New Methods for Seismic Reliability Evaluation of Structural Systems through Efficient Sampling and Optimization



Xuanli Sun

New College

University of Oxford

In Partial Fulfilment of the Requirements for the Degree of

Doctor of Philosophy

Michaelmas 2024

Acknowledgement

Above all, I would like to express my greatest gratitude to my supervisor Prof. Manolis N. Chatzis, for supporting, guiding, and working very closely with me during my D.Phil.. I am also truly grateful to Prof. Martin S. Williams for being my supervisor. He gave me the chance to work as I felt, total support and encouragement. For both of my supervisors, I will never forget the patience and understanding they have given. Their attitude towards research and passion for exploring the unknown have significantly shaped my perspective and approach towards research.

I would also like to thank all of those who I have collaborated with: first of all, my heartfelt appreciation goes to Dr. Xiaodong Shi, Dr. Emily Anderson and Dr. David Burton, for their insightful advice and inspirations on my research. I am also immensely grateful for Dr. Yunfang Yang, Dr. Bowen Cao and Dr. Lei Chen for the interesting discussions and generous help. I would also like to thank everyone in the Civil group, for all the engaging presentations and profound ideas given in the seminar.

Thanks should also go to my friends, both inside and outside the research office. I am deeply thankful to Jiayue Tao, Yue Zhou, Xiaonan Lu, Yifei Chen and many others. Their companion and support have been a source of joy and comfort during the

demanding times.

This work is also dedicated to my parents, Ms. Hong Zhu and Mr. Linghe Sun, for their unending understanding, support and love. This thesis owes its existence to them and my debt to them is beyond measure.

Finally, I would like to acknowledge Xinlei Liu, with profound gratitude. His patience, encouragement and understanding has made this work possible.

Abstract

The evaluation of the seismic reliability of a system plays an important role in its structural design and management, thus has been of interest in the field of earthquake engineering over decades. For this purpose, sampling and reliability methods are often used to effectively estimate the probabilistic response of structural systems under earthquakes. Furthermore, the probabilistic analysis is normally facilitated by adopting a synthetic earthquake model which simulates stochastic ground excitations.

This thesis develops new methods that provide more efficient and robust estimates for the seismic reliability of structural systems. For estimating the probabilistic responses of interest, a sampling method that adopts the concept of Unscented Transform (UT) is developed. It estimates the statistical information of the distribution, such as mean and covariance, of structural responses under earthquakes.

For evaluating the seismic reliability of the system, the Design point excitation (DPE) method, based on the concept of the First-order reliability method (FORM), is adopted. In the DPE method, a key step is finding the optimal design point, which can be expressed as an optimization problem. There are two methods developed in this thesis, which improve the robustness and efficiency of the DPE method: First, to

improve the efficiency of the gradient-based optimization method by developing an efficient Euler-analytical estimate of the derivative (EAD) to compute the gradients. Second, to treat the optimization problem as an optimal signal control problem solved by the Pontryagin's maximum principle (PMP). In the first approach, the EAD method is shown to effectively estimate the gradient of interest in the optimization. The DPE-EAD method is then further extended to excitation models with stochastic model parameters, upon which the seismic reliability of structures can be estimated for given seismological properties. In the second approach, the PMP effectively locates the design point by finding the optimal input signal. It inspires a novel application of the PMP in reliability estimations.

Incorporated into a probabilistic framework, the thesis also suggests a framework to estimate the reliability of structural systems under possibly occurring earthquakes over a period of interest. This can be used as a useful tool to indicate the resilience of a structural system to hazards. The constructed framework also has the potential to be extended for evaluating other reliabilities by incorporating different stochastic excitation models.

List of Publications & Presentations

X. Sun, M.S. Williams and M.N. Chatzis, *An efficient structural seismic reliability estimation through a recursive calculation of symbolic gradients*, Proceedings of the 17th World Conference of Earthquake Engineering (17WCEE), Sendai, Japan, 2020. Corresponding journal paper to be submitted.

X. Sun, K. Margellos, M.S. Williams and M.N. Chatzis, *A robust reliability algorithm for structures under earthquake excitations*, 4th International Conference on Uncertainty Qualification in Computer Sciences and Engineering (UNCECOMP), Athens, Greece, 2021

X. Sun, M.S. Williams and M.N. Chatzis, *An efficient seismic reliability method accounting for stochastic earthquake model parameters*, Engineering Mechanics Institute (EMI) Conference 2022, Baltimore, USA, 2022.

X. Sun, M.S. Williams and M.N. Chatzis, *A robust seismic reliability evaluation framework accounting for stochastic seismological properties*, Journal paper in progress

X. Sun, K. Margellos, M.N. Chatzis and M.S. Williams, *An effective reliability estimation method through the application of the Pontryagin's maximum principle (PMP) in optimizations*, Journal paper in progress

Contents

1 Introduction 1

1.1 Background and motivations 1

1.2 Literature review 5

1.2.1 Stochastic earthquake models 5

1.2.2 Sampling methods 9

1.2.3 Seismic reliability estimation 13

1.3 Objectives and navigation overview 18

2 Estimations of Seismic Responses of Dynamic Systems using the Unscented Transform 22

2.1 Synthetic earthquake model 23

2.1.1 The earthquake model parameters 26

2.1.2 Simulations of ground motions 29

2.1.3 Post-processing of the simulated ground motion 32

2.2 Methods for probabilistic response analysis 33

2.2.1 Monte Carlo (MC) simulation 33
2.2.2 Unscented Transform (UT) 35
2.3 Example and discussions: *A nonlinear hysteretic oscillator subjected to stochastic earthquake excitations.* 47
2.4 Conclusions 51
3 An Efficient Structural Seismic Reliability Estimation through a Recursive Calculation of Symbolic Gradients 53
3.1 Design Point Excitation (DPE) method 54
3.1.1 Initial guess of the design point 58
3.1.2 Line search optimization 63
3.2 Euler-Analytical estimate of the Derivative (EAD) 64
3.2.1 Selection of the discretization and integration time step ... 68
3.3 Derivative estimated by the Automatic Differentiation (AD) 70
3.4 Reliability problems with multiple limit states 72
3.4.1 The reliability over a time period 75
3.5 Examples and discussions 77
3.5.1 Example 1: *A 4-DoF system with Bouc-Wen nonlinearity subjected to earthquake excitations* 78
3.5.2 Example 2: *A 10-DoF system with polynomial nonlinearity subjected to earthquake excitations.* 102
3.6 Conclusion 114

4 Seismic Reliability of Structures Accounting for Stochastic Earthquake Model Parameters 116

4.1 Earthquake model with stochastic model parameters. 117

4.2 A modified Design Point Excitation (DPE) method - for excitations with stochastic model parameters..... 118

4.2.1 The reliability of a system at a specific time instant..... 118

4.2.2 The reliability of a system over an earthquake event..... 120

4.3 Euler-Analytical estimate of the Derivatives (EAD) 121

4.3.1 The general scheme 122

4.3.2 The analytical derivatives of the excitation $\frac{df(t_k)}{dU_i}$..... 123

4.4 Examples: Reliability of structures subjected to excitations with stochastic model parameters. 126

4.4.1 Example 1 - *Structural system with Bouc-Wen nonlinearity subjected to excitations with stochastic model parameters.* 127

4.4.2 Example 2 - *Structural system with polynomial nonlinearity subjected to excitations with stochastic model parameters.* 136

4.5 The extended DPE method - for excitations with stochastic seismological properties. 139

4.5.1 The analytical derivatives with respect to the model parameters $\boldsymbol{\mu}^{SD}$ and $\boldsymbol{\epsilon}^{SD}$ 142
4.5.2 Probabilistic distributions of the seismological properties 143
4.6 Reliability under repeated earthquakes 145
4.7 Examples: Reliability of structures subjected to excitations with stochastic seismological properties. 149
4.7.1 Example 3 – *Structural system with Bouc-Wen nonlinearity subjected to excitations with stochastic seismological properties.* 150
4.7.2 Example 4 - *Structural system with polynomial nonlinearity subjected to excitations with stochastic seismological properties.* 155
4.8 Conclusion 158
5 The Application of Pontryagin's Maximum Principle in the Optimizations in Seismic Reliability Estimations 160
5.1 Pontryagin's Maximum Principle (PMP) 161
5.1.1 The optimal signal 161
5.1.2 The concept of the PMP 162
5.2 The shooting method 167
5.2.1 The concept of the shooting method - single shooting 168

5.2.2 The multi-shooting method 169
5.3 Examples 172
5.3.1 Example 1: *A 3-DoF system with polynomial nonlinearity subjected to earthquake excitation.* 174
5.3.2 Example 2: *A 4-DoF system with Bouc-Wen nonlinearity subjected to earthquake excitation.* 182
5.4 Conclusion 187
6 Conclusions and Future Work 189
6.1 Summary and conclusions 189
6.2 Future works 192
Bibliography 195

Chapter 1

Introduction

1.1 Background and motivations

Significant earthquakes lead to serious damage to buildings and other infrastructure. For example, in the Sichuan (2008) [1,2], Haiti (2010) [3,4], Tohoku (2011) [5,6] and Turkey-Syria (2023) [7,8] earthquakes, buildings and bridges in town collapsed due to the severe ground shaking. Proper actions in advance of a seismic event may help prevent infrastructure damage and thus lower economic costs. For buildings entering an aging stage or being damaged, the starting point would be to carry out reliability evaluations to create a decision-making tool, thus enabling the formulation of optimal strategies for reducing or mitigating earthquake risks.

In this context, the term ‘reliability’ refers to the probability that system responses of interest do not exceed specified thresholds, while ‘risk’ is defined as the complementary concept to reliability. An accurate reliability evaluation often requires

a large number of simulations to be performed. Therefore, a key requirement is the number of available samples of earthquake time histories. One obvious source is accelerogram records in the database. Based on that, incremental Dynamic Analysis (IDA) [9,10] is a well-known method of estimating seismic risk through structural analysis. The accuracy of risk approximated by the IDA method is affected by the accelerogram records of the ground motions selected for the analysis, as well as the intensity measures chosen. Although certain earthquake selection methods, such as the Epsilon method [11] may improve the analysis, finding a significant number of earthquake records that would allow a probabilistic analysis remains a challenge. Alternatively, a large number of samples can be generated by employing a synthetic earthquake model. The models can be incorporated into a probabilistic framework to find the seismic reliability of dynamic systems [9].

The previous direction leads to the requirement of predicting the response of dynamic systems under stochastic earthquakes, which is one of the main subjects of the stochastic Earthquake Engineering community. However, the current methods are often computationally expensive to be able to obtain accurate estimations. One simple and very widely adopted approach is Monte Carlo (MC) simulation [12], in which probabilistic response estimates are obtained by generating samples of the earthquake time histories and seismic response of the dynamic system repeatedly. The inefficiency is mainly due to the large size of the sample set that is required before the statistics of the outcomes of interest converge.

This thesis focuses on exploring new approaches to estimating the probabilistic response of dynamic systems using synthetic earthquake models and ultimately suggesting new frameworks of seismic reliability evaluations. Efficient sampling and reliability methods are developed to reduce the computational cost in the seismic reliability evaluations of dynamic systems while retaining sufficient precision.

A brief literature review on the development of the synthetic ground model is provided in the following Section 1.2.1. A focus is placed on a robust ground motion model developed in [13,14] which is especially designed for simulating strong earthquakes. Since the model parameters have seismological properties, they follow certain distributions that can be found according to the earthquake database. This property serves as motivation for incorporating the synthetic ground motion model into a probabilistic framework, allowing for the probabilistic responses estimations and the seismic reliability evaluations of structural systems. Variations of this model are adopted in the majority of this research in the seismic reliability evaluation framework.

Section 1.2.2 gives a summary of existing sampling methods, outlining their respective advantages and limitations. Proper sampling methods can extensively reduce the computational costs in capturing the population of a target measurement. As the input variables in the ground motion model adopted, i.e., the white noise and the model parameters, follows Gaussian distributions, the concept of the Unscented Transform (UT) is anticipated to efficiently capture probabilistic information,

specifically the mean and variance, of the target measurement with appropriate accuracy, which motivates the research on the application of the UT sampling method in finding the probabilistic seismic response of structural systems written in Chapter 2.

Results from the sampling methods can be further processed to estimate the probability of the measurement response not exceeding a threshold, in order words the reliability. Alternatively, this information can also be directly obtained through reliability methods [15,16]. A literature review of the existing reliability methods is presented in Section 1.2.3. A focus is addressed on the Design Point Excitation (DPE) method which is specifically utilized for estimating the seismic reliability of structural dynamic systems [17]. The optimization problem in the DPE method is usually solved by a gradient-based optimization method which can be inefficient due to the challenges associated with calculating the gradient. A brief review of the gradient computation methods is presented in Section 1.2.3.1. To improve computational efficiency, an effective derivative estimation method is developed in Chapter 3 and associated with the DPE method to estimate the seismic reliability of structures efficiently. The current method [17] is only applicable to the examples with earthquake models having deterministic model parameters which is not representative for real earthquakes. This further motivates the work of the extension on the DPE method that evaluates the seismic reliability accounting for stochastic earthquake model parameters developed in Chapter 4.

Other optimization approaches may contribute to improving the performance of the DPE method in the reliability evaluations. Section 1.2.3.2 gives a literature review of the optimization methods. As per the literature of the DPE method, the design point is a discretized input signal. It motivates the research of the application of the Pontryagin's maximum principle (PMP) [18,19], a promising optimization method in finding a continuous time optimal signal, in the seismic reliability estimations in Chapter 5.

Finally, Section 1.3 at end of this chapter outlines the primary objectives and contributions and provides an overview of the thesis structure.

1.2 Literature review

1.2.1 Stochastic earthquake models

Though selecting and scaling existing earthquakes records to conduct probabilistic responses of dynamic system is common in a seismic risk assessment framework, the number of recorded earthquake time history in agreement with the seismological properties of an area of interest records are limited from a probabilistic analysis point of view. Thus, synthetic earthquake models which simulate the earthquake ground motion by a realization of an underlying stochastic process have been developed and employed for the probabilistic assessment of seismic demand. The literature review begins with a discussion on properties of earthquake time histories and followed by a review of the existing ground model developed.

An arbitrary earthquake time history can be thought of as one realization of an underlying stochastic process. It was found according to the accelerogram records that the stochastic process has nonstationary characteristics in both the time and frequency domains, referring to variations in both amplitude and frequency over time [13]. In this context, the variation of the amplitude, normally represented by the evolutionary spectra like Priestley [20], is known as the temporal non-stationarity. And the variation of the frequency, i.e. the frequency properties of the spectral density changing over time, is called the spectral non-stationarity. In terms of the temporal non-stationarity, the intensity of a typical ground motion gradually increases from zero to a high intensity which refers to a 'strong shaking' phase, and then gradually decays to zero with a total duration usually between 20–60s [21]. In terms of the spectral non-stationarity, it arises from the evolving nature of the seismic waves arriving at a site [13]. Typically, high-frequency (short wavelength) P waves tend to dominate the initial few seconds of the motion. These are followed by moderate-frequency (moderate wavelength) S waves, which tend to dominate the strong-motion phase of the ground motion. Toward the end of the shaking, the ground motion is dominated by low-frequency (long wavelength) surface waves. The complete ground motion is an evolving mixture of these waves with a dominant frequency that tends toward lower values with time [13]. Inelastic, degrading structures tend to have resonant frequencies, which often reduce with time as the structure responds inelastically to strong shaking. This trend could coincide with the variation in time of the predominant frequency of

the ground motion, thus enhancing the demand [22]. Thus, a realistic representation of both the temporal and spectral nonstationary characteristics of earthquake ground motions is essential for accurate predictions of the structural responses.

A series of pioneering ground motion models have been developed over the last decades, in which the spectral representation method [23] has been widely used and a series of different spectral density models are proposed. In the spectral representation method, sample functions of the stochastic process can be generated with great computational efficiency using a cosine series formula which is computed efficiently using the Fast Fourier Transform (FFT) technique [23]. Accounting for local site properties and a dominant frequency in the ground motion, stationary non-white process models were suggested by Kanai [24], Tajimi [25], Housner and Jennings [21], and Liu and Jhaveri [26]. Faravelli [27] formulated a stationary ground-motion model with mu1timodal spectral density. However, stationary models fail to produce the time-varying intensity, the temporal non-stationarities, which is typical in real earthquake ground-motion accelerograms. A time dependent envelope is introduced to the original model to partially remedy the deficiency [28-30]. A variety of time-modulating functions were then introduced to produce nonstationary ground models. These include the time-modulated harmonics [31], the modulated filtered white noise process [32], the modulated filtered Poisson process [33], the modulated stationary process [34], and the modulated filtered stationary process [35]. The improved models are not entirely satisfactory as they are uniformly modulated, i.e., the envelope only presents

the temporal non-stationarities in the ground motion. As such, the spectral non-stationarities in the frequency content, which is clearly shown in the earthquake accelerogram records, is not properly presented [20]. The model was further developed by introducing the non-stationarity using the mathematical concepts of random pulse train [36-39]. In the paper [98], a wavelet packet transform approach was used to characterize complex time-varying earthquake ground motions. In recent years, a spectral representation-based method is developed where the evolutionary spectrum for non-Gaussian processes is estimated to simulate non-stationary non-Gaussian stochastic processes using spectral representations [41]. A fully non-stationary Kanai-Tajimi ground motion model was developed by Vlachos et al. [99,100], utilizing time varying Kanai-Tajimi model parameters. The model parameters are linked with the seismological and local site properties to generate seismological and site-dependent ground motion. Studies have also been performed by Dabaghi et al. [101] and Lynne et al. [102] to construct non-stationary stochastic models for simulation of near-fault ground motions. These models have an evolutionary spectral representation [40] that represents the nonstationary characteristics in both the time and frequency domains.

Der Kiureghian et al. [14] developed a stochastic earthquake model constructed with model parameters that have seismological properties, i.e., the type of fault mechanism, the seismic magnitude, the source to site distance, and the soil condition, for which regional seismological authorities have further information. It is calibrated to a database of recorded ground motion so that the variability of the statistical

properties of the time histories generated by the synthetic ground motion is consistent with the variability observed in real records [13,14]. A ground model with separable spectral and temporal non-stationarities is constructed by a modulated filtered white noise process with a stochastic filter, and non-stationarities are achieved by introducing a time modulating function and introducing time-varying parameters in the stochastic filter. The model offers simplicity and ease of application as it is characterized by a minimal number of model parameters. In this thesis, this model proposed by Der Kiureghian et al. [14] has been adopted for probabilistic response and reliability analysis.

1.2.2 Sampling methods

Sampling methods attempt to obtain statistical information on the probability distributions of target measurement responses of dynamic systems through the generation of samples. Within the context of earthquake engineering those samples are different time histories. The MC simulation stands out as the most widely employed method due to its simplicity in the application [12]. The convergence of MC simulation does not depend on dimensionality; however, when a system model involves multiple sources of stochasticity, a large sample size is often required to accurately capture the distribution of a target measurement, especially in tail regions which correspond to rare events. This can lead to significant computational inefficiency. To address some of the limitations of the standard MC method, particularly in handling high-dimensional problems, rare-event probabilities, and computational inefficiencies, a

variety of sampling methods such as the Markov chain Monte Carlo (MCMC) simulation [42-45], the line sampling [50,51], the subset simulation [46], the importance sampling [47,48] and the Unscented Transform (UT) [49] have been successively developed over several decades. To capture the whole population, a smaller set of deterministic samples are generated and for some methods, prior knowledge of the measurement distribution is required. Each method has its strengths and limitations which are briefly summarized below. There is usually a trade-off between the accuracy level and the computational costs in sampling methods.

The MCMC method can be used for sampling from complex probability distributions and calculating numerical approximations of multi-dimensional integrals, with applications in Bayesian inference, probabilistic modelling, and rare event estimation [42,43]. One uses the previous sample values to randomly generate the next sample value, generating a Markov chain, which is a function of transition probabilities between sample values in terms of the most recent sample value [43]. Various algorithms have been developed for constructing the Markov chain. The Metropolis-Hastings algorithm [43,44], is most widely used, in which complex integrals are computed by expressing them as expectations for some distribution and then estimate this expectation by drawing samples from that distribution. By constructing a Markov chain that has the desired distribution, one can draw direct samples of the desired distribution by recording states from the chain. The more sample points included, the more closely the distribution of the sample matches the actual desired distribution. Due

to the residual effect of the starting position, the MCMC sampling only approximates a target distribution.

Line sampling is an attractive technique used in reliability engineering to compute small failure probabilities, often termed as ‘rare events’, in engineering systems [50]. This method is well-suited for addressing high-dimensional system challenges in reliability estimations, where the performance function has moderate non-linearity with respect to the stochastic parameters [51]. Similar to the subset simulation discussed below, the method does not necessitate detail knowledge of the system, thus is capable of analyzing ‘black box’ systems [50,52].

Subset simulation [46] is also very efficient in computing the reliability of the system when dealing with rare events. The basic idea is to express a small failure probability as a product of larger conditional probabilities by introducing intermediate failure events. This conceptually converts the original rare event problem into a series of frequent event problems that are easier to solve. In the actual implementation, samples conditional on intermediate failure events are adaptively generated to gradually populate from the frequent to rare event region. These ‘conditional samples’ provide information for estimating the complementary cumulative distribution function of the events that govern failure, covering the high as well as the low probability regions. They can also be used for investigating the cause and consequence of failure events. The generation of conditional samples is not trivial but can be performed efficiently using MCMC [46]. Subset Simulation takes the relationship

between the input random variables and the output response of interest as a ‘black box’. This can be attractive for complex systems where it is difficult to use other variance reduction or rare event sampling techniques, such as, that require prior information about the system behaviour. In cases where it is possible to incorporate prior information into the reliability estimation algorithm, for example, the system behaviour or the distributions of the model parameters, opting for other variance reduction techniques such as importance sampling is often more efficient [46-48]. In case of a fracture mechanics test problem, existing research shows that the subset simulation is more efficient than traditional MC simulation but less efficient than line sampling [52].

The Unscented Transform (UT) [49], first proposed by Julier and Uhlmann in 1997, was initially developed in the context of nonlinear extension of Kalman Filter. Distributions of random variables under arbitrary nonlinear transformation can be predicted by a minimal set of deterministic samples using UT. For Gaussian distributed input variables, the statistics of the transformed outputs are captured accurately to the 3rd order Taylor series expansion for any nonlinearity. While for non-Gaussian inputs, the method is accurate in approximation to the 2nd order. The accuracy of the 3rd and higher order moments can be achieved depending on the choice of model parameters [49]. The method can be used to develop a nonlinear generalization of Kalman Filter. It provides significant performance improvements over the Extended Kalman Filter (EKF) in many nonlinear filtering and control applications and has largely replaced

the EKF. In this thesis, since the inputs of the earthquake model adopted are Gaussian variables, the UT concept is used to estimate the probabilistic response of structural system under earthquakes and is further discussed in Chapter 2.

Over the last decade, a series of the variations of the UT, i.e., the higher order UT (HOUT) [53], the new UT [54], the improved UT [55] and a linear extension of UT [56], have been developed to improve the accuracy of the higher order distribution information for highly nonlinear transformations. A larger sample set with augmented sigma points are introduced to capture the higher order moments information. Research have shown that the improved methods have better performances in predicting the population distributions of the transformed outputs. The HOUT [53] and the linear extension of UT [56] allow capturing up to any order moments required. The HOUT requires higher computational cost when higher order information is desired, while the computational complexity of the linear extension of UT is considered as the same order as that of the original UT. Developing improved methods are still a topic of interest in the field so as to achieve high accuracy with a smaller sample set.

1.2.3 Seismic reliability estimation

This subsection focuses on reliability estimation methods. To begin with, there are several well-established methods for estimating the moments of the probability density function (PDF) of the system responses in reliability analysis. The Point Estimate Method (PEM) [103], including the variations of the UT methods discussed above, offers powerful approximation for the first and second-order probabilistic moments.

Recent research of variations of PEM shows capabilities to capture higher-order moments, i.e., skewness and kurtosis, in systems with complex random variables [53-56,104-107]. The Scaled Spherical Simplex Filter (S3F) method [104-106], which combines both sampling and filtering to improve the accuracy of moment estimation and is efficient in high-dimensional reliability problems. The Quadratic Point Estimate Method (QPEM) [107] uses quadratic expansion of the required sigma points to capture up to fifth-order input moments of the normal distribution.

Other than methods based on moments estimation, there are also probability-based methods that calculate the probability of failure and reliability directly, i.e., the first- and second-order reliability methods (FORM and SORM) [15,16,57]. As for the time-variant reliability problems, the PHI2 method [108] is a well-established method that deals with computing the outcrossing rate by using classical time-invariant reliability tools such as FORM and SORM. New reliability methods, the probability density evolution methods (PDEM) [58] and the Design Point Excitation (DPE) method [17] were developed in the last decade for the dynamic response analysis of structural system under stochastic excitations.

The FORM [15,16,57], also known as Hasofer -Lind Reliability Index, is first developed by Hasofer et al. in 1974 and is a well-known reliability method. The method introduces a performance function, named the Limit State Function (LSF), to search for the reliability index, which indicates the probability of a system response not exceeding a threshold limit. It is capable of handling non-linear systems with non-

normal variable inputs. The input variables are transformed into a standardized space of normal variables. The LSF, constructed in terms of the transformed standard normal variables, is approximated by its linearization using Taylor expansion. The FORM is a computationally more efficient alternative to the MC simulations in reliability analysis. Besides, to improve the performance of the FORM, the SORM [15,59], employing the second-order Taylor expansion of the LSF, is developed to provide better approximations to deal with problems incurred by the linearization. Both theoretical insights and practical examples have demonstrated that SORM provides a more accurate reliability approximation compared to FORM.

The reliability evaluation of structural systems subjected to stochastic excitations, such as earthquakes, is of significant interest to the earthquake engineering community. The PHI2 method allows to compute the evolution of the reliability in time and the Probabilistic Density Evolution Method (PDEM) tracks the evolution of the PDF of system responses over time. Both methods are effective for dynamic and time-dependent reliability problems [58,108]. The DPE method [17], which utilizes the fundamental theory of the FORM, is specifically designed for estimating the reliability of dynamic systems under stochastic excitations with random input. The continuous input signals are discretized to a series of independent variables such that the FORM can be applied to random process. It finds the design point excitation which is a most likely realization of the stochastic excitation that induces the threshold response [17] and approximates the reliability at the realization of the discretized random input that

has the highest joint probability. Finding this realization requires solving an optimization problem, which in turn involves gradient calculations. A brief literature review of the optimization methods and gradient computation methods are summarized below.

1.2.3.1 Gradient computation methods

An efficient derivative calculation method is critical in the application of gradient-based optimization algorithm, thus existing research on gradient computation for dynamic models has been explored in the context of optimization algorithms. The Finite Difference method [60] is the most commonly used method for estimating the gradients thanks to its simplicity in the applications. However, the Finite Difference scheme could potentially be imprecise and time-consuming when either a complex or a high dimensional dynamic model is considered. To pursue a better accuracy of the gradient approximations, variations of the Finite Difference method can be found in [61] but they are computationally more expensive. Other methods have also been developed to provide an estimate of the derivatives. For example, the adjoint method, first introduced in [62-64], approximates the gradient using the Lagrangian of the constraints implied by the dynamics. The stability of the adjoint equation for the underlying dynamical system may affect the application of the method. The Forward Sensitivity method [64], proposed in the context of modelling fMRI time series [62,65], stands out as a commonly applied technique in derivative estimations. It employs the chain rule to reformulate the differential equations in terms of implicit derivatives. The

Automatic Differentiation, a semi-analytical semi-numerical derivative calculation method, is another promising method widely used in the field of deep learning.

1.2.3.2 Optimization methods

A series of effective optimization methods such as the line search method [66,67] or the Improved HL-RF algorithm [68] have been developed over the decades. As mentioned earlier, the accuracy and efficiency of these gradient-based optimization methods rely much on the gradient computation method. If the optimization problem searches for a discretized signal, an alternative to traditional optimization algorithms is to approach them as optimal control problems which finds an optimal continuous input signal. This can be achieved by the Pontryagin's Maximum Principle (PMP) [18,19].

The PMP method proposed by Pontryagin [69] has been widely used in the field of optimal control [70-73] to select continuous control trajectories that maximize or minimize a desired objective, especially in the presence of constraints for the state or input controls. In Earthquake Engineering, the concept of the PMP has been adopted to find the optimal control signal for structures to resist earthquakes excitation [74-76]. The method constructs a Hamiltonian in terms of the objective function and the dynamic system in optimal control problem, and the principle states that the Hamiltonian is maximized at the optimal signal [18]. According to this property, the boundary conditions of the Hamiltonian system, also known as the transversality conditions, are defined according to first order optimality conditions of the continuous-

time problem in maximizing the Hamiltonian. Thus, the method converts the optimal control problem to a boundary-value problem (BVP) of the Hamiltonian system. The optimal solution is found by solving a system of differential equations that satisfies the endpoint conditions defined by the transversality conditions and the constraints in the optimization.

Various algorithms, commonly known as shooting methods [77,78], have been proposed for solving the boundary-value problem (BVP). The shooting methods replace the BVP with an initial-condition problem, starting with an arbitrary initial guess of the initial condition. In a single shooting method, a two-point BVP is considered. It is appealing due to its simplicity in applications; however, it may have problems with the numerical integration when the system has unstable modes, and a large time interval is considered in the integration. In order to overcome the numerical difficulties in the single shooting method, a modified method, called the multi-shooting method [79,80], has been developed. The integration time interval is divided into several sub-time intervals, and the shooting method is partitioned and applied at each sub-time interval. In this thesis, the PMP method is used to find the continuous-time optimal input signal to the earthquake model, and then incorporated into the DPE method to estimate the reliability.

1.3 Objectives and navigation overview

Motivated by the need to address the computational problems in the existing methods for the probabilistic estimates of seismic responses, the thesis develops robust methods

through efficient sampling and reliability methods for seismic reliability evaluations of structural systems. Both approaches adopt synthetic earthquake models to predict the probabilistic responses of dynamic systems.

The first research work presented in this thesis aims to improve the computational efficiency in probabilistic seismic response analysis through the use of the Unscented transform sampling method. The statistics of the probability distributions of the structural responses are captured by a minimal set of samples that are specially selected. The second contribution of this thesis is to improve the computational efficiency of the DPE method through an effective derivative estimation algorithm. The DPE method is further extended to improve the robustness of the method by accounting for the stochasticity of the ground model parameters in the seismic reliability evaluations. The final contribution of this work devoted to the pioneer application of the PMP method for seismic reliability evaluations.

The thesis is organized as follows:

- In chapter 2, the synthetic ground model generally adopted in this work is introduced. Two methodologies based on the UT sampling method, namely the Offline UT and the Online UT method, are developed to estimate the probability distributions of dynamic systems subjected to stochastic earthquake. The proposed methods are efficient because the distributions of the target responses are captured by a minimal set of weighted samples using the concept of UT. Algorithms of the developed Offline UT and the Online UT methods are

elaborated.

- In chapter 3, a reliability method, namely the Design Point Excitation (DPE) method is briefly introduced. An efficient Euler-Analytical estimation of the Derivative (EAD) is developed to be used in solving the optimization problem in the DPE method. The proposed method shows an outstanding computational efficiency over other existing gradient computation methods such as the finite difference method and the automatic differentiation methods. The DPE method with the use of the developed EAD is also applicable and accurate in estimating the reliability when multiple limit state criteria are examined. Applications and superior performance of the algorithm are demonstrated using multiple examples of nonlinear structural systems.

- In chapter 4, an extension of the DPE method capable of dealing with stochastic filters with stochastic seismological properties is developed. It finds optimized values of the seismic model parameters, whose probabilistic distributions are determined according to the seismological properties and the optimized values of seismological properties. Again, the efficient EAD is adopted and derivation procedure of the analytical expressions of the derivative with respect to the added seismic model parameters are elaborated. Examples of nonlinear structural systems are presented to demonstrate the efficiency and accuracy of the suggested method.

- In chapter 5, an alternative way to estimate reliability by using the Pontryagin's

maximum principle (PMP) is introduced. Rather than solving the optimization problem in the DPE method, the PMP treat it as an optimal signal control problem to find the design point. The fundamental theory is discussed and the developed DPE-PMP method is tested with examples of nonlinear structural systems. The developed method is robust, and it prompts an innovative path for tackling the optimization problem in the DPE method.

- In chapter 6, a conclusion of this thesis is presented followed by suggestions and foresights of the future work.

Chapter 2

Estimations of Seismic Responses of Dynamic Systems using the Unscented Transform

This chapter aims to develop efficient methods for estimating the probabilistic response of dynamic systems under stochastic excitations. The chapter starts with introducing the synthetic ground model adopted. Two novel methodologies, the Offline UT and the Online UT, based on the concept of the Unscented Transform (UT) sampling method are proposed to estimate the statistics of the probability distributions, i.e., mean and covariance, of the target responses. The concept of the UT sampling method is briefly introduced, and the algorithms of the Offline UT and Online UT are presented. The UT sampling method estimate the probability distributions of the target responses through a minimal set of samples which is substantially more efficient than the default, Monte Carlo (MC) simulations. For each sample, the former generates the whole earthquake and structural responses time history offline, while the later updates

the probability distributions of the earthquake and structural properties at each time step in an online manner. The performances of the proposed methods are demonstrated by an example of a nonlinear hysteretic oscillator with Bouc-Wen nonlinearity subjected to stochastic earthquakes. The results are compared to that of the default MC simulations to show the accuracy and the computational efficient of the proposed methods. Advantages and limitations of the proposed UT methods in estimating the probability distributions of the seismic responses of structural systems are discussed.

2.1 Synthetic earthquake model

A synthetic ground model, developed in [13,14], is adopted in this work to produce a necessary number of time histories and carry out the probabilistic analysis on the seismic responses of structures. The chapter provides an in-depth description of the ground model which is chosen as it represents well the non-stationarities in the earthquake time histories and due to its potential to match the statistical properties of the accelerogram time histories (real records) characteristics using a small number of model parameters. The synthetic ground model was constructed by regression applied on a suite of earthquake records. The regression procedure is briefly summarized. Further insights of the development of this ground model can be found in [13,14].

A modulated filtered white noise expressed by Eq. (2.1) is considered as the underlying stochastic process describing the earthquake ground motion $f(t)$.

$$f(t) = q(\boldsymbol{\alpha}, t)\left\{\frac{1}{\sigma_h(t)}\left[\int_{-\infty}^{t} h\big[t-\tau, \omega_f(\tau), \zeta_f(\tau)\big] w(\tau) d\tau\right]\right\} \tag{2.1}$$

In this ground model, $w(t)$ denotes the Gaussian white noise process, $q(\alpha, t)$ is the modulating function that controls the temporal non-stationarity and $h[t-\tau, \omega_f(\tau), \zeta_f(\tau)]$ is the impulse response function of the filter that controls the spectral non-stationarity. $\sigma_h(t) = \sqrt{\int_{-\infty}^{t} h^2[t-\tau, \theta(\tau)]d\tau}$ is the standard deviation of the filtered white noise represented by the integral in the squared bracket. Through normalization, the expression in the braces has unit variance. The temporal and spectral nonstationary characteristics of the stochastic process are separated by this ground model, thus can be carefully considered for the realization of the earthquake time histories.

The modulating function $q(\boldsymbol{\alpha}, t)$ is a deterministic and non-negative expressed by:

$$q(\boldsymbol{\alpha}, t) = \alpha_1 \cdot t^{\alpha_2 - 1} \cdot \exp(-\alpha_3 t) \tag{2.2}$$

where $\boldsymbol{\alpha} = [\alpha_1, \alpha_2, \alpha_3]$, in which $\alpha_1, \alpha_3 > 0$ and $\alpha_2 > 1$. The parameters α_1, α_2 and α_3 control the intensity, the shape and the duration of the modulating function respectively. Figure 2. 1 shows some realizations of the modulating functions with different α selected to show the effect of the parameters on the modulating function.

The spectral non-stationarity is achieved by introducing time-varying filter parameters. The unit-impulse response function of the filter corresponds to the pseudo-acceleration response of a single-degree-of-freedom linear oscillator is selected:

$$h[t-\tau, \omega_f(\tau), \zeta_f(\tau)] = \frac{\omega_f(\tau)}{\sqrt{1-\zeta_f^2(\tau)}} \exp[-\zeta_f(\tau)\omega_f(\tau)(t-\tau)] \cdot$$

$$\sin\left[\omega_f(\tau)\sqrt{1-\zeta_f^2(\tau)}(t-\tau)\right], \qquad \text{for } \tau \le t$$

$$= 0, \qquad \text{otherwise} \quad (2.3)$$

where $\omega_f(\tau)$ and $\zeta_f(\tau)$ denote the time-varying natural frequency and damping ratio of the filter which control the evolutionary predominant frequency and bandwidth of the motion respectively. Since the predominant frequency of an earthquake ground motion decays with time, $\omega_f(\tau)$ is selected as the linear form:

$$\omega_f(\tau) = \omega_0 - \frac{(\omega_0 - \omega_T)}{t_T}\tau \quad (2.4)$$

where t_T is the total duration of the ground motion. ω_0 and ω_T, the natural frequency of the filter at $t_0 = 0$ and t_T, are two parameters that describe the time-varying frequency content of the ground motion. While the filter damping $\zeta_f(\tau)$ is approximated as constant. Investigations of the existing accelerograms reveal that the variation of their bandwidth over time is relatively insignificant [13]. Thus, the filter damping $\zeta_f(\tau)$ is approximated as a constant.

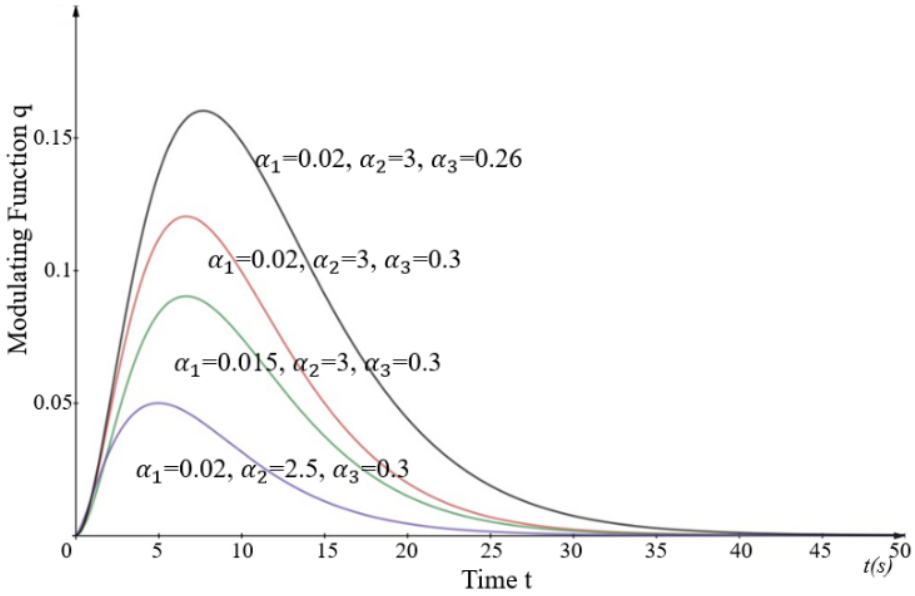


Figure 2. 1 Realizations of the modulating function with different $\boldsymbol{\alpha}$ selected.

For the ease of application and implementation, the ground model is discretized, as represented by:

$$f(t) = q(\boldsymbol{\alpha}, t) \cdot \sum_{i=1}^{N} s_i(t)\, w_i \tag{2.5}$$

The continuous white noise process, $w(t)$, is discretized to independent components, w_i, with a time step Δt_D, and thus $N = t/\Delta t_D$. $w_i = \sigma u_i$ represents the discretized white noise at $t_i = i \cdot \Delta t_D$, in which u_i is standard Gaussian and the standard deviation σ describes the intensity of the input white noise; $s_i(t) = \frac{h[t-t_i, \omega_f(t_i), \zeta_f(t_i)]}{\sigma_h(t)}$ is the normalized impulse response function associating the white noise w_i to the stochastic process.

2.1.1 The earthquake model parameters

The earthquake model parameters $\boldsymbol{\theta} = [\alpha_1, \alpha_2, \alpha_3, \omega_f, \zeta_f]$ has been further connected to quantities that have physical meanings in earthquake accelerograms. [14] The set of parameters $\boldsymbol{\theta}$ can be determined by the following properties vector, $\boldsymbol{\lambda} = [\bar{I}_a, D_{5-95}, t_{mid}, \omega_{mid}, \omega', \zeta]$ of the accelerogram time histories. The elements of $\boldsymbol{\lambda}$ are the Arias intensity $\bar{I}_a$, the effective duration of the motion D_{5-95} (time between 5 and 95% levels of Arias intensity), the time to the middle of the strong-shaking phase t_{mid} (time to the 45% level of Arias intensity), the filter frequency ω_{mid} at t_{mid}, the rate of change of the filter frequency ω' and the filter damping ratio ζ. The following equations link the two set of parameters $\boldsymbol{\lambda}$ and $\boldsymbol{\theta}$:

$$a_1 = \sqrt{\bar{I}_a \frac{(2a_3)^{2a_2-1}}{\Gamma(2a_2-1)}} \tag{2.6a}$$

$$\omega_f(t) = \omega_{mid} + \omega'(t - t_{mid}) \tag{2.6b}$$

$$\zeta_f(t) = \zeta \tag{2.6c}$$

in which $[\alpha_2, \alpha_3]$ are the solution to:

$$D_{5-95} = p_{95} - p_5 \tag{2.7a}$$

$$t_{mid} = p_{45} \tag{2.7b}$$

where p_j represent j-percentile variate, the inverse of the Gamma cumulative density function (CDF) with parameter $2\alpha_2 - 1$ and $2\alpha_3$ at probability $j\%$.

A regression model is then developed by Der Kiureghian et al. in [14] to relate the set of mathematical properties $\boldsymbol{\lambda} = [\bar{I}_a, D_{5-95}, t_{mid}, \omega_{mid}, \omega', \zeta]$ to the seismological properties of $\boldsymbol{\mu} = [F, M, R_{rup}, V_{s30}]$ for which regional seismological authorities have further information. Following the research work of [14], F represents the fault mechanism with $F = 0$ denoting a strike-slip fault and $F = 1$ denoting a reverse fault; M represents the moment magnitude of the earthquake; R_{rup} represents the closest distance from the site to the ruptured area and V_{s30} represents the shear-wave velocity of the top 30 meters of the site soil. The regression involves the following steps:

1) A set of recorded earthquakes is selected from the PEER NGA strong motion database [81,82].

2) The seismological properties of $\boldsymbol{\mu} = [F, M, R_{rup}, V_{s30}]$ are obtained for each record.

3) The mathematical properties $\boldsymbol{\lambda} = [\bar{I}_a, D_{5-95}, t_{mid}, \omega_{mid}, \omega', \zeta]$ of the accelerogram time histories are calculated for each record.

4) Probability distributions are assigned to fit the distribution of the samples $\boldsymbol{\lambda} = [\bar{I}_a, D_{5-95}, t_{mid}, \omega_{mid}, \omega', \zeta]$ obtained.

5) The mathematical properties $\boldsymbol{\lambda} = [\bar{I}_a, D_{5-95}, t_{mid}, \omega_{mid}, \omega', \zeta]$ are transformed into a normal space for satisfying the normality requirement of regression error. The transformed normal variables $\boldsymbol{v} = [v_i]$ for $i = 1,2, \ldots,6$, is given by

$$v_i = \phi^{-1}\left[F_{\lambda_i}(\lambda_i)\right] \tag{2.8}$$

where λ_i denotes the i^{th} element in the mathematical properties $\boldsymbol{\lambda}$, $F_{\lambda_i}(\cdot)$ denote the marginal cumulative distribution fitted to λ_i and $\phi^{-1}[\cdot]$ is the inverse standard normal CDF.

6) Through regression, a model that describes the relation between the seismological properties $\boldsymbol{\mu} = [F, M, R_{rup}, V_{s30}]$ and the transformed normal variables $\boldsymbol{v} = [v_i]$, which is shown later in Eq. (2.9).

It should be noted that the ground model is designed for simulating strong earthquakes, thus earthquakes records having the seismological properties of $M \geq 6$, $10km \leq R_{rup} \leq 100km$ and $V_{s30} \geq 600m/s$ are selected.

This regression model allows the synthetic earthquake model in Eq. (2.1) or Eq. (2.5) to generate time histories for a given seismological properties $\boldsymbol{\mu} =$

$[F, M, R_{rup}, V_{s30}]$. Through explanation of the development of this regression model and the transformation of the ground model parameters can be found in (Rezaeian & Der Kiureghian 2010).

2.1.2 Simulations of ground motions

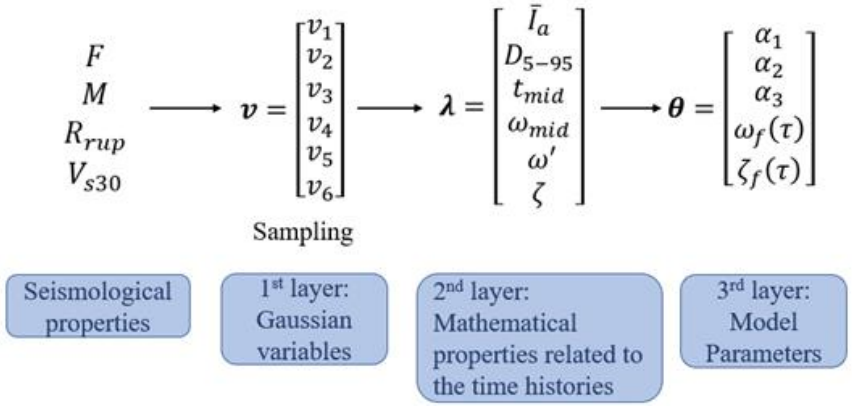


Figure 2. 2 Parametric transformations in the earthquake model

Based on the ground model in Eq. (2.1), earthquake time histories are generated with a realization of the model parameters $\boldsymbol{\theta} = [\alpha_1, \alpha_2, \alpha_3, \omega_f, \zeta_f]$ in agreement with the seismological properties $\boldsymbol{\mu}$ selected, and a random realization of the input white noise. Figure 2. 2 shows the procedure of determining the model parameters $\boldsymbol{\theta}$ from a given set of seismological properties $\boldsymbol{\mu} = [F, M, R_{rup}, V_{s30}]$. According to the regression model, the set of Gaussian parameters $\boldsymbol{v}$ are computed from the selected $\boldsymbol{\mu}$ using the following equations:

$$v_1 = \beta_{1,0} + \beta_{1,1} \cdot (F) + \beta_{1,2} \cdot \left(\frac{M}{7}\right) + \beta_{1,3} \cdot \left(\ln \frac{R_{rup}}{25km}\right) + \beta_{1,4} \cdot \left(\ln \frac{V_s}{750m/s}\right) + \eta_1 + \kappa_1 \quad (2.9a)$$

$$v_i = \beta_{i,0} + \beta_{i,1} \cdot (F) + \beta_{i,2} \cdot \left(\frac{M}{7}\right) + \beta_{i,3} \cdot \left(\frac{R_{rup}}{25km}\right) + \beta_{i,4} \cdot \left(\frac{V_s}{750m/s}\right) + \eta_i + \kappa_i \quad \text{for } i = 2, \dots, 6 \quad (2.9b)$$

where $\beta_{\cdot,\cdot}$ are dimensionless regression coefficients. For a given i, η_i and κ_i (for $i = 1, \dots, 6$) are independent, zero-mean, Gaussian distributed error terms with variance τ_i^2 and σ_i^2 respectively. The inter-event residuals η_i account for variability between different seismic events and the intra-event residuals κ_i correspond to variability within the same seismic event at different locations. Values of the dimensionless regression coefficients $\beta_{\cdot,\cdot}$ and the standard deviations τ_i and σ_i are shown in Table 2. 1. Let ϵ_i denote the total error in v_i for $i = 1, \dots, 6$, such that $\epsilon_i = \eta_i + \kappa_i$. The total errors ϵ_i are zero-mean, jointly Gaussian variables with variances $Var(\epsilon_i) = \tau_i^2 + \sigma_i^2$. Table 2. 2 shows the correlations in the error terms ϵ_i found by regression. The total error $\boldsymbol{\epsilon} = [\epsilon_i]$ is a zero-mean Gaussian vector with covariance matrix, $Cov(\boldsymbol{\epsilon})$, computed by the standard deviations $\varphi_i = \sqrt[2]{Var(\epsilon_i)} = \sqrt[2]{\tau_i^2 + \sigma_i^2}$ and the correlation matrix $\boldsymbol{R}_\epsilon$:

$$Cov(\boldsymbol{\epsilon}) = \text{diag}(\boldsymbol{\varphi}) \cdot \boldsymbol{R}_\epsilon \cdot \text{diag}(\boldsymbol{\varphi}) \tag{2.10}$$

where $\text{diag}(\boldsymbol{\varphi})$ refers to the diagonal matrix whose i[th] diagonal element correspond φ_i for $i = 1, \dots, 6$. $\boldsymbol{R}_\epsilon = [r_{ij}]$ is the correlation matrix in which r_{ij} is the correlation coefficient of ϵ_i and ϵ_j for $i = 1, \dots, 6$, $j = 1, \dots, 6$ as shown in Table 2. 2. The variances $Var(v_i)$, the correlations $\boldsymbol{R}_{\boldsymbol{v}}$ and the covariance matrix $Cov(\boldsymbol{v})$ of the Gaussian parameter $\boldsymbol{v}$ is identical to those of the error term vector $\boldsymbol{\epsilon}$, since $\boldsymbol{\epsilon} = [\epsilon_i] = [\eta_i + \kappa_i]$ is the only random variable in $\boldsymbol{v}$ as shown in Eq. (2.9). Thus, for a selected set of seismological properties $\boldsymbol{\mu}$, the means $\overline{v_i}$ and variances $Var(v_i)$ of the Gaussian parameters v_i, and the covariance matrix of $\boldsymbol{v}$ are well-determined: v_i

are jointly Gaussian variables with the means $\overline{v_i}$ as expressed in Eq. (2.11) and variances $Var(v_i) = Var(\epsilon_i) = \tau_i^2 + \sigma_i^2$.

$$\overline{v_1} = \beta_{1,0} + \beta_{1,1} \cdot (F) + \beta_{1,2} \cdot \left(\frac{M}{7}\right) + \beta_{1,3} \cdot \left(\ln \frac{R_{rup}}{25km}\right) + \beta_{1,4} \cdot \left(\ln \frac{V_s}{750m/s}\right) \quad (2.11a)$$

$$\overline{v_i} = \beta_{i,0} + \beta_{i,1} \cdot (F) + \beta_{i,2} \cdot \left(\frac{M}{7}\right) + \beta_{i,3} \cdot \left(\frac{R_{rup}}{25km}\right) + \beta_{i,4} \cdot \left(\frac{V_s}{750m/s}\right) \quad \text{for } i = 2, \dots, 6 \quad (2.11b)$$

And the covariance matrix $Cov(\boldsymbol{v})$ is computed by:

$$Cov(\boldsymbol{v}) = \text{diag}(\boldsymbol{\varphi}) \cdot \boldsymbol{R_v} \cdot \text{diag}(\boldsymbol{\varphi}) \quad (2.12)$$

where the correlation matrix $\boldsymbol{R_v} = \boldsymbol{R_\epsilon}$ is shown in Table 2. 2.

Table 2. 1 The regression coefficients and the standard deviation of the error components

i	$\beta_{i,0}$	$\beta_{i,1}$	$\beta_{i,2}$	$\beta_{i,3}$	$\beta_{i,4}$	τ_i	σ_i
1	−1.844	−0.071	2.944	−1.356	−0.265	0.274	0.594
2	−6.195	−0.703	6.792	0.219	−0.523	0.457	0.569
3	−5.011	−0.345	4.638	0.348	−0.185	0.511	0.414
4	2.253	−0.081	−1.810	−0.211	0.012	0.692	0.723
5	−2.489	0.044	2.408	0.065	−0.081	0.129	0.953
6	−0.258	−0.477	0.905	−0.289	0.316	0.682	0.760

Table 2. 2 Correlations between the error terms of model parameters $\boldsymbol{v}$

	ϵ_1/v_1	ϵ_2/v_2	ϵ_3/v_3	ϵ_4/v_4	ϵ_5/v_5	ϵ_6/v_6
ϵ_1/v_1	1	−0.36	0.01	−0.15	0.13	−0.01
ϵ_2/v_2		1	0.67	−0.13	−0.16	−0.20
ϵ_3/v_3			1	−0.28	−0.20	−0.22
ϵ_4/v_4				1	−0.20	0.28
ϵ_5/v_5		Sym.			1	−0.01
ϵ_6/v_6						1

With the mean and covariance matrix defined, a sample of the 1st layer Gaussian parameters $\boldsymbol{v}$ is drawn and then transformed into the 2nd layer parameters $\boldsymbol{\lambda}$

associated with the mathematical properties of the time history:

$$\lambda_i = {F_{\lambda_i}}^{-1}[\phi(v_i)] \tag{2.13}$$

where ${F_{\lambda_i}}^{-1}[\cdot]$ is the inverse marginal cumulative distribution of λ_i and $\phi(\cdot)$ denotes the standard normal CDF. Subsequently a realization of the 3rd layer model parameters $\boldsymbol{\theta}$ are determined by the parameters $\boldsymbol{\lambda}$ through Eq. (2.6) - (2.7).

To sum up, samples of model parameters and earthquake time histories can be generated for a selected site and earthquake characteristics $\boldsymbol{\mu} = [F, M, R_{rup}, V_{s30}]$ by following the steps:

1. Find the mean and covariance matrix of the Gaussian parameters $\boldsymbol{v}$ using Eq. (2.11) – (2.12).
2. Draw a sample of the Gaussian parameters $\boldsymbol{v}$ and transform them to a realization of the model parameters $\boldsymbol{\theta}$ through Eq. (2.13) and Eq. (2.6) - (2.7).
3. Substitute the model parameters $\boldsymbol{\theta}$ obtained in step 2 with a realization of the white noise input into Eq. (2.5) to generate an earthquake time history.

2.1.3 Post-processing of the simulated ground motion

The synthetic ground model is constructed through regression of earthquake records in the database. It was previously found that such stochastic ground models tend to overestimate the structural response at low frequencies [13]. This happens because the ground acceleration is simulated as a filtered white noise process which has a non-zero spectral density at zero frequency. Thus, the spectra of the ground velocity and displacement have infinite values of $\omega = 0$. To adjust the low-frequency content, a

critically damped oscillator is used as a high pass filter. The corrected ground motion, denotes $f_h(t)$, is obtained by the following differential equation:

$$\ddot{x}_h(t) + 2\omega_c \dot{x}_h(t) + \omega_c^2 x_h(t) = f(t) \tag{2.14a}$$

$$f_h(t) = \ddot{x}_h(t) \tag{2.14b}$$

where ω_c denotes the frequency of the high pass filter and $f(t)$ is the simulated ground motion by Eq. (2.5).

2.2 Methods for probabilistic response analysis

Several methods can be used to estimate the statistical properties of a selected structural response. The most commonly used method is through the use of Monte Carlo (MC) simulations which is a computational algorithm relying on random sampling. Samples of the target response measurements are drawn repeatedly through random sampling. The method is accurate when the sample set becomes sufficiently large which encounters the problem of computational inefficiency. An efficient sampling method, the UT, is then introduced in this section. The statistics of the probability distributions of a target response measurement are captured by a minimal set of samples that are specially selected. Based on the concept of UT, two novel algorithms, the offline and the online UT methods, are developed for estimating the statistical properties of structural responses under earthquake excitations.

2.2.1 Monte Carlo (MC) simulation

The process of generating each sample of the structural response of interest under

earthquake excitations is shown in the block diagram in Figure 2. 3 shown. To estimate seismic responses of structural systems, a realization of the white noise $w(t)$ and the earthquake model parameters $\boldsymbol{\theta}$ are input to the synthetic earthquake model to output the earthquake time history. The simulated earthquake time history is then input to the structural system as the excitation to generate the response time history of the target measurement. The state-space equation and output measurement of the structural system are written as:

$$\dot{\boldsymbol{x}}_s = \boldsymbol{l}(\boldsymbol{x}_s, f_h) \tag{2.15a}$$

$$y = \boldsymbol{h}(\boldsymbol{x}_s, f_h) \tag{2.15b}$$

where $\boldsymbol{x}_s$ is the state vector of the structural system and f_h is the post-processed ground excitation input obtained from Eq. (2.14b). $\boldsymbol{l}(\cdot,\cdot)$ is the state-space function that describes the dynamics of the structural system, and $\boldsymbol{h}(\cdot,\cdot)$ is the output measurement function that defines the output response of interest, y. The time histories of the structure responses of interest, $y(t)$, are obtained by the system of equations.

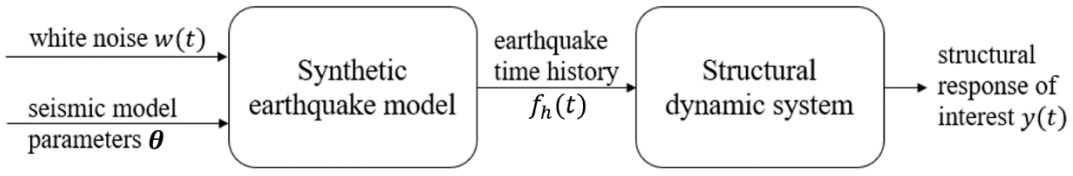


Figure 2. 3 Block diagram of the nonlinear transformation from the synthetic earthquake model inputs to the output of the target structural response.

Through the MC simulation, samples of the synthetic earthquake time histories are generated and then used as inputs to the structural system of interest to obtain

samples of the target response time histories $y(t)$ of the structural system. Statistical information on the probability distributions of the target responses is gathered using the generated sample set. Specifically, the mean and variance are computed by:

$$\bar{y}(t) = \frac{1}{N_n}\sum_{j=1}^{N_n} y_j(t) \tag{2.16}$$

$$Var[y(t)] = \frac{1}{N_n}\sum_{j=1}^{N_n} [\bar{y}(t) - y_j(t)]^2 \tag{2.17}$$

where $y_j(t)$ is the j^{th} sample of the target response. Depending on the target response, individual convergence test is run to determine the total number of samples N_n required in each MC simulation respectively.

2.2.2 Unscented Transform (UT)

The Unscented Transform (UT) is a sampling method to be used for estimating the statistics of the probability distributions, such as the mean, or covariance, of a random variable $\boldsymbol{X}$ which undergoes a nonlinear transformation, i.e.,

$$y = \boldsymbol{g}(\boldsymbol{X}) \tag{2.18}$$

where $\boldsymbol{g}(\cdot)$ denotes the non-linear transformation function. The probability distributions of the input random variables $\boldsymbol{X}$ are assumed to be Gaussian, and they are to be represented using a minimal set of deterministic sample points, named the sigma points $\boldsymbol{X}_I$. Figure 2. 4 illustrates the basic concept of the UT. Due to the property of statistical convergence, higher-order information about the distribution can be captured using only a very small number of samples.

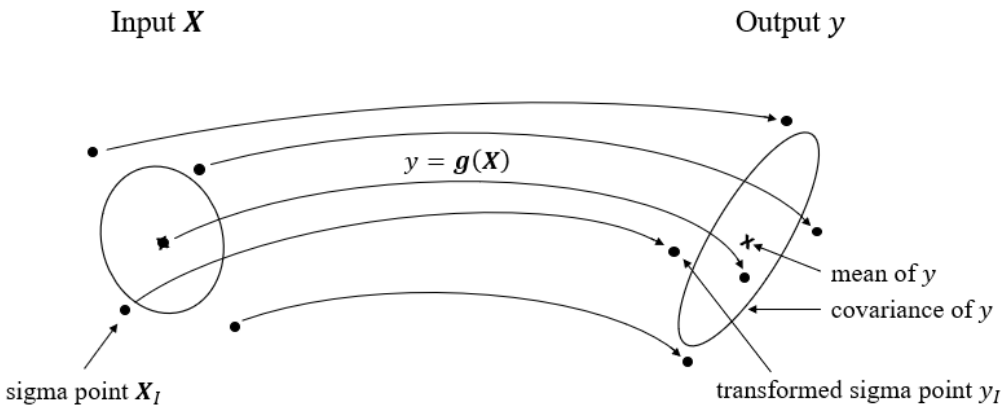


Figure 2. 4 A representation of the Unscented Transform (UT) concept

The UT uses a set of weighted sigma points $\boldsymbol{X}_I$ to propagate the means and covariances of nonlinear transformations of random variables given by Eq. (2.18). For a L-dimensional input random variable $\boldsymbol{X}$ with mean $\overline{\boldsymbol{X}}$ and covariance $\boldsymbol{P}_{XX}$, a minimal set of $2L + 1$ sigma points are required to capture the distributions. The sigma points $\boldsymbol{X}_I$ for $I = 0,1, \dots ,2L$ and their corresponding weight W_I are selected as follows:

$$\boldsymbol{X}_0 = \overline{\boldsymbol{X}} \tag{2.19a}$$

$$\boldsymbol{X}_I = \overline{\boldsymbol{X}} + \left(\sqrt{(L + \lambda_s) \cdot \boldsymbol{P}_{XX}}\right)_I \quad \text{for } I = 1,2, \dots , L \tag{2.19b}$$

$$\boldsymbol{X}_I = \overline{\boldsymbol{X}} - \left(\sqrt{(L + \lambda_s) \cdot \boldsymbol{P}_{XX}}\right)_I \quad \text{for } I = L + 1, \dots ,2L \tag{2.19c}$$

$$W_0^m = \frac{\lambda_s}{L + \lambda_s} \tag{2.19d}$$

$$W_0^c = \frac{\lambda_s}{L + \lambda_s} + (1 - {\alpha_s}^2 + \beta_s) \tag{2.19e}$$

$$W_I^m = W_I^c = \frac{1}{2(L + \lambda_s)} \quad \text{for } I = 1,2, \dots ,2L \tag{2.19f}$$

where $(\sqrt{(L + \lambda_s) \cdot \boldsymbol{P}_{XX}})_I$ refers to the I^{th} row or column of the matrix $\boldsymbol{A} = \sqrt{(L + \lambda_s) \cdot \boldsymbol{P}_{XX}}$, the Cholesky decomposition of the matrix $(L + \lambda_s) \cdot \boldsymbol{P}_{XX}$, i.e., $\boldsymbol{A} \cdot$

$\boldsymbol{A}^T = (L + \lambda_s) \cdot \boldsymbol{P}_{XX}$. W_I^m and W_I^c denote the weights associated with the sigma point $\boldsymbol{X}_I$, to be used for approximating the mean and covariance, respectively. $\lambda_s = {a_s}^2(L + \kappa_s) - L$ is a scaling parameter. The parameter a_s controls the spread of the sigma points around the mean, which is generally chosen in the range of $[10^{-3}, 1]$. A larger a_s spreads the sigma points further from the mean, which helps capture larger nonlinearities but increases the risk of introducing numerical instability. Generally, a_s is set to a small value, i.e., $a_s = 10^{-3}$, by default, but if strong nonlinearities in the transformation is expected, a_s is normally selected greater than 0.1. κ_s is a secondary scaling parameter which has a default choice of $\kappa_s = 0$. It provides an extra degree to "fine-tune" the higher-order moments of $\boldsymbol{X}$ to reduce the overall prediction error. β_s incorporates prior knowledge of the distribution of $\boldsymbol{X}$ and is set to 2 if Gaussian distribution is assumed.

Parameter selection is crucial for obtaining accurate, efficient, and stable approximations in UT. For highly nonlinear systems, parameters like a_s and κ_s must be carefully tuned to ensure appropriate spread of the sigma points. These parameters should be selected, based on the system's behavior, the dimensionality, and the nature of the noise involved.

The target responses are then obtained through the nonlinear transformation by Eq. (2.18), i.e., $y_I = \boldsymbol{g}(\boldsymbol{X}_I)$. The mean $\bar{y}$ and covariance P_{yy} of the target response y are estimated by the set of transformed sigma points y_I associated with their corresponding weights:

$$\bar{y} = \sum_{I=0}^{2L} W_I^m y_I \tag{2.20}$$

$$P_{yy} = \sum_{i=0}^{2L} W_i^c (y_I - \bar{y}\,)((y_I - \bar{y})^T \tag{2.21}$$

The method differs substantially from general sampling methods which normally require orders of magnitude more sample points to achieve an accurate prediction of the first moments of the distribution [83]. The accuracy of the method is adequately high for Gaussian input variables. The statistics of probability distributions of the transformed outputs are captured accurately to the 3rd order (Taylor series expansion) for any nonlinearity. For non-Gaussian inputs, the method is accurate in approximation to the 2nd order. The accuracy of the 3rd and higher order moments are determined by the choices of a_s and β_s.

The input variables, the earthquake model parameters $\boldsymbol{v}$ and the white noise input $w(t)$, to the synthetic earthquake model adopted in this chapter in Eq. (2.1) are Gaussian. The process of generating the seismic responses of structural systems through the use of the synthetic model, as shown in Figure 2. 3, is a non-linear transformation of the Gaussian random variables according to the earthquake model in Eq. (2.5) and the structural state-space equations in Eq. (2.15) and hence falls within the scope of the UT. The statistics of the probability distribution obtained can be further processed to approximate the reliability of the target response of the structural system under earthquakes.

Here, two implementation approaches based on the concept of the UT, namely

the Offline and the Online UT, are developed to estimate the mean and covariance of the structural responses under earthquakes. In the Offline UT, the whole targe response time histories of the structural systems under synthetic earthquakes are generated directly by the nonlinear transformation of the samples selected for the Gaussian model parameters $\boldsymbol{v}$ and the white noise input $w(t)$. Specifically, samples of the Gaussian model parameters $\boldsymbol{v}$ are selected by the UT scheme, and realizations of the white noise input $w(t)$ are sampled using the MC simulations. The later method, the Online UT, selects samples of both the Gaussian model parameters $\boldsymbol{v}$ and the white noise input $w(t)$ by the UT scheme. It propagates the statistics of the probability distributions of the earthquake ground motions and the structural responses recursively in an online manner. The thorough implementation algorithms are elaborated as follows.

2.2.2.1 Offline Unscented Transform

In the Offline UT, the two sources of randomness, the Gaussian model parameters $\boldsymbol{v}$ and the white noise input $w(t)$, are captured differently. Samples of the Gaussian model parameters $\boldsymbol{v}$ are selected by the UT scheme. The inputs variable $\boldsymbol{X}$ is a 6-dimensional input vector $\boldsymbol{v} = [v_1, \dots, v_6]^T$, i.e., $L = 6$, thus $2L + 1 = 13$ sigma points are required to fully capture the probability distributions according to the UT algorithm. The sigma points and their corresponding weights of the Gaussian model parameters $\boldsymbol{v}$ are selected by Eq. (2.19), in which $\overline{\boldsymbol{X}} = \overline{\boldsymbol{v}}$ and $\boldsymbol{P}_{XX} = Cov(\boldsymbol{v})$ are determined by Eq. (2.11) and Eq. (2.12) for a given set of earthquake and site

characteristics $\boldsymbol{\mu}$. The Gaussian model parameters are transformed to the model parameters $\boldsymbol{\theta}$ that define the properties of the modulating function in Eq. (2.2) and the filter in Eq. (2.3) in the ground model. Samples of the white noise input $w(t)$ are randomly drawn by the MC simulations. For each sigma point sample $\boldsymbol{X}_I$ selected for the Gaussian model parameters $\boldsymbol{v}$, N_m earthquake time histories are generated through random realizations of the white noise input $w(t)$. Thus, the Offline UT simulates $13 \cdot N_m$ samples of the earthquake time histories and the corresponding structural responses in total to estimate the probability distributions of the target structural responses under earthquakes.

To account for both sources of randomness, the Gaussian model parameters $\boldsymbol{v}$ and the white noise input $w(t)$, involved in the synthetic ground model, a simple modification to the UT formula that computes the mean and covariance of the target output responses is needed in the Offline UT. Let y_I^J denote the target response of the J^{th} sample at the sigma point $\boldsymbol{X}_I$, the expected value of the output response $y_I(t)$ corresponds to the sigma point $\boldsymbol{X}_I$ is given by:

$$y_I(t) = \frac{1}{N_m} \sum_{J=1}^{N_m} y_I^J(t) \tag{2.22}$$

The computed $y_I(t)$ are substituted in Eq. (2.20) to calculate the mean $\bar{y}(t)$ of the target response.

The expected value of the covariance $P_{yy}^I(t)$ of the output response corresponds to the sigma point $\boldsymbol{X}_I$ is given by:

$$P_{yy}^{I}(t) = \frac{1}{N_m}\sum_{J=1}^{N_m}[y_I^J(t) - \bar{y}(t)][y_I^J(t) - \bar{y}(t)]^T \tag{2.23}$$

And the covariance $P_{yy}(t)$ of the target output response $y(t)$ is then computed by:

$$P_{yy}(t) = \sum_{I=0}^{2L} W_I^c \cdot P_{yy}^I(t) \tag{2.24}$$

The covariances propagated from the randomness of the white noise input $w(t)$ is accounted by Eq. (2.23) and are then substituted to Eq. (2.24) to find the expected value of the covariances over the sigma points.

The means and covariances of the structural responses at any time instant t can be estimated by the structural response time histories through this approach. Both randomness of Gaussian model parameter $\boldsymbol{v}$ and the white noise input $w(t)$ are taken into account and $13 \cdot N_m$ samples are required to observe the convergence of the target measurements $\bar{y}(t)$ and $P_{yy}(t)$ in the Offline UT method.

If the focus of the study is on how model parameters $\boldsymbol{v}$ influence the mean and covariance of the target response, the proposed method will be more efficient than the MC simulation since the randomness $\boldsymbol{v}$ is accounted by a minimal set of samples through the more efficient sampling method of UT. In addition, the proposed method is also applicable to studies where the structural systems involve stochastic model parameters.

2.2.2.2 Online Unscented Transform

In the Online UT approach, the input variable $\boldsymbol{X}$ is redefined as a concatenation of

the process state $\boldsymbol{x}$, the parameters state $\boldsymbol{v}$ and the noise state $\boldsymbol{w}$ that defines the entire dynamic of transformation process i.e., $\boldsymbol{X} = [\boldsymbol{x}^T\ \boldsymbol{v}^T\ \boldsymbol{w}^T\ ]^T$. It should be noted that this structure of the input variable in the Online UT is normally seen in the literature of the application of UT in Kalman Filters. In this context, the process state $\boldsymbol{x} = [\boldsymbol{x_g}^T, \boldsymbol{x_h}^T, \boldsymbol{x_s}^T]^T$ refers to the states in the state-space equations describing the ground model, the high pass filter and the structural system, respectively; the parameters state $\boldsymbol{v}$ refers to the Gaussian model parameter and the noise state $\boldsymbol{w} = [w_i]$ refers to the discretized white noise in the synthetic earthquake model.

The construction of the process state $\boldsymbol{x}$ is further elaborated. As defined above in Section 2.1, the stochastic process in the squared bracket of the earthquake model in Eq. (2.1) is equivalent to the pseudo acceleration of a single-degree-of-freedom linear oscillator according to the impulse response function and it can be represented by the following state-space equations:

$$\dot{\boldsymbol{x}}_g = \boldsymbol{G}(\boldsymbol{x}_g, w) \tag{2.25a}$$

$$f = \boldsymbol{I}(\boldsymbol{x}_g, w) = \frac{q(\alpha, t)}{\sigma_h(t)}\ {\omega_f}^2 x_g \tag{2.25b}$$

where $\boldsymbol{x}_g = [x_g, \dot{x}_g]^T$ is the state vector of the dynamic system defining the ground motion, w is the input white noise, $\boldsymbol{G}(\cdot,\cdot)$ is state equation that describes the dynamic response of the top layer of the soil, and $\boldsymbol{I}(\cdot,\cdot)$ is the output equation that defines the ground motion, f. For ease of demonstration, the high pass filtering process in Eq. (2.14) is also written in terms of state-space equations as:

$$\dot{\boldsymbol{x}}_h = \boldsymbol{Q}(\boldsymbol{x}_h, f) \tag{2.26a}$$

$$f_h = \boldsymbol{R}(\boldsymbol{x}_h, f) = \ddot{x}_h \tag{2.26b}$$

where $\boldsymbol{x}_h = [x_h, \dot{x}_h]^T$ is the state vector of the high pass filter, f is the simulated ground motion, $\boldsymbol{Q}(\cdot,\cdot)$ is state equation of the high pass filter according to Eq. (2.14), and $\boldsymbol{R}(\cdot,\cdot)$ is the output function that defines the post-processed ground motion, f_h. As mentioned above, the process states $\boldsymbol{x}$ consist of the state vectors describing the ground model, the high pass filter, and the structural system, thus is constructed as $\boldsymbol{x} = [\boldsymbol{x}_g{}^T, \boldsymbol{x}_h{}^T, \boldsymbol{x}_s{}^T]^T$. The size of the process state $\boldsymbol{x}$ is the summation of the size of the state vector of the ground model $\boldsymbol{x}_g$, the high pass filter $\boldsymbol{x}_h$ and the structural system $\boldsymbol{x}_s$. The size L of the input variable $\boldsymbol{X}$ is the summation of the size of the process state $\boldsymbol{x}$, the parameters state $\boldsymbol{v}$ and the noise state $\boldsymbol{w}$.

A total of $2L + 1$ sigma points of the input variable $\boldsymbol{X}$ and their corresponding weights are selected by the UT using Eq. (2.19), in which the mean and the covariance of the input variable $\boldsymbol{X}$ are defined as:

$$\overline{\boldsymbol{X}} = \begin{bmatrix} \overline{\boldsymbol{x}} \\ \overline{\boldsymbol{v}} \\ \overline{\boldsymbol{w}} \end{bmatrix} \tag{2.27}$$

$$\boldsymbol{P}_{XX} = E[(\boldsymbol{X} - \overline{\boldsymbol{X}})(\boldsymbol{X} - \overline{\boldsymbol{X}})^T] = \begin{bmatrix} P_{\boldsymbol{x}} & 0 & 0 \\ 0 & P_{\boldsymbol{v}} & 0 \\ 0 & 0 & P_{\boldsymbol{w}} \end{bmatrix} \tag{2.28}$$

where $P_{\boldsymbol{x}}$, $P_{\boldsymbol{v}}$ and $P_{\boldsymbol{w}}$ are the covariance matrix of the process state $\boldsymbol{x}$, the parameters state $\boldsymbol{v}$ and the noise state $\boldsymbol{w}$, respectively.

In the Online UT, the mean and covariance of the target output response $y(t)$ at

any time instants t_k, denote y^k later for symbolic abbreviation, are obtained in an online manner by updating the input state variable $\boldsymbol{X}(t_k)$, denoted as $\boldsymbol{X}^k$ later for symbolic abbreviation, at each time instant t_k. At each time step t_k, the parameters state $\boldsymbol{v}^k$ and the noise state $\boldsymbol{w}^k$ in $\boldsymbol{X}^k$ remain the same as for the previous time step, because these parameters are time independent. The process state $\boldsymbol{x}^k$ updates at each time step and thus the mean and covariance of the input state variable $\boldsymbol{X}^k$ are updated recursively using Eq. (2.20) and Eq. (2.21). This allows for the selection of the sigma points of the input variable $\boldsymbol{X}^k$ at each time instant t_k using the concept of UT.

The recursive algorithm in the online approach starts at $t_0 = 0$. For initialization, the mean and covariance of the input state variable $\boldsymbol{X}^0$ are defined as follows. For the process state $\boldsymbol{x}^0$, the states vector in the ground model $\boldsymbol{x}_g$, the high pass filter $\boldsymbol{x}_h$ and the structural system $\boldsymbol{x}_s$ are initially uncorrelated and are zero at $t_0 = 0$. Thus, the mean $\overline{\boldsymbol{x}}^0$ of the process states set to zero and the covariances $P_{\boldsymbol{x}}$ are assumed to be infinitely small. For the parameter state $\boldsymbol{v}^0$, the mean $\overline{\boldsymbol{v}}^0$ and the covariance matrix $P_{\boldsymbol{v}}$ of the parameter states are determined by Eq. (2.11) and Eq. (2.12) for a given set of earthquake and site characteristics $\boldsymbol{\mu}$. For the noise state $\boldsymbol{w}^0$, the discretized white noise input at t_0 is $\boldsymbol{w}^0 = w_0 = \sigma u_0$, in which u_0 is the standard Gaussian and $\sigma = \sqrt{2\pi S_0 \Delta t_D}$ as defined in the ground model. Thus, the mean and the covariance of noise state are $\overline{\boldsymbol{w}}^0 = 0$ and $P_{\boldsymbol{w}} = \sigma^2$.

At any time step t_k, the mean and covariance of the state variable $\boldsymbol{X}^{k+1}$ and that of the target output response y^{k+1} at t_{k+1} are estimated. Due to the nature of the

nonlinear transformation considered, the input variable to the nonlinear transformation, i.e., $\boldsymbol{X}$ in Eq. (2.18), is the state variable $\boldsymbol{X}^k$ and the transformed output, i.e., y in Eq. (2.18), is $\boldsymbol{X}^{k+1}$ and y^{k+1}, respectively. The time updating algorithm finds mean and covariance of $\boldsymbol{X}^k$ and that of y^k at any time instant t_k through the following steps:

1. Select the sigma points $\boldsymbol{X}_I^k$ and their weights of the input state variables at t_k by Eq. (2.19).
2. Update the state variables at t_{k+1} by taking the selected sigma points $\boldsymbol{X}_I^k$ through a time updating model:

$$\boldsymbol{X}_I^{k+1|k} = \boldsymbol{K}\left[\boldsymbol{X}_I^k\right] \tag{2.29}$$

   where $\boldsymbol{K}[\cdot]$ is the nonlinear function that transforms the input state vector at t_k to t_{k+1}. The components in the process state $\boldsymbol{x} = [\boldsymbol{x}_g{}^T, \boldsymbol{x}_h{}^T, \boldsymbol{x}_s{}^T]^T$ are updated according to the state-space equations in Eq. (2.25), Eq. (2.26) and Eq. (2.15) respectively. There is no evolution in the parameter state $\boldsymbol{v}$ and the noise state $\boldsymbol{w}$ in the updates, i.e., $\boldsymbol{v}_I^{k+1|k} = \boldsymbol{v}_I^k$ and $\boldsymbol{w}_I^{k+1|k} = \boldsymbol{w}_I^k$, since the probability distributions the Gaussian model parameters and the discretized white noise remain the same at any time instants in the earthquake.
3. The mean and covariance of the updated state variable $\boldsymbol{X}^{k+1}$ are computed by:

$$\bar{\boldsymbol{X}}^{k+1} = \sum_{i=0}^{2L} W_I^m \, \boldsymbol{X}_I^{k+1|k} \tag{2.30a}$$

$$\boldsymbol{P}_{XX}^{k+1} = \sum_{i=0}^{2L} W_I^c \left[\boldsymbol{X}_I^{k+1|k} - \bar{\boldsymbol{X}}^{k+1}\right]\left[\boldsymbol{X}_I^{k+1|k} - \bar{\boldsymbol{X}}^{k+1}\right]^T \tag{2.30b}$$

4. Compute the target output responses of the structural system at t_{k+1}, $y_I^{k+1|k}$, for each sigma points. The target output y^{k+1} is simply a combination of the process states that represents the structural system, i.e., $[\boldsymbol{x}_s]^{k+1}$, in the obtained sigma point $\boldsymbol{X}^{k+1}$ according to Eq. (2.15b):

$$y_I^{k+1|k} = \boldsymbol{h}([\boldsymbol{x}_s]_I^{k+1|k}) \tag{2.31}$$

5. The mean and covariance of the target output response y^{k+1} are computed by:

$$\bar{y}^{k+1} = \sum_{i=0}^{2L} W_I^m \, y_I^{k+1|k} \tag{2.32}$$

$$P_{yy}^{k+1} = \sum_{i=0}^{2L} W_I^c \left[y_I^{k+1|k} - \bar{y}^k\right]\left[y_I^{k+1|k} - \bar{y}^k\right]^T \tag{2.33}$$

6. Set $k = k + 1$, update the time step t_k and the corresponding symbols, i.e., t_{k+1} and $\boldsymbol{X}^{k+1}$ in the current time step are denoted as t_k and $\boldsymbol{X}^k$. Then return to step 1 to compute the mean and covariance of the target output response y^{k+1} for the updated time instant t_k.

The Online UT method is applicable in systems that the states at t_{k+1} evolve from the states at the previous time step t_k. The mean and covariances of the target seismic responses y^k of a structural system at any time instants t_k are estimated by Eq. (2.32) and Eq. (2.33). It is expected that the Online UT method would further reduce the computational cost compared to the Offline UT, as it involves generating a substantially smaller set of deterministic samples to estimate the statistics of the probability distributions. This robustness comes with approximating the dynamic states at every time step as Gaussian.

2.3 Example and discussions: *A nonlinear hysteretic oscillator subjected to stochastic earthquake excitations.*

Both the Offline UT and Online UT are applied in this first example to estimate the statistical properties of the probability distribution, i.e., the mean and covariance, of target responses of a nonlinear hysteretic oscillator under stochastic earthquake excitations. The MC simulation is also applied and the result of which is used as a reference to show the performances of the methods proposed in this work.

The synthetic earthquake model of Eq. (2.5) introduced in Section 2.1 is adopted to simulate the ground excitations, in which a reverse fault ($F = 1$) is assumed and the seismological properties $M = 6$, $R_{rup} = 60$ km and $V_{s30} = 600$ m/s are chosen. The discretization time step $\Delta t_D = 0.01$s and the standard deviation $\sigma = 1$ are selected for the input white noise $w(t)$. The post-processed ground excitations $f_h(t)$ obtained by Eq. (2.14) is subject to a hysteretic oscillator defined by the following differential equation:

$$m\ddot{x}_s(t) + c\dot{x}_s(t) + k[\alpha x_s(t) + (1-\alpha)z(t)] = f_h(t) \tag{2.34a}$$

$$\dot{z}(t) = \boldsymbol{H}(x_s, \dot{x}_s, z) \tag{2.34b}$$

where $m = 3.0 \times 10^5$ kg, $c = 1.5 \times 10^2$ kNs/m and $k = 2.1 \times 10^4$ kN/m are selected. α that controls the degree of hysteresis is set to $\alpha = 0.1$. $z(t)$ is a hysteretic term governed by the nonlinear differential equation of Eq. (2.34b), in which the nonlinear function $\boldsymbol{H}(\cdot,\cdot,\cdot)$ defines the hysteresis law of the oscillator. Various

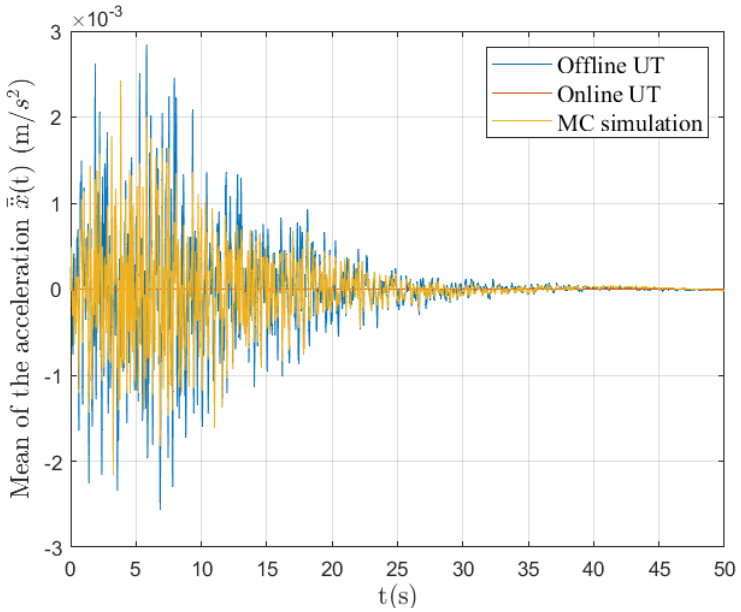
forms of this law are available for describing different types of inelastic behaviour. In the example, the Bouc-Wen hysteresis law is used:

$$\dot{z}(\mathrm{t}) = -\gamma|\dot{x}(t)||z(t)|^{n-1}z(t) - \eta|z(t)|^{n}\dot{x}_s(t) + Ax_s(t) \qquad (2.35)$$

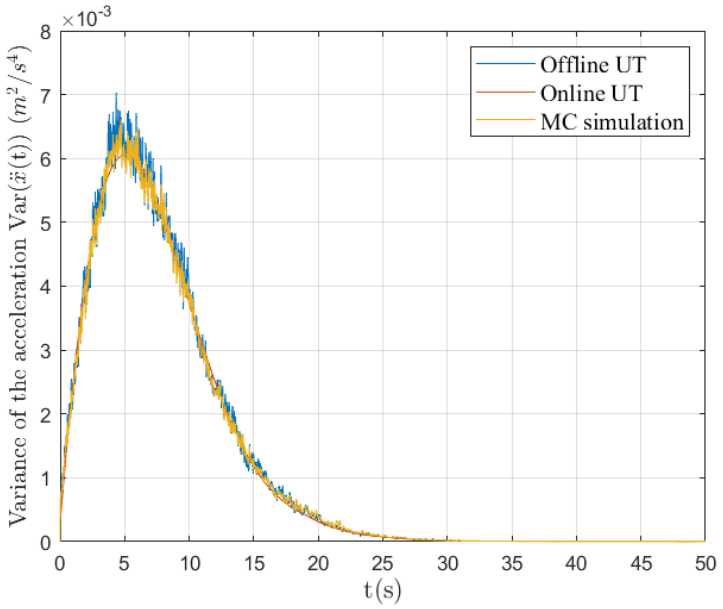
where the parameters are selected as $n = 3$, $A = 1$ and $\gamma = \eta = 1/(2{\sigma_0}^n)$, in which ${\sigma_0}^2 = \pi S m^2/(ck)$ is the mean-square of the linear oscillator ($\alpha = 1$).

In this example, the acceleration of the structural system, i.e., $y = \ddot{x}_s(t)$, is of interest. Figure 2. 5 plots the means and covariances of the accelerations $\ddot{x}_s(t)$ estimated by the MC simulations, the Offline UT and the Online UT methods in the vertical axis verses the corresponding time instants t concerned in the horizontal axis. The MC simulation is conducted with a converged sample size of $N_n = 10{,}000$. For the convergence test of the MC method, a time step $t = 10s$ during the strong motion period is selected which is found to have the slowest convergence rate. Subsequent convergence tests focus on this time step. Since the mean acceleration over time is approximately zero, instead of the Coefficient of Variance, root mean square (RMS) is used with a convergence tolerance of the error in RMS being less than 0.001. In the Offline UT, $N_m = 300$ realizations of the white noise are generated for each sigma point selected for the Gaussian model parameter $\boldsymbol{v}$ and 13 sigma points of $\boldsymbol{v}$ are selected according to the UT. Thus, a total of 3900 samples are simulated in the offline method to ensure that the estimated results closely match those of the MC simulation. In the Online UT, as the state $\boldsymbol{x}_s$ describing the structural system in the process state $\boldsymbol{x}$ is a 3-dimensional vector, the input state variable $\boldsymbol{X}^k$ in this example

is a 14-dimensional vector, i.e., $L = 14$, which requires only $2 \times \mathrm{L} + 1 = 29$ samples to be simulated according to the UT in the online method. For both the offline and online UT methods, the number of sigma points depends on the number of stochastic parameters associated with the earthquake model and the structure model.



(a) Estimated mean



(b) Estimated covariance

Figure 2. 5 Comparison of the mean and covariances of $\ddot{x}_s(t)$ estimated by the Offline and Online UT and MC simulations.

Thus, if there is structural model uncertainty, the number of samples required for both methods may increase.

For the offline and online UT method, as discussed in previous section, the accuracy of the results is highly dependent on the choice of a_s, κ_s and β_s parameters. These parameters are tuned to ensure that the estimated results closely match those of the MC simulation. In the results shown in Figure 2. 5, the parameters are set as $a_s = 0.55$, $\kappa_s = 0$ and $\beta_s = 2$.

As shown in Figure 2. 5, the estimated mean and covariance of the acceleration response $\ddot{x}_s(t)$ using the Offline UT and the Online UT methods closely match the MC results. Regarding the efficiency of different methods, the Offline UT method uses about half of the sample size as that of the MC simulation. The Online UT method extensively saves the computational cost, with an estimate of mean of the order of 10^{-6}.

In the above example, the result of the Online UT method is highly sensitive to the choice of a_s, κ_s and β_s. Improper selections of these parameters lead to inappropriate selection of the sigma points, which may not adequately represent the true distribution of the state. This could lead to an inaccurate approximation of the mean and covariance and instability in the numerical computations, and thus a failure of the method, especially for highly nonlinear systems. For such systems, a more rigorous selection of these parameters is required, or alternatively, a larger number of the sigma points may be used to capture the higher order information of the input

variables $\boldsymbol{X}$.

In addition, in the Online UT method, the covariance matrix of $\boldsymbol{X}^k$, $\boldsymbol{P}_{XX}^k$, is computed and updated at each time step t_k. By investigating the covariance matrix $\boldsymbol{P}_{XX}^k$ at each time step, the results indicate that the mean and covariance of $\boldsymbol{v}^k$ and $\boldsymbol{w}^k$ remain unchanged throughout the earthquake. And the covariances between $\boldsymbol{v}^k$, $\boldsymbol{w}^k$ and $\boldsymbol{x}^k$ are on the order of 10^{-40} suggesting that the numerical errors are negligible, where align with the theoretical relations.

2.4 Conclusions

Probabilistic response estimates of nonlinear structural systems subjected to stochastic earthquake excitations are usually computationally expensive. This chapter develops two approaches, the Offline UT and the Online UT methods, based on the concept of the UT sampling method to estimate the statistics of the probability distributions of the structural responses more efficiently. An example is introduced to demonstrate the accuracy and efficiency of the proposed methods. This work finds that the Offline UT method has a balance between the computational complexity and the accuracy. It saves about half the computation costs and the estimated results are reasonably accurate. The Online UT method is substantially more efficient. Only a small number of nonlinear dynamic analysis are needed to make estimations that closely match the MC results. Yet it should be noted that both UT methods are strongly dependent on the choice of a_s, κ_s and β_s parameters. For systems that exhibit high non-linearity, other modified UT schemes that construct a larger size sigma point may enhance the

accuracy of the estimations in the UT methods. The statistics obtained by the proposed methods can be further processed to estimate the probability distributions of the structural responses by assuming an expected distribution type, which can be used for seismic reliability evaluations. This first chapter illustrates that while the default MC method is accurate, its cost even in small systems is significant. The two sampling methods investigated in this chapter demonstrate the potential of such methods, where inevitably there is a compromise between the number of samples and the accuracy of the results. The focus in the following chapters will be turned to alternative methods.

Chapter 3

An Efficient Structural Seismic Reliability Estimation through a Recursive Calculation of Symbolic Gradients

One way to evaluate the seismic reliability is by using the Design Point Excitation (DPE) method. The line search algorithm [66] is demonstrated to successfully solve the optimization problem in the DPE method. An important part of the line search algorithm is to repeatedly approximate the gradient of the Limit State Function (LSF). And thus, it is vital to formulate an approach to estimate the gradient of interest which is both accurate and efficient. In this chapter, an analytical estimate of the derivative, named the Euler-Analytical estimate of the Derivatives (EAD) method is developed. The gradient calculations are performed by propagating the derivative term recursively,

adopting the idea of the Forward Sensitivity method which is applied together with an Euler approximation for the conversion of the continuous in time system to a discrete.

The chapter starts with a brief introduction to the DPE method. A line search algorithm and an algorithm that finds a warm initial guess used in the line search are presented. The EAD method is then elaborated, and the performance of the EAD method is presented by comparing it with two other gradient approximation methods, the Automatic Differentiation (AD) method and the finite-difference Numerical estimate of the Derivatives (ND) method. The reliabilities estimated by incorporating each derivative approximation method into the DPE method, i.e. DPE-EAD, DPE-AD and DPE-ND methods and the Monte Carlo (MC) simulations are compared, with examples of Multi Degree-of-Freedom systems featuring Bouc-Wen nonlinearities and polynomial nonlinearities. In addition, the DPE method only finds the reliability at a specific time instant. The DPE results are further applied to estimate the reliability of systems over a time period, by considering multiple failure criteria.

3.1 Design Point Excitation (DPE) method

This section provides a brief overview of the Design Point Excitation (DPE) method [17]. The DPE method estimates the probability of a system response y, not exceeding a given threshold, also known as the reliability P_R, when subjected to a random process $f(t)$. In seismic reliability estimations, the earthquake excitation is the random process of interest. A random process describing the earthquake ground motion can be represented by $f(t) = \int_0^t s(t_\tau)u(t_\tau)dt_\tau$, where $u(t)$ is a standard

Gaussian white noise process. After discretising $u(t)$ in the previous integral to independent components u_i, where $i = 1,..,N$ and $N = t/\Delta t$ when the discretization sampling time step Δt is selected, the earthquake model $f(t)$ is written as:

$$f(t) = \sum_{i=1}^{N} s_i(t)\, u_i \tag{3.1}$$

where $s_i(t)$ is an impulse response function associating u_i to $f(t)$, where it should be noted that the subscript i indicates the dependence of this function at the time instance t_i at which u_i is applied.

The response output, y, of a nonlinear structural system described by a state vector $\boldsymbol{x}$, subjected to a stochastic excitation $f(t)$ is of interest. Although a sensor is not used in this problem as the focus is put on an output y, as is typically the case in the Control literature, the system is described by its state-space and measurement equations, which are written as:

$$\dot{\boldsymbol{x}}(t) = \boldsymbol{l}\big(\boldsymbol{x}(t), f(t)\big) \tag{3.2a}$$

$$y(t) = \boldsymbol{h}\big(\boldsymbol{x}(t), f(t)\big) \tag{3.2b}$$

$\dot{\boldsymbol{x}}$ indicates the derivative with respect to time t, $\boldsymbol{l}(\cdot,\cdot)$ is state-space function that describes the dynamics of the structural system, and $\boldsymbol{h}(\cdot,\cdot)$ is the measurement function that defines the output response of interest. The measurement output, y, is a scalar here since the DPE method determines the reliability for a single output response. In the research work in this Chapter, the measurement output, y, is further assumed to be written as a linear function of the state vector $\boldsymbol{x}$ and the input excitation f. This

condition is retained for simplicity as several outputs of interest considered for seismic reliability satisfy it.

Considering the problem of whether a structural response $y(\tau)$ exceeds a threshold y_T at time τ, the Limit State Function (LSF), $G(\boldsymbol{u}, y_T, \tau)$, that separates the safety and the failure regions is constructed as:

$$G(\boldsymbol{u}, y_T, \tau) = y_T - y(\boldsymbol{u}, \tau) = 0 \tag{3.3}$$

where $\boldsymbol{u}$ is a vector of the standard Gaussian variables input to the system that generates the structural response $y(\tau)$. For the excitation model considered here, the input vector $\boldsymbol{u}$ is defined as the discretized standard white noise input to the earthquake model, i.e., $\boldsymbol{u} = [u_1, \dots, u_n]$ where $n = \tau/\Delta t$. $G(\boldsymbol{u}, y_T, \tau) > 0$ indicates the safety region.

According to the concept in the First Order Reliability Method (FORM), the reliability $P_R(\tau)$, i.e., the probability of the structural response y at the time τ not exceeding the threshold y_T, is evaluated using a linearization of the LSF G at a specially chosen point, named the design point $\boldsymbol{u}^*$, of the space spanned by the possible realizations of $\boldsymbol{u}$. This is the point on the limit state surface with the highest probability density in the $\boldsymbol{u}$ space. Since u_i are independent standard Gaussian variables, the design point is also found to be the point that minimizes the distance of the LSF to the origin [15-17]. Thus, the following optimization problem is formulated:

$$\boldsymbol{u}^*(y_T, \tau) = \arg\min \{\|\boldsymbol{u}\|^2 | G(\boldsymbol{u}, y_T, \tau) = 0\} \tag{3.4}$$

The reliability $P_R(\tau)$ of $y(\tau)$ is then approximated by:

$$P_R(\tau) = P(y(\tau) \leq y_T) = \boldsymbol{\phi}(\beta) \tag{3.5}$$

where $\boldsymbol{\phi}(\cdot)$ denotes the standard normal cumulative density function (CDF). β, known as the reliability index, is the distance of the origin to the hyperplane of the Limit State surface and is computed by:

$$\beta = \|\boldsymbol{u}^*\| = \boldsymbol{\alpha} \cdot \boldsymbol{u}^* \tag{3.6}$$

$$\boldsymbol{\alpha} = -\frac{\nabla_{\boldsymbol{u}} G}{\|\nabla_{\boldsymbol{u}} G\|} \tag{3.7}$$

in which $\boldsymbol{u}^*$ is the design point, the direction vector $\boldsymbol{\alpha}$ is a unit vector normal to the linearized hyperplane, and $\nabla_{\boldsymbol{u}} G$ is the derivative of the LSF with respect to $\boldsymbol{u}$ at the design point $\boldsymbol{u}^*$.

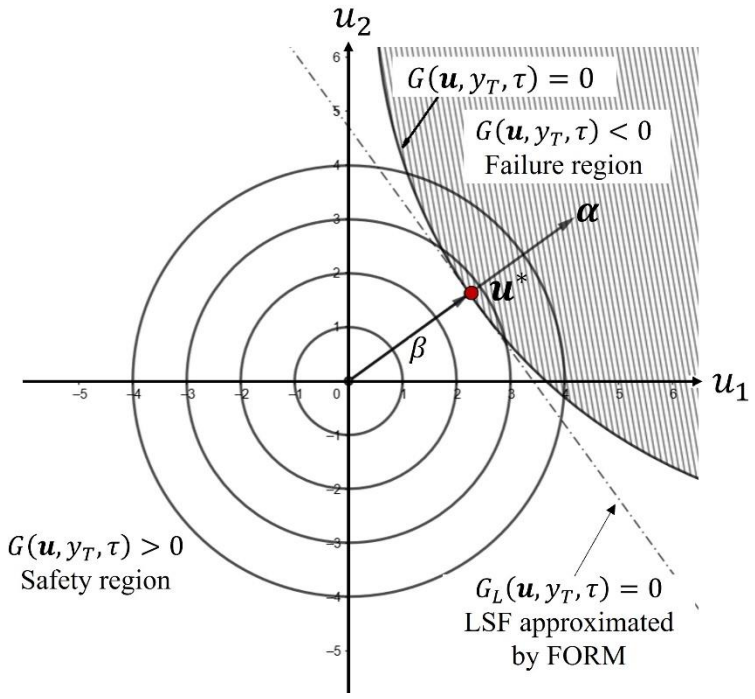


Figure 3. 1 A visualization of the design point in a bivariate system.

For a better understanding of how the method works, an example of a bivariate system with a non-linear Limit State Function (LSF) is illustrated by Figure 3. 1. The joint probability density of the input random variables $\boldsymbol{u} = [u_1, u_2]$ in the standard

normal space is represented by contours, i.e., all points on the same contour have the same probability density. It should be noted that the threshold y_T can be negative.

In seismic reliability analysis, the reliability of a response usually refers to the probability of the absolute value of the response, i.e., $|y|$, that does not exceed a threshold y_T. The reliability of the absolute response $|y|$ is defined as $P(|y| \leq y_T) = 1 - P(y \leq -y_T) \cup P(y \geq y_T)$. Since there is no intersection between the conditions of $y \leq -y_T$ and $y \geq y_T$, the reliability of the absolute response $|y|$ can be computed by:

$$\begin{aligned} P(|y| \leq y_T) &= 1 - [P(y \leq -y_T) + P(y \geq y_T)] \\ &= -P(y \leq -y_T) + P(y \leq y_T) \end{aligned} \tag{3.8}$$

The reliability the absolute response $P(|y| \leq y_T)$ can be calculated by Eq. (3.8) using the reliabilities $P(y \leq -y_T)$ and $P(y \leq y_T)$ obtained by the DPE method.

3.1.1 Initial guess of the design point

In the DPE method, finding the design point, $\boldsymbol{u}^*$, is a critical step. As defined above, the design point is found as the solution to the optimization problem in Eq. (3.4). A good initial estimate is often important in solving optimization problems efficiently.

Regarding the initial guess $\widehat{\boldsymbol{u}}^*$ of the design point, existing research [17] has shown that for Single Degree-of-Freedom (SDOF) systems, the Mirror Image Excitation [17] can help in locating a warm starting guess. Mirror image excitation refers to an excitation that produces a structural response mirroring or flipping the shape of the system's free vibration when subjected to initial conditions at the threshold of interest. However, for multi-degree-of-freedom (MDOF) systems, this

relationship does not hold due to the increased complexity of dynamic interactions [84]. For MDOF systems, a warm guess of the design point can be obtained by making use of the design points of the neighbouring optimization problems [84]. One may consider a sequence of ascending thresholds y_T^I where $I = 1,2,\dots,l$ and $y_T^1 < y_T^2 < \cdots < y_T^l$, and $\boldsymbol{u}^*(y_T^I,\tau) = \arg\min\{\|\boldsymbol{u}\|^2 | G(\boldsymbol{u}, y_T^I, \tau) = 0\}$ denotes the corresponding design point. If the increments between the successive thresholds y_T^{I-1}, y_T^I and y_T^{I+1} are small, the design point $\boldsymbol{u}^*(y_T^{I+1},\tau)$ can be approximated by the trajectory of the design points corresponding to the previous two consecutive thresholds $\boldsymbol{u}^*(y_T^I,\tau)$ and $\boldsymbol{u}^*(y_T^{I-1},\tau)$. The initial guess $\widehat{\boldsymbol{u}}^*(y_T^{I+1},\tau)$ of design point is obtained by solving the following equations:

$$\widehat{\boldsymbol{u}}^*(y_T^{I+1},\tau) = \boldsymbol{u}^*(y_T^I,\tau) + \lambda \frac{\boldsymbol{u}^*(y_T^I,\tau) - \boldsymbol{u}^*(y_T^{I-1},\tau)}{\|\boldsymbol{u}^*(y_T^I,\tau) - \boldsymbol{u}^*(y_T^{I-1},\tau)\|} \tag{3.9a}$$

$$y(\widehat{\boldsymbol{u}}^*(y_T^{I+1},\tau),\tau) = y_T^{I+1} \tag{3.9b}$$

where λ is a scalar defining the distance from $\widehat{\boldsymbol{u}}^*(y_T^{I+1},\tau)$ to $\boldsymbol{u}^*(y_T^I,\tau)$ along the vector connecting $\boldsymbol{u}^*(y_T^{I-1},\tau)$ and $\boldsymbol{u}^*(y_T^I,\tau)$ in the $\boldsymbol{u}$ space and is solved by the system equations of Eq. (3.9). The initial guess $\widehat{\boldsymbol{u}}^*(y_T^{I+1},\tau)$ is then obtained by substituting the solution of λ into Eq. (3.9a). Eq. (3.9a) locates the approximated design point $\widehat{\boldsymbol{u}}^*$ on the trajectory of the previous two design points, and Eq. (3.9b) confirms that $\widehat{\boldsymbol{u}}^*(y_T^{I+1},\tau)$ is on the LSF $G(\boldsymbol{u}, y_T^{I+1},\tau) = 0$. A maximum allowable distance indicator λ_{max} is introduced to ensure the increments of the successive thresholds selected are sufficiently small. Intermediate thresholds are required when λ solved from Eq. (3.9) exceeds λ_{max}.

For initialization, the first two design points in the sequence need to be chosen. For the systems studied in this work, the equations are formulated so that the response y of the autonomous system at equilibrium is zero. The first threshold y_T^1 is set to the response of the autonomous system at equilibrium. This is often zero as in the examples that follow in which case $y_T^1 = 0$ is selected. Since variables in $\boldsymbol{u}$ are standard Gaussian, the design point $\boldsymbol{u}^*(y_T^1, \tau)$ for y_T^1 corresponding to the equilibrium of the autonomous system is located at the origin, i.e., $\boldsymbol{u}^*(0, \tau) = 0$. The second threshold y_T^2 is selected as a small value where the response of the nonlinear system is nearly linear. In this case, the design point $\boldsymbol{u}_L^*(y_T^2, \tau)$ for the corresponding linear system, which can be solved deterministically through the analytical equations [84], is a good approximation of $\boldsymbol{u}^*(y_T^2, \tau)$ and can be used as a warm initial guess in the optimization. Considering the corresponding linear system of the structural system written in Eq. (3.2) which is represented by

$$\dot{\boldsymbol{x}}_L(t) = \boldsymbol{A}_L \cdot \boldsymbol{x}_L(t) + \boldsymbol{B}_L \cdot f(t) \tag{3.10a}$$

$$y(t) = \boldsymbol{C}_L \cdot \boldsymbol{x}_L(t) + \boldsymbol{D}_L \cdot f(t) \tag{3.10b}$$

where $\boldsymbol{x}_L$ is the state vector of the linearized system comprising of a subset of the elements of $\boldsymbol{x}$, e.g., plasticity related states are removed. The response $y(t)$ of a linear dynamic system subjected to the excitation $f(t)$ can also be written as

$$y(t) = \int_0^t h_L(t - t_\tau)\, f(t_\tau) dt_\tau \tag{3.11}$$

where $h_L(t)$ is the impulse response function of the linear dynamic system for the particular measurement response of interest. By substituting the excitation $f(t)$

represented in the form of Eq. (3.1), one has:

$$y(t) = \int_0^t h_L(t - t_\tau) \sum_{i=1}^{N} s_i(t_\tau)\, u_i dt_\tau = \mathbf{a}(t)\boldsymbol{u} \tag{3.12}$$

where $\mathbf{a}(t) = [\mathrm{a}_1(t) \dots \mathrm{a}_n(t)]$ and $\mathrm{a}_i(t) = \int_0^t h_L(t - t_\tau)\, s_i(t_\tau) dt_\tau$ for $i = 1,2, \dots, n$. Since the response of interest is written by $y(\tau) = \mathbf{a}(\tau)\boldsymbol{u}$ for a linear system according to Eq. (3.12), the corresponding LSF is given by $G_L(\boldsymbol{u}, y_T, \tau) = y_T - \mathbf{a}(\tau)\boldsymbol{u} = 0$, which defines a hyperplane in the $\boldsymbol{u}$ space with the gradient $\mathbf{a}(\tau)$. The design point $\boldsymbol{u}_L^*(y_T, \tau)$ for a linear system that corresponds to the hyperplane is given by

$$\boldsymbol{u}_L^*(y_T, \tau) = \frac{y_T}{\|\mathbf{a}(\tau)\|} \frac{\mathbf{a}(\tau)^T}{\|\mathbf{a}(\tau)\|} \tag{3.13}$$

where $\mathbf{a}(\tau)^T / \|\mathbf{a}(\tau)\|$ is the unit normal vector to the hyperplane.

With the first two points $\boldsymbol{u}^*(y_T^1, \tau)$ and $\boldsymbol{u}^*(y_T^2, \tau)$ determined, the method can proceed as described above. The algorithm of finding an initial guess $\hat{\boldsymbol{u}}^*(y_T, \tau)$ of the design point can be summarised as follows:

Algorithm 1

Initialization:

1. Set the maximum allowable distance indicator λ_{max}.
2. Select a sequence of ascending thresholds y_T^I where $I = 1,2, \dots, l$ and $y_T^I = y_T$.
3. The first two thresholds, y_T^1 as the response of the autonomous system at equilibrium and y_T^2 as a small value where the response of the nonlinear system is nearly linear, are selected to find the first two design points in the sequence for

initialization.

4. Compute the design point $\boldsymbol{u}_L^*(y_T^2, \tau)$ for the corresponding linear system by Eq. (3.13).
5. Find the 2nd design point $\boldsymbol{u}^*(y_T^2, \tau)$ by the optimization in Eq. (3.4), in which $\boldsymbol{u}_L^*(y_2, \tau)$ obtained in step 4 is used as an initial guess of $\boldsymbol{u}^*(y_2, \tau)$ in the line search optimization (*Algorithm 2*) elaborated later in Section 3.1.2.

From the Initialization steps, the design point $\boldsymbol{u}^*(y_T^1, \tau)$ and $\boldsymbol{u}^*(y_T^2, \tau)$ for the first two thresholds are obtained. The algorithm starts at the step $I = 2$ where the targeted initial guess of the design point $\widehat{\boldsymbol{u}}^*(y_T^{I+1}, \tau)$ for the original non-linear system can be obtained from $\boldsymbol{u}^*(y_T^{I-1}, \tau)$ and $\boldsymbol{u}^*(y_T^I, \tau)$ using the algorithm described below. For example, the first targeted initial guess of the design point $\widehat{\boldsymbol{u}}^*(y_T^3, \tau)$ is calculated from $\boldsymbol{u}^*(y_T^1, \tau)$ and $\boldsymbol{u}^*(y_T^2, \tau)$ that are obtained from Initialization steps. For threshold y_T^{I+1}, where $I = 2, \dots, l-1$:

1. Solve for λ by Eq. (3.9a-b).
2. If $\lambda \geq \lambda_{max}$, an intermediate threshold between y_T^I and y_T^{I+1} should be added to the sequence of ascending thresholds y_T^l and return to step 1. Otherwise, by substituting the λ obtained in Eq. (3.9a), the initial guess $\widehat{\boldsymbol{u}}^*(y_T^{I+1}, \tau)$ is found.
3. If $y_T^{I+1} = y_T$, the algorithm ends. Output $\widehat{\boldsymbol{u}}^*(y_T^{I+1}, \tau)$ as the initial guess of $\widehat{\boldsymbol{u}}^*(y_T, \tau)$. If $y_T^{I+1} < y_T$, continue to step 4.
4. Find $\boldsymbol{u}^*(y_T^{I+1}, \tau)$ by the optimization in Eq. (3.4) through the line search optimization (*Algorithm 2*), in which $\widehat{\boldsymbol{u}}^*(y_T^{I+1}, \tau)$ found in step 2 is used as the

initial guess.

5. Update $I = I + 1$ and start from step 1.

It should be noted that design points for negative thresholds y_T can be determined in the same manner by starting from the origin.

3.1.2 Line search optimization

Optimization methods such as the line search method [66, 67] or the Improved HL-RF algorithm [68] can be applied to find the design point as defined in Eq. (3.4). In this work, the line search method is adopted due to its ease of use and wide applicability with the DPE method [17].

The DPE method with line search iterations for non-linear systems is described in the following algorithm:

Algorithm 2

1. Select an initial guess $\widehat{\boldsymbol{u}}^*$ of the design point using *Algorithm 1*.
2. Calculate the gradient $\nabla_{\boldsymbol{u}} G$ and the corresponding direction vector using $\widehat{\boldsymbol{\alpha}} = -\nabla_{\boldsymbol{u}} G / \|\nabla_{\boldsymbol{u}} G\|$.
3. Find $\hat{\beta}$ by solving $G\left(-\hat{\beta}\widehat{\boldsymbol{\alpha}}, \tau, y_T\right) = y_T - y\left(-\hat{\beta}\widehat{\boldsymbol{\alpha}}, \tau\right) = 0$ using a root-finding algorithm.
4. Update the design point $\boldsymbol{u} = -\hat{\beta} \cdot \widehat{\boldsymbol{\alpha}}$.
5. Define the errors $e_1 = G(\boldsymbol{u}, \tau, y_T)/G(0, \tau, y_T)$ and $e_2 = 1 - \widehat{\boldsymbol{\alpha}} \cdot \boldsymbol{u}/\|\boldsymbol{u}\|$.
6. If $e_1 < 0.001$ and $e_2 < 0.001$, the algorithm ends, and the design point $\boldsymbol{u}^* = \boldsymbol{u}$ is obtained. Return the reliability index $\beta = \hat{\beta}$ and the reliability

$\boldsymbol{\phi}(\beta)$. Otherwise, continue to step 7.

7. Go back to step 2.

For implementation, the *fsolve* command in MATLAB which utilises the trust-region dogleg algorithm [97], is used as the root-finding algorithm in Step 3. It should also be noted that calculating gradient $\nabla_{\boldsymbol{u}} G$ is a critical step in the above steps.

3.2 Euler-Analytical estimate of the Derivative (EAD)

As shown in the previous section for the line search method, and more generally for gradient based optimization methods, the derivative calculations of the LSF $G(\boldsymbol{u}, y_T, \tau)$ with respect to the input vector $\boldsymbol{u}$ are needed repeatedly in each iteration step. A standard way of doing so is through calculating those gradients numerically, i.e., through the use of the finite-differences method. However, numerical differentiation can be both computationally inefficient and may not be sufficiently precise when computing the derivative $\nabla_{\boldsymbol{u}} G$ with respect to the input vector $\boldsymbol{u}$, especially when $\boldsymbol{u}$ is a large vector. In this section, a recursive method is introduced to calculate the derivatives symbolically using and Euler integration as an approximation of the discrete state-space equations of the state-space system from t_k to t_{k+1}.

According to Eq. (3.3), the derivative $\nabla_{\boldsymbol{u}} G = \left[\frac{dG}{du_1}, \frac{dG}{du_2}, \dots, \frac{dG}{du_n}\right]$ of interest in the optimization problem described by Eq. (3.4) is:

$$\nabla_{\boldsymbol{u}} G = -\nabla_{\boldsymbol{u}} y(\boldsymbol{u}, \tau) \tag{3.14}$$

The calculation of each element $\frac{dG}{du_i}$ in $\nabla_{\boldsymbol{u}} G$ through the numerical estimation using

the central-differences scheme is obtained by the following equation:

$$\frac{dG}{du_i} = -\frac{dy(\boldsymbol{u},\tau)}{du_i} = -\frac{y(\boldsymbol{u}+\Delta u_i,\tau) - y(\boldsymbol{u}-\Delta u_i,\tau)}{2\cdot\Delta u_i} \tag{3.15}$$

where Δu_i is the small increment selected for u_i for the derivative estimation. One needs to perturb each element in $\boldsymbol{u}$ and carry out structural analysis repeatedly to obtain $\nabla_{\boldsymbol{u}} G$, thus the computational cost of the finite-differences method is significant. The computational cost increases for complex higher-order nonlinear systems due to the cost in the structural analysis. Though appropriate Δu_i are required to be investigated for implementation, the obtained numerical estimates may not be sufficiently accurate.

To alleviate the previous problems in the numerical estimations, an analytical method is suggested in this work. If the state-space system is affine in the inputs and the measurement equation is a linear function of the state vector $\boldsymbol{x}(t)$ and the input excitation $f(t)$, the structural system defined by Eq. (3.2) can be rewritten as:

$$\dot{\boldsymbol{x}}(t) = \boldsymbol{l}_a\big(\boldsymbol{x}(t)\big) + \boldsymbol{l}_b\big(\boldsymbol{x}(t)\big)\cdot f(t) \tag{3.16a}$$

$$y(t) = \boldsymbol{C}_s\cdot\boldsymbol{x}(t) + \boldsymbol{D}_s\cdot f(t) \tag{3.16b}$$

For the purposes of approximating the gradients in Eq. (3.14) analytically, the Euler integration formula is adopted [85,62]:

$$\boldsymbol{x}_{k+1} \approx \boldsymbol{x}_k + \dot{\boldsymbol{x}}_k\cdot\Delta t \tag{3.17a}$$

$$y_{k+1} \approx \boldsymbol{C}_s\cdot\boldsymbol{x}_{k+1} + \boldsymbol{D}_s\cdot f(t_{k+1}) \tag{3.17b}$$

where $\boldsymbol{x}_k$, $\dot{\boldsymbol{x}}_k$ and y_k denote $\boldsymbol{x}(t_k)$, $\dot{\boldsymbol{x}}(t_k)$ and $y(t_k)$ respectively. $f(t_k)$ is the discretized excitation at t_k. The structural states $\boldsymbol{x}$ are integrated at the equally

spaced time steps $t_k = k \cdot \Delta t$ from t_k to t_{k+1} using the above equations as an approximation, in which the discretization time step Δt is selected as the integration time step such that $k = 0,1, \dots, n$. The derivative $\nabla_{\boldsymbol{u}} G$, as defined in Eq. (3.14), can be obtained by evaluating the following equations, i.e., differentiating Eq. (3.17) with respect to u_i, recursively until $t_{k+1} = \tau$:

$$\begin{aligned} &\frac{d\boldsymbol{x}_{k+1}}{du_i} = \frac{d\boldsymbol{x}_k}{du_i} + \frac{d\dot{\boldsymbol{x}}_k}{du_i} \cdot \Delta t && \text{for i} \le \text{k} \\ &\frac{d\boldsymbol{x}_{k+1}}{du_i} = 0 && \text{otherwise} \end{aligned} \quad (3.18a)$$

$$\begin{aligned} &\frac{dy_{k+1}}{du_i} = \boldsymbol{C}_s \cdot \frac{d\boldsymbol{x}_{k+1}}{du_i} + \boldsymbol{D}_s \cdot \frac{df(t_{k+1})}{du_i} && \text{for i} \le \text{k} \\ &\frac{dy_{k+1}}{du_i} = 0 && \text{otherwise} \end{aligned} \quad (3.18b)$$

Eq. (3.16a) is substituted into Eq. (3.18a) to obtain:

$$\frac{d\boldsymbol{x}_{k+1}}{du_i} = \frac{d\boldsymbol{x}_k}{du_i} + \frac{d\left(\boldsymbol{l_a}(\boldsymbol{x}_k) + \boldsymbol{l_b}(\boldsymbol{x}_k) \cdot f(t_k)\right)}{du_i} \cdot \Delta t$$

$$= \frac{d\boldsymbol{x}_k}{du_i} + \left[\nabla_{\boldsymbol{x}_k} \boldsymbol{l}_a(\boldsymbol{x}_k) \cdot \frac{d\boldsymbol{x}_k}{du_i} + \left[\nabla_{\boldsymbol{x}_k} \boldsymbol{l}_b(\boldsymbol{x}_k) \cdot \frac{d\boldsymbol{x}_k}{du_i}\right] \cdot f(t_k) + \boldsymbol{l}_b(\boldsymbol{x}_k) \cdot \frac{df(t_k)}{du_i}\right] \Delta t \quad (3.19)$$

The analytical expressions of the derivatives $\nabla_{\boldsymbol{x}} \boldsymbol{l}_a(\boldsymbol{x})$, $\nabla_{\boldsymbol{x}} \boldsymbol{l}_b(\boldsymbol{x})$ are calculated symbolically and then evaluated numerically for different realizations of $\boldsymbol{x}_k$; $\frac{df(t_k)}{du_i}$ can be obtained from Eq. (3.1), the deterministic function that describes the excitation; and $\frac{d\boldsymbol{x}_k}{du_i}$ is the term calculated in the previous time step k. Thus, $\frac{d\boldsymbol{x}_{k+1}}{du_i}$ can be calculated recursively using Eq. (3.19) and $\frac{dy_{k+1}}{du_i}$ is evaluated at the final time step $t_{k+1} = \tau$ by Eq. (3.18b). The derivatives $\nabla_{\boldsymbol{u}} G = -\nabla_{\boldsymbol{u}} y(\boldsymbol{u}, \tau) = -[\frac{dy(\boldsymbol{u},\tau)}{du_1}, \dots, \frac{dy(\boldsymbol{u},\tau)}{du_n}]$ can be finally approximated through recursion. It should be noted that $\boldsymbol{x}_k$ appearing in the above formulas is the numerical evaluations of the structural responses at different time instances. For the calculation of $\boldsymbol{x}_k$, Euler integration is not strictly

required as it simply involves determining the time history of the structural responses subjected to a given input excitation. For higher precision, in this work, the Runge-Kutta (4, 5) pair [86,87], i.e., the *ode45* command in MATLAB, is adopted to find $\boldsymbol{x}_k$, which is then substituted in Eq. (3.19) to obtain the gradients.

The algorithm of the Euler-Analytical estimate of Derivative (EAD) is summarized as follows:

Algorithm 3

Initialization: Analytically differentiate the state-space model of Eq. (3.16) and the excitation model of Eq. (3.1) to obtain the symbolic derivatives $\boldsymbol{\nabla_x l}_a(\boldsymbol{x})$, $\boldsymbol{\nabla_x l}_b(\boldsymbol{x})$ and $\frac{df(t)}{du_i}$. Set Δt. The algorithm starts at step $k = 0$, where $t_0 = 0$ and $\frac{d\boldsymbol{x}_k}{du_i} = \frac{d\boldsymbol{x}_0}{du_i} = 0$.

1. Find the discretized excitation $f(t)$ subjected to the updated input $\boldsymbol{u}$ obtained in step 4 of *Algorithm 2* at all t_k concerned using Eq. (3.1).
2. Find the responses $\boldsymbol{x}(t)$ of the structural system subjected to $f(t)$ obtained in step 1 at all t_k concerned.
3. At step k, the time step $t_k = k \cdot \Delta t$. Find $f(t_k)$ from the discretized excitation $f(t)$ obtained in step 1 and evaluate $\frac{df(t_k)}{du_i}$.
4. Find $\boldsymbol{x}_k$ from $\boldsymbol{x}(t)$ obtained in step 2 and evaluate $\boldsymbol{\nabla}_{\boldsymbol{x}_k}\boldsymbol{l}_a(\boldsymbol{x}_k)$, $\boldsymbol{\nabla}_{\boldsymbol{x}_k}\boldsymbol{l}_b(\boldsymbol{x}_k)$, $\boldsymbol{l}_b(\boldsymbol{x}_k)$.
5. Calculate $\frac{d\boldsymbol{x}_{k+1}}{du_i}$ using Eq. (3.19).
6. If $t_{k+1} = \tau$, the algorithm ends, output $\frac{dy(\tau)}{du_i} = \frac{dy_{k+1}}{du_i}$ using Eq. (3.18b).

Otherwise consider $k = k + 1$, replace the expression of $\frac{dx_{k+1}}{du_i}$ and $\frac{dy_{k+1}}{du_i}$ with $\frac{dx_k}{du_i}$ and $\frac{dy_k}{du_i}$, and return to step 3.

The recursive nature of the above algorithm allows for a robust calculation of the derivatives. It should be noted that all symbolic derivatives are calculated once for the system and output function studied in an offline manner. The method presented in *Algorithms 1,2 and 3* will be referred to as the Design Point Excitation method with an Euler-Analytical estimate of the Derivative (DPE-EAD).

3.2.1 Selection of the discretization and integration time step

Algorithm 3 is presented under the assumption that the sampling time step used to discretize the input $u(t)$ is the same as the integration time step used in the Euler integration in Eq. (3.17a). However, the latter may often need to be chosen as smaller than the former. While a small sampling time step would typically be unnecessary for an earthquake input, a highly non-linear system may require a small integration time-step for reasons related to accuracy of the calculated gradients.

Let Δt_I and Δt_D be the integration and the input sampling time step, respectively. The time instances at which the states of the system are updated through integration are then denoted as $t_k = k \cdot \Delta t_I$, where $k = 0,1, \dots, n_k$ and $n_k = \tau/\Delta t_I$, while Zero-Order-Hold is used to discretize the input between the time instances $t_j = j \cdot \Delta t_D$, where $j = 0,1, \dots, n_j$ and $n_j = \tau/\Delta t_D$. It is further assumed that $\Delta t_D = N_p \, \Delta t_I$ where N_p is a positive integer. In practice this means that the input is held constant for N_p integration time steps. With a small integration time step, the

accuracy of the integration is increased but the computational cost could be high. Thus, it is useful to select a robust integration time step ensuring balance between accuracy and efficiency.

In cases where different integration and the input sampling time step are selected, the analytical estimate of the derivative in Eq. (3.19) is rewritten as:

$$\frac{d\boldsymbol{x}_{k+1}}{du_i} = \frac{d\boldsymbol{x}_k}{du_i} + \frac{d\left(\boldsymbol{l_a}(\boldsymbol{x}_k) + \boldsymbol{l_b}(\boldsymbol{x}_k)\cdot f(t_j)\right)}{du_i}\cdot \Delta t_I \qquad \text{where } t_j \le t_k < t_{j+1}$$

$$= \frac{d\boldsymbol{x}_k}{du_i} + \left[\boldsymbol{\nabla}_{x_k}\boldsymbol{l_a}(\boldsymbol{x}_k)\cdot\frac{d\boldsymbol{x_k}}{du_i} + \left[\boldsymbol{\nabla}_{x_k}\boldsymbol{l_b}(\boldsymbol{x}_k)\cdot\frac{d\boldsymbol{x}_k}{du_i}\right]\cdot f(t_j) + \boldsymbol{l_b}(\boldsymbol{x}_k)\cdot\frac{df(t_j)}{du_i}\right]\Delta t_I \quad (3.20)$$

The algorithm of the EAD in *Algorithm 3* is amended as:

Algorithm 4

Initialization: Analytically derive the symbolic derivatives $\boldsymbol{\nabla_x} \boldsymbol{l}_a(\boldsymbol{x})$, $\boldsymbol{\nabla_x} \boldsymbol{l}_b(\boldsymbol{x})$ and $\frac{df(t)}{du_i}$. Select the sampling time step Δt_D and the integration time step Δt_I, where Δt_D is an integer multiple of Δt_I, i.e., $\Delta t_D = N_p\, \Delta t_I$. The algorithm starts at step $k = 0$ and $j = 0$, where $t_0 = 0$ and $\frac{dx_k}{du_i} = \frac{dx_0}{du_i} = 0$.

1. Find the discretized excitation $f(t)$ subjected to the updated input $\boldsymbol{u}$ obtained in step 4 of *Algorithm 1* at all t_j concerned using Eq. (3.1).
2. Find the responses $\boldsymbol{x}(t)$ of the structural system subjected to $f(t)$ obtained in step 1 at all t_k concerned.
3. At step k, the time step $t_k = k \cdot \Delta t_I$ and $t_j = j \cdot \Delta t_D$. Find $f(t_j)$ from the discretized excitation $f(t)$ obtained in step 1 and evaluate $\frac{df(t_j)}{du_i}$.
4. Find $\boldsymbol{x}_k$ from $\boldsymbol{x}(t)$ obtained in step 2 and evaluate $\boldsymbol{\nabla}_{\boldsymbol{x}_k}\boldsymbol{l}_a(\boldsymbol{x}_k)$, $\boldsymbol{\nabla}_{\boldsymbol{x}_k}\boldsymbol{l}_b(\boldsymbol{x}_k)$, $\boldsymbol{l}_b(\boldsymbol{x}_k)$.

5. Calculate $\frac{d\boldsymbol{x}_{k+1}}{du_i}$ using Eq. (3.20).
6. If $t_{k+1} = \tau$, the algorithm ends, output $\frac{dy(\tau)}{du_i} = \frac{dy_{k+1}}{du_i}$ using Eq. (3.18b). Otherwise consider $k = k + 1$, replace the expression of $\frac{d\boldsymbol{x}_{k+1}}{du_i}$ and $\frac{dy_{k+1}}{du_i}$ with $\frac{d\boldsymbol{x}_k}{du_i}$ and $\frac{dy_k}{du_i}$, and proceed to step 7.
7. If the updated $t_k \geq t_j + \Delta t_D$, update $j = j + 1$ and return to step 3. Otherwise, return to step 3 directly.

3.3 Derivative estimated by the Automatic Differentiation (AD)

Another approach of computing the derivative $\nabla_{\boldsymbol{u}} G$ shown in Eq. (3.14), as required in the DPE method repeatedly, is through the Automatic Differentiation (AD) method [89]. The AD method, widely used in deep learning for the computation of derivatives, may also be applied here in computing the derivatives in the optimization problems. The method uses symbolic rules for differentiation according to the analytical expression that relates the dependent, i.e., the LSF G, and the independent variable, i.e., the variable $\boldsymbol{u}$, and evaluates derivatives numerically. It requires that the dependent variable G is expressed in terms of the independent variable $\boldsymbol{u}$ fully analytically without any internal evaluation steps. The semi-analytical semi-numerical method is preferable compared to the Numerical estimate of the Derivatives (ND) method in terms of the accuracy and the computational efficiency. Compared to purely analytical approaches, AD evaluates expressions numerically early in the computations rather than carrying out large symbolic computations which could lead

to significant memory requirements [90]. It evaluates the derivatives at particular realization of the independent variables instead of constructing the whole symbolic expression of the derivatives [90].

Automatic differentiation evaluates the derivatives numerically at the intermediate transformed variables and using the Chain Rule to calculate the objective derivative symbolically [90]. The fundamental to the automatic differentiation is the decomposition of differentials according to the Chain rule. For the ease of demonstration, the analytical expression that relates the LSF G and the independent variable $\boldsymbol{u}$ to be differentiated with respect to is simplified as: $G = g_1\left(g_2\left(g_3(u)\right)\right)$. Let r_V denote the variables in the function operation, $V = 0,1,2 \dots, v$. It includes the independent variable $r_0 = u$, the dependent variable $r_v = G$ and the intermediate variables $[v_1, v_2, \dots, v_{n-1}]$. The function can then be rewritten in $G = g_1\left(g_2\left(g_3(u)\right)\right) = g_1\left(g_2\left(g_3(r_0)\right)\right) = g_1\left(g_2(r_1)\right) = g_1(r_2) = r_3 = G$, in which r_1, r_2 are the so-called intermediate variables. The Chain Rule gives $\frac{\partial G}{\partial u} = \frac{\partial G}{\partial r_2} \cdot \frac{\partial r_2}{\partial r_1} \cdot \frac{\partial r_1}{\partial u} = \frac{\partial g_1(r_2)}{\partial r_2} \cdot \frac{\partial g_2(r_1)}{\partial r_1} \cdot \frac{\partial g_3(u)}{\partial u}$. For more complicated systems, this approach works in two modes in the automatic differentiation method: the forward mode and the reverse mode. The forward mode finds $\frac{\partial G}{\partial u}$ by computing $\frac{\partial r_V}{\partial u} = \frac{\partial r_V}{\partial r_{V-1}} \cdot \frac{\partial r_{V-1}}{\partial u}$ recursively, in which V increases in ascending order from r_0 to r_v. In the forward mode, the independent variable to be differentiated with respect to is fixed. One computes the derivatives of each sub-expression recursively using Chain Rule:

$$\frac{\partial G}{\partial u} = \frac{\partial G}{\partial r_V} \cdot \frac{\partial r_V}{\partial u} = \frac{\partial y}{\partial x_V} \cdot \left(\frac{\partial r_V}{\partial r_{V-1}} \frac{\partial r_{V-1}}{\partial u}\right) = \cdots = \frac{\partial G}{\partial r_V} \cdot \left(\frac{\partial r_V}{\partial r_{V-1}} \cdot \frac{\partial r_{V-1}}{\partial r_{V-2}} \cdot \dots \cdot \frac{\partial r_1}{\partial u}\right) \quad (3.21)$$

The reverse mode finds $\frac{\partial G}{\partial u}$ through the opposite direction of the function operation order. It computes $\frac{\partial G}{\partial x_i} = \frac{\partial G}{\partial r_{V+1}} \cdot \frac{\partial r_{V+1}}{\partial x_V}$ recursively, in which i decreases in descending order from r_{V-1} to r_0. In the reverse mode, the dependent variable to be differentiated is fixed. The derivative is computed with respect to each sub-expression recursively using Chain Rule:

$$\frac{\partial G}{\partial u} = \frac{\partial G}{\partial r_1} \cdot \frac{\partial r_1}{\partial u} = \left(\frac{\partial G}{\partial r_2}\frac{\partial r_2}{\partial r_1}\right) \cdot \frac{\partial r_1}{\partial u} = \cdots = \left(\frac{\partial G}{\partial r_V} \cdot \frac{\partial r_V}{\partial r_{V-1}} \cdot \ldots \cdot \frac{\partial r_2}{\partial r_1}\right) \cdot \frac{\partial r_1}{\partial u} \tag{3.22}$$

The reverse mode AD is adopted in the *autodiff* command in the MATLAB Deep Learning package to evaluates the derivative $\nabla_{\boldsymbol{u}} G$**.** In the computation, the *dlgradient* command in MATLAB is used to calculate the derivative for a custom training loop. The *dlarray* command internally records the transformations of the independent variables in a trace, which enables the reverse mode AD. The *dlevel* command evaluates the numeric values of the *dlgradient* array function where the argument to the function is in a *dlarray* form.

The limitation of the AD method is that the function which transforms the independent variables to the dependent output variables needs to be deterministic and formulated symbolically. If any numerical estimation involves in the output response of interest, the *autodiff* is not capable of the derivative estimation.

3.4 Reliability problems with multiple limit states

The reliability analysis of a system may involve different response measurement criteria, and this leads to the need to account simultaneously for multiple Limit State Functions (LSFs). The reliability analysis that accounts for multiple LSFs

simultaneously is known as a System Reliability problem. In this case, the failure domain is expressed in terms of a system of continuous and differentiable LSFs G_M:

$$G_M(\boldsymbol{u}, y_T, \tau) = y_T - y(\boldsymbol{u}, \tau) \tag{3.23}$$

where $M = 1,2, \dots, q$. It should be noted that the LSFs G_M in a System Reliability problem may have variations in the responses y, the time instances τ, or the thresholds y_T of interest.

Two popular types of the System Reliability problems are: Series system problems and Parallel system problems [15]. In Series system problems, failure is defined by a system exceeding any of the thresholds y_T in the LSFs $G_M(\boldsymbol{u}, y_T, \tau)$ considered. The failure domain is the union of componential failure events:

$$D_f = \bigcup_M (G_M(\boldsymbol{u}, y_T, \tau) \leq 0) \tag{3.24}$$

In Parallel system problems, failure is defined by a system exceeding all the thresholds y_T in the LSFs $G_M(\boldsymbol{u}, y_T, \tau)$ considered. The failure mode considers a redundant system that requires failure of several components, each defined by the LSF $G_M(\boldsymbol{u}, y_T, \tau)$. The failure domain is the intersection of componential failure events:

$$D_f = \bigcap_M (G_M(\boldsymbol{u}, y_T, \tau) \leq 0) \tag{3.25}$$

The FORM estimate of the failure probability is obtained by linearizing each of the LSFs $G_M(\boldsymbol{u}, y_T, \tau)$ at the design point $\boldsymbol{u}_M^*$. Each limit state surface is approximated by the tangent hyperplane:

$$\beta_M - \boldsymbol{\alpha}_M \boldsymbol{u} = 0 \tag{3.26}$$

where $\boldsymbol{\alpha}_M$ and β_M are the direction vector and the reliability index regarding the M^{th} limit state surface. A reasonable choice for the linearization point $\boldsymbol{u}_M^*$ is the minimum distance point on each Limit State surface from the origin, as defined in Eq. (3.4). It should be noted that this is a good choice in approximating the failure domain for Series systems, while for Parallel systems the Limit State surfaces linearized at the

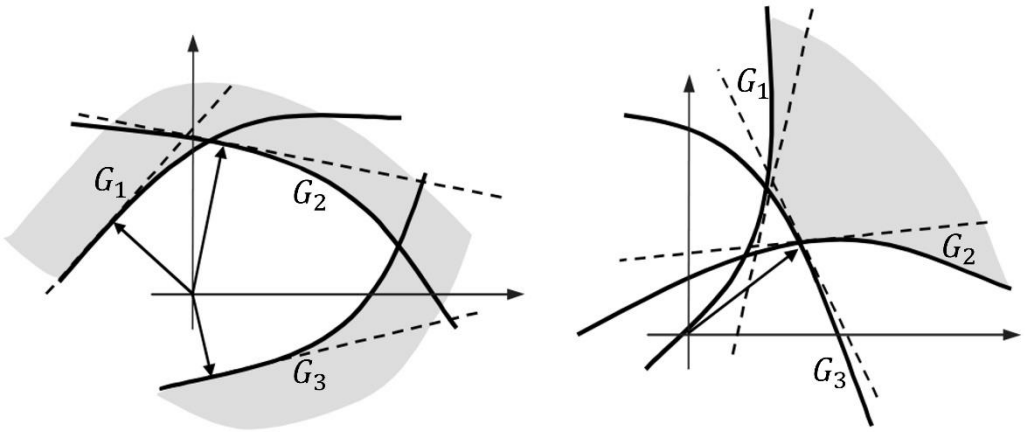


Figure 3. 2 Linearization points selected for series and parallel systems [15].

joint design point, defined by $\boldsymbol{u}_{joint}^* = \arg\min\{\|\boldsymbol{u}\| | G_M \leq 0, M = 1,2,\dots,q\}$, provide a better approximation of the failure domain [15]. Figure 3. 2 illustrates the above choices for linearization, which shows that the joint design point $\boldsymbol{u}_{joint}^*$ is a better choice for Parallel systems. Nonetheless, the linearization point $\boldsymbol{u}_M^*$ define by Eq. (3.4) is commonly used in practice since it is much easier to obtain.

With the limit states surfaces linearized, the failure domain of a system problem is approximated by a hyper polygon. According to the concept of system reliability by FORM [15], the corresponding approximations of the failure probability are derived as follows : Let $v_M = \boldsymbol{\alpha}_M \cdot \boldsymbol{u}$, $\boldsymbol{v} = [v_1, v_2, \dots, v_q]$ be standard normal variables with the correlation coefficient: $\rho_{hl} = \boldsymbol{\alpha}_h \boldsymbol{\alpha}_l^T$, where $h, l = 1,2,\dots,q$. For a Series system,

the failure probability is

$$P_f = P\left[\bigcup_{M=1}^{q}(\beta_M \le v_M)\right] = 1 - P\left[\bigcap_{M=1}^{q}(v_M < \beta_M)\right] = 1 - \boldsymbol{\phi}_m(\boldsymbol{B}, \boldsymbol{R}) \qquad (3.27)$$

where $\boldsymbol{\phi}_m(\boldsymbol{B}, \boldsymbol{R})$ is the multi-variate standard normal CDF with correlation matrix $\boldsymbol{R} = [\rho_{hl}]$ evaluated at $\boldsymbol{B} = [\beta_1, \dots, \beta_q]$. For a Parallel system, according to the symmetric nature of the probability density of standard normal variables, the failure probability is

$$P_f = P\left[\bigcap_{M=1}^{q}(\beta_M \le v_M)\right] = P\left[\bigcap_{M=1}^{q}(v_M < -\beta_M)\right] = \boldsymbol{\phi}_m(-\boldsymbol{B}, \boldsymbol{R}) \qquad (3.28)$$

Both Eq. (3.27) and Eq. (3.28) can be reduced to Eq. (3.5) for a single LSF problem when $q = 1$.

3.4.1 The reliability over a time period

The reliability obtained for each LSF only considers a specific time instant τ as defined in the LSF of either Eq. (3.3) or Eq. (3.23). In the seismic reliability analysis of a structural system, it is more of interest to deduce the possibility of whether an output response of a system is exceeded at any time instances in an earthquake than at one specific time instance. The concept of the System Reliability helps find the reliability of a system over a time period, which is categorized as a Series system by definition.

The reliability over a time period T is defined by the output response not exceeding a threshold y_T at a sequence of equally spaced time instants $\tau_J = J \cdot \Delta\tau$ for $J = 1,2, \dots, j$ considered in the time period T, where $j = T/\Delta\tau$ and $\Delta\tau$ controls

frequency of the time instants concerned in the reliability estimations. It should be noted that the selection of $\Delta\tau$ affect the accuracy of the reliability estimation. The design point at each time instants τ_J is found by the solving the optimization problem, as shown in Eq. (3.4), in the DPE method, in which the LSFs $G_J(\boldsymbol{u}, y_T, \tau_J) = y_T - y(\boldsymbol{u}, \tau_J)$ are constructed as the set of the LSFs concerned in the Series system. According to Eq. (3.27), the reliability (P_R) of the output response of a system over a time period is computed by:

$$P_R = 1 - P_f = \boldsymbol{\phi}_m(\boldsymbol{B}, \boldsymbol{R}) \tag{3.29}$$

where the reliability index β_J and the direction vector $\boldsymbol{\alpha}_J$ obtained by the DPE method for each limit state surface of $G_J = 0$ are substituted to determine the parameters $\boldsymbol{B}$ and $\boldsymbol{R}$.

An efficient way to find a warm starting guess $\hat{\boldsymbol{u}}^*$ of the design point at the time instant τ_J is to use the design points $\boldsymbol{u}^*$ at its neighbouring time instants $\tau_J \pm \Delta\tau$ [17]. Let $u^*(t)$ denotes the element in the design point $\boldsymbol{u}^*$ correspond to the time instant t. If the design point $[u^*(t)](y_T, \tau_J)$ for a selected time τ_J is obtained, a good approximation to the design point $[u^*(t)](y_T, \tau_J+\Delta\tau)]$ for a later time instant $\tau_J + \Delta\tau$ can be obtained from the neighbouring time steps τ_J by time shifting, i.e., $[u^*(t - \Delta\tau)](y_T, \tau_J)$. Similarly, if a former time instant $\tau_J - \Delta\tau$ is of interest, a good approximation to the design point $[\boldsymbol{u}^*(t)](y_T, \tau_J - \Delta\tau)$ for the former time instant $\tau_J - \Delta\tau$ is $[u^*(t + \Delta\tau)](y_T, \tau_J)$. The approximation obtained are used as a warm starting guess in the line search optimization in *Algorithm 2* to find the exact solution

of the design point $\boldsymbol{u}^*(y_T, \tau_J+\Delta\tau)$ and $\boldsymbol{u}^*(y_T, \tau_J-\Delta\tau)$. It should be noted that selecting a time instant in the strong motion period is reasonable to initialize. A small time instant does not capture the majority shape of the design point and a large time instant, consist of a large size design point, has a large size of unknown variables in the optimization and is computationally expensive in finding the exact design point.

3.5 Examples and discussions

In this section, examples are used to demonstrate the methods suggested. The examples are chosen from systems exhibiting nonlinearities relevant to structural engineering systems whose earthquake engineering. Variations of Design Point Excitation method using the Euler-Analytical estimate of the Derivative (DPE-EAD), the Numerical estimate of the Derivative (DPE-ND) [88] and the Automatic Differentiations (DPE-AD) [90] and the Monte Carlo (MC) simulations [12] are applied to estimate the seismic reliability of the structural systems considered. The accuracies and the computational efficiencies of the four approaches applied in the reliability estimations are elaborated. In the DPE methods, the design point $\boldsymbol{u}^*$ in the optimization problem in Eq. (3.4) is solved by the line search optimization in *Algorithm 2*, in which the initial guess $\widehat{\boldsymbol{u}}^*$ is obtained through *Algorithm 1*. In the MC simulations, samples of earthquake time histories and the structural responses are generated repeatedly, and the seismic reliabilities are estimated according to the generate sample set. The MC simulations, a default method widely used in finding the reliabilities, is accurate when the sample set is sufficiently large [12], thus it is implemented here as a reference to

indicate the accuracies of the reliabilities estimated by other methods. The Runge-Kutta (4,5) pair [86,87] (*ode45* command in MATLAB) is implemented in all four approaches to integrate the state-space equation of the structural system and the structural response y written by Eq. (3.2).

The newly proposed EAD method is capable of computing the derivative used in optimization more efficiently. The results of the DPE-EAD method are compared to the MC simulations and variations of the DPE method when using the ND through the central-differences scheme of Eq. (3.15) and AD through the *autodiff* command in MATLAB. It should be noted that *Algorithm 3* is used when the integration time step Δt_I selected in the EAD method is identical to the input-sampling time step Δt_D and *Algorithm 4* is used when different time steps of Δt_I and Δt_D are selected.

3.5.1 Example 1: *A 4-DoF system with Bouc-Wen nonlinearity subjected to earthquake excitations*.

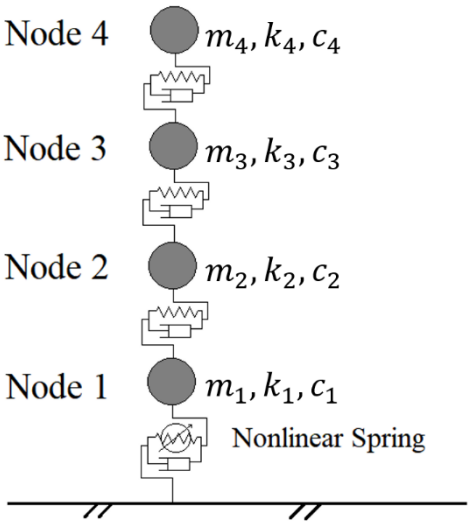


Figure 3. 3 The structural model considered in *Example 1*.

In this example, the seismic reliability of a 4-degree-of-freedom structural system with a Bouc-Wen nonlinearities is examined. Details of the structural model and the earthquake ground model are introduced as follows. The 4-storey shear building shown in Figure 3. 3 is considered.

The mass, stiffness, and damping coefficient of the i^{th} storey appearing in Figure 3. 3 are denoted as m_i, k_i and c_i, respectively. The first story of the shear building has a Bouc-Wen nonlinearity, and the rest of the stories are linear elastic. The 4-story shear building model is represented by the following differential equations:

$$\boldsymbol{M}\ddot{\boldsymbol{x}}(t) + \boldsymbol{C}\dot{\boldsymbol{x}}(t) + \boldsymbol{K}(\boldsymbol{\alpha}\boldsymbol{x}(t) + (\boldsymbol{I}_4 - \boldsymbol{\alpha})\boldsymbol{Z}(t)\,) = \boldsymbol{F}(t) \tag{3.30a}$$

$$\dot{z}(t) = -\gamma|\dot{x}_1(t)||z(t)|^{n-1}z(t) - \eta|z(t)|^n\dot{x}_1(t) + A\dot{x}_1(t) \tag{3.30b}$$

where the displacement vector $\boldsymbol{x}$ is denoted as $\boldsymbol{x} = [x_1, x_2, x_3, x_4]^T$. The Bouc-Wen hysteretic term associated to the elastic displacements of the structure is denoted as $\boldsymbol{Z} = [z, 0, 0, 0]^T$, in which z is the hysteretic term for the first storey governed by Eq. (3.30b) and the parameters $n = 3$, $A = 1$ and $\gamma = \eta = 1/(2\sigma_0^n)$ are selected where $\sigma_0^2 = \pi S m^2/ck$ is the mean square response of the corresponding single DoF linear oscillator with $S = 0.0156\text{m}^2/\text{s}^3$. $\boldsymbol{M}$, $\boldsymbol{C}$ and $\boldsymbol{K}$ are the mass matrix, damping matrix and the stiffness matrix of the corresponding linear-elastic shear building respectively, written by:

$$\boldsymbol{M} = \begin{bmatrix} m_1 & 0 & 0 & 0 \\ 0 & m_2 & 0 & 0 \\ 0 & 0 & m_3 & 0 \\ 0 & 0 & 0 & m_4 \end{bmatrix},\ \boldsymbol{C} = \begin{bmatrix} c_1 + c_2 & -c_2 & 0 & 0 \\ -c_2 & c_2 + c_3 & -c_3 & 0 \\ 0 & -c_3 & c_3 + c_4 & 0 \\ 0 & 0 & -c_4 & c_4 \end{bmatrix} \text{ and}$$

$$\boldsymbol{K} = \begin{bmatrix} k_1 + k_2 & -k_2 & 0 & 0 \\ -k_2 & k_2 + k_3 & -k_3 & 0 \\ 0 & -k_3 & k_3 + k_4 & 0 \\ 0 & 0 & -k_4 & k_4 \end{bmatrix}$$

where $m_i = 30$ Mg, $k_i = 10000(2\pi)^2$ N/m and $c_i = 8000\pi$ Ns/m for $i = 1,2,3,4$ are selected for the structure model. The α_i in the diagonal matrix $\boldsymbol{\alpha} = \text{diag}([\alpha_1, \alpha_2, \alpha_3, \alpha_4]^T)$ controls the degree of hysteresis for the i^{th} storey, where $\alpha_1 = 0.2$ is assumed for the first story and the rest of the stories are assumed to be linear ($\alpha_2 = \alpha_3 = \alpha_4 = 1$). The excitation is defined by $\boldsymbol{F}(t) = [m_1, m_2, m_3, m_4]^T \cdot f(t)$, where $f(t)$ is the ground excitation.

In this example, the stochastic earthquake model developed by Der Kiureghian et al. [13] is adopted. The ground excitation $f(t)$ is simulated by a modulated filtered white noise defined as:

$$f(t) = q(t) \cdot \sum_{i=1}^{N} h(t - t_i) w_i \tag{3.31}$$

in which the discretized white noise $w_i = \sigma u_i$ and $N = t/\Delta t_j$. The standard deviation $\sigma = \sqrt{2\pi S_0 \Delta t_j}$ describes the intensity of the white noise input and $S_0 = 10^4$. The modulating function is given by $q(t) = 0.03 \cdot t^2 \cdot \exp(-0.2t)$, and the unit-impulse response function of the filter is defined by:

$$h(t) = -\left[\frac{\omega_f}{\sqrt{1-\zeta_f^2}} \sin\left(\omega_f t \sqrt{1-\zeta_f^2}\right) + 2\zeta_f \omega_f \cos\left(\omega_f t \sqrt{1-\zeta_f^2}\right)\right] \exp\left(-\zeta_f \omega_f t\right) \tag{3.32}$$

where $\omega_f = 5\pi$ rad/s and $\zeta_f = 0.4$. Figure 3. 4 shows the amplitude of the modulating function and a sample realization of the ground excitation by the earthquake model selected. The input-sampling time step of $\Delta t_D = 0.01$s is selected

for the earthquake model and the integration time step of $\Delta t_I = 0.01\text{s}$ is selected in the EAD method in computing the derivative $\nabla_{\boldsymbol{u}} G$.

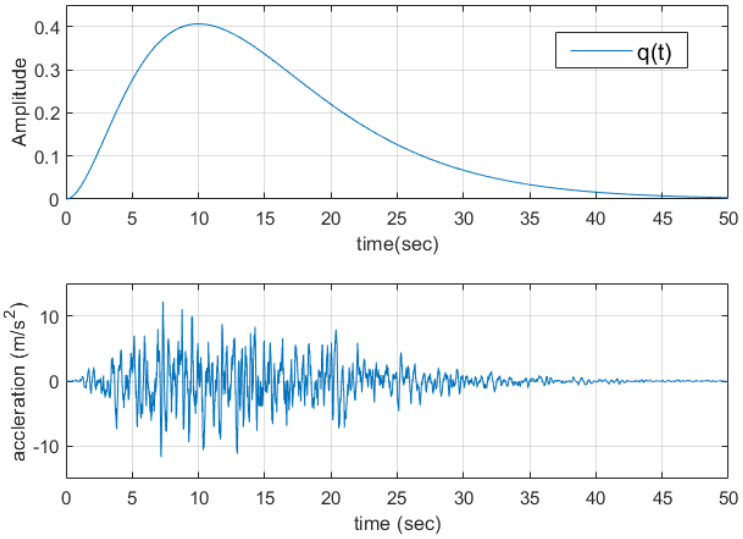


Figure 3. 4 The modulating function and a sample realization of the ground excitation.

The seismic reliability of the 4th storey displacement, i.e., $y(\tau) = x_4(\tau)$, which is a state element in the state vector $\boldsymbol{x}$ of the structural system, is of interest. The time instant $\tau = 15\text{ s}$ is selected since it is during the strong motion period of the earthquake according to the envelope function. The reliability that considers a sequence of thresholds $[y_T^I] = \pm[10^{-3} \cdot (I-2)]$ m where $I = 3,4,\ldots,27$ are examined in this example. It should be noted that the notation of the thresholds y_T^I starts from y_T^3 since y_T^1 and y_T^2 are specifically selected for initialization in *Algorithm 1*. The DPE method is applicable to the examples with negative thresholds that correspond to negative directions. The reliability of the absolute responses of $y(\tau) = |x_4(\tau)|$, which is usually more significant in reliability analysis, is then computed by Eq. (3.8) from the reliability obtained for the threshold y_T^I in both

positive and negative signs.

To find the initial guess $\widehat{\boldsymbol{u}}^*$ of the design point in the DPE method, $\lambda_{max} = 0.3$ is considered in *Algorithm 1* and the first two thresholds $y_T^1 = 0$ m and $y_T^2 = 10^{-5}$ m are selected. Figure 3. 5 compares the design point $\boldsymbol{u}_L^*(y_T^2, \tau)$ for the corresponding linear system, i.e., $\alpha_i = 1$ in Eq. (3.29), computed by Eq. (3.13) to the design point $\boldsymbol{u}^*(y_T^2, \tau)$ for the nonlinear system obtained by Eq. (3.4) using the line search optimization with EAD. The elements of u_i in design points are plotted in the vertical axis versus the corresponding time instant t_i at which u_i is applied in the horizontal axis. As can be seen in Figure 3. 5, the design point for the linear system $\boldsymbol{u}_L^*(y_T^2, \tau)$ and that for the nonlinear system $\boldsymbol{u}^*(y_T^2, \tau)$ are practically identical for $y_T^2 = 10^{-5}$ m. In order to further show that the nonlinear system is practically linear when the selected threshold of $y_T^2 = 10^{-5}$ m is considered, Figure 3. 6 plots the 1st storey displacement $x_1(t)$ of the linear and the nonlinear system subjected to the ground excitation $f(t)$ with the input $\boldsymbol{u}^*(y_T^2, \tau)$ in the vertical axis versus the corresponding time instant t in the horizontal axis. It shows that the nonlinear term z in the structural system is practically x_1, i.e., the elastic and total displacement of the 1st storey are identical. The threshold y_T^2 selected is sufficiently small to reasonably approximate the response $x_4(\tau)$ of the nonlinear system with its linearization.

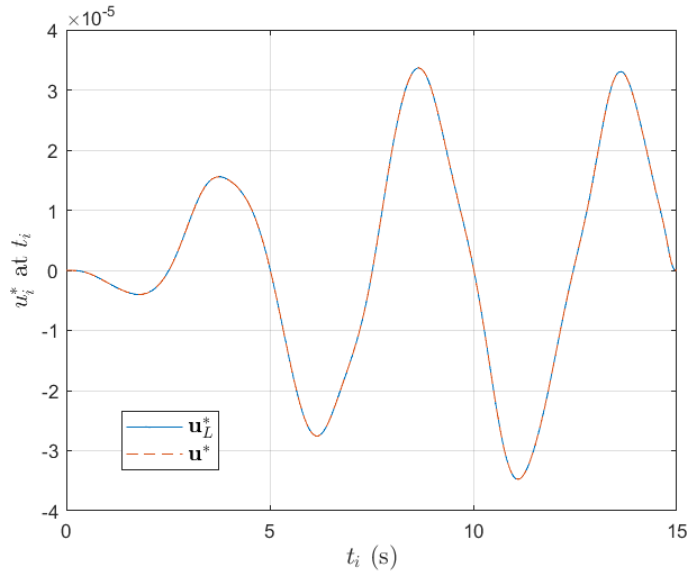


Figure 3. 5 $\boldsymbol{u}_L^*(y_T^2, \tau)$ and $\boldsymbol{u}^*(y_T^2, \tau)$ obtained for $y_T^2 = 10^{-5}$ m.

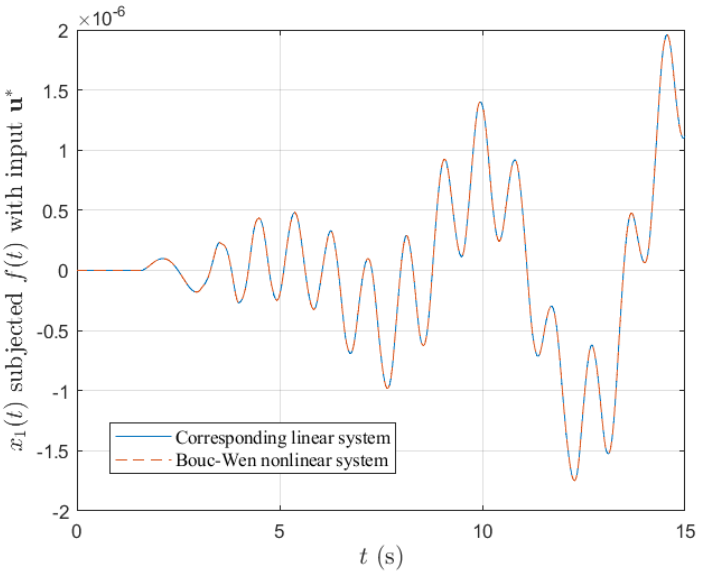
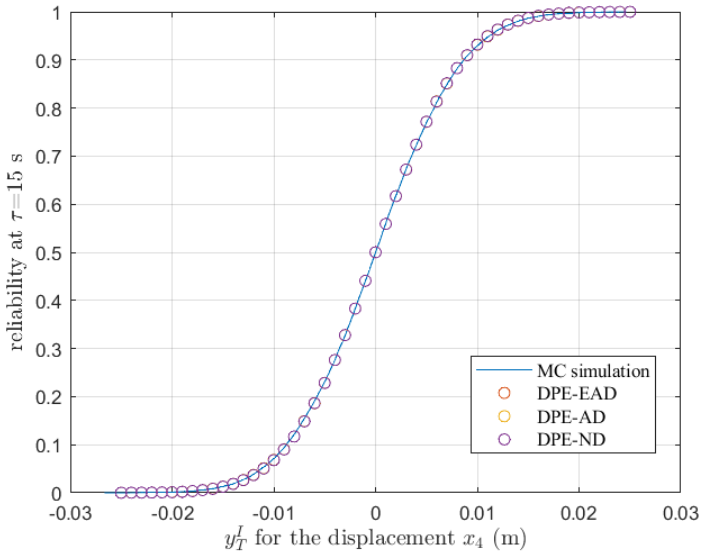


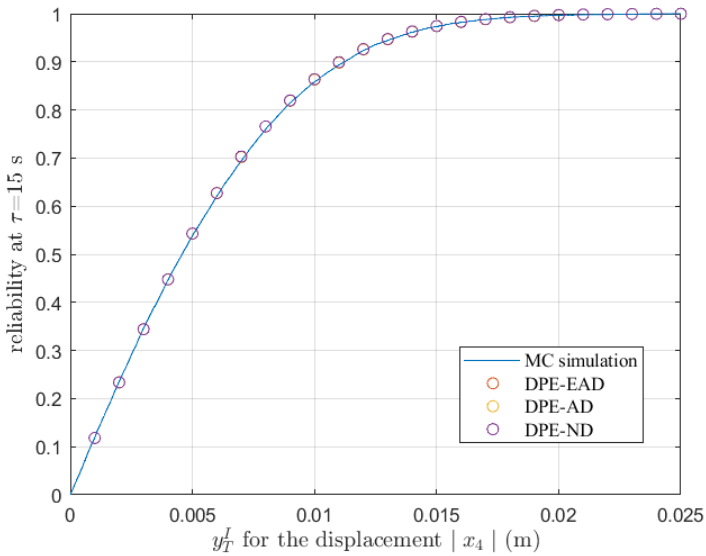
Figure 3. 6 The 1st storey displacement $x_1(t)$ of the linear and the nonlinear system subjected to the ground excitation $f(t)$ with the input $\boldsymbol{u}^*(y_T^2, \tau)$.

The reliabilities of $y(\tau) = x_4(\tau)$ and $y(\tau) = |x_4(\tau)|$ obtained by the DPE methods are plotted in Figure 3. 7 as scatter points. The vertical axis indicates the reliability values plotted against the corresponding thresholds y_T^I on the horizontal axis. As shown in Figure 3. 7(a), the reliabilities obtained by different derivative estimation methods, i.e., DPE-EAD, DPE-ND and DPE-AD are identical. By using

the derivative $\nabla_{\boldsymbol{u}} G$ approximated by the EAD, ND and AD method, 1 iteration, 2 iterations and 1 iteration on average are required in the line search optimization (*Algorithm 2*) in locating the design point $\boldsymbol{u}^*(y_T^I, \tau)$ for each LSFs $G(\boldsymbol{u}, y_T^I, \tau) = y_T^I - x_4(\boldsymbol{u}, \tau)$. This observation potentially indicates that the derivatives $\nabla_{\boldsymbol{u}} G$ obtained by the EAD and AD methods provide better accuracy than the ND method.



(a) $y = x_4(\tau)$



(b) $y = |x_4(\tau)|$

Figure 3. 7 The reliability of $x_4(\tau)$ and $|x_4(\tau)|$ at $\tau = 15\text{s}$ approximated by the DPE methods for a sequence of thresholds versus the CDF of which obtained by the MC simulation.

The cumulative density function (CDF) of $x_4(\tau)$ and $|x_4(\tau)|$ obtained by the MC simulations using 15000 samples are plotted on the corresponding figures for comparison. A convergence test is carried out to ensure the MC sample set is adequately large to provide accurate results [12]. By using the MC sample set, the reliability is computed by:

$$P_R(\tau) = P(y(\tau) \le y_T) = \frac{\text{No. of samples of } y(\tau) \le y_T}{\text{Total No. of the samples simulated}} \tag{3.33}$$

The reliabilities considering the thresholds of $y_T = 4.5 \cdot 10^{-4}\text{m}$, $y_T = 4.5 \cdot 10^{-3}\text{m}$ and $y_T = 0.013\text{m}$, which have the corresponding reliability of 5%, 50% and 95%, are of interest in the convergence analysis. Figure 3. 8 shows the evolutions of the reliabilities, i.e., $P(|x_4(\tau)| \le 4.5 \cdot 10^{-4}\text{m})$, $P(|x_4(\tau)| \le 4.5 \cdot 10^{-3}\text{m})$ and $P(|x_4(\tau)| \le 0.013\text{m})$ estimated by the MC simulation of an increasing number of samples. After investigations, the tail regions having the extreme probability would require a larger sample set to converge. If a maximum accepted relative error of 3% is considered, then generating 12000 samples of the earthquake time histories and the corresponding structural responses is sufficient in the reliability estimation when considering the threshold of $y_T = 4.5 \cdot 10^{-3}$ m, which has the reliability of 50%, and generating 15000 samples is sufficient when considering the thresholds of $y_T = 4.5 \cdot 10^{-4}$ m and $y_T = 0.013$ m, which have the extreme reliabilities of 5% and 95%, respectively.

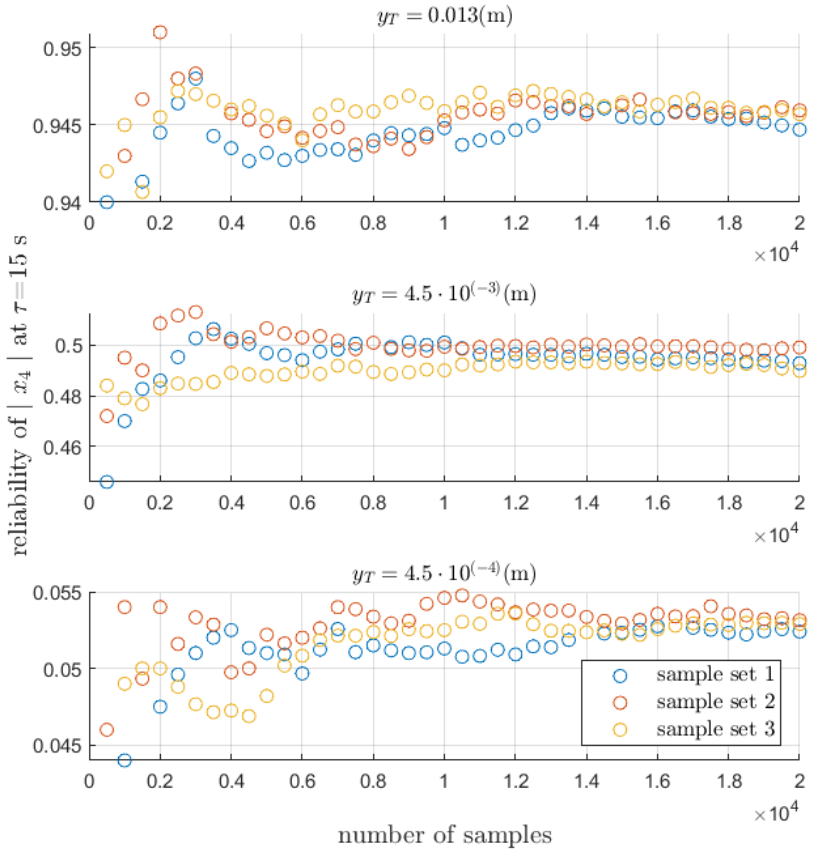


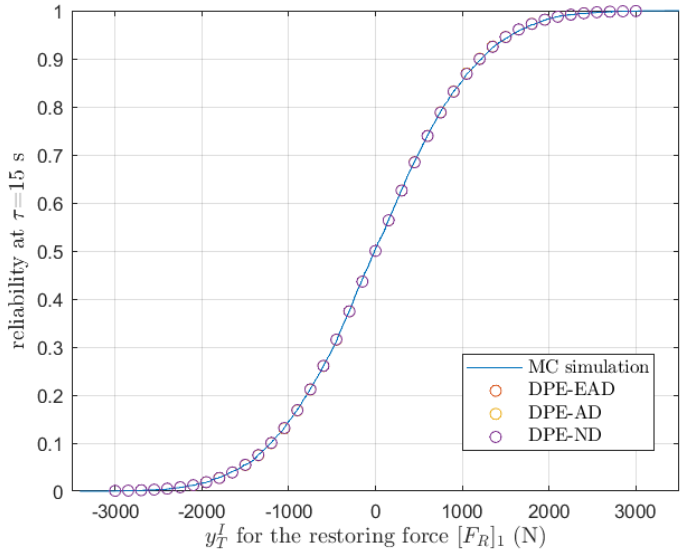
Figure 3. 8 The evolution of the reliability approximated by the MC simulation with an increased size of the sample set.

As can be seen in Figure 3. 7, the reliabilities obtained by the DPE methods agree well with the CDF of $x_4(\tau)$ and $|x_4(\tau)|$. The derivative $\nabla_{\boldsymbol{u}} G$ estimated by the EAD, ND and AD methods are sufficiently accurate to be used in the line search of *Algorithm 2* and the design point $\boldsymbol{u}^*$ located are accurate for a large range of thresholds y_T^l considered, even in the tail regions with small probabilities of exceedance or non-exceedance. The maximum relative differences between the DPE methods and the MC estimations are about 1% at $y_T^9 = \pm 0.007$m which shows a superior accuracy of the DPE method approximations in this example where the response of interest is a state element in the state vector $\boldsymbol{x}$ of the structural system.

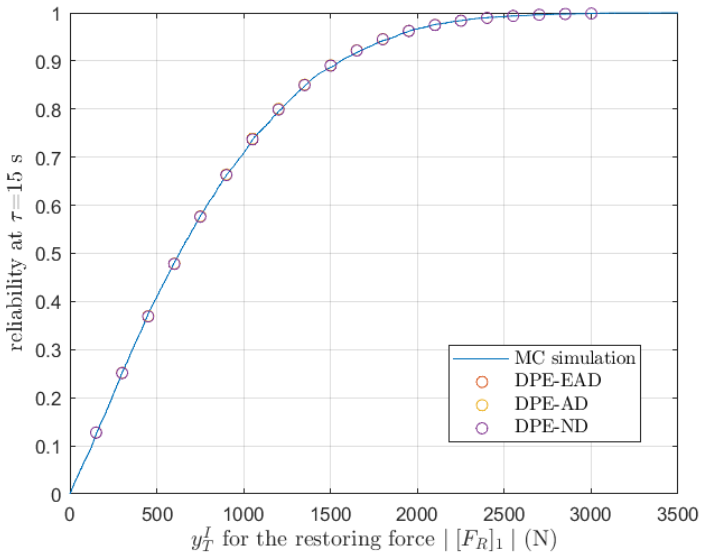
The restoring force is another important measure in reliability analysis which indicates the yielding behaviour of a nonlinear system. Here, the seismic reliability of the 1st storey restoring force is of interest, i.e., $y(\tau) = [\boldsymbol{F}_R]_1(\tau)$, where $[\cdot]_1$ denotes the first element in the vector in the square bracket and the time instant $\tau = 15$ s is selected. The 1st storey restoring force is expressed by $[\boldsymbol{F}_R]_1(\tau) = [1,0,0,0] \cdot \left[\boldsymbol{K}\left(\boldsymbol{\alpha x}(\tau) + (\boldsymbol{I}_4 - \boldsymbol{\alpha})\boldsymbol{Z}(\tau)\right)\right] = (k_1 + k_2) \cdot [\alpha_1 \cdot x_1 + (1 - \alpha_1)z_1] - k_2 \cdot x_2$ according to the structural model. The thresholds $[y_T^I] = \pm[150 \cdot (I - 2)]$ N where $I = 3,4, \dots, 22$ are selected. The reliability of the absolute responses of $y(\tau) = |[\boldsymbol{F}_R]_1(\tau)|$ is computed by Eq. (3.8). In the DPE method, $\lambda_{max} = 0.3$ and the first two thresholds $y_T^1 = 0$ N and $y_T^2 = 0.5$ N are selected in *Algorithm 1* to find the initial guess $\widehat{\boldsymbol{u}}^*$. Similar as before, an investigation is carried out to show that the response $[\boldsymbol{F}_R]_1(\tau)$ of the nonlinear structural system can be approximated by the corresponding linear system at the selected threshold y_T^2.

The reliability of $y(\tau) = [\boldsymbol{F}_R]_1(\tau)$ and $y(\tau) = |[\boldsymbol{F}_R]_1(\tau)|$ obtained by the DPE method are plotted in Figure 3. 9 as the scatter points and are compared to the CDF of $[\boldsymbol{F}_R]_1(\tau)$ and $|[\boldsymbol{F}_R]_1|(\tau)$ obtained by the MC simulations of 15000 samples. A convergence test is carried out to ensure the sample set of 15000 samples provides accurate results for the response $[\boldsymbol{F}_R]_1(\tau)$. As shown in Figure 3. 9(a), the reliability obtained by DPE method with different derivative estimation methods, i.e., DPE-EAD, DPE-ND and DPE-AD are identical for the response $y(\tau) = [\boldsymbol{F}_R]_1(\tau)$. An average of 1 iteration, 1.7 iterations and 1 iteration are required in the line search of *Algorithm 2*

with the derivative $\nabla_{\boldsymbol{u}} G$ approximated by the EAD, ND and EAD method respectively to locate the design point $\boldsymbol{u}^*$ for each LSF $G(\boldsymbol{u}, y_T^I, \tau) = y_T^I - [\boldsymbol{F}_R]_1(\boldsymbol{u}, \tau)$. In the EAD method, the analytical expression of the derivative $\frac{dy(\boldsymbol{u},\tau)}{du_i}$ in this example is $\frac{d[\boldsymbol{F}_R]_1}{du_i} = (k_1 + k_2) \cdot [\alpha_1 \cdot \frac{dx_1}{du_i} + (1 - \alpha_1)\frac{dz_1}{du_i}] - k_2 \cdot \frac{dx_2}{du_i}$, according to Eq. (3.18b) and the measurement equation of the response $[\boldsymbol{F}_R]_1$.



(a) $y = [\boldsymbol{F}_R]_1(\tau)$



(b) $y = |[\boldsymbol{F}_R]_1(\tau)|$

Figure 3. 9 The reliability of $[\boldsymbol{F}_R]_1(\tau)$ and $|[\boldsymbol{F}_R]_1(\tau)|$ at $\tau = 15\text{s}$ approximated by the DPE method for a sequence of thresholds versus the CDF of which obtained by the MC simulations.

As can be seen in Figure 3. 9, the reliabilities obtained by the DPE methods agree well with the CDF of $[\boldsymbol{F}_R]_1(\tau)$ and $|[\boldsymbol{F}_R]_1(\tau)|$ where the response of interest is a linear function of the state vector of the structural system. The derivative $\nabla_{\boldsymbol{u}} G$ estimated by the EAD, ND and AD methods are sufficiently accurate to be used in the line search of *Algorithm 2* to locate the design point $\boldsymbol{u}^*$ and find the reliability for a large range of thresholds y_T^I considered. The maximum relative differences between the DPE method and the MC estimations is about 0.9% at $y_T^{10} = \pm 1200\text{N}$ which further shows that the DPE-EAD, the DPE-ND and the DPE-AD methods are reliable in this example in estimating seismic reliabilities. More specifically, the developed DPE-EAD method shows high accuracy in estimating the reliability of nonlinear structural systems with Bouc-Wen nonlinearity subjected to stochastic earthquake excitations.

Though the DPE methods with different approaches, i.e., EAD, ND and AD, used in computing the derivative $\nabla_{\boldsymbol{u}} G$ achieve the same level of accuracy in the reliability approximations in this example, the computational costs and the accuracies of the derivative approximations vary. Details of the comparisons of the derivative approximation methods are elaborated later in Section 3.5.1.1.

In terms of the computational efficiency of the applied methods, Table 3. 1 summarizes the time taken in finding the reliabilities of the responses $y(\tau) = x_4(\tau)$ and $y(\tau) = [\boldsymbol{F}_R]_1(\tau)$ as shown in Figure 3. 7 and Figure 3. 9 using the four approaches, the DPE-EAD, the DPE-ND, the DPE-AD and the MC simulations. The

calculation time of the DPE methods in finding the reliabilities for all $(\dim(I)+1)$ thresholds are shown in the 3rd column in Table 3. 1, in which the time for per threshold refers to the average time required in locating each design point $\boldsymbol{u}^*(y_T^I,\tau)$ using the line search optimization. It should be noted that the time required for $(\dim(I)+1)$ thresholds is concerned in the DPE methods because the design point $\boldsymbol{u}^*(y_T^1,\tau)$ for the threshold y_T^1 is at the origin by definition, which is a known vector. The cost of the DPE methods vary with the total number of thresholds selected accordingly. Regarding the efficiency of locating the design point $\boldsymbol{u}^*(y_T^I,\tau)$, it depends on the efficiency of the derivative approximation method in finding $\nabla_{\boldsymbol{u}}G$ shown in the 4th column, the root-finding algorithm (the *fzero* command in MATLAB) in finding $\hat{\beta}$ shown in the 5th column and the number of iterations needed which are indicated in the above discussions according to the line search of *Algorithm 2*.

According to the 3rd and 4th column in Table 3. 1, the DPE-EAD is the most efficient attributed to the outstanding computational efficiency of the EAD method in the derivative approximation. As evident from the 5th column, the root-finding procedures for computing $\hat{\beta}$ in the DPE-EAD and the DPE-AD methods are slightly more efficient than that in the DPE-ND method since the approximated derivatives $\nabla_{\boldsymbol{u}}G$ are more precise as shown later in Section 3.5.1.1. The precision of the approximated derivative $\nabla_{\boldsymbol{u}}G$ also affects the number of iterations needed in the line search optimization. As indicated in the above discussions, the DPE-ND needs more iterations on average in locating the design point $\boldsymbol{u}^*$ than the DPE-EAD and the DPE-

AD, which makes the DPE-ND method even less efficient than the other two methods.

In terms of the efficiency of the DPE-EAD, DPE-ND and DPE-AD methods when different response is considered, Table 3. 1 shows that the average time taken in locating the design point $\boldsymbol{u}^*(y_T^I, \tau)$ shown in the 3rd column and in computing the derivative $\nabla_{\boldsymbol{u}} G$ shown in the 4th column for the responses of $y(\tau) = x_4(\tau)$ and $y(\tau) = [\boldsymbol{F}_R]_1(\tau)$ considered have little differences in general, which indicates that the computational efficiency of the DPE method is not highly affected by the complexity of the response of interest. More specifically, the computational cost of the developed DPE-EAD method is slightly higher in locating $\boldsymbol{u}^*$ and computing $\nabla_{\boldsymbol{u}} G$ when a relatively more complex response of $y(\tau) = [\boldsymbol{F}_R]_1(\tau)$ is considered, while the computational cost is not necessarily higher in the DPE-ND and the DPE-AD methods.

The calculation time of the MC simulation is shown separately in the last column in Table 3. 1, which indicates the total time taken in generating the entire sample set as required according to the convergence test, i.e., for this example, it is 15000 samples of the earthquake time histories and the corresponding structural responses. In the MC simulation, the information of any responses can be computed through simple mathematical calculations from the evolutions of the structural system states, which are available in a generated sample set. The extra computation to find the reliabilities for different responses that consider different thresholds are negligible in the MC simulation.

According to the time required in the methods applied in the reliability estimations as summarized in Table 3. 1, the developed method of DPE-EAD is the most efficient and it substantially saves the computational cost compared to the DPE-ND and the MC simulation in this example when the selected number of thresholds is considered.

Table 3. 1 The computational costs of the DPE-EAD, DPE-ND, DPE-AD and the MC method in *Example 1*.

Design Point Excitation (DPE) method					**MC sim.**
Response of interest	Method	Finding reliabilities or $\boldsymbol{u}^*(y_T^l, \tau)$	Computing $\nabla_{\boldsymbol{u}} G$ (Avg.)	Root-finding algo. (Avg.)	Generating the sample set
$y = x_4(\tau)$	DPE-EAD	4.0 min. 9.5 s per threshold	4.9 s	2.6 s	4.8 h (1.15 s per sample)
	DPE-ND	2.1 h 5.2 min. per threshold	2.4 min.	5.4 s	
	DPE-AD	11.5 min. 27.6 s per threshold	22.9 s	3.0 s	
$y = [\boldsymbol{F}_R]_1(\tau)$	DPE-EAD	4.2 min. 12.7 s per threshold	6.7 s	3.1 s	
	DPE-ND	1.3 h 4.0 min. per threshold	2.3 min.	4.1 s	
	DPE-AD	8.6 min. 26.0 s per threshold	19.7 s	3.0 s	

The efficiencies of all the variations of the DPE methods are influenced by the time instant τ and the sampling time step Δt_D selected which define the size of $\boldsymbol{u}$, i.e., the number of unknows, in the optimization problem. The line search optimizations in DPE methods are expected to be more efficient in finding the design point $\boldsymbol{u}^*$ when the size of the variable $\boldsymbol{u}$, i.e., the number of unknowns, reduces. Thus, the DPE methods may be further improved by selecting a different sampling time step Δt_D for discretization. Table 3. 2 indicates the computational cost in the DPE-EAD, DPE-ND and DPE-AD when different sampling time step Δt_D are selected in finding

the reliabilities of the response $y(\tau) = x_4(\tau)$ where $\tau = 15$ s. It is found that when a larger sampling time step Δt_D is selected, the DPE methods are more efficient. The average computational efficiencies of the line search optimizations in finding $\boldsymbol{u}^*$ are shown in the 3rd column, in which the average time taken for both computing the derivatives $\nabla_{\boldsymbol{u}} G$ and the root-finding algorithm, as listed in the 4th and 5th column respectively, are improved with a larger Δt_D selected. However, this improvement comes at the cost of sacrificing the accuracies of the estimated reliabilities, as indicated by the maximum relative errors shown in Table 3. 2 in the final column. One may select an appropriate Δt_D in the DPE methods that estimate the reliabilities having relative errors within the maximum relative error allowed efficiently.

Table 3. 2 The computational costs of the DPE-EAD, DPE-ND, DPE-AD with different Δt_D selected.

Δt_D	Method	Line search in finding $\boldsymbol{u}^*(y_T^I, \tau)$ (Avg.)	Computing $\nabla_{\boldsymbol{u}} G$ (Avg.)	Root-finding algo. (Avg.)	Max. relative estimation error
0.005	DPE-EAD	15.5 s	6.0 s	5.4 s	0.8%
	DPE-ND	11.7 min.	5.6 min.	11.7 s	
	DPE-AD	34.3 s	24.2 s	5.9 s	
0.01	DPE-EAD	9.5 s	4.9 s	2.6 s	1%
	DPE-ND	5.2 min.	2.4 min.	5.4 s	
	DPE-AD	27.6 s	22.9 s	3.0 s	
0.02	DPE-EAD	5.7 s	3.8 s	1.1 s	4.2%
	DPE-ND	2.5 min.	67.5 s	2.5 s	
	DPE-AD	23.9 s	22.0 s	1.1 s	
0.05	DPE-EAD	3.6 s	2.5 s	0.6 s	6.8%
	DPE-ND	26.7 s	11.6 s	1.3 s	
	DPE-AD	21.5 s	20.4 s	0.6 s	

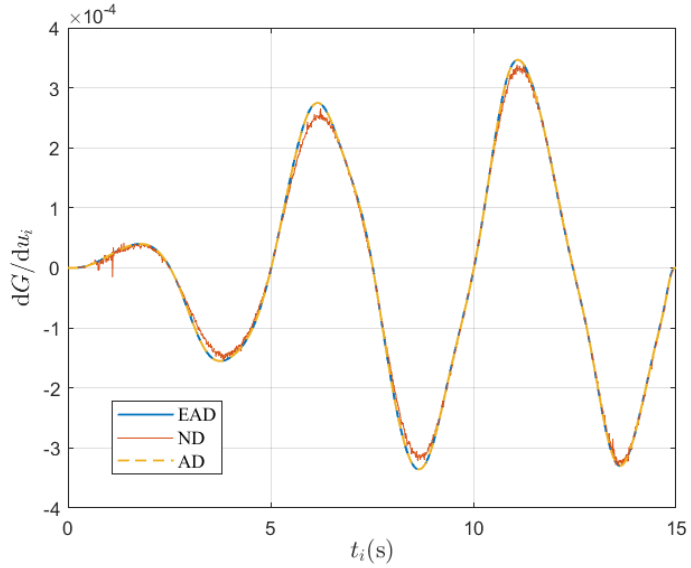
3.5.1.1 Computing the derivative $\nabla_{\boldsymbol{u}} G$

The discussions so far have been focused on the performance of the reliability estimations using the DPE-EAD, DPE-AD and DPE-ND methods. In this section, the estimation process of the derivative $\nabla_{\boldsymbol{u}} G$ is elaborated further. The accuracy and

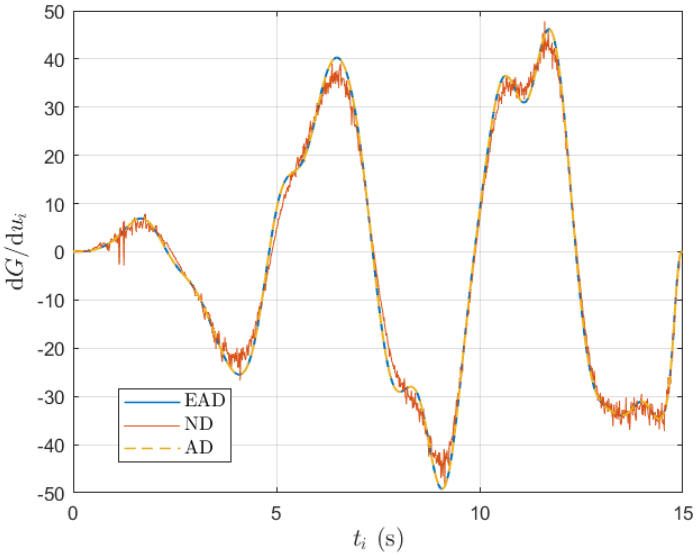
computational efficiency of the derivative $\nabla_{\boldsymbol{u}} G$ estimated by the EAD, ND and AD methods are discussed in the following lines.

The gradient $\nabla_{\boldsymbol{u}} G$ estimated at the first iteration step in the line search considering the threshold y_T^3 is selected for illustration for both responses $y(\tau) = x_4(\tau)$ and $y(\tau) = [\boldsymbol{F}_R]_1(\tau)$. Figure 3. 10 plots the gradient $\nabla_{\boldsymbol{u}} G$ estimated by the EAD, ND, and AD methods, where the vertical axis is the gradient of the LSF G with respect to u_i applied at the time t_i as shown in the horizontal axis. As shown in Figure 3. 10, the gradients $\nabla_{\boldsymbol{u}} G$ approximated by the EAD method agree with the AD method and is more precise than the ND method using the central-differences. It should be noted that proper increments of Δu_i are selected in the ND method of the central-differences in Eq. (3.15), such that the estimated gradient converges. Figure 3. 11 plots the gradient approximated by the central-differences with different Δu_i selected, demonstrating that the precision of the approximated gradient is directly affected by the chosen increment Δu_i. An improper selection of Δu_i, which leads to inaccurate approximations of $\nabla_{\boldsymbol{u}} G$, may ultimately cause failure in the root-finding algorithm in solving for the reliability index β or a divergence in the line search optimization in finding the design point $\boldsymbol{u}^*$. According to the implementation of the ND method in the examples considered, it is difficult and time-consuming to find a proper Δu_i for each of the element in the variable $\boldsymbol{u}$ and the $\nabla_{\boldsymbol{u}} G$ calculated by central-differences is noisy even with carefully selected increments of Δu_i. Variations of the finite-differences and other numerical estimates of derivative methods [88] that produce a

higher precision can be adopted, but they are more expensive in terms of the computational cost and consequently weaken the computational advantage of the DPE method over the MC simulation.



(a) $y = x_4(\tau)$ with $y_T^3 = 0.001\text{m}$



(b) $y = [\boldsymbol{F}_R]_1(\tau)$ with $y_T^3 = 150\text{N}$

Figure 3. 10 The gradient $\nabla_{\boldsymbol{u}} G$ approximated by the EAD, ND and AD algorithms.

As pointed out in the previous section, more iterations are required in the DPE-ND method, where the derivative $\nabla_{\boldsymbol{u}} G$ approximated lacks precision, than the DPE-

EAD and the DPE-AD methods in the line search method in finding the design point $\boldsymbol{u}^*$. Table 3. 1 compares the computational cost of the root-finding algorithm in the line search method, i.e., step 3 in *Algorithm 2*, using the $\nabla_{\boldsymbol{u}} G$ estimated by the three different approaches, which shows that the efficiency of the root-finding algorithm is also affected by the accuracy of the $\nabla_{\boldsymbol{u}} G$ estimated.

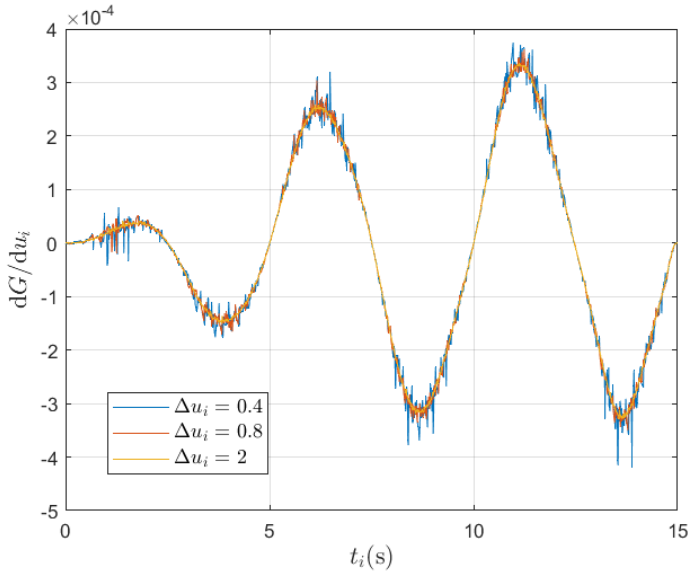


Figure 3. 11 The gradient $\nabla_{\boldsymbol{u}} G$ approximated by the central-differences algorithm with different Δu_i selected.

The average time taken in computing the derivative $\nabla_{\boldsymbol{u}} G$ using EAD, ND and AD methods are summarized in the 4th column of Table 3. 1. The developed method of the EAD has an outstanding computational efficiency over the ND and the AD methods. Since the derivative $\nabla_{\boldsymbol{u}} G$ is computed repeatedly in the line search optimization (*Algorithm 2*), an efficient derivative estimation method essentially saves the computational cost of the DPE method. Table 3. 3 compares the number of earthquake simulations and the structural analyses required in each method, which is an indication of the computational costs and explains the observation shown in the 4th

column of Table 3. 1. The ND method through finite-differences is especially time consuming compared to the EAD and AD methods because the process is taken repeatedly in the calculation of the structural response $y(\boldsymbol{u} \pm \Delta u_i, \tau)$ when each element in the input vector $\boldsymbol{u}$ changes. According to the central-differences scheme as in Eq. (3.15), the number of the responses $y(\boldsymbol{u} \pm \Delta u_i, \tau)$ required to be computed increases proportionally with the size of the input vector $\boldsymbol{u}$, n in the ND method, which is usually a huge value that leads to costly computation. N_1, N_2 and N_3 are the total number of iterations needed in the line search algorithm using the derivative $\nabla_{\boldsymbol{u}} G$ estimated by the EAD, ND and AD respectively. It should be noted that N_1, N_2 and N_3 can be different because the precision of the derivative $\nabla_{\boldsymbol{u}} G$ approximation affects the predictions in line search.

Table 3. 3 Comparison of the number of structural response analyses required.

Method	The number of structural response analyses involved
DPE-EAD	N_1
DPE-ND	$N_2 \cdot (2n)$
DPE-AD	N_3
MC	The number of samples simulated (N_{MC})

3.5.1.2 System reliability - reliability over a time period

To find the reliability for a response over the entire event of an earthquake, the reliability estimated at a sequence of time instants is required. Again, the responses of $y = x_4$ and $y = [\boldsymbol{F}_R]_1$ considered above are examined, in which the thresholds $y_T = 0.01\,\text{m}$ and $y_T = 1800\,\text{N}$ are chosen for x_4 and $[\boldsymbol{F}_R]_1$ respectively. Assuming that the total duration of the earthquake is $T = 50\text{s}$, the time instants $[\tau_J] = [J]\,\text{s}$ for $J = 1,2,\ldots,50$ evenly spread in the earthquake with $\Delta\tau = 1\text{s}$ are

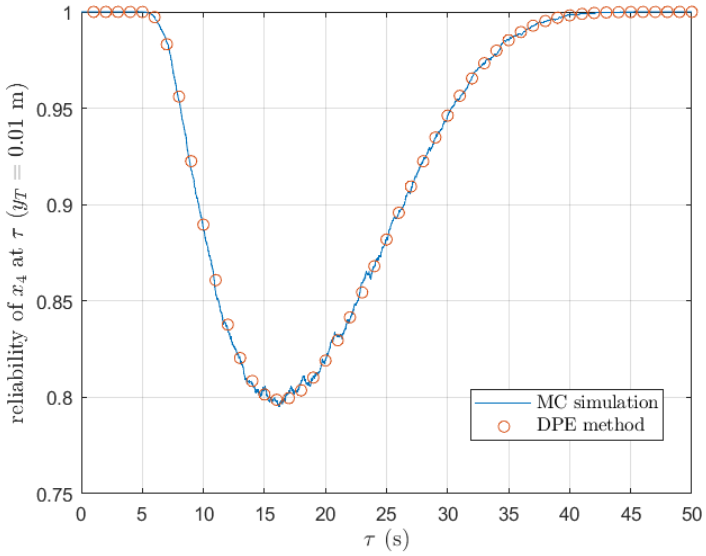
selected.

The DPE-EAD method introduced in this work is adopted and examined here to find the reliability for each LSF $G_J(\boldsymbol{u}, y_T, \tau_J)$ considered in the Series system as it is accurate and is the most efficient in the variations of the DPE method. To find the initial guess $\hat{\boldsymbol{u}}^*$ of the design point for the LSFs $G_J(\boldsymbol{u}, y_T, \tau_J)$, the starting point at $\tau_J = 15\text{s}$ is considered where the design point $\boldsymbol{u}^*(y_T, \tau_J = 15\text{s})$ was obtained in the above examples. The initial guesses $\hat{\boldsymbol{u}}^*$ of the design point for the LSFs $G_J(\boldsymbol{u}, y_T, \tau_J)$ at the nearby time instants are approximated gradually by time shifting. An average of 1 iteration is required in *Algorithm 2* to search for the design points $\boldsymbol{u}^*$ for the other time instants τ_J considered, which shows that the initial guess $\hat{\boldsymbol{u}}^*$ obtained by time shifting provides a good approximation.

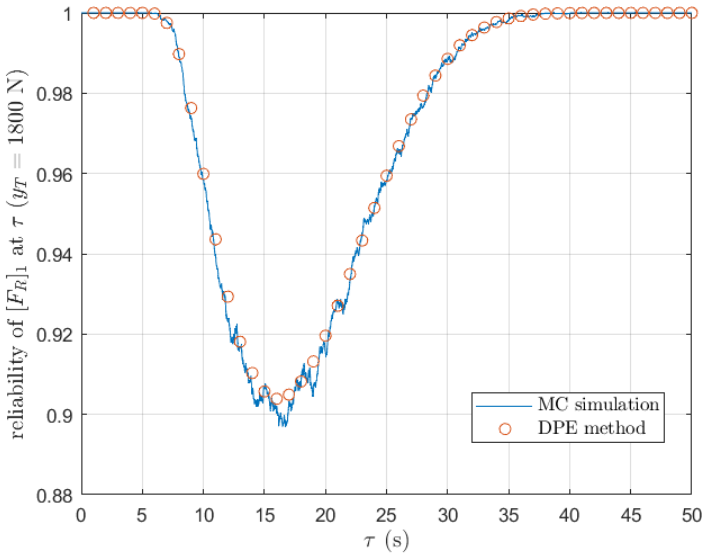
The reliabilities estimated by the DPE-EAD method are plotted in Figure 3. 12, where the reliability is indicated by the vertical axis and the corresponding time instant τ considered is indicated by the horizontal axis. To demonstrate the accuracy of the results obtained by DPE-EAD method, the reliabilities estimated by the MC simulations of 15000 samples are also plotted in the figure. It should be noted that the reliability $P_R(\tau) = P(y(\tau) \leq y_T)$ at any time instant τ is available from the MC sample set, given by Eq. (3.33). The figure indicates that the MC estimates appear to be noisy in the strong motion period from the sample set of 15000 samples, but they are acceptable as the maximum relative error is found to be 1% and 0.8% in estimating the reliability of $|x_4(\tau)|$ and $|F_R(\tau)|$ respectively, according to the convergence test.

After investigations, the unsmooth shape can be eliminated with a substantially large sample set but is hardly avoided. And the MC simulation is not efficient in this case for generating a substantially larger sample set. The maximum relative estimation differences between the MC and the DPE method is about 0.6% observed at τ_{23} for the response $|x_4|$, and 0.9% at τ_{19} for the response $|[\boldsymbol{F}_R]_1|$ with the thresholds y_T considered in the examples.

In terms of the reliability over the period T, it is the System reliability (P_R) computed by Eq. (3.29) using the β_J and α_J obtained above in finding the design point $\boldsymbol{u}^*(y_T, \tau_J)$ for the time instances τ_J considered in T. In this example, the reliabilities of $|x_4|$ and $|F_R|$ over the time period T are $P_R = 0.593$ and $P_R = 0.783$ respectively, according to the DPE-EAD method. The MC estimate of the reliability over the period T is given by $P_R = P(\max(y(\tau)) \leq y_T) = \frac{\text{No.of samples of } \max(y(\tau)) \leq y_T}{\text{Total No.of the samples simulated}}$, where τ belongs to any time instants in the period of T, i.e., $\tau \in [0,50]$ in this case. According to the MC sample set of 15000 samples, the reliabilities of $|x_4|$ and $|F_R|$ are found to be $P_R = 0.604$ and $P_R = 0.803$, with relative estimation errors of 0.6% and 0.2%, respectively. The relative differences between the DPE-EAD and the MC simulations results are 1.8% and 2.5% in the reliability estimations of $|x_4|$ and $|F_R|$ over the time period T, respectively, which shows that the developed DPE-EAD method is reasonably accurate in the reliability estimations for a structural system with Bouc-Wen nonlinearities subjected to earthquake excitations over a time period.



(a) $y = |x_4(\tau)|$ with $y_T = 0.01$ m



(b) $y = |\boldsymbol{F}_R(\tau)|$ with $y_T = 1800$ N

Figure 3. 12 The reliability estimated by the DPE method and the MC simulations at a sequence of time instant τ.

Regarding the computational cost, the time required for the DPE method depends on the number of time instances considered in finding the System reliability. In this example, with $\Delta\tau = 1\text{s}$ selected and $J = T/\Delta\tau = 50$ time instances considered, as shown in Figure 3. 12, the DPE-EAD method takes about 18.6 minutes. In contrast, the MC simulations take 18 hours to generate 15000 samples of the earthquake time

histories and the corresponding structural responses over the period of $T = 50\text{s}$, as required according to the convergence test discussed earlier. The DPE-EAD method demonstrates significantly greater efficiency than the MC simulations in determining the reliability over a time period with a very good accuracy as indicated in the previous paragraph.

The choice of the sampling time step $\Delta\tau$, determining the total number of time instants τ_J considered in the System reliability, affects the computational efficiency of the DPE methods in finding reliability over a time period. Less computational cost is required if a smaller number of time instants τ_J is concerned. We may adjust $\Delta\tau$ to find an optimal estimation frequency that finds the reliability over a time period efficiently and accurately as required. To demonstrate how $\Delta\tau$ affects the accuracy and the efficiency of the estimations, the reliability of the response $y = |x_4|$ over $T = 50\text{s}$ with $y_T = 0.01\text{m}$ considered is estimated with different $\Delta\tau$ selected. Table 3. 4 presents the estimated System reliabilities, the relative estimation errors compared to the MC result and the computational time taken in the 3rd, 4th and 5th column respectively using the DPE-EAD method. $\Delta\tau = 1\text{s}$ is selected in this example under the consideration of both the computational efficiency and accuracy.

Table 3. 4 The accuracy and efficiency of the System reliability estimated by the DPE-EAD method with different $\Delta\tau$ selected.

$\Delta\tau$	The number of τ_J considered (dim (J))	Estimated reliability	Relative error compared to the MC result	Computational time
0.5	100	0.6	0.7 %	53.1 min.
1	50	0.593	1.8 %	18.6 min.
1.5	33	0.571	5.4 %	8.8 min.
2	25	0.55	9.0 %	6.3 min.

3.5.2 Example 2: *A 10-DoF system with polynomial nonlinearity subjected to earthquake excitations.*

A 10-storey shear building subjected to earthquake ground motions adopted in [91] is considered in this example. The 10-storey shear building model is defined by a 10-degree-of-freedom system through the following differential equation:

$$\boldsymbol{M}\ddot{\boldsymbol{x}}(t) + \boldsymbol{C}\dot{\boldsymbol{x}}(t) + \boldsymbol{K}\big(\boldsymbol{x}(t)\big)\boldsymbol{x}(t) = \boldsymbol{F}(t) \tag{3.34}$$

where the displacement vector $\boldsymbol{x}$ is denoted as $\boldsymbol{x} = [x_1, x_2, \dots, x_{10}]^T$. The mass matrix and damping matrix are written by:

$$\boldsymbol{M} = \begin{bmatrix} m_1 & 0 & 0 & \cdots & 0 \\ 0 & m_2 & 0 & \cdots & 0 \\ \vdots & \vdots & \vdots & \ddots & \vdots \\ 0 & 0 & 0 & \cdots & m_{10} \end{bmatrix}, \quad \boldsymbol{C} = \begin{bmatrix} c_1 + c_2 & -c_2 & 0 & \cdots & 0 \\ -c_2 & c_2 + c_3 & -c_3 & \cdots & 0 \\ \vdots & \vdots & \vdots & \ddots & \vdots \\ 0 & 0 & 0 & -c_{10} & c_{10} \end{bmatrix}$$

with $\boldsymbol{K}\big(\boldsymbol{x}(t)\big)$ being a displacement dependent stiffness matrix defined as:

$$\boldsymbol{K}\big(\boldsymbol{x}(t)\big) = \begin{bmatrix} k_1 + k_2 & -k_2 & 0 & \cdots & 0 \\ -k_2 & k_2 + k_3 & -k_3 & \cdots & 0 \\ \vdots & \vdots & \vdots & \ddots & \vdots \\ 0 & 0 & 0 & -k_{10} & k_{10} \end{bmatrix}$$

and $k_i = k^i \cdot (1 + \epsilon \cdot (\frac{\delta x_i(t)}{\delta x_{ref}})^2)$ for $i = 1,2,\dots,10$, where $\epsilon = 0.1$ and $\delta x_{ref} = 0.02\text{m}$ are selected. $\delta x_i(t) = x_i(t) - x_{i-1}(t)$ represents the relative displacement between adjacent floors and $x_0(t) = 0$. It is assumed that $m_1 = m_2 = \cdots = m_{10} = 10\ \text{Mg}$, $k_1 = k_2 = k_3 = 40\ \text{MN/m}$, $k_4 = k_5 = k_6 = 36\ \text{MN/m}$, $k_7 = k_8 = k_9 = k_{10} = 32\ \text{MN/m}$, $c_i = 2\zeta_i\sqrt{m_i k_i}$, and $\zeta_i = 0.04$ for $i = 1,2,\dots,10$.

The excitation $\boldsymbol{F}(t)$ has the form $\boldsymbol{F}(t) = [m_1, m_2, \dots, m_{10}]^T \cdot f(t)$. The stochastic earthquake model used in the benchmark problem is adopted, which simulates the ground excitation $f(t)$ by a modulated filtered white noise defined as:

$$f(t) = {\omega_1}^2 v_{f1}(t) + 2\zeta_1\omega_1 v_{f2}(t) - {\omega_2}^2 v_{f3}(t) - 2\zeta_2\omega_2 v_{f4}(t) \tag{3.35}$$

where $\boldsymbol{v}_f = [v_{f1}, v_{f2}, v_{f3}, v_{f4}]^T$ is the state vector in the following state-space equation defining the ground motion:

$$\dot{\boldsymbol{v}}_f(t) = \begin{bmatrix} 0 & 1 & 0 & 0 \\ -{\omega_1}^2 & -2\zeta_1\omega_1 & 0 & 0 \\ 0 & 0 & 0 & 1 \\ {\omega_1}^2 & 2\zeta_1\omega_1 & -{\omega_2}^2 & -2\zeta_2\omega_2 \end{bmatrix} \cdot \boldsymbol{v}_f(t) + \begin{bmatrix} 0 \\ w(t) \\ 0 \\ 0 \end{bmatrix} \tag{3.36}$$

The white noise input $w(t)$ is defined as $w(t) = h(t) \cdot I_w \cdot u(t)$, where $u(t)$ denotes a standard white noise, I_w denotes the intensity of the white noise, and

$$h(t) = \begin{cases} \dfrac{t}{2} & \text{for } 0 \le t \le 2 \\ 1 & \text{for } 2 \le t \le 10 \\ e^{(-0.1(t-10))} & \text{for } t \ge 10 \end{cases} \tag{3.37}$$

The values $\omega_1 = 15\ \text{rad/s}$, $\omega_2 = 0.3\ \text{rad/s}$, $\zeta_1 = 0.8$, $\zeta_2 = 0.995$ and $I_w = 0.08\ \text{m}^2/\text{s}^3$ are selected for the model of the filter. The input-sampling time step of $\Delta t_D = 0.01\text{s}$ is selected for the discretization of the white noise $u(t)$ in this example and the integration time step of $\Delta t_I = 0.01\text{s}$ is selected in the EAD method in computing the derivative $\nabla_{\boldsymbol{u}} G$.

The reliability of the 1st storey acceleration, i.e., $y(\tau) = \ddot{x}_1(\tau)$ is examined, in which the time instant $\tau = 10\text{s}$ is selected as it is in the strong motion period of the seismic model described by Eq. (3.35) - (3.37) and a set of thresholds $[y_T^I] = \pm[1.5 \cdot 10^{-3} \cdot (I-2)]\ \text{m/s}^2$ where $I = 3,4,\dots,20$ is considered. According to the structural model, the 1st storey acceleration is $\ddot{x}_1(\tau) = \left[-\boldsymbol{M}^{-1} \cdot \left(\boldsymbol{C}\dot{\boldsymbol{x}}(\tau) + \boldsymbol{K}\big(\boldsymbol{x}(\tau)\big)\boldsymbol{x}(\tau)\right)\right]_1$, which is a nonlinear output as $\boldsymbol{K}\big(\boldsymbol{x}(t)\big)$ is state-dependent. As the EAD method developed in this work considers linear output only, the state-dependent

stiffness matrix $\boldsymbol{K}(\boldsymbol{x}(t))$ is evaluated at each time instant and considered as a time-varying scalar parameter in the EAD method. The DPE-EAD, DPE-ND and DPE-AD methods are applied to estimate the reliability, in which $\lambda_{max} = 0.2$ and the first two thresholds $y_T^1 = 0\ \mathrm{m/s^2}$ and $y_T^2 = 10^{-8}\ \mathrm{m/s^2}$ are selected in *Algorithm 1* to find the initial guess $\widehat{\boldsymbol{u}}^*$. Figure 3. 13 plots the 1st storey acceleration $\ddot{x}_1(t)$ of the linear and the nonlinear system subjected to the ground excitation $f(t)$ with the input $\boldsymbol{u}^*(y_T^2, \tau)$ which shows that the response behaviour of the nonlinear system can be approximated by the corresponding linear system, i.e., $\epsilon = 0$, when the threshold y_T^2 is considered for the response $\ddot{x}_1(\tau)$. The chosen threshold $y_T^2 = 10^{-8}\ \mathrm{m/s^2}$ is sufficiently small in which case the design point $\boldsymbol{u}_L^*(y_T^2, \tau)$ for the corresponding linear system computed by Eq. (3.13) can be used as an approximation to $\boldsymbol{u}^*(y_T^2, \tau)$ for the nonlinear system.

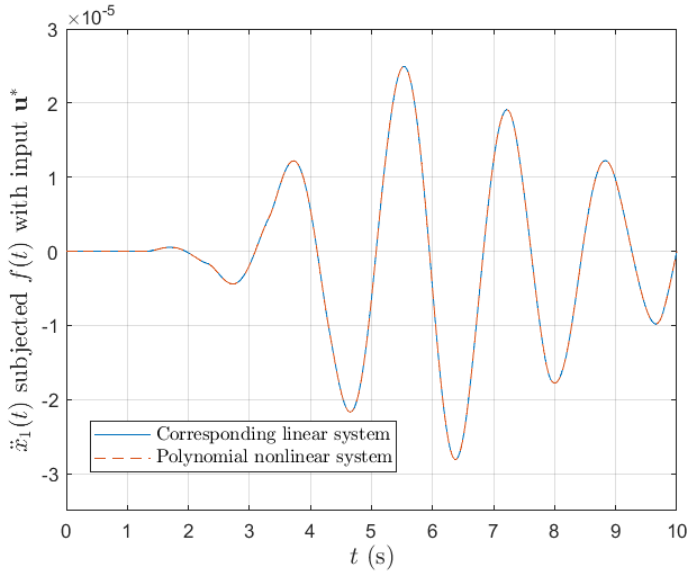


Figure 3. 13 The 1st storey acceleration $\ddot{x}_1(t)$ of the linear and the nonlinear system subjected to the ground excitation $f(t)$ with the input $\boldsymbol{u}^*(y_T^2, \tau)$.

The reliabilities of the absolute responses of $y(\tau) = |\ddot{x}_1(\tau)|$ is computed by Eq. (3.8) using the reliabilities obtained by the DPE-EAD, DPE-AD and DPE-ND methods and are plotted by scatter points in Figure 3. 14. The CDF of $|\ddot{x}_1(\tau)|$ obtained by the sample set of 20000 MC simulations, which is sufficient when a maximum relative error of 3% is considered according to the convergence test, is plotted on the same figure as a reference. For the reliabilities obtained by different DPE methods as shown in Figure 3. 14, similar results are obtained by the DPE-EAD and DPE-AD methods while a small difference is observed for the DPE-ND method. Compared to the MC estimates, the maximum relative errors in reliability estimations are 1.7% found at $y_T^6 = 6 \cdot 10^{-3}\ \mathrm{m/s^2}$ for the DPE-EAD and the DPE-AD methods and 1.9% found at $y_T^8 = 9 \cdot 10^{-3}\ \mathrm{m/s^2}$ for the DPE-ND method. In addition, the DPE-EAD and DPE-AD methods take an average of 1.5 iterations in the line search of *Algorithm 2* to find the design point $\boldsymbol{u}^*$ for each LSF $G(\boldsymbol{u}, y_T^I, \tau)$. The DPE-ND method takes an average of 2 iterations in the line search of *Algorithm 2* to find the design point $\boldsymbol{u}^*$. One specific example of the design points $\boldsymbol{u}^*(y_T^3, \tau)$ found by different methods is shown in Figure 3. 15. The results show that the design points obtained by the DPE-EAD and DPE-AD methods are identical while having discrepancy with that obtained by the DPE-ND method. The differences in the design points and number of iterations required for the DPE-ND method are caused by the gradient $\nabla_{\boldsymbol{u}} G$ estimated by the ND using the finite difference method being less accurate.

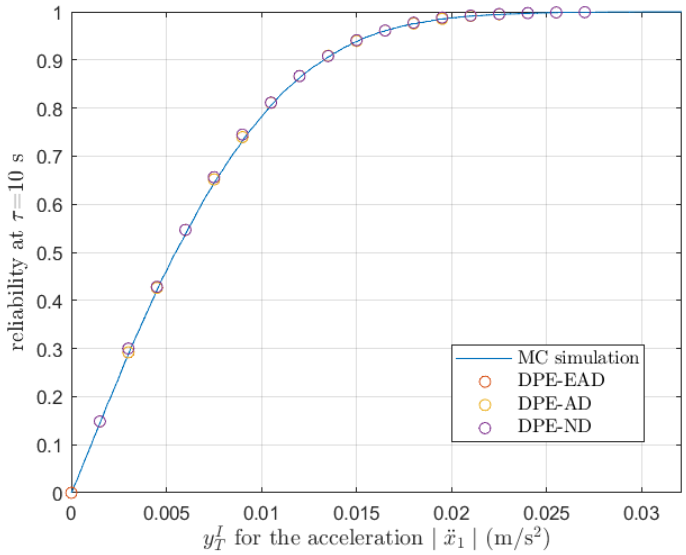


Figure 3. 14 The reliability of $|\ddot{x}_1(\tau)|$ at $\tau = 10\text{s}$ approximated by the DPE methods for a sequence of thresholds versus the CDF of which obtained by the MC simulations.

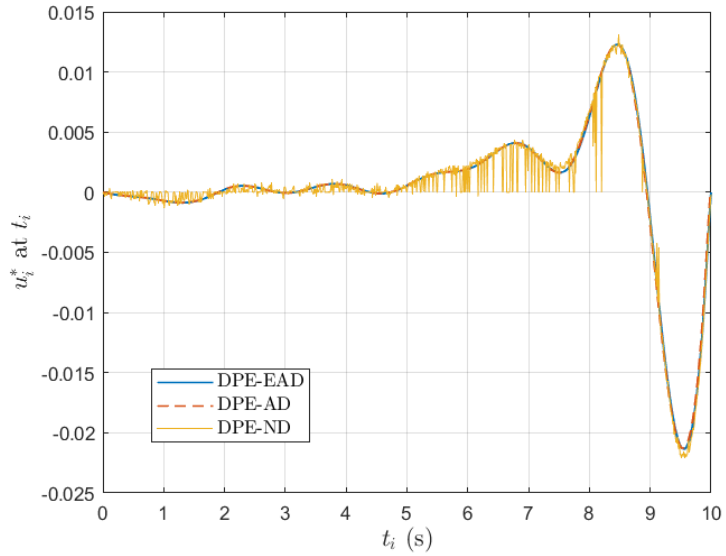


Figure 3. 15 The design point $\boldsymbol{u}^*(y_T^3, \tau)$ found by the DPE-EAD, DPE-AD and the DPE-ND methods for $y = \ddot{x}_1(\tau)$ with $y_T^3 = 1.5 \cdot 10^{-3}$ m/s^2.

Figure 3. 16 plots the example of the gradient $\nabla_{\boldsymbol{u}} G$ estimated at the first iteration step in the line search considering the threshold y_T^3 using the EAD, ND, and AD methods. The gradient $\nabla_{\boldsymbol{u}} G$ estimated by the EAD agrees with that estimated by the AD method, which explains why the design points as well as the reliabilities obtained by the DPE-EAD and DPE-AD methods are identical and same number of iterations

are required in the line search algorithm as mentioned above. The failure of the ND method to capture the gradient of responses $\ddot{x}_1$ with respect to specific u_i is potentially due to an improper selection of the increment Δu_i. The convergence test is performed to obtain better selection of the increment Δu_i, but no substantial improvement is observed. It suggests that large computational cost is required to find a proper increment Δu_i in the ND method. The inaccurate approximation of $\nabla_{\boldsymbol{u}} G$ causes a divergence in finding the design point $\boldsymbol{u}^*$ and failure in the root-finding algorithm in the line search optimization.

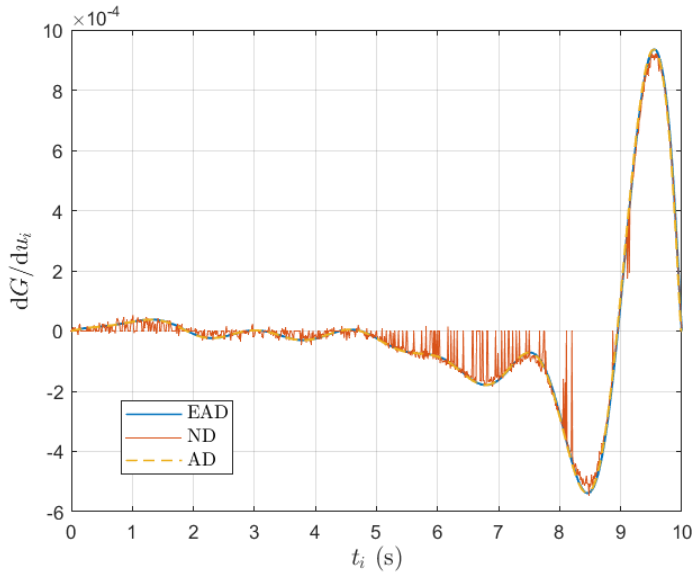


Figure 3. 16 The gradient $\nabla_{\boldsymbol{u}} G$ approximated by the EAD, ND and AD algorithms, where $y = \ddot{x}_1(\tau)$ and the threshold $y_T^3 = 1.5 \cdot 10^{-3}\ \mathrm{m/s^2}$ are considered.

Table 3. 5 summarizes the calculation time required by the DPE-EAD, the DPE-ND, the DPE-AD and the MC simulation in finding the reliabilities of $|\ddot{x}_1(\tau)|$ shown in Figure 3. 14. The computational cost of the MC simulation indicated in the last column refers to the time in generating the entire sample set of 20000 simulations as required according to the convergence test. The calculation time of the DPE methods

in finding the reliabilities for all $(\dim(I)+1)$ thresholds and the average time taken for per threshold are shown in the 3rd column in Table 3. 5. The efficiency of the derivative estimation methods and the root-finding algorithm are highlighted in the 4th and 5th column respectively. Attributed to the great accuracy and efficiency of the EAD method in computing the derivative $\nabla_{\boldsymbol{u}} G$, the DPE-EAD method developed in this work is the most robust and efficient among the three DPE methods and it substantially saves the computational cost compared to the MC simulation.

Compared to the computational cost in *Example 1* shown in Table 3. 1, the DPE-EAD method takes less time in the reliability estimations for per threshold on average when a higher-order structural system is considered. The size of state vector $\boldsymbol{x}$ of the structural system considered in this example is about twice larger than that considered in *Example 1*. By comparing the 4th and 5th columns in Table 3. 1 and Table 3. 5, it is found that the derivative estimation and the root-finding algorithm are more efficient in this example. This is potentially due to a former time instant $\tau = 10\text{s}$ is considered in this example, thus length of the integration time intervals and the size of the input vector $\boldsymbol{u}$, i.e., the number of unknows are smaller. According to this observation, the computational efficiency of the DPE method is not necessarily affected by the size or the complexity of the nonlinearity of the structural system but is significantly influenced by the time instant τ and the size of $\boldsymbol{u}$, i.e., the number of unknows considered in the optimization problem. In contrast, the time taken in MC simulation is substantially larger in this example. This is not only because a larger sample set is

required in this example, but also because the average time taken in generating per sample is longer as shown in the final column. Apparently, the computational efficiency of the MC simulation is apparently affected by size and the complexity of the nonlinearity of the structural system. The observations suggests that the DPE-EAD is potentially more beneficial over the MC simulation in the application to complex systems.

Table 3. 5 The computational costs of the DPE-EAD, DPE-ND, DPE-AD and the MC method in *Example 2*.

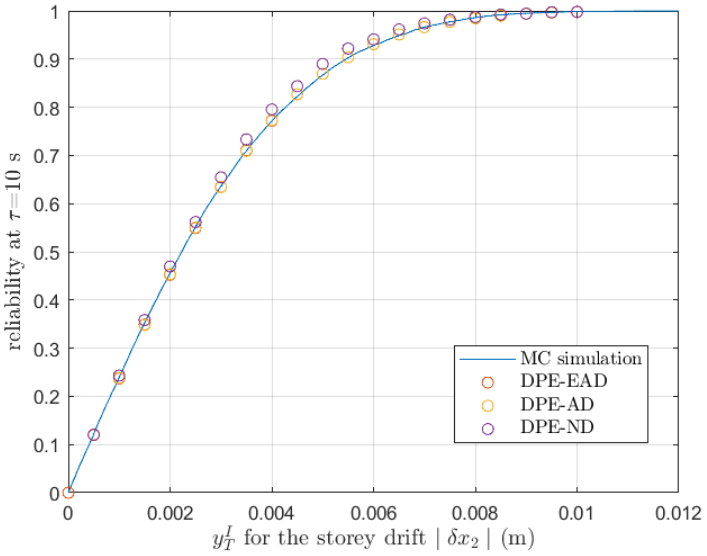
Design Point Excitation (DPE) method					**MC sim.**
Response of interest	Method	Finding reliabilities or $\boldsymbol{u}^*(y_T^l, \tau)$	Computing $\nabla_{\boldsymbol{u}} G$ (Avg.)	Root-finding algo. (Avg.)	Generating the sample set
$y = \ddot{x}_1(\tau)$	DPE-EAD	1.7 min. 5.7 s per threshold	3.1 s	1.4 s	12.9 h (2.3 s per sample)
	DPE-ND	2.1 h 7.1 min. per threshold	3.4 min.	4.0 s	
	DPE-AD	8.8 min. 29.2 s per threshold	26.1 s	1.7 s	
$y = \delta x_2(\tau)$	DPE-EAD	2.0 min. 6.0 s per threshold	2.9 s	1.6 s	
	DPE-ND	2.5 h 7.4min. per threshold	3.6 min.	4.4 s	
	DPE-AD	8.6 min. 25.9 s per threshold	22.6 s	1.9 s	
$y = \delta x_{10}(\tau)$	DPE-EAD	1.7 min. 5.5 s per threshold	3.0 s	1.4 s	
	DPE-ND	2.0 h 6.5 min. per threshold	3.1 min.	4 s	
	DPE-AD	7.6 min. 25.5 s per threshold	22.6 s	1.5 s	

3.5.2.1 System reliability

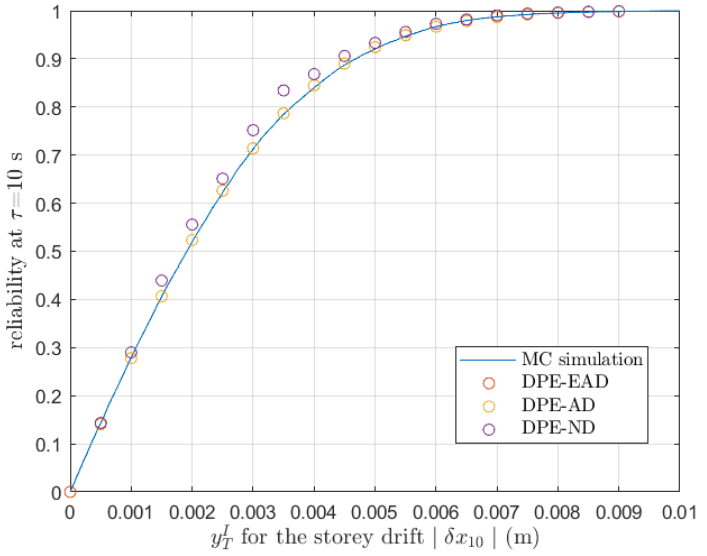
The reliabilities of the structural system having the failure criteria defined by multiple LSFs in a Series system and a Parallel system are both examined. Here in the example, the failure criteria on the response of the 2nd storey drift, i.e., $y(\tau) = \delta x_2(\tau) = x_2(\tau) - x_1(\tau)$ and the 10th storey drift, i.e., $y(\tau) = \delta x_{10}(\tau) = x_{10}(\tau) - x_9(\tau)$ are

considered where $\tau = 10\text{s}$ is selected. The componential LSFs $G_1(\boldsymbol{u}, y_{T_1}^I, \tau)$ and $G_2(\boldsymbol{u}, y_{T_2}^I, \tau)$ are constructed for the response $\delta x_2(\tau)$ and $\delta x_{10}(\tau)$ respectively in which the thresholds of $[y_{T_1}^I] = \pm[0.5 \cdot 10^{-3} \cdot (I-2)]$ m where $I = 3,4,\dots,22$ and $[y_{T_2}^I] = \pm[0.5 \cdot 10^{-3} \cdot (I-2)]$ m where $I = 3,4,\dots,20$ are selected. The DPE methods are applied to find the design point $\boldsymbol{u}^*$ for each response that considers a single componential LSF of either G_1 or G_2 only. The corresponding reliability indexes β and direction vectors $\boldsymbol{\alpha}$ of the $\boldsymbol{u}^*$ obtained are used in Eq. (3.27) and Eq. (3.28) to compute the System reliability. In finding the initial guesses $\widehat{\boldsymbol{u}}^*$, $\lambda_{max} = 0.2$ and the first two thresholds $y_{T_1}^1 = y_{T_2}^1 = 0\text{m}$ and $y_{T_1}^2 = y_{T_2}^2 = 10^{-8}\text{m}$ are selected in *Algorithm 1* for both of the responses $\delta x_2(\tau)$ and $\delta x_{10}(\tau)$. The reliabilities of the absolute responses of $|\delta x_2(\tau)|$ and $\delta|x_{10}(\tau)|$ obtained by the DPE methods are plotted in Figure 3. 17 by scatter points and compared to the CDF of $|\delta x_2(\tau)|$ and $\delta|x_{10}(\tau)|$ obtained by the MC sample set of 20000 simulations. As shown in the figures, the reliability estimated by the DPE-EAD and the DPE-AD method are identical and is more accurate than that found by the DPE-ND method. The maximum relative differences of the estimations in the DPE-EAD and the DPE-AD methods are found to be 1.4% at $y_{T_1}^3 = 1.5 \cdot 10^{-3}$ m for the response $\delta x_2(\tau)$ and 0.8% at $y_{T_2}^4 = 2 \cdot 10^{-3}$ m for the response $\delta x_{10}(\tau)$, and those in the DPE-ND method are found to be 3.3% at $y_{T_1}^7 = 3.5 \cdot 10^{-3}$ m for the response $\delta x_2(\tau)$ and 6.3% at $y_{T_2}^7 = 3.5 \cdot 10^{-3}$ m for the response $\delta x_{10}(\tau)$. The results depicted in Figure 3. 17 show that the DPE-EAD method developed in this work estimates the reliabilities of the responses

$|\delta x_2(\tau)|$ and $\delta|x_{10}(\tau)|$ accurately. Details of the computational cost of the DPE methods and the MC simulation for reliability estimations are summarized in Table 3. 5. Once the design points $\boldsymbol{u}^*$ for all the componential LSFs considered are obtained, the extra computations in computing the System reliability by Eq. (3.27) and Eq. (3.28) are negligible.



(a) $y = |\delta x_2(\tau)|$



(b) $y = |\delta x_{10}(\tau)|$

Figure 3. 17 The reliability of $|\delta x_2(\tau)|$ and $|\delta x_{10}(\tau)|$ at $\tau = 10\text{s}$ approximated by the DPE methods for a sequence of thresholds versus the CDF of which obtained by the MC simulations.

If the failure criterion is defined by a Series system, the failure condition refers to any of the responses, either δx_2 or δx_{10}, exceeding the thresholds considered in their corresponding componential LSFs, i.e., $G_1 \leq 0$ or $G_2 \leq 0$. The thresholds of $y_{T_1}^8 = 4 \cdot 10^{-3}$, $y_{T_1}^{12} = 6 \cdot 10^{-3}$ and $y_{T_1}^{14} = 7 \cdot 10^{-3}$ in (m) which has the corresponding reliability of about 80%, 90% and 95% are concerned for δx_2 in G_1 and a sequence of ascending thresholds $\left[y_{T_2}^I\right]$ for $I = 3,4,\ldots,20$ are concerned for δx_{10} in G_2. Figure 3. 18 presents the reliabilities of the Series system computed by Eq. (3.27) using the reliability indexes β and their direction vectors $\boldsymbol{\alpha}$ obtained by the DPE-EAD method with the reliabilities estimated according to the MC sample set of 20000 simulations. The System Reliabilities are shown in the vertical axis versus the thresholds considered for the response δx_{10} in G_2 shown in the horizontal axis. Each set of the scatter points specifies the System Reliabilities for the example of one specific threshold considered for δx_2 in G_1 as specified in the legends and a sequence of ascending thresholds $\left[y_{T_2}^I\right]$ considered for δx_{10} in G_2. The maximum relative difference of the estimations between the DPE-EAD method and the MC simulations in the examples is found to be 1.4% in finding the System Reliabilities for a Series system.

If the failure condition is defined by both responses δx_2 and δx_{10} exceeding the thresholds considered in their corresponding componential LSFs, i.e., $G_1 \leq 0$ and $G_2 \leq 0$, it is a Parallel system. Again, the thresholds of $y_{T_1}^8$, $y_{T_1}^{12}$ and $y_{T_1}^{14}$ are selected for the response of δx_2 in G_1 and the sequence of thresholds $y_{T_2}^I$ for $I =$

$3,4,\ldots,20$ is considered for the response of δx_{10} in G_2. Figure 3. 19 presents the reliabilities of the Parallel system computed by Eq. (3.28) using the reliability indexes β and their direction vectors $\boldsymbol{\alpha}$ obtained by the DPE-EAD method with the reliabilities estimated according to the MC sample set of 20000 simulations. The maximum relative difference between the DPE-EAD method and the MC simulations is found to be 0.6% in finding the System Reliabilities for a Parallel system.

The observation suggests that the reliability indexes β and the direction vectors $\boldsymbol{\alpha}$ found by the DPE-EAD method are sufficiently accurate to be used in Eq. (3.27) or Eq. (3.28) to find the System Reliability when multiple response measurement criteria are considered. The DPE-EAD method is efficient and accurate in calculating the System reliabilities of either a Series system or a Parallel system defined by multiple LSFs.

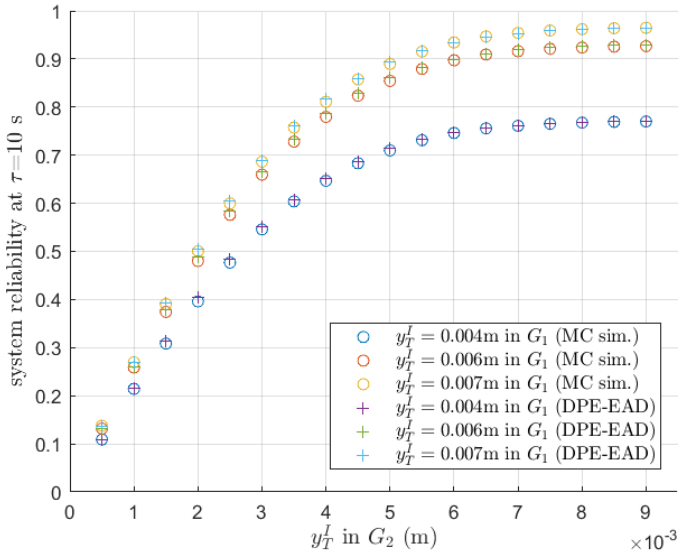


Figure 3. 18 Series system reliability approximated by the DPE method and MC simulations.

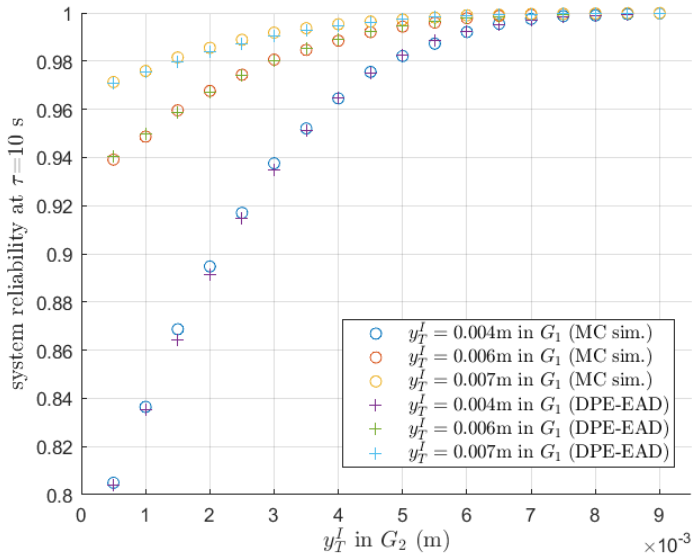


Figure 3. 19 Parallel system reliability approximated by the DPE method and MC simulations.

3.6 Conclusion

In this chapter, an effective reliability method for seismic reliability evaluation, the Design Point Excitation (DPE) method, is briefly introduced. A line search optimization method is suggested to solve the optimization problem that defines the design point crucial for computing reliability. A key part in the line search algorithm is to repeatedly compute the gradient of the LSF. To improve the DPE method, an Euler-Analytical estimate of the Derivatives (EAD) is developed and elaborated in this chapter to estimate the gradient of interest in the line search iterations. The located design points are further used to calculate system reliability under multiple failure criteria. A novel application is introduced to compute the seismic reliability of structural systems over a time period by considering multiple limit states.

In the example scenarios featuring structural systems exhibiting polynomial nonlinearity and Bouc-Wen nonlinearity, the developed EAD method is compared with

the Automatic Differentiation (AD) method and the finite-difference Numerical estimate of the Derivatives (ND) method. The results suggest that the developed EAD method is sufficiently accurate in computing the gradient of the LSF to solve the optimization problem. The DPE-EAD method, which integrates the EAD method into the DPE approach, is then compared with the DPE-AD, DPE-ND and the MC simulations and is observed to be the most efficient while maintaining the accuracy. The calculated design points are subsequently utilized to evaluate system reliability under multiple failure criteria. The results show that the reliability index and the direction vectors of the located design points are sufficiently accurate to approximate the system reliability with multiple limit states considered.

Since the DPE method utilizes the fundamental theory of the FORM, it is computationally efficient but can be less accurate for highly nonlinear systems. In such cases, SORM improves upon FORM by using a quadratic approximation, which accounts for the curvature of the limit state function in addition to the linear approximation in FORM when calculating the reliability index. Further work could be performed to adapt the DPE method to work within the SORM framework and modify the EAD method to compute the second derivative. The modified DPE-EAD method could potentially work with highly nonlinear systems, which require further investigation.

Chapter 4

Seismic Reliability of Structures Accounting for Stochastic Earthquake Model Parameters

This work extends the Euler-Analytical estimate of the Derivative (EAD) in estimating the derivative of the Limit State Function (LSF), constructed in the Design Point Excitation (DPE) method, with respect to the seismic model parameters and the seismological properties that define a stochastic filter. The derivation procedure is elaborated, and a general scheme of the EAD is provided where the response of interest can be expressed by any nonlinear observation functions. A modified DPE-EAD method is developed to estimate the seismic reliabilities that accounts for the randomness of the seismic model parameters, enabling the evaluation of the seismic reliability of structures for given seismological properties of interest. The developed method is subsequently applied to two structural systems featuring Bouc-Wen nonlinearity and polynomial nonlinearity, and then compared to Monte Carlo (MC)

simulations. With the assumption that the occurrence of the earthquake events follows a Poisson arrival process, the estimated reliability is further applied to estimate the reliability of the structure under possible earthquakes in the future years.

4.1 Earthquake model with stochastic model parameters.

In the previous chapter, the DPE method applies to excitation models with deterministic parameters. To extend the application of the DPE method to problems involving excitation models with stochastic parameters, the earthquake model, proposed in [14] and summarized in Section 2.1 in Chapter 2 is adopted. The ground excitation is simulated by a modulated filtered white noise with stochastic model parameters. The discretized model is written in terms of Eq. (2.5), where $s_i(t)$ is the impulse response function defined as $s_i(t) = h\left[t - t_i, \omega_f(t_i), \zeta_f(t_i)\right]$, and the expression of $f(t)$ is given by:

$$f(t) = q(\boldsymbol{\alpha}, t) \cdot \sum_{i=1}^{N} h[t - t_i, \omega_f(t_i), \zeta_f(t_i)]\, w_i \tag{4.1}$$

where $N = t/\Delta t_D$ and Δt_D is the discretization time step. The modulating function $q(\boldsymbol{\alpha}, t)$ defined in Eq. (2.2) and the unit-impulse response function of the filter $h\left[t - t_i, \omega_f(t_i), \zeta_f(t_i)\right]$ defined in Eq. (2.3) are selected. The discretized white noise w_i at $t_i = i \cdot \Delta t_D$ is written as $w_i = \sigma u_i$, with u_i being standard Gaussian, $\sigma = \sqrt{2\pi S_0 \Delta t_D}$ and S_0 controlling the intensity of the white noise.

According to the earthquake model discussed in Section 2.1, the model parameters $\boldsymbol{\theta} = \left[\alpha_1, \alpha_2, \alpha_3, \omega_f, \zeta_f\right]$ are stochastic since they are transformed from the parameters $\boldsymbol{\nu}$ that are Gaussian variables. A succinct outline of the parameter transformations

from seismological properties $\boldsymbol{\mu}$ to the model parameters $\boldsymbol{\theta}$ is presented in Figure 2. 2, with detailed explanations provided in Section 2.1.1 and Section 2.1.2. The model parameters with given distributions can be transformed to standard Gaussian variables and incorporated as the additional terms in the Gaussian input variable $\boldsymbol{u}$ in the DPE method.

4.2 A modified Design Point Excitation (DPE) method - for excitations with stochastic model parameters.

A brief overview of the DPE method was provided in Section 3.1 in Chapter 3. In this section, the DPE method is extended to estimate the reliability, P_R, i.e., the probability of a system response, y, not exceeding a given threshold, when subjected to excitation $f(t)$ generated by the earthquake model with stochastic model parameters as described in Eq. (4.1) in Section 4.1.

4.2.1 The reliability of a system at a specific time instant

Regarding the excitation model written by Eq. (4.1), the stochastic variables input to the system that generates the response $y(\tau)$ are not only the discretized standard white noise $\boldsymbol{u} = [u_i]$ for $i = 1,2,\dots.,n$, where $n = \tau/\Delta t_D$, as what was considered in the work of Chapter 3, but also the stochastic model parameters. Following the concept of FORM, it is necessary to have knowledge of the distributions of stochastic input variables and subsequently transform them into independent standard Gaussian variables in the application of the DPE method to estimate reliability. According to the properties of the earthquake model parameters presented in Section 2.1.1, the

distributions of the 1st layer Gaussian parameters $\boldsymbol{v}$ are defined, thus is considered as the stochastic variables input to the system. The synthetic earthquake model in Eq. (4.1) is written in the following form accordingly:

$$f(t) = F_g(\boldsymbol{u}, \boldsymbol{v}, t) \tag{4.2}$$

The set of earthquake model parameters $\boldsymbol{v}$ consists of correlated Gaussian variables defined by Eq. (2.9) which has the mean and the covariance matrix specified in Eq. (2.11) and Eq. (2.12). The correlated Gaussian model parameter $\boldsymbol{v}$ is further transformed to an independent standard Gaussian variable $\boldsymbol{v}^{SD}$ by orthogonal transformation. This transformation demonstrates the relation between a correlated multi-variate Gaussian vector and a non-correlated standard Gaussian vector, in this case $\boldsymbol{v}$ and $\boldsymbol{v}^{SD}$, as:

$$\boldsymbol{v} = \boldsymbol{L} \cdot \boldsymbol{v}^{SD} + \overline{\boldsymbol{v}} \tag{4.3}$$

where $\overline{\boldsymbol{v}}$ is the mean of $\boldsymbol{v}$ and $\boldsymbol{L}$ is the Cholesky decomposition of the covariance matrix of $\boldsymbol{v}$, $Cov(\boldsymbol{v})$, i.e., $Cov(\boldsymbol{v}) = \boldsymbol{L} \cdot \boldsymbol{L}^T$. Thus, the vector of standard Gaussian variables input to the system is augmented and denoted as $\boldsymbol{U} = [\boldsymbol{p}^T \ \boldsymbol{u}^T]^T$, where $\boldsymbol{p}$ is the variables related to the stochastic model parameters, i.e., regarding the earthquake model considered here, $\boldsymbol{p} = \boldsymbol{v}^{SD}$, and $\boldsymbol{u}$ is the discretized standard white noise. The size of $\boldsymbol{U}$, $\boldsymbol{p}$ and $\boldsymbol{u}$ are denoted as N_d, m and n respectively, i.e., $N_d = m + n$. The LSF is amended accordingly and written as:

$$G(\boldsymbol{U}, y_T, \tau) = y_T - y(\boldsymbol{U}, \tau) = 0 \tag{4.4}$$

The optimization problem is refined as:

$$\boldsymbol{U}^*(y_T,\tau) = \arg\min\{\|\boldsymbol{U}\|^2 | G(\boldsymbol{U}, y_T, \tau) = 0\} \tag{4.5}$$

And the reliability index and the direction vector of the design point are defined as:

$$\beta = \|\boldsymbol{U}^*\| = \boldsymbol{\alpha}\cdot\boldsymbol{U}^* \tag{4.6}$$

$$\boldsymbol{\alpha} = -\frac{\nabla_{\boldsymbol{U}} G}{\|\nabla_{\boldsymbol{U}} G\|} \tag{4.7}$$

The refined optimization problem can also be solved by the line search method as written in *Algorithm 2* with the input variable $\boldsymbol{u}$ being replaced by the augmented input variable $\boldsymbol{U}$, and the gradient $\nabla_{\boldsymbol{U}} G$ is computed repeatedly in the iterations. To calculate the gradient $\nabla_{\boldsymbol{U}} G$ efficiently, the EAD method is adopted.

4.2.2 The reliability of a system over an earthquake event

As discussed in Section 3.4.1 in Chapter 3, the reliability over a time period or the entire event of an earthquake can be computed by Eq. (3.29) using the reliability indexes β_J and the direction vectors α_J of the design points obtained by the DPE method for a series of time instants τ_J, where $J = 1,2,\dots,j$ in the period of interest.

As stated above, an effective approach to find a series of consecutive time design points is to use the design point $\boldsymbol{U}^*(y_T,\tau_J)$ for a selected time instant τ as an approximation of the design point for the nearby time instants $\widehat{\boldsymbol{U}}^*(y_T,\tau_J \pm \Delta\tau)$. This is based on the anticipation that the excitation generated by the input at the design point, also referred to as the design point excitation $f(t)$, remains similar for the adjacent time instants of interest. As per the algorithm introduced in section 3.4.1 in the previous chapter, the warm starting guesses for the terms of the discretized white noise $\widehat{\boldsymbol{u}}^*(y_T, \tau_J \pm \Delta\tau)$ is the corresponding terms $\boldsymbol{u}^*(y_T, \tau_J)$ in the design point for

the neighbouring time instants τ_J after time shifting. For the starting guesses of the rest of the elements in $\boldsymbol{U}^*(y_T, \tau_J \pm \Delta\tau)$, i.e., the seismic model parameters $\widehat{\boldsymbol{p}}^*(y_T, \tau_J \pm \Delta\tau)$, the corresponding terms in the design point for the neighbouring time instants $\boldsymbol{p}^*(y_T, \tau_J)$ are directly used. The above can form up a warm starting guess $\widehat{\boldsymbol{U}}^*(y_T, \tau_J \pm \Delta\tau) = [\widehat{\boldsymbol{u}}^*(y_T, \tau_J \pm \Delta\tau), \widehat{\boldsymbol{p}}^*(y_T, \tau_J \pm \Delta\tau)]$. The obtained starting guess of $\widehat{\boldsymbol{U}}^*$ are used in *step 1* in the line search optimization of *Algorithm 2* to find the design point $\boldsymbol{U}^*$. Selecting a time instant τ_J in the strong motion period of the earthquake excitation is reasonable to initialize.

4.3 Euler-Analytical estimate of the Derivatives (EAD)

To find the design point $\boldsymbol{U}^*$ using the line search optimization, the derivative $\nabla_{\boldsymbol{U}} G$ is computed repeatedly. The EAD method introduced in Chapter 3 is adopted to calculate the gradient of the LSF $G(\boldsymbol{U}, y_T, \tau)$ with respect to the input vector $\boldsymbol{U}$ as it is found to be efficient and accurate according to the work in Chapter 3.

According to the LSF defined in Eq. (4.4), the derivative $\nabla_{\boldsymbol{U}} G$ of interest in the optimization is:

$$\nabla_{\boldsymbol{U}} G = -\nabla_{\boldsymbol{U}} y(\boldsymbol{U}, \tau) \tag{4.8}$$

The state-space and measurement equations in Eq. (3.2) describe the structural system and the output response of interest, $y(\tau)$. The measurement function $\boldsymbol{h}(\cdot,\cdot)$ in Eq. (3.2b) is not limited to be a linear expression in this research work. A general EAD scheme for computing the derivative of any output response $y(\boldsymbol{U}, \tau)$ is developed in the sub-section 4.3.1. The general scheme extends the applicability of the DPE method

which allows for the reliability estimations on any output response written by a general measurement function $\boldsymbol{h}(\cdot,\cdot)$.

By considering excitation models with stochastic model parameters, the derivative $\nabla_{\boldsymbol{U}} G$ is constructed as $\nabla_{\boldsymbol{U}} G = \left[\nabla_{\boldsymbol{p}} G, \nabla_{\boldsymbol{u}} G\right] = [\frac{dG}{dp_1}, \dots, \frac{dG}{dp_m}, \frac{dG}{du_1} \dots, \frac{dG}{du_n}]$. An analytical expression of $\nabla_{\boldsymbol{u}} G = -\nabla_{\boldsymbol{u}} y(\boldsymbol{U}, \tau)$, the derivative with respect to the standard white noise $\boldsymbol{u}$ has been derived and constructed in Section 3.2. Here in the sub-section 4.3.2 below, the analytical expression of $\nabla_{\boldsymbol{p}} G = -\nabla_{\boldsymbol{p}} y(\boldsymbol{U}, \tau)$, the derivative with respect to the additional input variables $\boldsymbol{p} = \boldsymbol{v}^{SD}$ related to the earthquake model parameters are derived.

4.3.1 The general scheme

The general concept of recursive EAD method was introduced and developed in Chapter 3, where the measurement function is assumed to be linear. Here in this section, a general scheme of the EAD that calculates the derivative in Eq. (4.8) for an output defined by any measurement functions written by $\boldsymbol{h}(\cdot,\cdot)$ is provided.

As the standard Gaussian input variable is augmented and now denoted by $\boldsymbol{U}$, the independent variable being differentiated with respect to is refined as U_i and the analytical expression of the derivative $\frac{d\boldsymbol{x}_{k+1}}{dU_i}$ is amended accordingly:

$$\frac{d\boldsymbol{x}_{k+1}}{dU_i} = \frac{d\boldsymbol{x}_k}{dU_i} + \frac{d\dot{\boldsymbol{x}}_k}{dU_i} \cdot \Delta t_I = \frac{d\boldsymbol{x}_k}{dU_i} + \frac{d\left(\boldsymbol{l_a}(\boldsymbol{x}_k) + \boldsymbol{l_b}(\boldsymbol{x}_k) \cdot f(t_k)\right)}{dU_i} \cdot \Delta t_I$$

$$= \frac{d\boldsymbol{x}_k}{dU_i} + \left\{ \boldsymbol{\nabla}_{\boldsymbol{x}_k} \boldsymbol{l}_a(\boldsymbol{x}_k) \cdot \frac{d\boldsymbol{x}_k}{dU_i} + \left[\boldsymbol{\nabla}_{\boldsymbol{x}_k} \boldsymbol{l}_b(\boldsymbol{x}_k) \cdot \frac{d\boldsymbol{x}_k}{dU_i}\right] \cdot f(t_k) + \boldsymbol{l}_b(\boldsymbol{x}_k) \cdot \frac{d\, f(t_k)}{dU_i} \right\} \Delta t_I \quad (4.9)$$

where Δt_I is the integration time step selected in the Euler integration formula. Regarding the output response y expressed by the general measurement function

$\boldsymbol{h}(\cdot,\cdot)$ as in Eq. (3.2b), the output response y_{k+1} is approximated by the Euler integration formula as:

$$y_{k+1} \approx \boldsymbol{h}\big(\boldsymbol{x}_{k+1}, f(t_{k+1})\big) \tag{4.10}$$

By differentiating the above measurement equation with respect to U_i, an analytical expression of the derivative $\frac{dy_{k+1}}{dU_i}$ is constructed:

$$\frac{d\, y_{k+1}}{dU_i} = \frac{d\, \boldsymbol{h}\big(\boldsymbol{x}_{k+1}, f(t_{k+1})\big)}{dU_i}$$

$$= \frac{d\, \boldsymbol{h}\big(\boldsymbol{x}_{k+1}, f(t_{k+1})\big)}{d\boldsymbol{x}_{k+1}} \frac{d\boldsymbol{x}_{k+1}}{dU_i} + \frac{d\, \boldsymbol{h}\big(\boldsymbol{x}_{k+1}, f(t_{k+1})\big)}{df(t_{k+1})} \frac{df(t_{k+1})}{dU_i} \tag{4.11}$$

where $\frac{d\boldsymbol{x}_{k+1}}{dU_i}$ is obtained by Eq. (4.9) through recursion. The expression of $\frac{d\, \boldsymbol{h}(\boldsymbol{x},f)}{d\boldsymbol{x}}$ and $\frac{d\, \boldsymbol{h}(\boldsymbol{x},f)}{df}$ are derived symbolically according to the measurement equation and evaluated numerically at the realizations of $\boldsymbol{x}_{k+1}$. The gradient $\frac{dy(\boldsymbol{U},\tau)}{dU_i}$ is approximated by evaluating Eq. (4.11) at $t_{k+1} = \tau$ and the gradient $\nabla_{\boldsymbol{U}} G = [-\frac{dy(\boldsymbol{U},\tau)}{dU_1}, \ldots, -\frac{dy(\boldsymbol{U},\tau)}{dU_{N_d}}]$, as defined in Eq. (4.8), can be obtained through recursion. To apply the EAD method to the earthquake model with stochastic model parameters introduced in Section 4.1, similar procedures as listed in *Algorithm 3* and *Algorithm 4* are taken. *Algorithm 3* is used when the time steps Δt_I and Δt_D are identical, and *Algorithm 4* is applied when the time steps differ. To adapt to the earthquake model with stochastic model parameters, in both algorithms, u_i are replaced by the updated input U_i. In addition, according to the general scheme, the gradients $\frac{d\boldsymbol{x}_{k+1}}{dU_i}$ and $\frac{d\, y_{k+1}}{dU_i}$ are computed using Eq. (4.9) and Eq. (4.11) instead.

4.3.2 The analytical derivatives of the excitation $\frac{df(t_k)}{dU_i}$

To obtain the analytical expression of $\frac{df(t_k)}{dU_i}$ in Eq. (3.19), one needs to consider the derivatives with respect to the discretized standard white noise $\boldsymbol{u}$, $\frac{df(t_k)}{d\boldsymbol{u}}$, and the derivatives with respect to the parameters $\boldsymbol{v}^{SD}$, $\frac{df(t_k)}{d\boldsymbol{v}^{SD}}$, separately. According to the excitation model, as shown in Eq. (4.1), the discretized white noise $\boldsymbol{u}$ directly appears in the expression of the excitation $f(t)$, while the parameter $\boldsymbol{v}^{SD}$ does not. Thus, the analytical expression of $\frac{df(t_k)}{d\boldsymbol{u}}$ can be simply obtained from Eq. (4.1), while the analytical expression of $\frac{df(t_k)}{d\boldsymbol{v}^{SD}}$ needs to be derived using the chain rule. Details of the derivation procedures are expanded as follows.

a) The derivatives with respect to the discretized white noise $\boldsymbol{u}$.

Regarding the analytical derivative of the excitation with respect to the discretized standard white noise $\boldsymbol{u}$, it is simply $\frac{df(t_k)}{dU_i} = \frac{df(t_k)}{du_i} = q_k h(t_k - t_i)$ according to Eq. (4.1).

b) The derivatives with respect to the model parameters $\boldsymbol{v}^{SD}$.

Regarding the analytical derivative of the excitation with respect to the standard Gaussian model parameters $\boldsymbol{v}^{SD}$, $\frac{df(t_k)}{dU_i} = \frac{df(t_k)}{dv_i^{SD}}$ cannot be derived directly. The expression of $f(t_k)$ in Eq. (4.1) is written in terms of the model parameter $\boldsymbol{\theta}$ which is a deterministic transformation of the variable $\boldsymbol{v}^{SD}$. Thus, the analytical expression of the derivative $\frac{df(t_k)}{dv_i^{SD}}$ is computed by chain rule according to the equations of parameter transformations:

$$\frac{df(t_k)}{dv_i^{SD}} = \frac{df(t_k)}{d\boldsymbol{\theta}} \cdot \frac{d\boldsymbol{\theta}}{d\boldsymbol{\lambda}} \cdot \frac{d\boldsymbol{\lambda}}{d\boldsymbol{v}} \cdot \frac{d\boldsymbol{v}}{dv_i^{SD}}$$

$$\frac{df(t_k)}{dv_i^{SD}} = \sum_{ij=1}^{\dim(\boldsymbol{v})} \left(\sum_{j=1}^{\dim(\boldsymbol{\lambda})} \left(\sum_{l=1}^{\dim(\boldsymbol{\theta})} \frac{df(t_k)}{d\theta_l} \cdot \frac{d\theta_l}{d\lambda_j} \right) \cdot \frac{d\lambda_j}{dv_{ij}} \right) \cdot \frac{dv_{ij}}{dv_i^{SD}} \tag{4.12}$$

in which $\frac{df(t_k)}{d\boldsymbol{\theta}} = \frac{\partial f(t_k)}{\partial \boldsymbol{\theta}}$, $\frac{d\boldsymbol{\lambda}}{d\boldsymbol{v}} = \frac{\partial \boldsymbol{\lambda}}{\partial \boldsymbol{v}}$ and $\frac{d\boldsymbol{v}}{dv_i^{SD}} = \frac{\partial \boldsymbol{v}}{\partial v_i^{SD}}$ according to Eq. (4.1), Eq. (2.13) and Eq. (4.3) respectively. While the parameters in $\boldsymbol{\theta}$ are correlated according to Eq. (2.6a), thus the total derivatives in $\frac{d\boldsymbol{\theta}}{d\boldsymbol{\lambda}}$ is given by:

$$\frac{d\theta_l}{d\lambda_j} = \sum_{lj=1}^{size(\boldsymbol{\lambda})} \frac{\partial \theta_l}{\partial \theta_{lj}} \cdot \frac{\partial \theta_{lj}}{\partial \lambda_j} \tag{4.13}$$

in which $\frac{\partial \theta_l}{\partial \theta_{lj}}$ is computed according to Eq. (2.6a), the equation that correlates the parameters in $\boldsymbol{\theta}$.

The analytical expressions of the derivatives $\frac{\partial f(t_k)}{\partial \boldsymbol{\theta}}$, $\frac{\partial \boldsymbol{\theta}}{\partial \boldsymbol{\lambda}}$, $\frac{\partial \boldsymbol{\lambda}}{\partial \boldsymbol{v}}$ and $\frac{\partial \boldsymbol{v}}{\partial \boldsymbol{v}^{SD}}$ are derived from Eq. (4.1), Eq.(2.6) - (2.7), Eq. (2.13) and Eq. (4.3) that transform $\boldsymbol{v}^{SD}$ to $\boldsymbol{\theta}$ accordingly, in which $\frac{\partial f(t_k)}{\partial \boldsymbol{\theta}}$, $\frac{\partial \boldsymbol{\lambda}}{\partial \boldsymbol{v}}$ and $\frac{\partial \boldsymbol{v}}{\partial \boldsymbol{v}^{SD}}$ can be obtained directly since the dependent variables are written in terms of the independent variables to be differentiated with respect to. While in $\frac{\partial \boldsymbol{\theta}}{\partial \boldsymbol{\lambda}}$, the dependent variables a_2 and a_3 in $\boldsymbol{\theta}$ are the solution to the coupled Eq. (2.7a-b) with the independent variable D_{5-95} and t_{mid} in $\boldsymbol{\lambda}$. Thus, the four terms $\frac{\partial a_2}{\partial D_{5-95}}$, $\frac{\partial a_3}{\partial D_{5-95}}$, $\frac{\partial a_2}{\partial t_{mid}}$ and $\frac{\partial a_3}{\partial t_{mid}}$ cannot be obtained directly. Alternatively, they are derived using the following method: According to the definition of p_{95}, p_5 and p_{45}, they represent the inverse of the Gamma CDF with parameters written in terms of a_2 and a_3. Thus, one can write Eq. (2.7a-b) as functions of a_2 and a_3:

$$f_1(a_2, a_3) = p_{95} - p_5 = D_{5-95} \tag{4.14a}$$

$$f_2(a_2, a_3) = p_{45} = t_{mid} \tag{4.14b}$$

and then differentiate both equations above with respect to D_{5-95} and t_{mid} to obtain:

$$\frac{df_1(a_2,a_3)}{dD_{5-95}} = \sum_{i=2}^{3} \frac{\partial f_1(a_2,a_3)}{\partial a_i} \frac{\partial a_i}{\partial D_{5-95}} = \frac{dD_{5-95}}{dD_{5-95}} \tag{4.15a}$$

$$\frac{df_1(a_2,a_3)}{dt_{mid}} = \sum_{i=2}^{3} \frac{\partial f_1(a_2,a_3)}{\partial a_i} \frac{\partial a_i}{\partial t_{mid}} = \frac{dD_{5-95}}{dt_{mid}} \tag{4.15b}$$

$$\frac{df_2(a_2,a_3)}{dD_{5-95}} = \sum_{i=2}^{3} \frac{\partial f_2(a_2,a_3)}{\partial a_i} \frac{\partial a_i}{\partial D_{5-95}} = \frac{dt_{mid}}{dD_{5-95}} \tag{4.15c}$$

$$\frac{df_2(a_2,a_3)}{dt_{mid}} = \sum_{i=2}^{3} \frac{\partial f_2(a_2,a_3)}{\partial a_i} \frac{\partial a_i}{\partial t_{mid}} = \frac{dt_{mid}}{dt_{mid}} \tag{4.15d}$$

in which, $\frac{\partial f_1(a_2,a_3)}{\partial a_2}$, $\frac{\partial f_1(a_2,a_3)}{\partial a_3}$, $\frac{\partial f_2(a_2,a_3)}{\partial a_2}$, $\frac{\partial f_2(a_2,a_3)}{\partial a_3}$ can be obtained from the derivatives of the inverse Gamma CDF with respect to the distribution parameters. The four unknowns $\frac{\partial a_2}{\partial D_{5-95}}$, $\frac{\partial a_3}{\partial D_{5-95}}$, $\frac{\partial a_2}{\partial t_{mid}}$ and $\frac{\partial a_3}{\partial t_{mid}}$ can be solved by the above coupled equations. The rest terms in $\frac{\partial \boldsymbol{\theta}}{\partial \boldsymbol{\lambda}}$ can be computed according to Eq. (2.6a-c). The analytical derivatives related to the CDF and inverse CDF in this work are obtained using Maple.

4.4 Examples: Reliability of structures subjected to excitations with stochastic model parameters.

In this section. a 4-Degrees-of-Freedom structural system with a Bouc-Wen nonlinearity and a 10-Degrees-of-Freedom structural system with polynomial nonlinearity are considered to examine the developed DPE-EAD method in estimating the reliability of structures subjected to earthquake model with stochastic model parameters. The stochastic earthquake model introduced in Section 4.1 is adopted, where the intensity of the white noise $S_0 = 5 \cdot 10^5$ and the seismological properties

$F = 1$, $M = 7$, $R_{rup} = 100\text{km}$, $V_{s30} = 800\text{m/s}$ are selected. In the seismological parameters $\boldsymbol{\lambda}$ computed by Eq. (2.13), $\bar{I}_a$ follows a lognormal distribution, D_{5-95}, t_{mid} and ζ follow Beta distributions, ω_{mid} follows a Gamma distribution and ω' follows a Two-Sided Exponential distribution. The discretization time step $\Delta t_D = 0.01\text{s}$ is chosen in Eq. (4.1) in the excitation model. And the integration time step $\Delta t_I = 0.01\text{s}$ is used in Eq. (4.9) in finding the analytical derivatives in the implementation of the DPE-EAD method.

As a reference to show the accuracy and the efficiency of the developed DPE-EAD method, the Monte Carlo (MC) simulations are also implemented in which samples of earthquake time histories and the structural responses are generated repeatedly to estimate the reliability. It is known that the result obtained from the MC simulation is accurate when the sample set is sufficiently large. And thus, in each example, convergence tests are run respectively for each response. Both the MC simulation and the DPE-EAD approaches use the Runge-Kutta (4, 5) pair (*ode45* command in MATLAB) [86,87], to integrate the state-space equation of the structural system and the structural response y written by Eq. (3.2a-b) in all examples discussed in this chapter.

4.4.1 Example 1 - *Structural system with Bouc-Wen nonlinearity subjected to excitations with stochastic model parameters*.

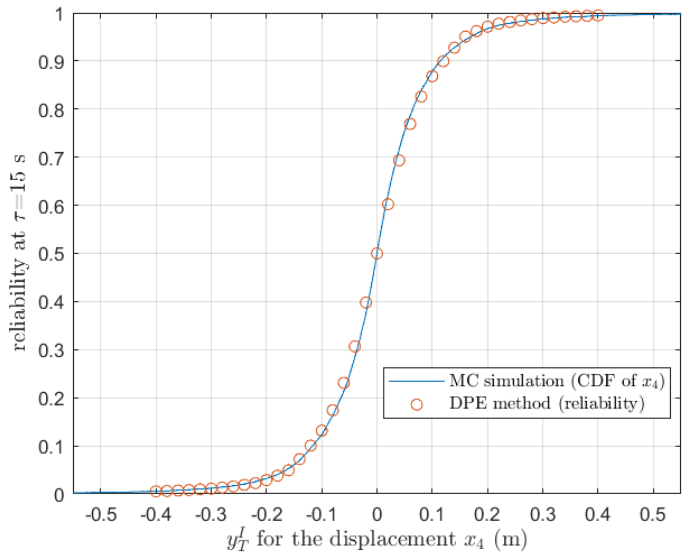
The 4-story shear building studied in Section 3.5.1 *Example 1* is considered. The 4-DoF structural system with Bouc-Wen nonlinearity is represented by the differential

equations written in Eq. (3.30) and the parameters selected were introduced in Section 3.5.1. The excitation $f(t)$ subjected to the structure is the ground acceleration generated by the earthquake model introduced in Eq. (4.1) that has stochastic model parameters. The reliability of the 4th storey displacement, $y(\tau) = x_4(\tau)$ and the 1st storey restoring force, $y(\tau) = [\boldsymbol{F}_R]_1(\tau)$ are examined to demonstrate the DPE-EAD method developed for excitations with stochastic model parameters.

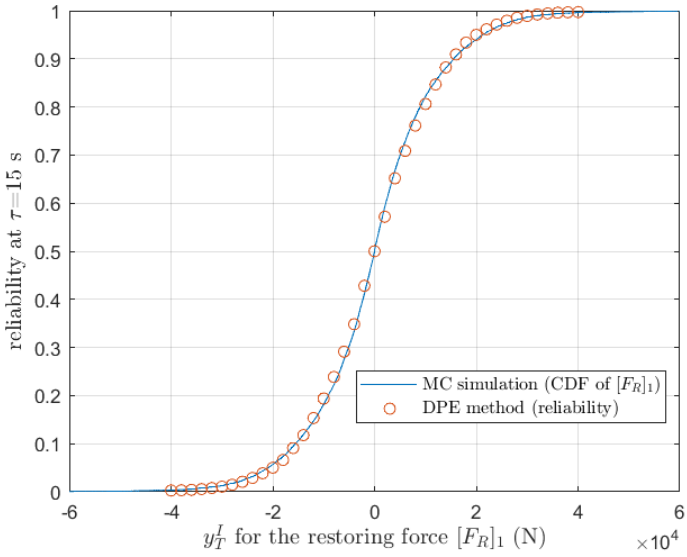
To ensure the MC sample set is adequately large and the results from the MC simulation are sufficiently accurate, a convergence test is carried out, where a set of thresholds are considered. From the sample set obtained in the MC simulation, the reliability is computed by Eq. (3.33). After investigations, the tail regions having the extreme probabilities of less than 5% or greater than 95% would require a larger sample set to converge. Generating 15000 samples of time histories and the corresponding structural responses is sufficient for estimating the reliabilities of the responses considered in this example if a maximum accepted relative error of 5% is chosen.

To begin with, the response of the 4th storey displacement, i.e., $y(\tau) = x_4(\tau)$, at 15 seconds is studied. The time instant $\tau = 15\text{s}$ is selected since it is a time instance during the strong motion period of the earthquake according to the envelope function. In the DPE-EAD method, a series of equally spaced threshold limits $[y_T^I] = \pm[0.02 \cdot I]$ m, where $I = 1,2,\dots,20$, are selected in estimating the reliability for the 4th storey displacement $x_4(\tau)$. It should be noted that in case of negative thresholds

that correspond to negative directions, the reliability computed by this method refers to $P(y \leq -y_T^I)$. One iteration on average is required in the line search optimization (*Algorithm 2*) in locating each design point $\boldsymbol{U}^*$ for the LSFs $G(\boldsymbol{U}, \tau) = y_T^I - x_4(\boldsymbol{U}, \tau)$, which shows a good accuracy of the Euler-analytical estimate of the derivatives. In the following Figure 4. 1(a), the reliabilities obtained are shown in the vertical axis versus the corresponding limits y_T^I shown in the horizontal axis. The cumulative density function (CDF) of $x_4(\tau)$ obtained from the MC simulation is plotted on the same figure for comparison. As can be seen in Figure 4. 1(a), the reliabilities obtained from the DPE-EAD method agree well with the CDFs of $x_4(\tau)$. This indicates that the design points located by the line search optimization with the Euler-analytical estimate of derivatives are sufficiently accurate for a large range of the threshold limits of interest, even in the tail regions with small probabilities of exceedance or non-exceedance. The maximum relative difference between the DPE-EAD method and the MC estimations is about 4% (at $y_T^2 = \pm 0.04\text{m}$) which shows a reasonable level of accuracy of the DPE-EAD method approximation. Thus, the developed DPE-EAD method is adequate in reliability estimations for structures subjected to seismic excitations with stochastic model parameters when the response of interest (y) is a simple state variable of the structure.



(a) $y = x_4(\tau)$



(b) $y = [\boldsymbol{F}_R]_1(\tau)$

Figure 4. 1 The reliability of $x_4(\tau)$ and $[\boldsymbol{F}_R]_1(\tau)$ at $\tau = 15\text{s}$ approximated by the DPE-EAD method for a sequence of thresholds versus the CDF of which obtained by the MC simulations.

The reliability of the 1st storey restoring force, $y(\tau) = [\boldsymbol{F}_R]_1(\tau)$ at $\tau = 15\text{s}$ is also examined. It is usually an important measure in reliability analysis which indicates the yielding behaviour of a nonlinear system. It is expressed by $[\boldsymbol{F}_R]_1(\tau) = [1,0,0,0] \cdot \left[\boldsymbol{K}\left(\boldsymbol{\alpha x}(\tau) + (\boldsymbol{I}_4 - \boldsymbol{\alpha})\boldsymbol{Z}(\tau)\right)\right] = (k_1 + k_2) \cdot [\alpha_1 \cdot x_1 + (1 - \alpha_1)z_1] - k_2 \cdot x_2$, a linear

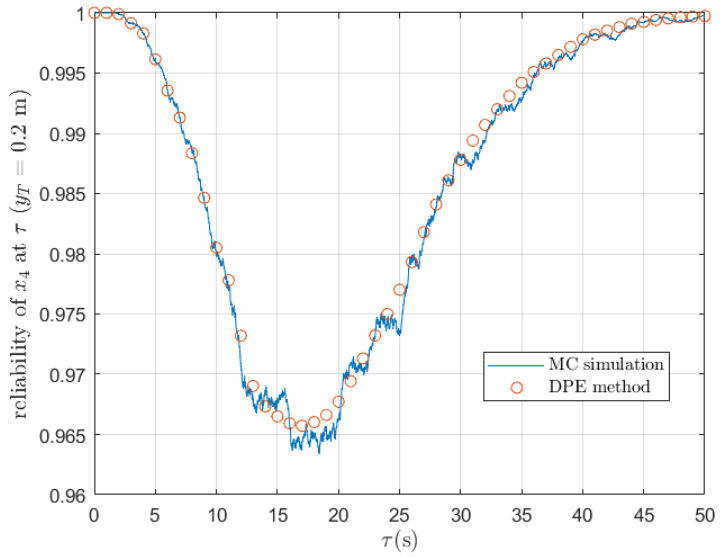
function of the states of the structural system. The thresholds $[y_T^I] = \pm[2000 \cdot I]$ N, where $I = 1,2,\dots,20$, are considered. The corresponding reliability estimated by the DPE-EAD method are plotted in Figure 4. 1(b), which are compared to the CDF of $[\boldsymbol{F}_R]_1$ (at $\tau = 15$s) found by the MC simulation of 15000 samples. An average of 1.3 iterations are required in locating each design point $\boldsymbol{U}^*$ for the LSF $G(\boldsymbol{U},\tau) = y_T^I - [\boldsymbol{F}_R]_1(\boldsymbol{U},\tau)$ using line search optimization (*Algorithm 2*), in which the analytical derivative $\frac{d[\boldsymbol{F}_R]_1}{dU_i}$ is expressed by Eq. (4.11). The maximum relative differences between the DPE-EAD method to the MC estimations is about 3.7% (at $y_T^3 = 6000$N) which is acceptable. The DPE method with the developed Euler-analytical estimate of derivatives is sufficiently accurate in finding the design point as well as the reliability when the response of interest (y) is in terms of a measurement function written as a linear combination of the state variable of a structure.

To find the reliability for a response over an earthquake event, the reliability at a series of time instants is required. The responses of the 4th storey displacement, i.e., $y = x_4$ and the 1st storey restoring force, i.e., $y = [\boldsymbol{F}_R]_1$ that were considered above are examined, in which the threshold limits $y_T = 0.2$m and $y_T = 1.8 \cdot 10^4$N are chosen for x_4 and $[\boldsymbol{F}_R]_1$ respectively. Assuming that the total duration of the earthquake is 50 seconds, time instants evenly spread in the earthquake $[\tau_J] = [J]$ s, where $J = 1,2,\dots,50$, are selected.

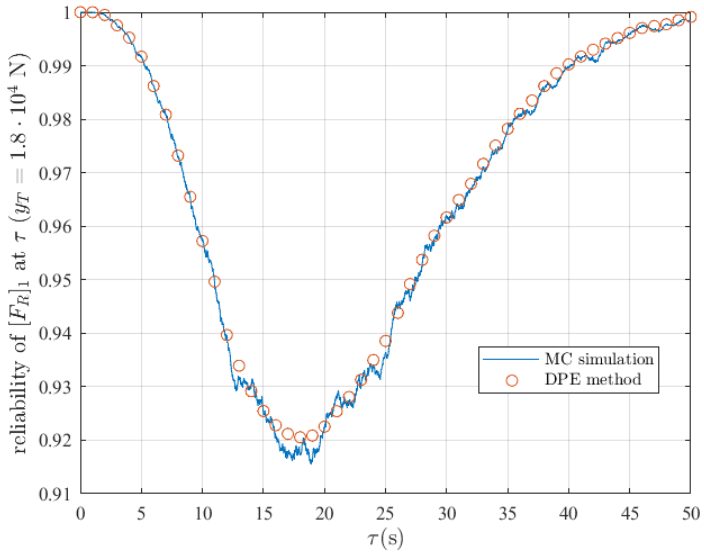
The starting point is the design vector $\boldsymbol{U}^*$ at $\tau = 15$s which was obtained in the above examples. The initial guesses of the design points $\boldsymbol{U}^*(y_T, \tau_J)$ at the nearby time

instants are approximated gradually by time shifting. Starting with these initial guesses, each design point $\boldsymbol{U}^*(y_T, \tau_J)$ can be located in just one iteration in the line search optimization (*Algorithm 2*) for both responses in case of the LSF $G(\boldsymbol{U}, \tau_J) = 0.2\text{m} - x_4(\boldsymbol{U}, \tau_J)$ and the LSF $G(\boldsymbol{U}, \tau_J) = 1.8 \cdot 10^4\text{N} - [\boldsymbol{F}_R]_1(\boldsymbol{U}, \tau_J)$ constructed. The corresponding reliabilities $P_R(\tau_J)$ estimated for a series of time instants are plotted in Figure 4. 2(a) and (b), where the vertical axis indicates the reliability and the horizontal axis indicates the time instant τ_J considered. The reliability at each time instant obtained by the MC sample set is also plotted in the figures for comparison. In Figure 4. 2(a) and (b), the MC estimates are noisy in the strong motion period. This is because the threshold limits correspond to reliability in the tail region are selected and MC simulation is normally not efficient in finding tail probabilities [12]. After investigations, the unsmooth shape can be eliminated with a substantially large sample set but is hardly avoided. The maximum relative estimation differences between the DPE-EAD method to the MC simulation is about 0.4% observed at $\tau_{25} = 25\text{s}$ for the response x_4 with $y_T = 0.2\text{m}$, and 0.6% at $\tau_{19} = 19\text{s}$ for the response $[\boldsymbol{F}_R]_1$ with $y_T = 1.8 \cdot 10^4\text{N}$. The reliability indexes β_J and the direction vectors α_J obtained for all the time instants τ_J considered in the DPE-EAD method are then used in Eq. (3.29) to find the reliabilities for the responses x_4 and $[\boldsymbol{F}_R]_1$ of the 4-storey shear building that undergoes an earthquake. The reliabilities of x_4 and $[\boldsymbol{F}_R]_1$ in the period of 50 seconds considered are $P_R = 0.674$ and $P_R = 0.343$, respectively, approximated by the DPE-EAD method. Compared to the reliabilities estimated by the MC sample set,

$P_R = 0.652$ for x_4 and $P_R = 0.325$ for $[\boldsymbol{F}_R]_1$, relative estimation differences of 3.2% and 5.2% are observed in estimating the reliabilities of the 4th storey displacement ($y = x_4$) and the 1st storey restoring force ($y = [\boldsymbol{F}_R]_1$) in an earthquake. The DPE-EAD method is reasonably accurate in estimating the reliability of a structure with Bouc-Wen nonlinearities that undergoes an earthquake event.



$(a)\ y = x_4(\tau)$ with $y_T = 0.2$ m



(b) $y = [\boldsymbol{F}_R]_1(\tau)$ with $y_T = 1.8 \cdot 10^4$ N

Figure 4. 2 The reliability of $x_4(\tau)$ and $[\boldsymbol{F}_R]_1(\tau)$ estimated at a sequence of time instants τ using the DPE method and the MC simulations.

Regarding the computational efficiency of both methods, details of the calculation time are summarized in Table 4. 1. For the DPE-EAD method, the responses $y = x_4$ and $y = [\boldsymbol{F}_R]_1$ are examined in this example. It is found that the efficiency of locating each design point $\boldsymbol{U}^*(y_T^I, \tau)$ using the line search algorithm depends on the efficiency of the root-finding procedure (*fzero* command in MATLAB) in finding $\hat{\beta}$ in step 3 of *Algorithm 2* and the number of iterations needed in *Algorithm 2*. The time required for finding the reliabilities of the responses at $\tau = 15\text{s}$ with all $\dim(I)$ threshold limits considered in Figure 4. 1(a) and (b) are shown in the 1st column, in which the time for per threshold also refers to the average time required in locating each design point $\boldsymbol{U}^*(y_T^I, \tau)$. The time taken for finding the reliabilities at all $\dim(J)$ time instants as shown in Figure 4. 2(a) and (b) are in the 2nd column. It should be noted that the efficiency of the method is influenced by the time instant τ and the discretization step Δt_D selected which define the size of $\boldsymbol{U}$ (the number of unknows) in the optimization problem. The calculation time also varies with the number of thresholds $\dim(I)$ and the number of time instants $\dim(J)$ selected accordingly. In terms of the time cost in computing the derivatives $\nabla_{\boldsymbol{U}} G$ using the Euler-analytical estimation, it varies with the time instant τ and the integration step Δt_I selected since the size of $\boldsymbol{U}$ and the integration step needed in the Euler integration vary accordingly. The average time in computing the derivatives $\nabla_{\boldsymbol{U}} G$ for $\tau = 15\text{s}$ and $\Delta t_I = 0.01\text{s}$ are specifically pointed out in the 3rd column. As shown in Table 4. 1, the computational time of locating each design point (time for per threshold) and computing the derivative for

$y = x_4$ and $y = [\boldsymbol{F}_R]_1$ has little difference, thus the computational efficiency of the DPE-EAD method is not highly affected by the complexity of the response of interest. The calculation time of the MC simulation is shown separately in the last column in Table 4. 1, which is the total time taken in generating the entire sample set of 15000 samples of the earthquake time histories and the corresponding structural responses.

Table 4. 1 The computational costs of the DPE-EAD method and the MC simulations in *Example 1* and *Example 2*.

	Response of interest	**Design Point Excitation method (DPE-EAD)**			**MC sim.**
		Find $\boldsymbol{U}^*(y_T^I, \tau)$ for dim (I) thresholds	Find $\boldsymbol{U}^*(y_T, \tau_j)$ for dim (J) time instants	Computing $\nabla_{\boldsymbol{U}} G$ (Avg.)	Generating the sample set
Ex. 1	$y = x_4$	7.6 min. 22.9 s per threshold	32.4 min.	9.2 s	7.1 h
	$y = [\boldsymbol{F}_R]_1$	9.8 min. 29.3 s per threshold	41.4 min.	10.1 s	
Ex. 2	$y = \ddot{x}_1$	13.9 min. 41.6 s per threshold	58.9 min.	14.7 s	10 h

In contrast to the MC simulation which calculates the reliability for the overall time period in an earthquake, the DPE method finds the reliability for one specific time of interest for each calculation. If a different time instant is considered, an additional computation is required. Nonetheless, the developed DPE-EAD method is still competitive over the MC simulation in estimating the reliabilities of a targeted response over a time period. The time taken to perform a DPE-EAD reliability estimation for a series of time instants, as shown in 2nd column of DPE-EAD in minutes, is significantly lower than that of a MC simulation shown in last column in hours. In general, if the reliabilities of specific responses are of interest, the developed DPE-EAD method is sufficiently accurate and efficient in the reliability estimations for

structures with Bouc-Wen nonlinearities subjected to seismic excitations with stochastic model parameters.

4.4.2 Example 2 - *Structural system with polynomial nonlinearity subjected to excitations with stochastic model parameters*.

The 10-story shear building studied in Section 3.5.2 *Example 2* is considered in this example. The 10-DoF structural system is described by the differential equation in Eq. (3.33). The parameters are chosen as discussed in Section 3.5.2 and the excitation $f(t)$ is determined by the earthquake model in Eq. (4.1) with stochastic model parameters characterized by seismological properties selected at the beginning of this section. The reliability for the 1st storey acceleration, i.e., $y(\tau) = \ddot{x}_1(\tau)$ is examined. For the MC simulation, a sample size of 15000 is required in this example according to the convergence test with 5% of the maximum accepted relative error considered.

To begin with, the reliability for the 1st storey acceleration $\ddot{x}_1(\tau)$ at the time instant $\tau = 15\text{s}$ in the strong motion period of the seismic model is calculated. According to the structural model, the 1st storey acceleration is $\ddot{x}_1(t) = \left[-\boldsymbol{M}^{-1} \cdot \left(\boldsymbol{C}\dot{\boldsymbol{x}}(t) + \boldsymbol{K}\left(\boldsymbol{x}(t)\right)\boldsymbol{x}(t)\right)\right]_1$, in which $\boldsymbol{K}\left(\boldsymbol{x}(t)\right)$ is state-dependent. Thus, the response of interest in this example is not a simple linear combination of the states. This example focuses on this additional challenge for the DPE method, which applies to a more general case as described by the nonlinear Eq. (3.2b). The set of threshold limits $[y_T^I] = \pm[(6 \cdot 10^{-3}) \cdot I]\ \text{m/s}^2$, where $I = 1,2,\ldots,20$, is considered. Figure 4. 3 compares the reliabilities found by the DPE-EAD method to the CDF of $\ddot{x}_1(\tau)$

according to the MC sample set. An average of 1.3 iterations are required in locating each design point $\boldsymbol{U}^*(y_T^I, \tau)$ for the LSFs $G(\boldsymbol{U}, \tau) = y_T^I - \ddot{x}_1(\boldsymbol{U}, \tau)$ in the line search optimization. The maximum relative difference of the reliability estimations is about 5% at $y_T^2 = \pm 1.2 \cdot 10^{-2}\ \mathrm{m/s^2}$, which is equal to the maximum accepted error considered in the MC convergence test. The result shows that the analytical estimate of the derivative by Eq. (4.11) is sufficiently accurate in this example, and the DPE method with the developed Euler-analytical derivative estimation is applicable in estimating the reliabilities of the responses expressed by a nonlinear measurement function.

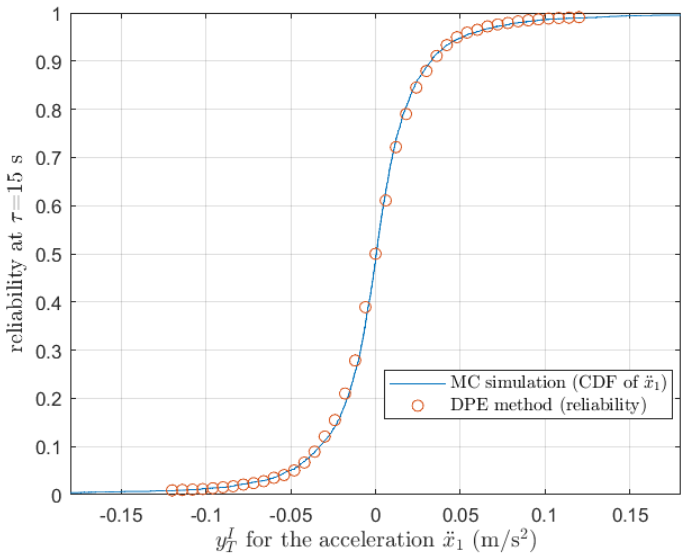


Figure 4. 3 The reliability of $\ddot{x}_1(\tau)$ at $\tau = 15\mathrm{s}$ approximated by the DPE-EAD method for a sequence of thresholds versus the CDF of which obtained by the MC simulations.

The reliability for the 1st storey acceleration $\ddot{x}_1$ at a set of different time instants in the earthquake $[\tau_J] = [J]$ s, where $J = 1,2,\ldots,50$, is also examined and is used to find the reliability for the whole period considered. The threshold limit $y_T = 0.05\mathrm{m/s^2}$ is selected. Each design point for the constructed LSF $G(\boldsymbol{U}, \tau_J) = y_T -$

$\ddot{x}_1(\boldsymbol{U}, \tau_J)$ is located by one iteration on average in the optimization starting with the initial guess obtained by time shifting. The corresponding reliabilities $P_R(\tau_J)$ are plotted in Figure 4. 4, in which the maximum relative differences between the DPE-EAD method and the MC estimations is found to be 0.6% at about $\tau_{16} = 16\text{s}$. By substituting the obtained reliability indexes β_J and the direction vectors α_J in Eq. (3.29), the reliability of $\ddot{x}_1$ in the period of the 50 seconds of interest is $P_R = 0.412$. Compared to the MC simulation result of $P_R = 0.397$, a relative estimation errors of 3.6% is observed, which shows that the DPE-EAD method can be used to estimate reliability of a structure with polynomial nonlinearities for a time period.

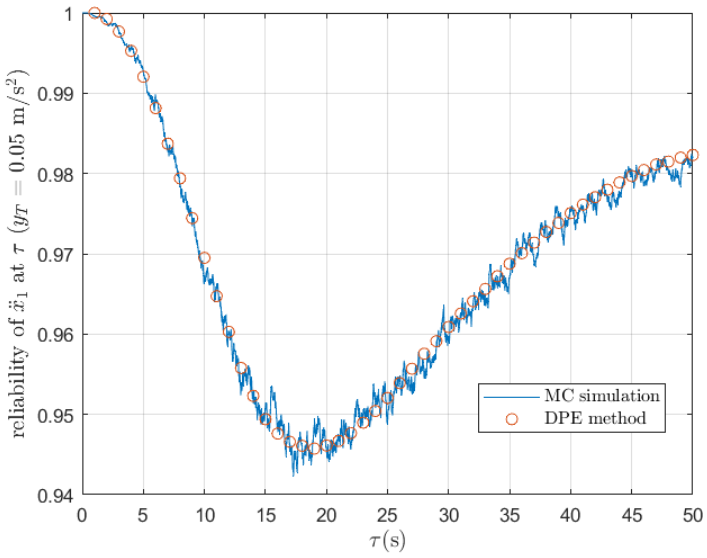


Figure 4. 4 The reliability of $\ddot{x}_1(\tau)$ with $y_T = 0.05\text{m/s}^2$ estimated at a sequence of time instants τ using the DPE method and the MC simulations.

The computational costs of finding the reliabilities for the 1st storey acceleration $\ddot{x}_1$ are summarized in Table 4. 1. Both the DPE-EAD method and the MC simulation method experience similar proportional increase in calculation time compared to that of *Example 1*. The main reason is that a higher-order structural system is considered

in this example, which leads to larger size of the state variable $\boldsymbol{x}$. In addition, the system is more complicated since the polynomial non-linearities are applied to all storeys. The time taken for generating the structural responses is thus higher, which results in the increase in cost for the MC simulation. As for the developed DPE-EAD method, in addition to the previous reason, another important cause is the dependency of the size of $\frac{d\boldsymbol{x}}{dU_i}$ in Eq. (4.9) in computing the derivative $\nabla_{\boldsymbol{U}} G$ on the state variable $\boldsymbol{x}$. The number of iterations required in the line search optimization (*Algorithm 2*) is similar in both *Example 1* and *2*, suggesting that it is weakly affected by the complexity of the structure and the response of interest. In conclusion, the results show that the developed DPE method with Euler-analytical estimate of the derivative is capable of estimating the reliability of structures with polynomial nonlinearities subjected to excitations with stochastic model parameters and is substantially more efficient than the MC simulations.

4.5 The extended DPE method - for excitations with stochastic seismological properties.

When considering the seismicity of an area, the seismological properties $\boldsymbol{\mu}$ would also follow their own probabilistic distributions. Hence, considering the seismological properties, i.e., the moment magnitude (M), the source to site distance (R_{rup}), and the site-soil shear-wave velocity (V_{s30}), as variables in the earthquakes model allows estimating the expected seismic responses of structural systems more accurately. In this section, the design point excitation method (DPE) is extended accordingly.

To do so, the variable $\boldsymbol{p}$ related to the stochastic model parameters in the standard Gaussian variable $\boldsymbol{U}$ appearing in the Limit State Function (LSF) in Eq. (4.4) is amended and augmented, where the variables $\boldsymbol{\mu} = [M, R_{rup}, V_{s30}]$ are transformed to standard Gaussian variables and added as additional terms in $\boldsymbol{p}$. According to Eq. (2.9a-b), the stochastic model parameter $\boldsymbol{v}$ is expressed in terms of the seismological properties $\boldsymbol{\mu} = [M, R_{rup}, V_{s30}]$ and the error term $\boldsymbol{\epsilon}$. In the former case in Section 4.2 when deterministic seismological properties $\boldsymbol{\mu}$ are assumed, the model parameter $\boldsymbol{v}$ is focused on as the independent variable input to the excitation model as shown in Eq. (4.2). It follows a Gaussian distribution since the error term $\boldsymbol{\epsilon}$, which is a Gaussian variable, is the only variable in the expression of $\boldsymbol{v}$. Here in this case when the seismological properties $\boldsymbol{\mu}$ are stochastic, the seismological properties $\boldsymbol{\mu}$ and the error term $\boldsymbol{\epsilon}$ are the model parameters considered as the independent variables input to the excitation model. The earthquake model in Eq. (4.1) is expressed in terms of the variables $\boldsymbol{\mu}$, $\boldsymbol{\epsilon}$ and $\boldsymbol{u}$ accordingly as:

$$f(t) = F_g(\boldsymbol{u}, \boldsymbol{\mu}, \boldsymbol{\epsilon}, t) \tag{4.16}$$

The probabilistic distributions selected for the seismological properties $\boldsymbol{\mu}$ are elaborated later in Section 4.5.2, and the probabilistic distribution of the error term $\boldsymbol{\epsilon}$ is known to be a zero-mean Gaussian variable with the covariance matrix $Cov(\boldsymbol{\epsilon})$ computed by Eq. (2.10) as discussed in Section 2.1.2.

Since the stochastic model parameters $\boldsymbol{\mu}$ and $\boldsymbol{\epsilon}$ are not independent standard Gaussian, they are further transformed to standard Gaussian variables, denoted as $\boldsymbol{\mu}^{SD}$

and $\boldsymbol{\epsilon}^{SD}$. The seismological properties $\boldsymbol{\mu}$ are transformed to the $\boldsymbol{\mu}^{SD}$ through the Rosenblatt transformation:

$$F_{\boldsymbol{\mu}}(\boldsymbol{\mu}) = \boldsymbol{\phi}(\boldsymbol{\mu}^{SD}) \tag{4.17}$$

where $F_{\boldsymbol{\mu}}(\cdot)$ is cumulative density function (CDF) of $\boldsymbol{\mu}$. And since the error term $\boldsymbol{\epsilon}$ is a correlated multi-variant vector, it is transformed to $\boldsymbol{\epsilon}^{SD}$ by Orthogonal transformation:

$$\boldsymbol{\epsilon} = \boldsymbol{L} \cdot \boldsymbol{\epsilon}^{SD} + \bar{\boldsymbol{\epsilon}} \tag{4.18}$$

where $\boldsymbol{L}$ is the Cholesky decomposition of $Cov(\boldsymbol{\epsilon})$, which has $Cov(\boldsymbol{\epsilon}) = \boldsymbol{L} \cdot \boldsymbol{L}^T$. As the mean of the $\boldsymbol{\epsilon}$ is $\bar{\boldsymbol{\epsilon}} = 0$, one has $\boldsymbol{\epsilon} = \boldsymbol{L} \cdot \boldsymbol{\epsilon}^{SD}$. The transformed variables $\boldsymbol{\mu}^{SD}$ and $\boldsymbol{\epsilon}^{SD}$ form the input variable $\boldsymbol{p}$, the term related to the model parameters in the standard Gaussian variable $\boldsymbol{U}$. Thus, the augmented input variable $\boldsymbol{U}$ is constructed as $\boldsymbol{U} = [\boldsymbol{p}^T \ \boldsymbol{u}^T]^T$, where $\boldsymbol{p} = \begin{bmatrix} \boldsymbol{\mu}^{SD} \\ \boldsymbol{\epsilon}^{SD} \end{bmatrix}$. The LSF $G(\boldsymbol{U}, y_T, \tau)$ in Eq. (4.4) as well as the optimization problem in Eq. (4.5) are updated accordingly with the augmented input variable $\boldsymbol{U}$.

Again, the line search algorithm (*Algorithm 2*) suggested above is utilized to solve the updated optimization problem, determining the design point of the augmented variable $\boldsymbol{U}$. In the computation of the gradient $\nabla_{\boldsymbol{U}} G$ using the EAD method, additional derivations are necessary to obtain the analytical expressions of the derivatives of the LSF $G(\boldsymbol{U}, y_T, \tau)$ with respect to the augmented terms $\boldsymbol{\mu}^{SD}$ and $\boldsymbol{\epsilon}^{SD}$ in $\boldsymbol{U}$. These derivations are elaborated upon in the subsequent Section 4.5.1. With these adjustments, the reliability of a structure subjected to earthquake excitations with

stochastic seismological properties can be estimated using the DPE-EAD method in a similar manner.

4.5.1 The analytical derivatives with respect to the model parameters $\boldsymbol{\mu}^{SD}$ and $\boldsymbol{\epsilon}^{SD}$.

To find the derivative $\nabla_{\boldsymbol{U}} G$ with respect to $\boldsymbol{\mu}^{SD}$ and $\boldsymbol{\epsilon}^{SD}$ which are the amended terms in $\boldsymbol{U}$, the Euler-Analytical estimate of derivative scheme introduced in Section 4.3 is applied. It should be noted that all terms in Eq. (4.9) have been derived analytically already in the former case in Section 4.3 except the term $\frac{df(t_k)}{dU_i}$, i.e., in this case $\frac{df(t_k)}{d\boldsymbol{\mu}^{SD}}$ and $\frac{df(t_k)}{d\boldsymbol{\epsilon}^{SD}}$. The derivations of the analytical expressions of $\frac{df(t_k)}{d\boldsymbol{\mu}^{SD}}$ and $\frac{df(t_k)}{d\boldsymbol{\epsilon}^{SD}}$ are presented in this section.

Since both $\boldsymbol{\mu}^{SD}$ and $\boldsymbol{\epsilon}^{SD}$ do not directly appear in Eq. (4.1), the analytical expressions of $\frac{df(t_k)}{d\boldsymbol{\mu}^{SD}}$ and $\frac{df(t_k)}{d\boldsymbol{\epsilon}^{SD}}$ are derived using the Chain Rule:

$$\frac{df(t_k)}{d\mu_i^{SD}} = \frac{df(t_k)}{d\boldsymbol{\theta}} \cdot \frac{d\boldsymbol{\theta}}{d\boldsymbol{\lambda}} \cdot \frac{d\boldsymbol{\lambda}}{d\boldsymbol{v}} \cdot \frac{d\boldsymbol{v}}{d\boldsymbol{\mu}} \cdot \frac{d\boldsymbol{\mu}}{d\mu_i^{SD}}$$
$$= \sum_{lj=1}^{\dim(\boldsymbol{\mu})} \left(\sum_{ij=1}^{\dim(\boldsymbol{v})} \left(\sum_{j=1}^{\dim(\boldsymbol{\lambda})} \left(\sum_{l=1}^{\dim(\boldsymbol{\theta})} \frac{df(t_k)}{d\theta_l} \cdot \frac{d\theta_l}{d\lambda_j} \right) \cdot \frac{d\lambda_j}{dv_{ij}} \right) \cdot \frac{dv_{ij}}{d\mu_{lj}} \right) \cdot \frac{d\mu_{lj}}{d\mu_i^{SD}} \tag{4.19}$$

$$\frac{df(t_k)}{d\epsilon_i^{SD}} = \frac{df(t_k)}{d\boldsymbol{\theta}} \cdot \frac{d\boldsymbol{\theta}}{d\boldsymbol{\lambda}} \cdot \frac{d\boldsymbol{\lambda}}{d\boldsymbol{v}} \cdot \frac{d\boldsymbol{v}}{d\boldsymbol{\epsilon}} \cdot \frac{d\boldsymbol{\epsilon}}{d\epsilon_i^{SD}}$$
$$= \sum_{lj=1}^{\dim(\boldsymbol{\epsilon})} \left(\sum_{ij=1}^{\dim(\boldsymbol{v})} \left(\sum_{j=1}^{\dim(\boldsymbol{\lambda})} \left(\sum_{l=1}^{\dim(\boldsymbol{\theta})} \frac{df(t_k)}{d\theta_l} \cdot \frac{d\theta_l}{d\lambda_j} \right) \cdot \frac{d\lambda_j}{dv_{ij}} \right) \cdot \frac{dv_{ij}}{d\epsilon_{lj}} \right) \cdot \frac{d\epsilon_{lj}}{d\epsilon_i^{SD}} \tag{4.20}$$

The first three terms in both equations, $\frac{df(t_k)}{d\boldsymbol{\theta}}$, $\frac{d\boldsymbol{\theta}}{d\boldsymbol{\lambda}}$ and $\frac{d\boldsymbol{\lambda}}{d\boldsymbol{v}}$, are the same terms as obtained in Eq. (4.12) and can be computed analytically as described in Section 4.3. The 4th terms, $\frac{d\boldsymbol{v}}{d\boldsymbol{\mu}}$ and $\frac{d\boldsymbol{v}}{d\boldsymbol{\epsilon}}$, can be simply derived according to the expressions of $\boldsymbol{v}$

written in Eq. (2.9a-b). And the 5th terms, $\frac{d\boldsymbol{\mu}}{d\mu_i^{SD}}$ and $\frac{d\boldsymbol{\epsilon}}{d\epsilon_i^{SD}}$, can be obtained from the expressions of the Rosenblatt transformation in Eq. (4.17) and the Orthogonal transformation in Eq. (4.18). The analytical expression of the derivatives related to the CDF and inverse CDF are derived using Maple.

4.5.2 Probabilistic distributions of the seismological properties

This section discusses the distributions assumed for the seismological properties of M, R_{rup} and V_{s30} in $\boldsymbol{\mu}$. It is assumed that the moment magnitude (M) follows the Gutenberg-Richter law [92,93], the source to site distance (R_{rup}) follows a uniform distribution and the site-soil shear-wave velocity (V_{s30}) follows a Gaussian distribution. Details and discussions on the probabilistic distributions assumed for M and R_{rup} are elaborated.

a) *Distribution of the moment magnitude (M)*

The distribution of the moment magnitude (M) used in this work is described by the Gutenberg-Richter law, which expresses the relationship between the earthquake moment magnitude and the frequency of occurrence for any region and timescale specified. The expected number of earthquakes (N) with moment magnitude greater than $\widehat{M}$ in the timescale (T_{G-R}) inherent to the Gutenberg-Richter parameters is given by:

$$N_{M \geq \widehat{M}} = 10^{a - b\widehat{M}} \tag{4.21}$$

where a and b are the Gutenberg-Richter parameters defined by the seismicity of the region and the timescale of interest. The a-value represents the total seismicity rate

of the region and is dependent of the timescale considered. The b-value describes the proportional frequency of occurrence versus the moment magnitude $\widehat{M}$ and is independent of the timescale. The values of the a and b may vary significantly from region to region and most quoted values are in an annual-basis context. The model indicates the expected total number of earthquakes (N_{total}) by setting $\widehat{M} = 0$, which shows that the total number of earthquakes depends only on the a-value:

$$N_{total} = 10^{a} \tag{4.22}$$

The cumulative density function (CDF) $\phi_M(\cdot)$ and the probability density function (PDF) $f_M(\cdot)$ of the moment magnitude (M) are defined from Eq. (4.21) as:

$$\phi_M(\widehat{M}) = 1 - \frac{N_{M \geq \widehat{M}}}{N_{total}} = 1 - 10^{-b\widehat{M}} \tag{4.23a}$$

$$f_M(\widehat{M}) = 10^{-b\widehat{M}} \cdot b \cdot \ln(10) \tag{4.23b}$$

b) *Distribution of the source to site distance (R_{rup})*

The source to site distance (R_{rup}), also known as the rupture distance, is the closest distance from the site to the rupture area on the fault plane. Assuming that *point A* in Figure 4. 5 indicates the site location and *plane B* is the only fault plane nearby the site for simplification. The rupture can occur at any point on the fault plane with the same probability of occurrence. The closest distance from the site to the rupture area is evenly distributed from l_1 to l_2. Thus, a uniform distribution is assumed for the source to site distance (R_{rup}). The CDF $\phi_R(\cdot)$ and PDF $f_R(\cdot)$ of the R_{rup} are defined as:

$$\phi_R(R_{rup}) = \begin{cases} 0 & \text{for } R_{rup} < l_1 \\ \dfrac{R_{rup} - l_1}{l_2 - l_1} & \text{for } R_{rup} \in [l_1, l_2] \\ 0 & \text{for } R_{rup} > l_2 \end{cases} \quad (4.24a)$$

$$f_R(R_{rup}) = \begin{cases} \dfrac{1}{l_2 - l_1} & \text{for } R_{rup} \in [l_1, l_2] \\ 0 & \text{otherwise} \end{cases} \quad (4.24b)$$

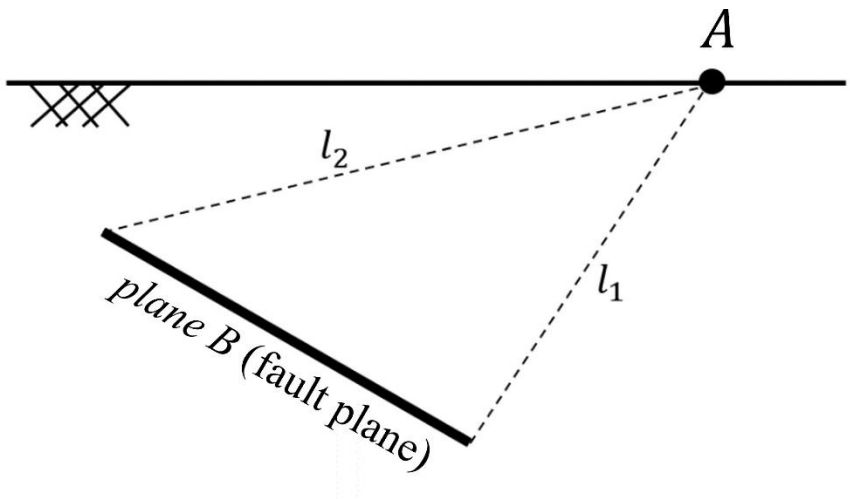


Figure 4. 5 Illustration of the possible source to site distances (R_{rup})

4.6 Reliability under repeated earthquakes

For a structure its seismic reliability over a period of time over which it will be subjected to repeated earthquakes is ultimately the main quantity of interest. This section links the developments of the previous sections for a single seismic event, P_R, to its reliability under any possibly occurring earthquakes in a time period of interest. Again, in this work, failure is defined as a structural response exceeding a threshold. The failure probability, P_f, refers to the probability of the structural response exceeding the threshold and the reliability P_r, also known as the survival probability, refers to the probability of non-exceedance. It is further assumed that if failure occurs after an earthquake, it is immediately repaired.

To obtain the seismic reliability of a structure in the next T years, information regarding the occurrence of earthquakes in this period and the seismic reliability of the structure in multiple earthquakes is needed. The seismic reliability of a structure over a period T is computed by:

$$P_R{}^{(T)} = 1 - P_F^{(T)} = 1 - \sum_{i=0}^{\infty} P_f(n_e = i) P^{(T)}(n_e = i) \tag{4.25}$$

where $P_F^{(T)}$ is the failure probability of a structure over the period T, n_e is the number of earthquakes that the structure may be subjected to over that period, $P_f(n_e = i)$ is the failure probability of the structure after i earthquakes and $P^{(T)}(n_e = i)$ is the probability of i earthquakes occurring over the period. Here, we consider structural responses exceeding the threshold in any of the occurring earthquakes in time T as failure. Under this assumption, the failure probability of a structure under repeated earthquakes, $P_f(n_e = i)$, is the union of the probability of each failure event, while the reliability, $P_r(n_e = i)$, is the intersection of the probability of each survival event:

$$P_f(n_e = i) = \bigcup_{j=1}^{i} P_f^{(j)} \tag{4.26a}$$

$$P_r(n_e = i) = \bigcap_{j=1}^{i} P_r^{(j)} \tag{4.26b}$$

where $P_f^{(j)}$ and $P_r^{(j)}$ is the failure probability and the reliability of structure in the j^{th} earthquake, respectively. As post each earthquake the structure is assumed to be repaired, the survival events are mutually independent, the reliability of a structure after i earthquakes is simply $P_r(n_e = i) = \bigcap_{j=1}^{i} P_r^{(j)} = P_r(n_e = 1)^i$, and the failure

probability, $P_f(n_e = i)$, is obtained accordingly:

$$P_f(n_e = i) = 1 - P_r(n_e = i) = 1 - P_r(n_e = 1)^i \tag{4.27}$$

By substituting Eq. (4.27) into Eq. (4.25), the failure probability of a structure in time T, $P_F^{(T)}$, can be rewritten as:

$$\begin{aligned} P_F^{(T)} &= \sum_{i=0}^{\infty} \left(1 - P_r(n_e = 1)^i\right) \cdot P^{(T)}(n_e = i) \\ &= \sum_{i=0}^{\infty} P^{(T)}(n_e = i) - \sum_{i=0}^{\infty} P_r(n_e = 1)^i \cdot P^{(T)}(n_e = i) \\ &= 1 - \sum_{i=0}^{\infty} P_r(n_e = 1)^i \cdot P^{(T)}(n_e = i) \end{aligned} \tag{4.28}$$

The expression is simplified since the total summation of the probability of i earthquakes ($i = 1,2, \dots, \infty$) occurring in time T is 1. The reliability of a structure in a time T, ${P_R}^{(T)}$, is then expressed by:

$${P_R}^{(T)} = \sum_{i=0}^{\infty} P_r(n_e = 1)^i \cdot P^{(T)}(n_e = i) \tag{4.29}$$

To find the probability of i earthquakes occurring in time T, $P^{(T)}(n_e = i)$ in the above equations, we assume that the occurrence of the earthquake events follows a Poisson arrival process, i.e., the number of the earthquake events occurring in a time interval of interest is Poisson distribution. The likelihood of observing i earthquakes in time T is given by:

$$P^{(T)}(n_e = i) = \frac{e^{-\lambda}(\lambda)^i}{i!} \tag{4.30}$$

in which the distribution parameter λ is defined as the total number of earthquakes expected to occur in time T, i.e., $\lambda = N_{total}^{(T)}$, which can be obtained from the Gutenberg Richter model. As mentioned above, the Gutenberg-Richter model

indicates the number of earthquakes with magnitude $M \geq \widehat{M}$ that are expected to occur in a given time period T_{G-R}. The total number of earthquakes expected to occur in time T is given by:

$$N_{total}^{(T)} = N_{total}^{(A)} \cdot T \tag{4.31}$$

where $N_{total}^{(A)} = 10^{a} / T_{G-R}$ is the number of earthquakes expected to occur annually. By substituting Eq. (4.31) into Eq. (4.30), the probability of i earthquakes occurring in time T is given by:

$$P^{(T)}(n_e = i) = \frac{e^{-\left(N_{total}^{(A)} \cdot T\right)} \cdot \left(N_{total}^{(A)} \cdot T\right)^{i}}{i!} \tag{4.32}$$

Then by replacing Eq. (4.32) into Eq. (4.29), the expression of the reliability ${P_R}^{(T)}$ of a structure in time T is:

$${P_R}^{(T)} = \sum_{i=0}^{\infty} P_r(n_e = 1)^{i} \cdot \frac{e^{-\left(N_{total}^{(A)} \cdot T\right)} \cdot \left(N_{total}^{(A)} \cdot T\right)^{i}}{i!} \tag{4.33}$$

After mathematical simplification, the expression can be written as

$${P_R}^{(T)} = e^{\left(N_{total}^{(A)} \cdot T\right)(P_r(n_e=1)-1)} \tag{4.34}$$

where $P_r(n_e = 1) = P_R$ is the reliabilities of structural responses over a single earthquake event modelled within a stochastic framework, where the ground motion is treated as a random process rather than being defined by a specific earthquake event, which can be obtained using the DPE-EAD method through *Algorithm 2* and Eq. (3.29) introduced in Section 3.4.1. To sum up, when the reliability P_R over an earthquake event is obtained, seismic reliability over a period of time T under the possibly occurring repeated earthquakes is estimated by Eq. (4.34).

4.7 Examples: Reliability of structures subjected to excitations with stochastic seismological properties.

The 4-DoF structural system with Bouc-Wen nonlinearity and the 10-DoF structural system with polynomial nonlinearity introduced in *Example 1* and *Example 2* are considered to examine the developed DPE-EAD method in estimating the reliability of structures subjected to earthquake model with stochastic seismological properties. The stochastic earthquake model introduced in Section 4.1 is adopted. Regarding the seismological properties, the reverse fault type ($F = 1$) is considered. The parameters $a = 0.45$ and $b = 0.51$ (for an annual basis context) are selected in the Gutenberg-Richter model to define the distribution of M. Since the earthquake model define by Eq. (4.1) in Section 4.1 is designed by regression of earthquake records with moment magnitude $M \geq 6$, simulating severe earthquake is desirable for this model. Thus, the reliability is only estimated for the occurrence of severe earthquakes with $M \geq 6$. The CDF of the moment magnitude M is amended accordingly, in which $N_{total} = N_{M\geq 6}$:

$$\phi_M(\widehat{M}) = \begin{cases} 1 - \dfrac{N_{M\geq\widehat{M}}}{N_{total}} = 1 - \dfrac{N_{M\geq\widehat{M}}}{N_{M\geq 6}} = 1 - 10^{-b\widehat{M}+6b} & \text{for } \widehat{M} \geq 6 \\ 0 & \text{otherwise} \end{cases} \tag{4.35}$$

For the selected Gutenberg-Richter parameters, the expected probability of the occurrence of an earthquake with $M \geq 6$ over a period of 100 years is about 0.25 (a return period of 400 years). In the uniform distribution of R_{rup}, the parameters $l_1 = 85\text{km}$ and $l_2 = 120\text{km}$ are selected in Eq. (4.24a-b). And in the Gaussian distribution of V_{s30}, the mean $\mu_V = 800\text{m/s}$ and standard deviation $\sigma_V = 50$ are selected. The values of the intensity of the white noise $S_0 = 5 \cdot 10^5\ \text{N}^2\text{s/rad}$, the

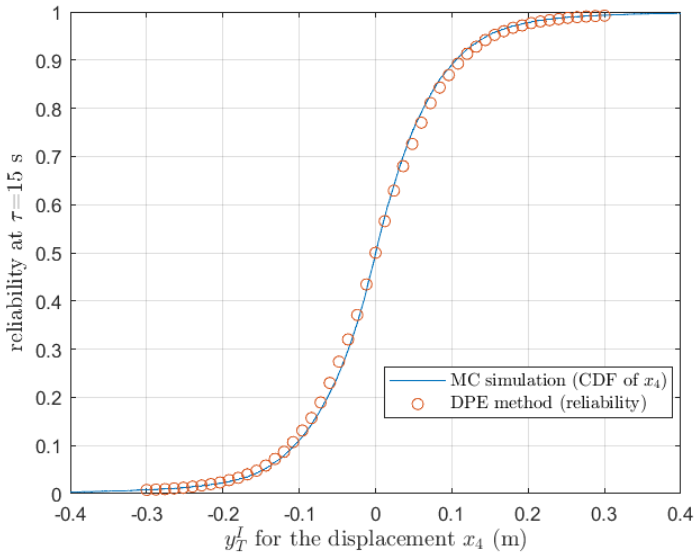
discretization time step $\Delta t_D = 0.01\text{s}$ and the integration time step $\Delta t_I = 0.01\text{s}$ in *Examples 1* and *2* are used. The MC simulation is used as a reference for the results.

4.7.1 Example 3 – *Structural system with Bouc-Wen nonlinearity subjected to excitations with stochastic seismological properties.*

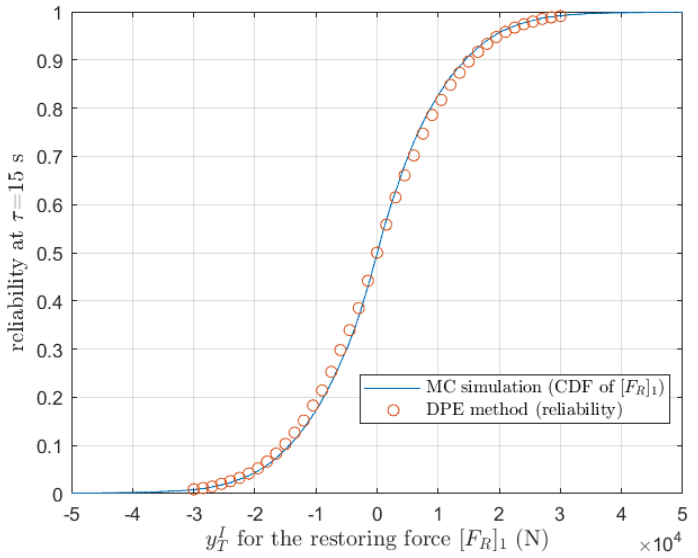
The same 4-storey shear building studied in *Example 1* with Bouc-Wen nonlinearity is now subjected to the earthquake model of Eq. (4.1) with stochastic seismological properties in this example. For the ease of comparison, the responses of interest chosen in *Example 1*, the 4th storey displacement (x_4) and the 1st storey restoring force ($[\boldsymbol{F}_R]_1$), are also considered here to examine the effectiveness of the extended DPE-EAD method for finding reliabilities of the structure subjected to earthquakes with stochastic seismological properties. A convergence test is performed in the MC simulation and finds that at least 20000 samples are required to estimate the reliability properly if a 5% maximum accepted relative error is considered.

First, the reliability for the responses at the time instant $\tau = 15\text{s}$ is concerned. Figure 4. 6(a) and (b) illustrate the reliabilities for the 4th storey displacement, i.e., $y = x_4$, regarding thresholds $[y_T^I] = \pm[0.012 \cdot I]$ m where $I = 1,2,\dots,25$ and the reliabilities for the 1st storey restoring force, i.e., $y = [\boldsymbol{F}_R]_1$, regarding thresholds $[y_T^I] = \pm[1500 \cdot I]$ N, where $I = 1,2,\dots,20$ estimated by the extended DPE-EAD method. An average of 1.2 iterations are required in finding each design point $\boldsymbol{U}^*(y_T^I, \tau)$ for both responses using the line search optimization (*Algorithm 2*). Compared to the iterations required in *Example 1*, the number of iterations needed

does not necessarily increase with the additional randomness associated with the seismological properties in this seismic model. Compared to the CDF obtained from the MC sample set, the DPE-EAD method underestimates the reliability. The maximum relative differences are about 5.5% at $y_T^4 = \pm 0.048\text{m}$ for $y = x_4$ and 5.2% at $y_T^4 = \pm 6000\text{N}$ for $y = [\boldsymbol{F}_R]_1$. Nonetheless, the estimated reliabilities still agree



(a) $y = x_4(\tau)$



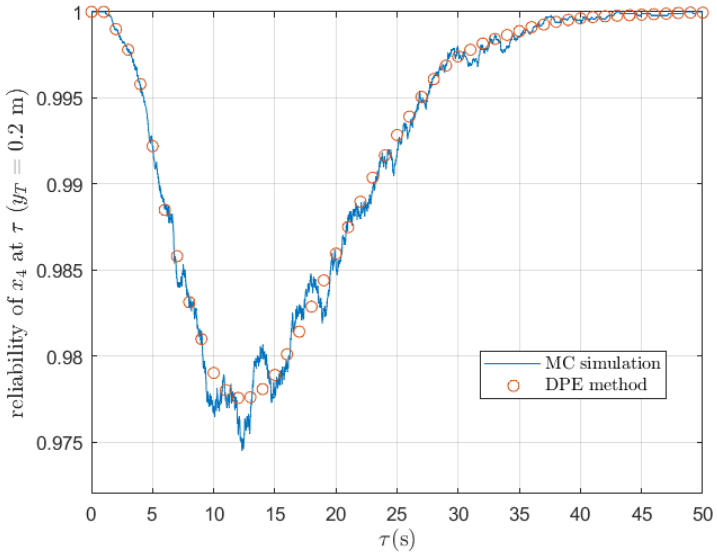
(b) $y = [\boldsymbol{F}_R]_1(\tau)$

Figure 4. 6 The reliability of $x_4(\tau)$ and $[\boldsymbol{F}_R]_1(\tau)$ at $\tau = 15\text{s}$ approximated by the DPE method for a sequence of thresholds versus the CDF of which obtained by the MC simulations.

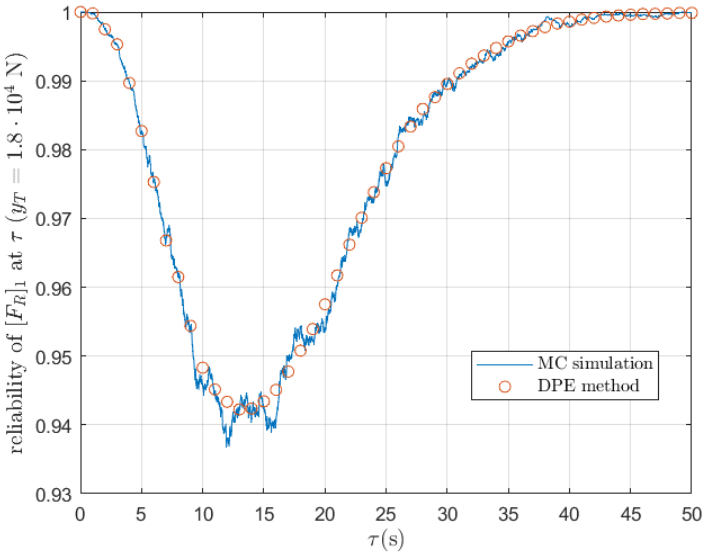
well in general, which tells that the Euler-analytical estimate of the derivatives, especially the new derived terms with respect to the amended terms in $\boldsymbol{U}$, i.e., the seismological properties and the error terms, are sufficiently accurate in solving the optimization problems. The extended DPE-EAD method is effective in reliability estimations for structures with Bouc-Wen nonlinearities subjected to seismic excitations with stochastic seismological properties.

The reliabilities for the responses at time instants $[\tau_J] = [J]\,\mathrm{s}$, where $J = 1,2,\ldots,50$ in the earthquake are then estimated to find the reliability of the responses for a time period concerned. The threshold limits $y_T = 0.2\mathrm{m}$ and $y_T = 1.8 \cdot 10^4\mathrm{N}$ are chosen for x_4 and $[\boldsymbol{F}_R]_1$ respectively. Starting with the initial guess obtained by time shifting, each design point $\boldsymbol{U}^*(y_T, \tau_J)$ for the constructed LSF $G(\boldsymbol{U}, \tau_J)$ is located by one iteration on average for both responses using the line search optimization. The corresponding reliabilities $P_R(\tau_J)$ for x_4 and $[\boldsymbol{F}_R]_1$ are plotted in Figure 4. 7(a) and (b), where the maximum relative differences between the DPE-EAD method and the MC estimations are found to be 0.3% at about $\tau_{12} = 12\mathrm{s}$ for the response x_4 with $y_T = 0.2$ m, and 0.7% at $\tau_{12} = 12\mathrm{s}$ and at about $\tau_{16} = 16\mathrm{s}$ for the response $[\boldsymbol{F}_R]_1$ with $y_T = 1.8 \cdot 10^4$ N. The reliability indexes β_J and the direction vectors α_J obtained are then used in Eq. (3.29) to find the reliabilities for the responses in the 50 seconds considered, which are $P_R = 0.78$ for x_4 and $P_R = 0.491$ for $[\boldsymbol{F}_R]_1$. Compared to the reliabilities found by the MC simulation, $P_R = 0.758$ for x_4 and $P_R = 0.459$ for $[\boldsymbol{F}_R]_1$, a relative estimation errors of 2.8% and

6.5% are observed. The reliability (P_R) obtained for one earthquake, together with the information of the Gutenberg-Richter model selected, can be further used in Eq. (4.34) to estimate the reliability of the structure in the future T years of interest. In this example, by only considering earthquakes with $M \geq 6$, i.e. $N_{total}^{(A)} = 10^{a-6b}$, the reliabilities for the responses x_4 and $[\boldsymbol{F}_R]_1$ in the next $T = 100$ years are $P_R{}^{(T)} =$



(a) $y = x_4(\tau)$ with $y_T = 0.2$ m



(b) $y = [\boldsymbol{F}_R]_1(\tau)$ with $y_T = 1.8 \cdot 10^4$ N

Figure 4. 7 The reliability of $x_4(\tau)$ and $[\boldsymbol{F}_R]_1(\tau)$ estimated at a sequence of time instants τ using the DPE-EAD method and the MC simulations.

0.947 and $P_R{}^{(T)} = 0.883$ respectively.

The computational costs in finding the reliabilities for the responses $y = x_4$ and $y = [\boldsymbol{F}_R]_1$ are summarized in Table 4. 2. The computational cost of the MC simulation for this example is higher than that of *Example 1* shown in Table 4. 1 due to the larger sample set required for convergence. While in the DPE-EAD method, the time taken to calculate the reliability as shown in the 1st and 2nd columns of DPE-EAD and to compute the derivatives (with $\tau = 15\text{s}$ and $\Delta t_I = 0.01\text{s}$) as shown in the 3rd column of DPE-EAD in Table 4. 2 does not vary significantly compared to the same measures in *Example 1*. The computational efficiency of the DPE-EAD method, or more specifically, the number of iterations needed in *Algorithm 2* in locating the design point $\boldsymbol{U}^*$ and the efficiencies of the computation of the derivative $\nabla_{\boldsymbol{U}} G$ and the root-finding procedure (*fzero* command in MATLAB) in finding $\hat{\beta}$ in step 3 of *Algorithm 2*, are not essentially affected by the higher order randomness involved in the seismic model. These efficiencies are extensively influenced by the size of the variable $\boldsymbol{U}$. Regarding the more complex seismic model with stochastic seismological properties used in this example, the size of $\boldsymbol{U}$ is only expanded with three extra terms ($\boldsymbol{\mu}^{SD}$) related to the seismological properties, and thus does not affect much in terms of computational efficiency. Also, as shown in Table 4. 2, the time needed in locating each design point (time for per threshold), as shown in the 1st column of DPE-EAD and computing the derivative, shown in the 3rd column of DPE-EAD for $y = x_4$ and $y = [\boldsymbol{F}_R]_1$ has little difference. It suggests that the effectiveness of the extended DPE-EAD method

is not necessarily affected by the complexity of the response of interest. This example illustrates that the extended DPE-EAD method is substantially more efficient than the MC simulation in estimating the reliability for structures with Bouc-Wen non-linearities subjected to excitations with stochastic seismological properties.

Table 4. 2 The computational costs of the DPE-EAD method and the MC simulations in *Example 3* and *Example 4*

	Response of interest	**Design Point Excitation method (DPE-EAD)**			**MC sim.**
		Find $\boldsymbol{U}^*(y_T^I,\tau)$ for dim (I) thresholds	Find $\boldsymbol{U}^*(y_T,\tau_j)$ for dim (J) time instants	Computing $\nabla_{\boldsymbol{U}} G$ (Avg.)	Generating the sample set
Ex. 3	$y = x_4$	10.9 min. 26.3 s per threshold	37.2 min.	10.5 s	11.1 h
	$y = [\boldsymbol{F}_R]_1$	8.9 min. 26.7 s per threshold	37.8 min.	10.2 s	
Ex. 4	$y = \ddot{x}_1$	14.2 min. 42.5 s per threshold	60.2 min.	13.6 s	16.1 h

4.7.2 Example 4 - *Structural system with polynomial nonlinearity subjected to excitations with stochastic seismological properties.*

The 10-storey shear building with polynomial nonlinearity introduced in *Example 2* is subjected to the earthquake model in Eq. (4.1) with stochastic seismological properties. For the ease of comparison, the response of interest chosen in *Example 2*, the 1st storey acceleration $(\ddot{x}_1)$, is considered in this example to examine the extended DPE-EAD method for finding reliabilities for the structure subjected to earthquakes with stochastic seismological properties. The convergence test suggests that 20000 samples are required in the MC simulation to estimate the reliability properly.

Firstly, the reliability for $y = \ddot{x}_1(\tau)$ at $\tau = 15\text{s}$ with a set of thresholds $[y_T^I] = \pm[(4 \cdot 10^{-3}) \cdot I]\ \text{m/s}^2$, where $I = 1,2,\dots,20$ is estimated and plotted in Figure 4. 8.

An average of 1.4 iterations are required in locating each design point $\boldsymbol{U}^*(y_T^I, \tau)$ by the line search in this example, which is also not highly affected by the higher order randomness in the seismic model. The maximum relative difference of the reliability estimations is about 3% at $y_T^2 = \pm 8 \cdot 10^{-3}\ \mathrm{m/s^2}$, which is reasonably accurate. It indicates that the derivatives with respect to the seismological properties and the error terms derived in this work are sufficiently accurate and the extended DPE-EAD method is effective in estimating reliability for a nonlinear response of a structure with polynomial nonlinearities subjected to excitations with stochastic seismological properties.

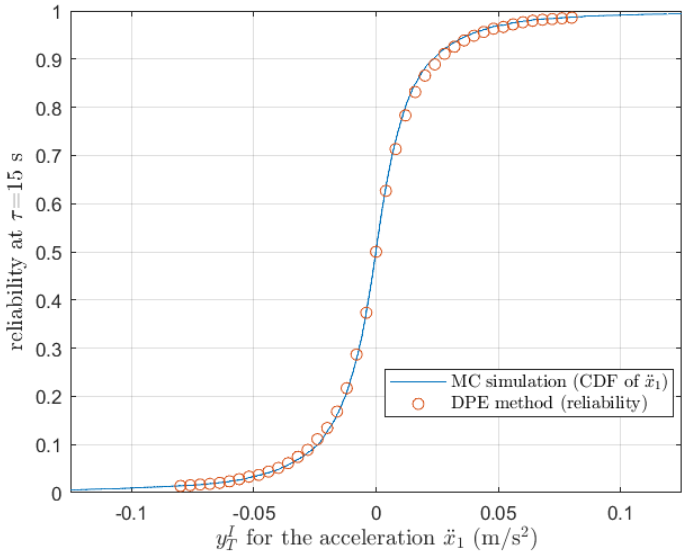


Figure 4. 8 The reliability of $\ddot{x}_1(\tau)$ at $\tau = 15\mathrm{s}$ approximated by the DPE-EAD method for a sequence of thresholds versus the CDF of which obtained by the MC simulations.

The reliabilities for the responses at a set of consecutive time instants $[\tau_J] = [J]$ s, where $J = 1,2,\ldots,50$ are estimated with the threshold $y_T = 0.05\mathrm{m/s^2}$ selected. The design points $\boldsymbol{U}^*(y_T, \tau_J)$ are located by an average of one iteration, benefited from a good initial guess obtained by time shifting. The corresponding reliabilities

$P_R(\tau_J)$ are plotted in Figure 4. 9, in which the maximum relative differences between the DPE-EAD method and the MC estimations are found to be 0.4% at about $\tau_{11} = 11\text{s}$ and $\tau_{23} = 23\text{s}$. Using the reliability indexes β_J and the direction vectors α_J obtained, the reliability of $\ddot{x}_1$ in the period of the 50 seconds considered is $P_R = 0.576$ computed by Eq. (3.29). Compared to the MC simulation result of $P_R = 0.535$, a relative estimation errors of 7.1% is observed. Then according to Eq.(4.34), by only considering earthquakes with $M \geq 6$, i.e. $N_{total}^{(A)} = 10^{a-6b}$, the reliability for $\ddot{x}_1$ in the next $T = 100$ years is $P_R{}^{(T)} = 0.901$.

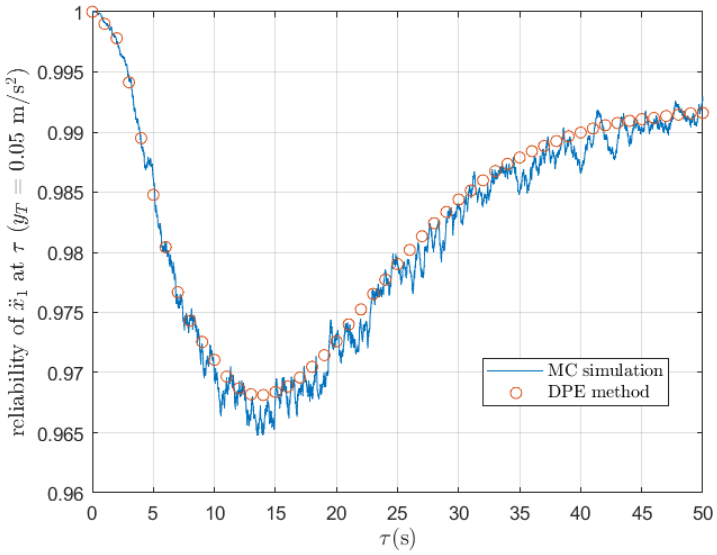


Figure 4. 9 The reliability of $\ddot{x}_1(\tau)$ with $y_T = 0.05\ \text{m/s}^2$ estimated at a sequence of time instants τ using the DPE method and the MC simulations.

The time required to find the reliability for $y = \ddot{x}_1$ in both methods are summarized in Table 4. 2. In the DPE-EAD method, the efficiency is not highly influenced by the higher order randomness in the seismic model. The computational cost of finding the reliability and computing the derivatives in this example is comparable to the same measures in *Example 2*. The superior efficiency of the

extended DPE-EAD method also indicates that the effectiveness of the extended DPE-EAD method is not essentially affected by the complexity of the response of interest. The extended DPE-EAD method substantially saves the computational cost in estimating the reliability of the structure subjected to excitations with stochastic seismological properties.

4.8 Conclusion

This work develops an effective seismic reliability estimation framework accounting for the randomness of the seismic model parameters. To begin with, an extension of the DPE-EAD method that deals with structures subjected to seismic models with stochastic model parameters is introduced. The method is further extended to estimate the reliability of structures subjected to the seismic model with stochastic seismological properties. The stochastic seismic model parameters and the stochastic seismological properties are added to construct an augmented variable in the optimization problem considered in the DPE-EAD method. As an important role in the optimization procedure to find the design point and so to estimate the reliability, the gradient of the LSF with respect to the stochastic model parameters is obtained using the EAD method, in which the analytical expressions of the derivatives with respect to the stochastic model parameters are derived in this chapter through the use of Chain Rule.

The extended DPE-EAD method is examined in examples of one structure system with Bouc-Wen nonlinearity and another with polynomial nonlinearity. Comparing to

the MC simulations, the developed method is robust and allows accurate evaluation of the seismic reliability of structures for given seismological properties of interest. The results also validate the accuracy of the gradient estimated by the EAD method using the derived analytical expression of the derivatives with respect to the stochastic model parameters. Additionally, the DPE-EAD method, as demonstrated in the examples studied, is substantially more efficient than the commonly employed MC sampling method for calculating the reliability. With the information of the likelihood of earthquake events in the future years, the developed framework can also predict the seismic reliability of structural systems under the possibly occurring earthquakes.

Chapter 5

The Application of Pontryagin's Maximum Principle in the Optimizations in Seismic Reliability Estimations

This Chapter presents a novel application of the Pontryagin's maximum principle (PMP) in reliability estimations. As in Chapter 3 and Chapter 4, the design point is normally determined using optimization methods in the DPE method. In this chapter, rather than solving for a discretized optimal input white noise, represented by a vector of standard Gaussian variables in the optimization problem, the PMP method finds the continuous-time optimal signal in an optimal signal control problem. To solve for the optimal signal using the PMP, a multi-shooting method is adopted to prevent the instability in numerical integrations of the state-space equations of the system defined by the Hamiltonian. The application of the PMP method incorporated into the DPE

method for finding the design point is elaborated and the corresponding algorithms are presented. Subsequently, the performance of the so-called DPE-PMP method to find the reliability is compared to the results of the DPE-EAD method and MC simulations, through the illustrative examples of two structural systems with polynomial nonlinearity and Bouc-Wen nonlinearity. Further insights into the design points obtained by the DPE-PMP and DPE-EAD methods are also discussed later in the chapter.

5.1 Pontryagin's Maximum Principle (PMP)

In this Chapter, the concept of the Pontryagin's maximum principle (PMP) is applied for the optimizations in reliability estimations. According to the DPE method introduced in Section 3.1, in the process of determining the reliability of the structural response $y(\tau)$ under a random process, solving the optimization problem in Eq. (3.4) that finds the design point $\boldsymbol{u}^*$ plays a crucial role and it directly influences the accuracy and the efficiency of the DPE method. To enhance the application and efficiency of the DPE method, there is a continual interest in developing robust methods that effectively determine the design points. In this research work, a novel method that adopts the PMP is developed to find the design points.

5.1.1 The optimal signal

The random process considered in this work is represented by an excitation model with deterministic model parameters, as introduced in Eq. (3.1) and considered in Chapter 3, in which case the standard Gaussian input vector $\boldsymbol{u}$ considered in the optimization

problem in Eq. (3.4) is essentially the input signal $u(t)$ after discretization. The common way to solve the optimization problem in Eq. (3.4) is through optimization methods, which finds the discretized signal $\boldsymbol{u}^*$ directly. According to the nature of $\boldsymbol{u}$, the optimization problem can also be treated as an optimal signal control problem which finds the optimal input signal $u^*(t)$ in a continuous time form.

In order to define the input signal $u(t)$, the stochastic excitation $f(t)$, subject to the structural system defined by state-space equations in Eq. (3.2), is represented by the continuous time form as:

$$f(t) = \int_0^t s(t_\tau)u(t_\tau)dt_\tau \tag{5.1}$$

where $u(t)$ is a standard white noise and $s(t_\tau)$ is a function in terms of deterministic model parameters. In this case, the Limit State Function (LSF) that separates the safety and the failure regions is refined accordingly as:

$$G(u(t), y_T, \tau) = y_T - y(u(t), \tau) = 0 \tag{5.2}$$

where $G(u(t), y_T, \tau) > 0$ indicates the safety region. The optimal signal $u^*(t)$ is defined accordingly as:

$$[u^*(t)](y_T, \tau) = \arg\min\left\{\int_0^\tau u^2(t)dt \,|G(u(t), y_T, \tau) = 0\right\} \tag{5.3}$$

which is an optimal signal control problem that can be solved using the Pontryagin's maximum principle (PMP).

5.1.2 The concept of the PMP

The Pontryagin's maximum principle (PMP) [18,69] states a set of conditions that

holds on the trajectory of a system subjected to the optimal control signal $u^*(t)$. The optimal control signal, $u^*(t)$, is defined as the signal that minimizes an objective function J over the time period for $t \in [0, \tau]$ subjected to a constraint function C defined by the following equations:

$$\text{minimize} \qquad J = \psi_J\big(\boldsymbol{X}(\tau)\big) + \int_0^\tau L_J(\boldsymbol{X}(t), u(t))dt \tag{5.4a}$$

$$\text{subjected to} \quad C = \psi_C\big(\boldsymbol{X}(\tau)\big) + \int_0^\tau L_C(\boldsymbol{X}(t), u(t))dt \tag{5.4b}$$

According to Eq. (5.3), the optimization problem in the DPE method is to find the optimal signal $u^*(t)$ that

$$\text{minimize} \qquad J = \int_0^\tau u^2(t)dt \tag{5.5a}$$

$$\text{subjected to} \quad C = G(u(t), y_T, \tau) \tag{5.5b}$$

with the system of equations in Eq. (5.5) being a special subcase of equations in Eq. (5.4) where $\psi_J\big(\boldsymbol{X}(\tau)\big) = 0$, $L_J\big(\boldsymbol{X}(t), u(t)\big) = u^2(t)$, $\psi_C\big(\boldsymbol{X}(\tau)\big) = G(u(t), y_T, \tau)$ and $L_C\big(\boldsymbol{X}(t), u(t)\big) = 0$. The PMP states that the optimal control signal $u^*(t)$ is found when the Hamiltonian H is maximized, which is defined as:

$$\begin{aligned} H\big(\boldsymbol{X}(t), \boldsymbol{p}(t), u(t)\big) &= \boldsymbol{p}^T(t) \cdot \boldsymbol{l}_P\big(\boldsymbol{X}(t), u(t)\big) - L_J\big(\boldsymbol{X}(t), u(t)\big) \\ &= \boldsymbol{p}^T(t) \cdot \boldsymbol{l}_P(\boldsymbol{X}(t), u(t)) - u^2(t) \end{aligned} \tag{5.6}$$

The Hamiltonian in PMP is different to the physical Hamiltonians used in classical mechanics. Instead of describing the conservation of physical energy, this time-dependent Hamiltonian integrates system dynamics and cost functions to achieve the optimal control strategy. $\boldsymbol{l}_P(\boldsymbol{X}(t), u(t))$ is the state-space equation that describes the dynamic system of interest. Since $u(t)$ is the input considered in the system,

$\boldsymbol{l}_P(\boldsymbol{X}(t), u(t))$ represents the dynamics of both the structural model and the excitation model. The state vector $\boldsymbol{x}(t)$ of the structural system is defined in the state-space equation Eq. (3.2a). The excitation model $f(t)$ adopted, input to the structural system in Eq. (3.2a), is required to be represented by a state-space and measurement equations with the $u(t)$ being the input in the application of the PMP method as:

$$\dot{\boldsymbol{x}}_w(t) = \boldsymbol{l}_g\big(\boldsymbol{x}_w(t), u(t)\big) \tag{5.7a}$$

$$f(t) = \boldsymbol{h}_g\big(\boldsymbol{x}_w(t), u(t)\big) \tag{5.7b}$$

where $\boldsymbol{x}_w(t)$ is the state vector of the dynamic system that represents the excitation $f(t)$. By substituting the expression of the excitation in Eq. (5.7b) into the state-space equation of the structural system in Eq. (3.2a), we have $\boldsymbol{l}\big(\boldsymbol{x}(t), f(t)\big) = \boldsymbol{l}\Big(\boldsymbol{x}(t), \boldsymbol{h}_g(\boldsymbol{x}_w(t), u(t))\Big)$ which can be written in the form of $\boldsymbol{l}_P(\boldsymbol{X}(t), u(t))$ as abbreviation, where the state vector $\boldsymbol{X}(t)$ is defined as a congregation of the state vector that describes the structural system and that describes the excitation model:

$$\boldsymbol{X}(t) = [\boldsymbol{x}^T(t), \boldsymbol{x}_w^T(t)]^T \tag{5.8}$$

As shown in the above equation, $\boldsymbol{l}_P(\boldsymbol{X}(t), u(t))$ is adjoined to the Lagrangian L by introducing time-varying Lagrange multiplier vector $\boldsymbol{p}(t)$, whose elements are called the co-states of the system. The adjoint co-state vector $\boldsymbol{p}$ has the same size as the system state $\boldsymbol{X}$, i.e., $\dim(\boldsymbol{p}) = \dim(\boldsymbol{X})$. The maximum principle states that the Hamiltonian is maximized at the optimal control signal $u^*(t)$, i.e, the condition:

$$[u^*(t), \boldsymbol{X}^*(t), \boldsymbol{p}^*(t)] = \arg\max \{H(\boldsymbol{X}(t), u(t), \boldsymbol{p}(t), t)\} \tag{5.9}$$

holds on the optimal control signal $u^*(t)$, the optimal state trajectory $\boldsymbol{X}^*(t)$ and the

adjoint co-state trajectory $\boldsymbol{p}^*(t)$. The optimal control signal $u^*(t)$ that maximizes the Hamiltonian is found when the derivative of the Hamiltonian with respect to the input $u(t)$ is zero, i.e.,

$$\left.\frac{\partial H\big(\boldsymbol{X}(t),\boldsymbol{p}(t),u(t)\big)}{\partial u(t)}\right|_{u(t)=u(t)^*} = 0 \tag{5.10}$$

Solving to Eq. (5.10), w.r.t. the optimal signal, $u^*(t)$ is in terms of the trajectories of the system states in $\boldsymbol{X}^*(t)$ and the adjoint co-states in $\boldsymbol{p}^*(t)$, i.e.,

$$u^*(t) = \boldsymbol{r}\big(\boldsymbol{X}^*(t),\boldsymbol{p}^*(t)\big) \tag{5.11}$$

where the function $\boldsymbol{r}(\cdot,\cdot)$ is constructed according to the property of the maximum principle stated in Eq. (5.10) To find the optimal trajectories of the state $\boldsymbol{X}^*(t)$ and the adjoint co-state $\boldsymbol{p}^*(t)$, firstly, the state-space equation of the state $\dot{\boldsymbol{X}}$ and the adjoint co-state $\dot{\boldsymbol{p}}$ are defined. The paired system with both the original system states in $\boldsymbol{X}$ and the adjoint co-states in $\boldsymbol{p}$ satisfy:

$$\dot{\boldsymbol{X}} = \frac{\partial H(\boldsymbol{X},u,\boldsymbol{p})}{\partial \boldsymbol{p}} = l_p(\boldsymbol{X},u) \tag{5.12a}$$

$$\dot{\boldsymbol{p}} = -\frac{\partial H(\boldsymbol{X},u,\boldsymbol{p})}{\partial \boldsymbol{X}} = -\boldsymbol{p}^T \cdot \frac{\partial l_p(\boldsymbol{X},u)}{\partial \boldsymbol{X}} \tag{5.12b}$$

when $u(t)$ and $\boldsymbol{x}(t)$ are the optimal control signal and the optimal state trajectory. It should be noted that in Eq. (5.12), the state-space equations of the state $\boldsymbol{X}$ and the co-state $\boldsymbol{p}$ have opposite signs. If the dynamic system of the state $\boldsymbol{X}$ is positively damped which stabilizes the system, the dynamic system of the co-state $\boldsymbol{p}$ exhibits negative damping behaviour, leading to a destabilizing effect. This 'opposite' damping behaviour arises because the co-state dynamics reflect the sensitivity to future costs, effectively compensating for the state dynamics. The PMP also states a transversality

condition which defines the terminal values of the co-states $\boldsymbol{p}(t)$ at $t = \tau$:

$$\boldsymbol{p}(t = \tau) = -\lambda \cdot \nabla_{\boldsymbol{X}} G(u(t), y_T, \tau) \tag{5.13}$$

$$= \lambda \cdot \nabla_{\boldsymbol{X}} y(u(t), \tau)$$

where λ is a scalar constant that does not have physical meaning. The equation is simplified since $\nabla_{\boldsymbol{X}} G(u(t), y_T, \tau) = -\nabla_{\boldsymbol{X}} y(u(t), \tau)$ according to the constraint function $G(u(t), y_T, \tau)$ defined in Eq. (5.2) where y_T is a constant. Together with the constraint condition stated in Eq. (5.2), one would have sufficient number of equations to solve for the initial conditions of the co-states $\boldsymbol{p}(t = 0)$ and the parameter λ. It should be noted that the excitation signal $u(t)$ is expressed in terms of the state $\boldsymbol{X}(t)$ and the co-state $\boldsymbol{p}(t)$ Eq. (5.11).

A shooting method is typically adopted to solve for $\boldsymbol{p}(t = 0)$ and λ. In this work, we employ a more robust variation of the shooting method, known as the multi-shooting method. Further details on the multi-shooting method are provided in Section 5.2. With the initial conditions of the co-states $\boldsymbol{p}(t = 0)$ defined, the trajectories of the state $\boldsymbol{X}^*(t)$ and the co-state $\boldsymbol{p}^*(t)$ for $t \in [0, \tau]$ are obtained through the time integrations of the state-space equations in Eq. (5.12a-b), and the optimal control signal $u^*(t)$ is then computed by Eq. (5.11).

The algorithm of suggested PMP method in finding the optimal control signal $u^*(t)$ concerned in the DPE method for reliability estimation is summarized:

Algorithm 5

Initialization:

Derive the analytical expression of the derivatives $\frac{\partial H(\boldsymbol{X}(t),\boldsymbol{p}(t),u(t))}{\partial u(t)}$, $\frac{\partial l_p(\boldsymbol{X},u)}{\partial \boldsymbol{X}}$ and $\nabla_{\boldsymbol{X}} y(u(t),\tau)$. Construct the state-space equation of the state $\dot{\boldsymbol{X}}$ and the adjoint co-state $\dot{\boldsymbol{p}}$ by Eq. (5.12a-b).

1. Define the $\boldsymbol{r}(\cdot,\cdot)$ function in Eq. (5.11) by the property of the maximum principle stated in Eq. (5.10).
2. Solve for the initial condition of the co-states $\boldsymbol{p}(t=0)$ and the parameter λ that satisfy the transversality and constraint conditions defined in Eq. (5.13) and Eq. (5.2) by a shooting method.
3. Obtain the trajectory of the state $\boldsymbol{X}^*(t)$ and the co-state $\boldsymbol{p}^*(t)$ using the solution to $\boldsymbol{p}(t=0)$ and λ found in step 3.
4. Calculate for the optimal control signal $u^*(t)$ using Eq. (5.11).

To find the reliability index β that ultimately approximate the reliability, the optimal control signal $u^*(t)$ is discretized to $\boldsymbol{u}^* = [u_i^*]$ where u_i^* is the discretized optimal signal at $t_i = i * \Delta t_D$, $i = 1,2,\dots,n$, $n = \tau/\Delta t_D$ and Δt_D is the discretization time step. The reliability index β and the corresponding reliability $P_R(\tau)$ is then calculated by Eq. (3.6) and Eq. (3.5).

5.2 The shooting method

The problem of finding initial conditions $\boldsymbol{p}(t=0)$ that satisfy the transversality and constraint conditions stated in Eq. (5.13) and Eq. (5.2) in the PMP method is defined as a Boundary Value Problems (BVP). It can be solved by a shooting method that is widely used in the BVPs to find the initial conditions at $t=0$ that satisfy a given

boundary condition at $t = \tau$. In this section, the concept of the shooting method [77-80,94] is elaborated, and the method is summarized as an algorithm to solve for the BVP defined in the PMP method (step 5 in *Algorithm 5*).

5.2.1 The concept of the shooting method - single shooting

The shooting method converts a BVP to an Initial Value Problem (IVP). It takes advantage of the speed and adaptivity of methods for IVPs [94]. In the shooting method, for a system defined by differential equations as in Eq. (5.12a-b), the boundary conditions at $t = \tau$ are considered as a multivariate function of the initial conditions at $t = 0$. The method uses iterative guesses of the initial conditions until it finds the set that satisfies the boundary conditions defined in the BVP. Thus, for solving the BVP in the PMP method, the shooting method is an iterative method [94] that finds the initial conditions $\boldsymbol{p}(t = 0)$ and the parameter λ that satisfy the boundary conditions at $t = \tau$, in this case the transversality condition and the constraint condition defined by Eq. (5.13) and Eq. (5.2). The algorithm is summarized as follows:

Algorithm 6

1. Select an arbitrary value for the $\boldsymbol{p}(t = 0)$ and λ.
2. Integrate the state- space equation in Eq. (5.12a-b) for $\boldsymbol{X}$ and $\boldsymbol{p}$ from $t = 0$ to $t = \tau$ with the initial condition $\boldsymbol{p}(t = 0)$ selected in step 1.
3. If the obtained $\boldsymbol{p}(t = \tau)$ and $G(u(t), y_T, \tau)$ satisfy the transversality and the constraint conditions, the algorithm ends. Otherwise, go back to step 1 and repeat iteratively.

For implementations, a root-finding algorithm [96,77,78] which follows the above iterative procedure is adopted since it selects appropriate iterative values of $\boldsymbol{p}(t=0)$ and λ in a smart and efficient way.

5.2.2 The multi-shooting method

The numerical integration can be unstable in finding the solution to the IVP for systems that have unstable modes as in the case of the adjoint system in the PMP, especially when an inappropriate initial condition is selected [95]. To overcome the instability of the system in the numerical integrations, the concept of multi-shooting is considered [79,80].

In the state-space system defined by Eq. (5.12a-b) in the BVP in the Pontryagin's Maximum principle (PMP) method, the state-space equation of the adjoint co-states $\boldsymbol{p}$ in Eq. (5.12b) has a negative damping, thus is unstable when it is integrated directly from $t=0$ to $t=\tau$. To reduce the numerical integration error induced by the instability, the multi-shooting method partitions the original time interval $[0,\tau]$ given by BVP into a set of smaller sub-time intervals $\left[t^j, t^{j+1}\right]$ by introducing equally spaced time grids in $t \in [0,\tau]$, where $t^j = j \cdot \Delta t_g$ for $j = 0,1,2,\ldots,N_g$ and $\Delta t_g = \tau/N_g$. N_g is the number of sub-time intervals formed and $N_g - 1$ is the number of additional time grids introduced. Instead of integrating the system from $t^0 = 0$ to $t^{N_g} = \tau$ in one go, as would be the case for single shooting, the differential equations are integrated gradually in each sub-time intervals $\left[t^j, t^{j+1}\right]$. The initial conditions of the state $\boldsymbol{X}$ and the co-state $\boldsymbol{p}$ at the added $N_g - 1$ time grids are extra unknowns

imposed. To solve the extra unknowns, $N_g - 1$ matching conditions are constructed at each added time grids t^j for $j = 1,2,\dots,N_g - 1$. Together with the transversality condition Eq. (5.13), one has a system of N_g equations that is sufficient to solve for the conditions of $\boldsymbol{X}$ and $\boldsymbol{p}$ in all the N_g sub-time intervals. The conditions of $\boldsymbol{X}$ and $\boldsymbol{p}$ solved in each sub-time intervals form a solution to the original BVP for the whole-time interval.

To further alleviate the instability imposed by the adjoint co-states $\boldsymbol{p}$ in forward integrations from t^j to t^{j+1}, a variation of multi-shooting method is adopted, in which backward integrations from t^{j+1} to t^j take place in half of the sub-time intervals. In backward integrations, the state-space equation of the adjoint co-states $\boldsymbol{p}$ in Eq. (5.12b) are stable and effectively have positive damping and state-space equation of the states $\boldsymbol{X}$ in Eq. (5.12a) have negative damping. The system is integrated in either a forward or a backward direction in a sub-time interval. To balance the instability imposed by the states $\boldsymbol{X}$ and the adjoint co-states $\boldsymbol{p}$, forward integration is applied in the sub-time interval where j in t^j is odd and the backward integration is applied where j in t^j is even. The condition matching equations are constructed as follows:

Forward (for odd j):

$$\boldsymbol{X}\left(t = t^{j+1}\right) = \int_{t^j}^{t^{j+1}} \dot{\boldsymbol{X}}\, dt \tag{5.14a}$$

$$\boldsymbol{p}\left(t = t^{j+1}\right) = \int_{t^j}^{t^{j+1}} \dot{\boldsymbol{p}}\, dt \tag{5.14b}$$

Backward (for even j):

$$\boldsymbol{X}(t = t^j) = \int_{t^{j+1}}^{t^j} \dot{\boldsymbol{X}}\, dt \tag{5.15a}$$

$$\boldsymbol{p}(t = t^j) = \int_{t^{j+1}}^{t^j} \dot{\boldsymbol{p}}\, dt \tag{5.15b}$$

It should be noted that finding the conditions of the state $\boldsymbol{X}$ and the adjoint co-state

$\boldsymbol{p}$ at $t = t^{j+1}$ is an IVP when forward integration in Eq. (5.14a-b) is applied, while it is a BVP when backward integration in Eq. (5.15a-b) is applied since the unknown condition at $t = t^{j+1}$ is an initial condition in Eq. (5.15a-b) and the known condition at $t = t^{j}$ is a boundary condition. The conditions of the states $\boldsymbol{X}$ and the adjoint co-states $\boldsymbol{p}$ at all time grid t^{j} as well as the solution to the original BVP in the PMP method, i.e., $\boldsymbol{p}(t = 0)$ and λ, are solved by the above system of equations in Eq. (5.14) and Eq. (5.15) together with the constraint and the transversality conditions written in Eq. (5.2) and Eq. (5.13) using a root-finding algorithm. The algorithm of the multi-shooting method, a modified *Algorithm 6*, is summarized as follows:

Algorithm 7

1. Select a proper number of sub-time intervals N_g.
2. Construct the condition matching equations as in Eq. (5.14a-b) and Eq. (5.15a-b) for each sub-time interval $[t^{j}, t^{j+1}]$.
3. Select an arbitrary value for the $\boldsymbol{p}(t = 0)$ and λ.
4. Integrate the state $\boldsymbol{X}$ and the co-state $\boldsymbol{p}$ gradually in each sub-time interval $[t^{j}, t^{j+1}]$ from $t = 0$ to $t = \tau$ with the $\boldsymbol{p}(t = 0)$ selected in step 3.
5. If the obtained $\boldsymbol{p}(t = \tau)$ and $G(u(t), y_T, \tau)$ satisfy the transversality and the constraint conditions, the algorithm ends. The conditions of $\boldsymbol{X}$ and $\boldsymbol{p}$ at all t^{j} are solved simultaneously. Otherwise, go back to step 3 and repeat iteratively.

For implementations, a root-finding algorithm which follows the iterative procedure in step 3 to step 5 is applied to find the solution to $\boldsymbol{p}(t = 0)$ and λ

efficiently. In this work, the trust-region dogleg algorithm [97], i.e., *fsolve* command in MATLAB is used.

5.3 Examples

A 3-Degrees-of-Freedom structural system with a polynomial nonlinearity and a 4-Degrees-of-Freedom structural system with Bouc-Wen nonlinearity are considered to examine the Design Point Excitation method with the suggested Pontryagin's Maximum Principle (DPE-PMP) method, implemented by *Algorithm 5* and *7*, in estimating the reliability of structural responses subjected to earthquakes. Both linear function of the structural system state vector $\boldsymbol{x}$, i.e., the storey displacement and drift, and nonlinear function of $\boldsymbol{x}$, i.e., the acceleration, are considered in the observation function of Eq. (3.2b) as the response of interest. The Design Point Excitation method with the Euler Analytical estimate of the Derivative (DPE-EAD) and the Monte Carlo simulation (MC) are applied for cross-comparison. The DPE-EAD method applied solves the original optimization problem in Eq. (3.4) using the line search with gradients estimated by the EAD method. Details of the method can be found in Chapter 3. The design point and the reliability obtained are used as references to show the reliability estimation performance of the DPE-PMP method. The trust-region dogleg algorithm (*fsolve* command in MATLAB) [97] is used for root-finding in the multi-shooting method (*Algorithm 7*). All approaches use the Runge-Kutta (4, 5) pair (*ode45* command in MATLAB) [86,87] to integrate the differential equations.

To facilitate cross-comparison, the Der Kiureghian's stochastic earthquake model

[13,14] utilized to illustrate the DPE-EAD method in Section 3.5.1 is employed in the following illustrative examples. The ground excitation is expressed in continuous time as:

$$f(t) = q(t) \cdot \int_0^t h(t - t_\tau) w(t_\tau) dt_\tau \tag{5.16}$$

where the white noise $w(t) = \sigma u(t)$ and $\sigma = \sqrt{2\pi S_0}$ describes the intensity of the white noise and $S_0 = 10^4$. The modulating function is given by $q(t) = 0.03 \cdot t^2 \cdot \exp(-0.2t)$. The unit-impulse response function of the filter corresponds to the pseudo-acceleration of a single Degree-of-Freedom linear oscillator is selected:

$$h(t) = \frac{\omega_f}{\sqrt{1-\zeta_f^2}} \cdot \sin\left(\omega_f t \sqrt{1-\zeta_f^2}\right) \cdot \exp(-\zeta_f \omega_f t) \tag{5.17}$$

where $\omega_f = 5\pi$ rad/s and $\zeta_f = 0.4$. First, for the applications of the PMP and DPE-EAD method, the expression of the ground excitation $f(t)$ is amended as follows. In the PMP method, the ground motion is required to be represented by a states-space and measurement equation in Eq. (5.7). As defined earlier in the impulse response function $h(t)$ selected, $\int_0^t h(t - t_\tau) w(t_\tau) dt_\tau$ in Eq. (5.16) is equivalent to the pseudo acceleration $a_{psu}(t)$ of the linear system defined by the following differential equation:

$$\ddot{x}_w(t) + 2\,\omega_f \zeta_f \dot{x}_w(t) + {\omega_f}^2 x_w(t) = w(t) \tag{5.18}$$

where $\boldsymbol{x}_w = [x_w, \dot{x}_w]^T$ is the state vector of the dynamic system defining the ground excitation and $w(t)$ is the white noise excitation. The pseudo acceleration is defined as $a_{psu}(t) = {\omega_f}^2 x_w(t)$. The differential equation in Eq. (5.18) defines the state-

space equation in Eq. (5.7a). And the measurement equation of Eq. (5.7b) for the ground excitation defined in Eq. (5.16) is expressed by:

$$f(t) = \boldsymbol{h}_g\big(\boldsymbol{x}_w(t), u(t)\big) = q(t) \cdot {\omega_f}^2 x_w(t) \tag{5.19}$$

In the implementation of the DPE-EAD method, since the design point $\boldsymbol{u}^*$ found by the optimization problem defined in Eq. (3.4) is a vector of the discretized input excitation, the ground model is discretized as:

$$f(t) = \ q(t) \cdot \sum_{i=1}^{N} h(t - t_i) w_i \tag{5.20}$$

in which the discretized white noise $w_i = \sigma u_i$ for $i = 1,2, \dots, n$ and $\sigma = \sqrt{2\pi S_0 \Delta t_D}$. A discretization time step $\Delta t_D = 0.01\text{s}$ is chosen and $N = t/\Delta t_D$. For cross-comparison, the time step used for discretizing the seismic model in the DPE-EAD method is selected for discretizing the optimal control signal found by the DPE-PMP method.

A series of equally spaced threshold limits are considered in each response to examine the performance of the suggested DPE-PMP method. It should be noted that threshold limits may have negative signs which refer to negative directions. Here in the examples, since the structure studied is symmetric, only positive threshold limits are selected.

5.3.1 Example 1: *A 3-DoF system with polynomial nonlinearity subjected to earthquake excitation.*

The 3-story shear building with the structural model shown in Figure 5. 1 is considered:

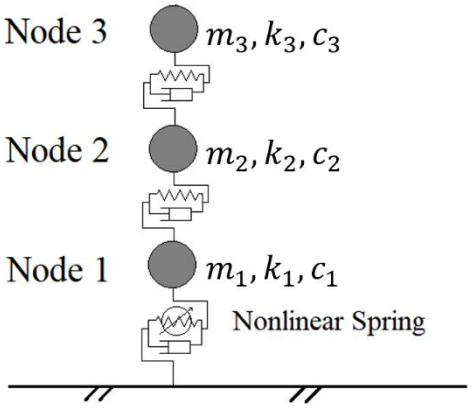


Figure 5. 1 The structural model considered in *Example 1*

m_i, k_i and c_i denote the mass, stiffness and damping coefficient of the i^{th} storey, respectively. Suppose the first storey of the shear building has a cubic nonlinearity, and the rest of the stories are linear elastic. The 3-storey shear building model is represented by the following differential equations:

$$\boldsymbol{M}\ddot{\boldsymbol{x}}(t) + \boldsymbol{C}\dot{\boldsymbol{x}}(t) + \boldsymbol{K}(\boldsymbol{x}(t) + \boldsymbol{\gamma}\boldsymbol{x}(t)^3) = \boldsymbol{F}(t) \tag{5.21}$$

where the displacement vector is denoted as $\boldsymbol{x} = [x_1, x_2, x_3]^T$. $\boldsymbol{M}$, $\boldsymbol{C}$ and $\boldsymbol{K}$ are the mass matrix, damping matrix and the stiffness matrix of the corresponding linear-elastic shear building, respectively:

$$\boldsymbol{M} = \begin{bmatrix} m_1 & 0 & 0 \\ 0 & m_2 & 0 \\ 0 & 0 & m_3 \end{bmatrix},\ \boldsymbol{C} = \begin{bmatrix} c_1 + c_2 & -c_2 & 0 \\ -c_2 & c_2 + c_3 & -c_3 \\ 0 & -c_3 & c_3 \end{bmatrix} \text{ and}$$

$$\boldsymbol{K} = \begin{bmatrix} k_1 + k_2 & -k_2 & 0 \\ -k_2 & k_2 + k_3 & -k_3 \\ 0 & -k_3 & k_3 \end{bmatrix}$$

Suppose that $m_i = 3000\,\text{kg}$, $k_i = 5000(2\pi)^2\,\text{N/m}$ and $c_i = 1000\pi\,\text{Ns/m}$ for $i = 1,2,3$ are selected for the structure model. $\boldsymbol{\gamma}$ is a diagonal matrix written by $\boldsymbol{\gamma} = \begin{bmatrix} \gamma_1 & 0 & 0 \\ 0 & \gamma_2 & 0 \\ 0 & 0 & \gamma_3 \end{bmatrix}$, where γ_i controls the degree of nonlinearity for the i^{th} storey. In this

example, $\gamma_1 = 1\, m^{-2}$ is assumed for the first storey and the rest of the storeys are assumed to be linear, i.e., $\gamma_2 = \gamma_3 = 0$. The excitation is defined by $\boldsymbol{F}(t) = [m_1, m_2, m_3]^T \cdot f(t)$, where $f(t)$ is the ground excitation defined above in Eq. (5.16).

In this example, the reliability of the top storey displacement $y = x_3(\tau)$ and the first storey acceleration $y = \ddot{x}_1(\tau)$ are of interest. The time instant $\tau = 12\text{s}$ is selected since it is in the strong motion period of the earthquake according to the envelope function. For the response $y = x_3(\tau)$, the thresholds $[y_T^I] = [\, 2 \cdot 10^{-3} \cdot I]$ m where $I = 1,2, \dots, 20$ are selected. For the response $y = \ddot{x}_1(\tau)$, the first storey acceleration is expressed by $\ddot{x}_1(\tau) = [-\boldsymbol{M}^{-1} \cdot \boldsymbol{K}(\boldsymbol{x}(\tau) + \boldsymbol{\gamma}\boldsymbol{x}(\tau)^3)]_1$. It should be noted that this output is a non-linear function of the state vector $\boldsymbol{x}$. The thresholds $[y_T^I] = [1.5 \cdot 10^{-2} \cdot I]\ \text{m/s}^2$ where $I = 1,2, \dots, 20$ are selected.

To ensure a good performance of the PMP method, an appropriate number of sub-time intervals N_g should be selected in the application of the multi-shooting. A small value of N_g is preferred in terms of the computational efficiency since fewer unknown conditions of the state $\boldsymbol{X}$ and the adjoint co-state $\boldsymbol{p}$ are solved in the root-finding of step 3 to step 5 in *Algorithm 7*. The least number N_g of sub-time intervals needed depends not only on the time instant τ for which the reliability estimation is pursued but also on the stability of the differential equations of the state $\boldsymbol{X}$ and the adjoint co-states $\boldsymbol{p}$, which is related to the seismic model and structural system considered. It may also vary when a different response is of interest in which case the transversality and the constraint conditions are different. It is necessary to ensure that

lengths of the sub-time intervals (corresponding to the selected N_g) are sufficiently small for stable integrations. An improper value of N_g leads to either failure in finding the initial condition $\boldsymbol{p}(t=0)$ and the parameter λ or inefficiency problems in the multi-shooting method. After investigations, $N_g = 13$ and $N_g = 15$ sub-time intervals are selected for $y = x_3(\tau)$ and $y = \ddot{x}_1(\tau)$ respectively in the numerical integrations.

The reliability obtained by the DPE-PMP method for the response $y = x_3(\tau)$ and $y = \ddot{x}_1(\tau)$ are plotted as scatter points in Figure 5. 2 and Figure 5. 3 respectively, in which the vertical axis indicates the reliability value and the horizontal axis specifies the corresponding thresholds y_T^I considered. It should be noted that the reliability starts at 0.5 since only positive thresholds are examined. The results obtained by the DPE-EAD method and by the MC simulation are plotted on the same figure for cross-comparison. To ensure the MC sample set is adequately large to generate accurate CDF

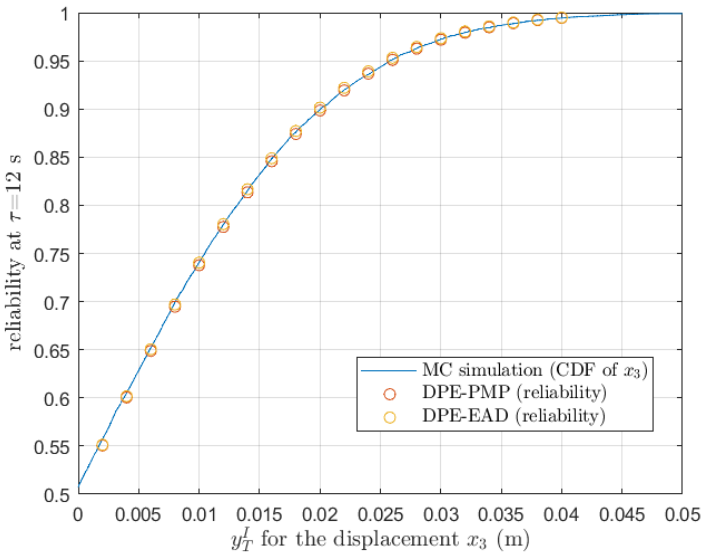


Figure 5. 2 The reliability of $x_3(\tau)$ at $\tau = 12\text{s}$ estimated by the DPE-PMP and DPE-EAD methods for a sequence of thresholds versus the CDF of which obtained by the MC simulation.

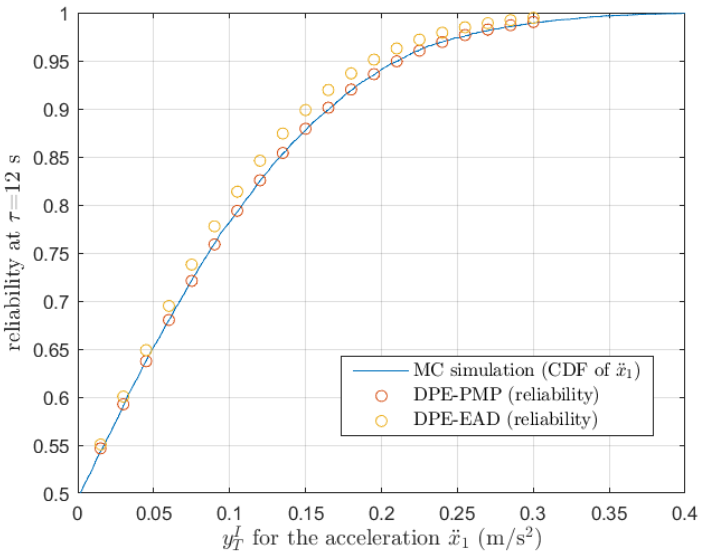


Figure 5. 3 The reliability of $\ddot{x}_1(\tau)$ at $\tau = 12\text{s}$ estimated by the DPE-PMP and DPE-EAD methods for a sequence of thresholds versus the CDF of which obtained by the MC simulation.

as references, a convergence test is carried out which finds that at least 15000 samples are required if a maximum of 5% relative error is allowed. The results show that for $y = x_3(\tau)$, the reliability estimated by both the DPE-PMP and the DPE-EAD method agree well with the CDF plot. While for $y = \ddot{x}_1(\tau)$, expressed by a non-linear function of the state vector $\boldsymbol{x}$, the reliability estimated by the DPE-PMP method have a better accuracy than that by the DPE-EAD method. This is potentially due to the different design points obtained by the two optimization approaches as discussed later. As shown in Figure 5. 2 and Figure 5. 3, the reliability estimated using the optimal signals $u^*(t)$ found by the PMP with the multi-shooting method (*Algorithm 7*) are sufficiently accurate for a large range of the thresholds, even in the tail regions with small probabilities of exceedance or non-exceedance. The maximum relative error of the DPE-PMP method is about 1.1% at $y_T^1 = 0.002\text{m}$ for $y = x_3(\tau)$ and 0.6% at $y_T^1 = 0.015\text{m/s}^2$ for $y = \ddot{x}_1(\tau)$ by referring to the MC estimations computed by Eq. (3.33)

which illustrates a great accuracy of the DPE-PMP method in the reliability estimation. The result shows that the suggested DPE-PMP method is applicable in the seismic reliability estimation of a response (y) in terms of either a linear or non-linear function of the state vector $\boldsymbol{x}$ for a structure with polynomial nonlinearity.

For a better understanding of the differences observed in the reliabilities estimated by the DPE-PMP and the DPE-EAD methods, the design points $\boldsymbol{u}^*$ found by both methods are plotted on the same figure for comparison in Figure 5. 5 and Figure 5. 4. Figure 5. 5 plots the design points $\boldsymbol{u}^*(y_T^{10}, \tau)$ for the response $y = x_3(\tau)$ with the threshold $y_T^{10} = 0.02\text{m}$ considered. Though the reliability estimated for the response $y = x_3(\tau)$ by the two methods are almost identical, the shape of the design points $\boldsymbol{u}^*$ are different in amplitude. This indicates that the optimized design point $\boldsymbol{u}^*$ found by different optimization approaches could potentially be a local minimum, although the reliability index and the reliability estimated are closely identical. This is because both DPE-PMP and DPE-EAD methods search for the optimized design point $\boldsymbol{u}^*$ by setting constraints only on the states in the state vector $\boldsymbol{x}$ that define the response of interest. The evolutions of the other states in $\boldsymbol{x}$ may vary in different optimized design points $\boldsymbol{u}^*$ obtained. For the response $y = \ddot{x}_1(\tau)$ where the estimated reliability has discrepancies, the design point $\boldsymbol{u}^*(y_T^8, \tau)$ with the threshold $y_T^8 = 0.12\text{m/s}^2$ obtained by the DPE-PMP and the DPE-EAD methods are plotted in Figure 5. 4 and are found to be different in both frequency and amplitude as expected.

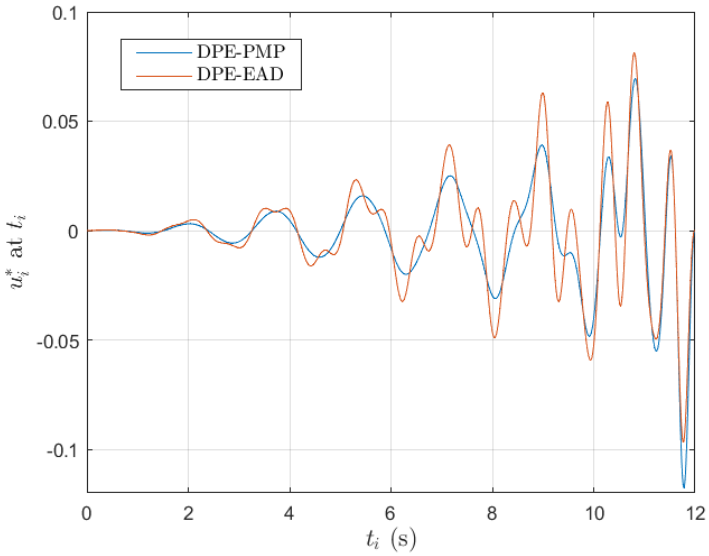


Figure 5. 5 The design point $\boldsymbol{u}^*(y_T^8, \tau)$ found by the DPE-PMP and the DPE-EAD methods for $y = \ddot{x}_1(\tau)$ with $y_T^8 = 0.12\text{m/s}^2$.

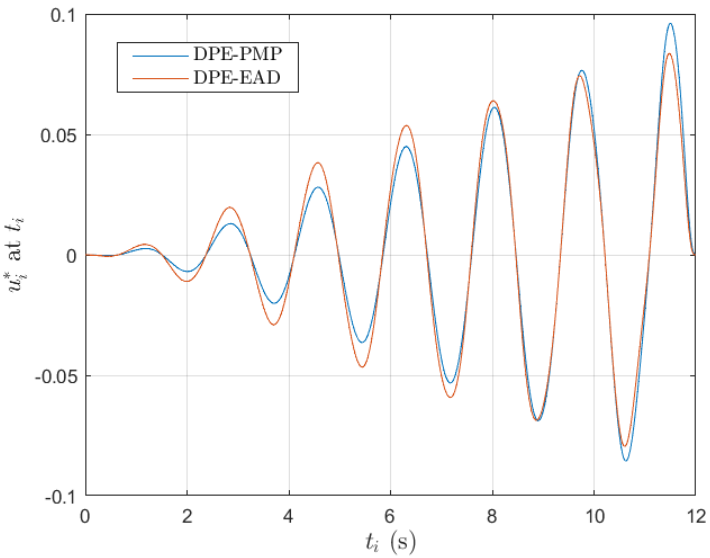


Figure 5. 4 The design point $\boldsymbol{u}^*(y_T^{10}, \tau)$ found by the DPE-PMP and the DPE-EAD methods for $y = x_3(\tau)$ with $y_T^{10} = 0.02\text{m}$.

In terms of computational efficiency, the calculation time in the reliability estimations using all three methods is summarized in Table 5. 1. The time required in the DPE-PMP and the DPE-EAD method, shown in the 2nd and 3rd column, refers to the total time of finding the reliability for all $\dim(I)$ thresholds considered in Figure

5. 2 and Figure 5. 3. The computational time for per threshold considered is also pointed out which is essentially the average time required in finding a design point $\boldsymbol{u}^*$ since the time for computing the reliability from $\boldsymbol{u}^*$ is negligible. In the DPE-PMP method, this is the time taken in finding the optimal signal $u^*(t)$ by the multi-shooting method (*Algorithm 7*) using the trust-region dogleg algorithm (*fsolve* command in MATLAB). Since as mentioned above, the efficiency of the root-finding algorithm is affected by the number of sub-time interval N_g selected and a proper value of N_g depends on the length of the total time interval τ considered, the computational cost of the root-finding algorithm varies with the time instant τ of interest. The computational efficiency of the DPE-PMP method also varies with the threshold y_T^I selected, since the smoothness nearby the actual solution of initial condition $\boldsymbol{p}(t=0)$ and the parameter λ and the number of iterations required in the root-finding vary in different y_T^I considered. As shown the 2nd column in Table 5. 1, the time cost for the DPE-PMP method in finding the reliability considering the response $y = x_3$ is about half of that considering the response $y = \ddot{x}_1$. This infers that the computational cost of the DPE-PMP is dependent on the complexity of the response of interest and is different to that of DPE-EAD method which is not necessarily dependent on the response of interest as shown in the 3rd column. The time required in the MC simulation, as shown in the 4th column, refers to the time for generating the whole sample set, i.e., in this example, it is 15000 samples of the earthquake time histories and the structural responses. The CDF of any responses of

interest can be computed through simple mathematical calculations from the evolutions of the structure state vector $\boldsymbol{x}$, which are available in the generated sample set. According to the time cost summarized in Table 5. 1, though the suggested DPE-PMP method is not as efficient as the DPE-EAD, it saves the computational cost compared to the MC simulation in estimating the seismic reliability of a response of a 3-DoF structure with polynomial nonlinearity.

Table 5. 1 The computational cost of the DPE-PMP, the DPE-EAD and the MC simulation in *Example 1*

Response of interest	**DPE-PMP method**	**DPE-EAD method**	**MC simulation**
	Find the reliabilities for $\dim(I)$ thresholds	Find the reliabilities for $\dim(I)$ thresholds	Generate the whole sample set
$y = x_3$	24.9 mins	7.2 mins	4.9 hours
	1.2 mins per threshold	21.5 s per threshold	
$y = \ddot{x}_1$	54.7 mins	8.4 mins	
	2.7 mins per threshold	25.2 s per threshold	

5.3.2 Example 2: *A 4-DoF system with Bouc-Wen nonlinearity subjected to earthquake excitation.*

The structural model of a 4-storey shear building with Bouc-Wen nonlinearity introduced in Section 3.5.1 *Example 1* is adopted for illustration. The 4-story shear building model is represented by the differential equations written in Eq. (3.30). Details of the parameters selected were introduced in Section 3.5.1. The excitation is defined by $\boldsymbol{F}(t) = [m_1, m_2, m_3, m_4]^T \cdot f(t)$, where $f(t)$ is the ground excitation defined above in Eq. (5.16).

In this example, the reliability of the top storey drift $y = \delta x_4(\tau)$ and the first storey restoring force $y = [\boldsymbol{F}_R]_1(\tau)$ are estimated. The time instant $\tau = 15\text{s}$ in the

strong motion period of the earthquake is selected. For the response $y = \delta x_4(\tau)$, the expression of the fourth storey drift $\delta x_4(\tau) = x_4(\tau) - x_3(\tau)$ is a linear function of state vector $\boldsymbol{x}$ of the structural system. The thresholds $[y_T^I] = [\pm 1 \cdot 10^{-4} \cdot I]$ m where $I = 1,2,\dots,20$ are selected. For the response $y = [\boldsymbol{F}_R]_1(\tau)$, the first storey restoring force is expressed by a linear function of the state vector $\boldsymbol{x}$ and the Bouc-Wen hysteretic term $\boldsymbol{Z}$. The thresholds $[y_T^I] = [100 \cdot I]$ N where $I = 1,2,\dots,20$ are selected. After investigations, $N_g = 17$ sub-time intervals are selected in the multi-shooting (*Algorithm 7*) in PMP method for both $y = \delta x_4(\tau)$ and $y = [\boldsymbol{F}_R]_1(\tau)$ in the numerical integrations.

The reliability of the response $y = \delta x_4(\tau)$ and $y = [\boldsymbol{F}_R]_1(\tau)$ for the thresholds y_T^I considered are plotted by scatter points in Figure 5. 6 and Figure 5. 7 respectively. The CDF of the responses obtained by the MC simulation are plotted on the same figures as references. According to a convergence test that considers a 5% relative error allowance, the CDF are plotted by a MC sample set with 20000 simulated samples. Figure 5. 6 and Figure 5. 7 show that for both responses considered in this example, $y = \delta x_4(\tau)$ and $y = [\boldsymbol{F}_R]_1(\tau)$, the reliability estimated by both the DPE-PMP and the DPE-EAD method are almost identical and agree well with the CDF plot. It reinforces the previous statement that PMP is robust in finding the optimal control signal $u^*(t)$. The maximum relative error of the DPE-PMP method is about 1.2% at $y_T^5 = 5 \cdot 10^{-4}$m for $y = \delta x_4(\tau)$ and 0.5% at $y_T^7 = 700$N for $y = [\boldsymbol{F}_R]_1(\tau)$ by referring to the MC estimations which illustrates a great accuracy of the DPE-PMP

method approximation. The results show that the suggested DPE-PMP method is sufficiently accurate yet robust in the seismic reliability estimation of a response (y) in terms of the state vector $\boldsymbol{x}$ and the hysteretic term $\boldsymbol{Z}$ for a structure with Bouc-Wen nonlinearity.

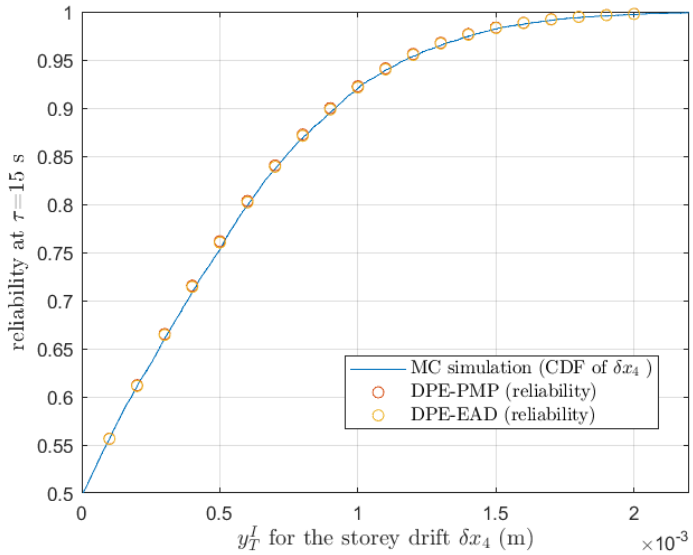


Figure 5. 6 The reliability of $\delta x_4(\tau)$ at $\tau = 15\text{s}$ estimated by the DPE-PMP and DPE-EAD methods for a sequence of thresholds versus the CDF of which obtained by the MC simulation.

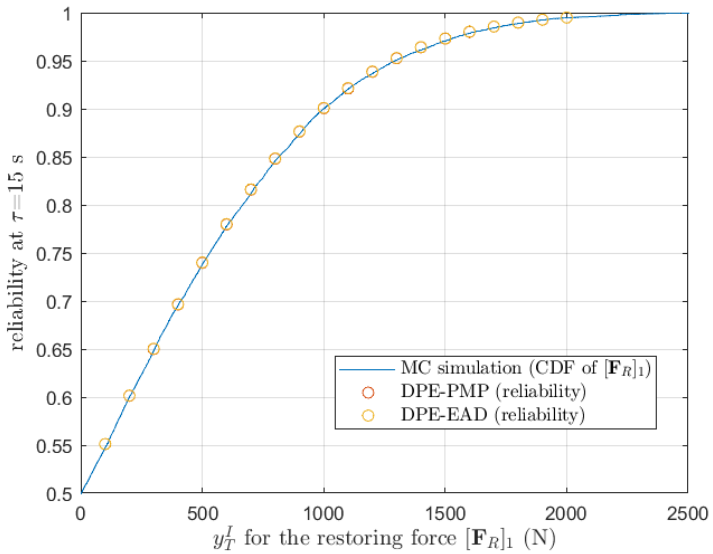


Figure 5. 7 The reliability of $[\boldsymbol{F}_R]_1(\tau)$ at $\tau = 15\text{s}$ estimated by the DPE-PMP and DPE-EAD methods for a sequence of thresholds versus the CDF of which obtained by the MC simulation.

The design point $\boldsymbol{u}^*$, which determines the reliability, found by the PMP and the DPE-EAD methods in the examples of $y = \delta x_4(\tau)$ with the threshold value $y_T^{10} = 10^{-3}\text{m}$ and the example of $y = [\boldsymbol{F}_R]_1(\tau)$ with the threshold value $y_T^5 = 500\text{N}$ are plotted in Figure 5. 8 and Figure 5. 9 respectively for comparison. Similar to the

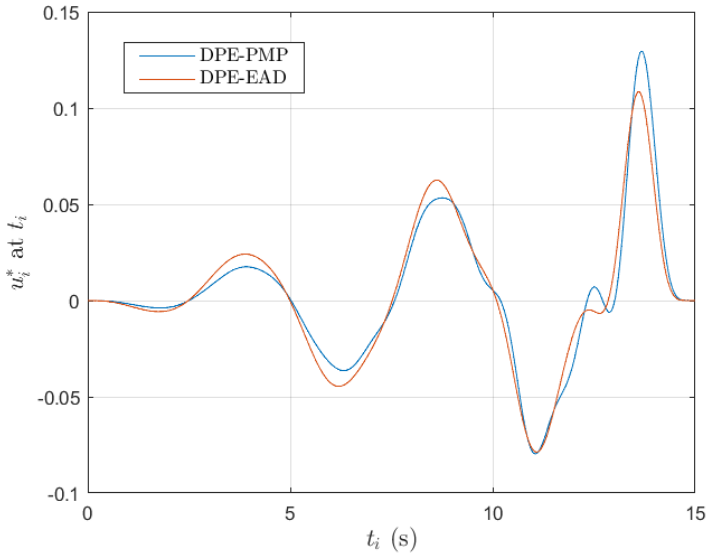


Figure 5. 8 The design point $\boldsymbol{u}^*(y_T^{10}, \tau)$ found by the DPE-PMP and the DPE-EAD methods for $y = \delta x_4(\tau)$ with $y_T^{10} = 10^{-3}\text{m}$.

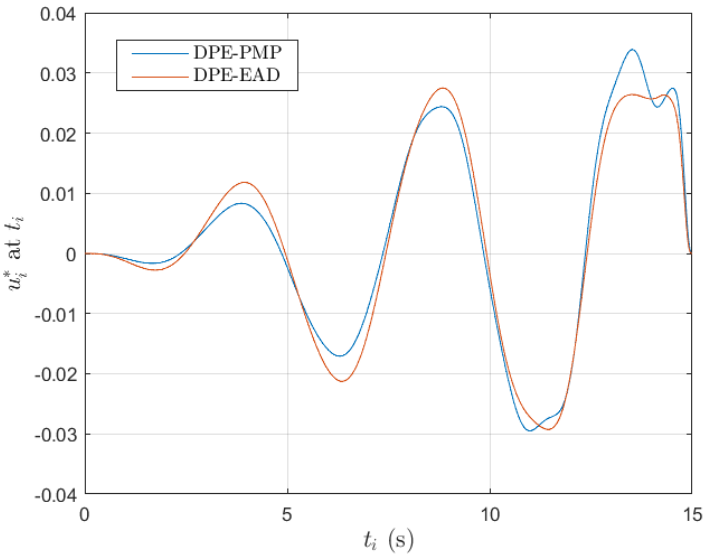


Figure 5. 9 The design point $\boldsymbol{u}^*(y_T^{10}, \tau)$ found by the DPE-PMP and the DPE-EAD methods for $y = [\boldsymbol{F}_R]_1(\tau)$ with $y_T^5 = 500\text{N}$.

observation in *Example 1*, the shapes of the design points $\boldsymbol{u}^*$ are not identical, yet provide similar reliability estimates.

The calculation time in this example is summarized in Table 5. 2. The time required in the DPE-PMP and the DPE-EAD method, shown in the 2nd and 3rd column, refers to the total time of finding the reliability for all $\dim(I)$ thresholds considered in Figure 5. 6 and Figure 5. 7. And the average time required in finding a design point $\boldsymbol{u}^*$, shown as the computational time for per threshold in Table 5. 2, is also pointed out. Compare to the computational cost shown in Table 5. 1 for *Example 1*, the cost in the DPE-PMP method increases evidently in this example where a higher order system is considered. The time cost in the DPE-PMP method, shown in the 2nd column in Table 5. 2, again points out that efficiency of the method is affected by the complexity of the response of interest. In this example, the time required in the MC simulation, as shown in the 4th column, refers to the time for generating 20000 samples of the earthquake time histories and the structural responses. According to the time cost summarized in Table 5. 2, the suggested DPE-PMP method is not as efficient as the DPE-EAD but would still save the computational cost in estimating the seismic reliability of a response of a 4-DoF structure with Bouc-Wen nonlinearity when it is compared to the MC simulation.

Table 5. 2 The computational cost of the DPE-PMP, the DPE-EAD and the MC simulation in *Example 2*

Response of interest	**DPE-PMP method**	**DPE-EAD method**	**MC simulation**
	Find the reliabilities for $\dim(I)$ thresholds	Find the reliabilities for $\dim(I)$ thresholds	Generate the whole sample set
$y = \delta x_4$	52.5 mins	11mins	5.7 hours
	2.6 mins per threshold	33.2 s per threshold	
$y = [\boldsymbol{F}_R]_1$	93 mins	4.9 mins	
	4.6 mins per threshold	14.6 s per threshold	

5.4 Conclusion

This research work develops an application of the PMP method in reliability estimations. It is incorporated in the DPE method to find the design point by treating the optimization problem as an optimal signal control problem. The optimal signal is found according to the conditions that the PMP stated. To apply the method, the state-space equation of the state $\dot{\boldsymbol{X}}$ and the adjoint co-state $\dot{\boldsymbol{p}}$ are constructed by the Hamiltonian. A forward and backward multi-shooting method is adopted to overcome the problem of instability of the system governing the co-states in numerical integrations due to a negative damping.

In the illustrative examples of structural systems with polynomial nonlinearity and with Bouc-Wen nonlinearity, the seismic reliabilities of the structural responses are estimated using the DPE-PMP method. The DPE-EAD method and the MC simulations are also performed for comparison. It is observed that the optimized design point $\boldsymbol{u}^*$ found by various optimization approaches may potentially represent a local minimum, yet the estimated reliabilities are accurate. The developed DPE-PMP method is robust in solving the optimization problem. Although the DPE-PMP method

is more expensive than the DPE-EAD method, it is significantly cheaper than the MC simulations and it inspires a novel direction to solve for the optimization problem.

Chapter 6

Conclusions and Future Work

In this chapter, the main contributions of this thesis are summarized, and some important directions of future work are discussed.

6.1 Summary and conclusions

The thesis focuses on the developments of robust and efficient frameworks for estimating the probabilistic response and the seismic reliability of structural systems under earthquake excitations. Efficient sampling methods and reliability methods have been considered and developed for estimating the response of structural systems subjected to stochastic excitations. The developed methods are expected to play impactful roles in any scientific or industrial field where reliability assessments are conducted. In a more detailed perspective, the contribution of each chapter is summarized in the following:

In Chapter 2, the concept of the Unscented Transform (UT), commonly used in the context of nonlinear extension of Kalman Filter, is adopted to estimate the statistics

of probability distributions, such as mean and covariance, of the seismic response of structural systems under stochastic earthquakes. The UT method potentially simplifies the computational complexity of the Monte Carlo (MC) simulation, as only a small number of nonlinear dynamic analyses at the selected sigma points need to be conducted to approximate the probability distribution of the structural responses. Two approaches based on the concept of the UT, the Offline and Online UT methods have been developed, each exhibiting distinct strengths. Specifically, the Offline UT method saves about half the computation costs of the MC simulations and if the focus of the study is on how model parameters influence mean and covariance of the target response, the method is more efficient than MC. The Online UT method stands out for its substantial efficiency and its accurate approximation of the mean and variance. The proposed methods can be further applied for seismic reliability evaluations.

In Chapter 3, the Design Point Excitation (DPE) method is introduced, which is based on the design point to estimate seismic reliability. The design point that computes the reliability is defined as the solution to an optimization problem. It is calculated using a line search optimization method, in which a vital part is to repeatedly compute the gradient of the Limit State Function (LSF). An Euler-Analytical estimate of the Derivatives (EAD) is developed to estimate the gradient of interest in the line search iterations. It is robust, yet significantly more efficient than the Automatic Differentiation (AD) and the finite-difference Numerical estimate of the Derivatives (ND) in computing the gradient. The developed EAD method is potentially

useful in other optimization methods where gradients are computed. The EAD, AD and ND methods are then incorporated into the DPE method and compared with the MC simulations to estimate the reliability of nonlinear structural systems and the DPE-EAD method is shown to be the most efficient while being accurate. It is also observed that the reliability index and the direction vectors of the located design points are accurate such that the DPE-EAD method can be further applied to approximate system reliability when multiple failure criteria are considered.

In Chapter 4, the DPE-EAD method is modified and for the estimation of the seismic reliability of structures subjected to an earthquake model with stochastic model parameters. It further extended to allow estimation of the seismic reliability of structures at a specific site when the probability distributions of the seismological properties of the site are available from the earthquake database. The analytical expression of the derivative with respect to the stochastic model parameters are derived which allows accurate and efficient gradient estimation through the use of EAD. Compared to MC simulations, the developed DPE-EAD method is robust yet more efficient when applying to structural systems with different nonlinearities. This chapter also provides a framework to compute the seismic reliability of structures under any possibly occurring earthquakes in an upcoming time period. It is a useful tool in practical structural design and reinforcement, especially for the reliability assessment of structural systems at earthquake pone regions where extensive seismic information are available.

In Chapter 5, the concept of Pontryagin's Maximum Principle (PMP) is introduced to find the design point in the DPE method, that computes the reliability by considering the optimization problem as an optimal control problem. The optimal signal is determined based on the conditions stated by the PMP. By constructing extra matching conditions on the states and the co-states of the structural system, a forward and backward multi-shooting method is adopted to overcome the instability in the numerical integration caused by negative damping. Illustrative examples of the nonlinear structural systems subjected to earthquake excitations show that although the optimized design point $\boldsymbol{u}^*$ found by various optimization methods could potentially be a local minimum, the estimated reliabilities are accurate. The developed DPE-PMP method is robust in estimating reliabilities and this work provides a novel application of the PMP in reliability estimations.

6.2 Future works

The research conducted in this thesis leads to a number of directions that can be further investigated. This section briefly points out several interesting directions:

The implemented example illustrated in Chapter 2 finds that the UT sampling method applied is not sufficiently accurate in estimating the variance of the structural responses under stochastic earthquakes. This is potentially due to the lack of sample points selected for matching the higher order central moments of the random variables. Variations of the UT, i.e. the higher order UT (HOUT) [53], the new UT [54], the improved UT [55] and a linear extension of UT [56], can be adopted to improve the

accuracy for highly nonlinear transformations by introducing an augmented set of sigma points. Previous research has shown that the variations of the UT have better performances in predicting the population distributions of the transformed outputs, which has the potential to improve the estimations of the probability distribution of the structural responses under earthquakes.

The DPE-EAD reliability method developed in Chapter 3-4 is applied to estimate the reliability of structural systems. It is also interesting to investigate whether the DPE-EAD method can be applied to non-structural elements, or in other words rocking bodies, which is also crucial in the seismic risk assessment framework. For rocking systems, in the application of the EAD, there could be challenges in obtaining the symbolic derivative of the states-space equations with respect to the states. The velocity states are discontinuous when an impact occurs. And specifically for irregular rocking bodies, the state-space equations vary depending on the active rocking corner of the body. And thus, further investigation is required to address this special case in the EAD method. The DPE-EAD method can also be extended to estimate the reliability of black-box systems, where the state-space equations of the system of interest are unavailable. It could be achieved by evaluating the gradient $\boldsymbol{\nabla}_{\boldsymbol{x}_k}\boldsymbol{l}_a(\boldsymbol{x}_k)$ and $\boldsymbol{\nabla}_{\boldsymbol{x}_k}\boldsymbol{l}_b(\boldsymbol{x}_k)$ in the EAD formula numerically. This two future research would potentially widen the applicability and improve the robustness of the EAD method.

Following the development of the application of the PMP in reliability evaluations as in Chapter 5, it is also interesting to investigate whether the PMP can be applied to

earthquake models with stochastic model parameters or any other types of stochastic excitations.

Finally, for the methods developed in this thesis, only earthquake models are adopted because the main focus of the research is to evaluate the seismic response. Extending the developed reliability estimation framework by adopting other excitation models with stochasticity, such as wind or wave load models, for wider applications is another interesting future work.

Bibliography

[1] Lu, A. (Ed.). (2008, May 18). *Magnitude of SW China earthquake revised to 8.0*. Chinese Government's Official Web Portal. https://web.archive.org/web/20120229-091938/http:/english.gov.cn/2008-05/18/content_981724.htm

[2] Bryner, J. (2008, May 15). *Why the China quake was so devastating*. Yahoo Live Science. https://web.archive.org/web/20080517233751/http:/news.yahoo.com/s/live-science/whythechinaquakewassodevastating

[3] National Earthquake Information Center (NEIC). (2010, January 12). *Magnitude 7.0 - HAITI REGION*. United States Geological Survey (USGS). https://web.archive.org/web/20100115110510/http:/earthquake.usgs.gov/earthquakes/eqinthenews/2010/us2010rja6/

[4] RENOIS, C. (2010, February 5). *Haitians angry over slow aid*. THE AGE. https://web.archive.org/web/20100207005409/http:/www.theage.com.au/world/haitians-angry-over-slow-aid-20100204-ng2g.html

[5] Agency, J. M. (2011, March 11). *Information on the 2011 Great East Japan earthquake*. Japan Meteorological Agency. https://www.jma.go.jp/jma/en/2011_-Earthquake/Information_on_2011_Earthquake.html

[6] Japanese Gov. (2011, March 11). *3.11 Footage: What Happened That Day*. NHK Disaster Archives. https://web.archive.org/web/20221125045643/ http:/www9.-nhk.or.jp/archives/311shogen/summary/area/

[7] Earthquake Hazards Program. (2023, February 6). *M 7.8 - Pazarcik earthquake, Kahramanmaras earthquake sequence*. United States Geological Survey (USGS). https://earthquake.usgs.gov/earthquakes/eventpage/us6000jllz/executive

[8] World Health Organization (WHO). (2023, July 20). *Kahramanmaraş earthquakes – Türkiye and Syria, 31 May 2023 - Türkiye*. ReliefWeb. https://reliefweb.int/-report/turkiye/kahramanmaras-earthquakes-turkiye-and-syria-31-may-2023

[9] Vamvatsikos D, & Cornell, C.A. (2002). Incremental dynamic analysis. *Earthquake Engineering & Structural Dynamics*, *31* (3), 491-514. https://doi.org-/10.1002/eqe.141

[10] Kiani, J., & Khanmohammadi, M. (2015). New approach for selection of Real Input Ground Motion Records for Incremental Dynamic Analysis (IDA). *Journal of Earthquake Engineering*, *19*(4), 592–623. https://doi.org/10.1080/13632469.2014.-997901

[11] Baker, J. W. (2011). Conditional mean spectrum: Tool for ground-motion selection. *Journal of Structural Engineering*, *137*(3), 322–331. https://doi.org-/10.1061/(asce)st.1943-541x.0000215

[12] Robert, C. P., & Casella, G. (2004). *Monte Carlo Statistical Methods*. Springer, 2nd edition.

[13] Rezaeian, S., & Der Kiureghian, A. (2008). A stochastic ground motion model with separable temporal and spectral nonstationarities. *Earthquake Engineering & Structural Dynamics*, *37*(13), 1565–1584. https://doi.org/10.1002/eqe.831

[14] Rezaeian, S., & Der Kiureghian, A. (2010). Simulation of synthetic ground motions for specified earthquake and site characteristics. *Earthquake Engineering & Structural Dynamics*, *39*(10), 1155–1180. https://doi.org/10.1002/eqe.997

[15] Der Kiureghian, A., Nikolaidis, E., Singhal, S., & Ghiocel, D. M. (2005). Chapter 14: First- and Second-Order Reliability Methods. In *Engineering Design Reliability Handbook*. CRC Press.

[16] Zhao, Y.-G., & Ono, T. (1999). A general procedure for first/second-order reliability method (FORM/SORM). *Structural Safety*, *21*(2), 95–112. https://doi.org-/10.1016/s0167-4730(99)00008-9

[17] Koo, H., Kiureghian, A. D., & Fujimura, K. (2005). Design-point excitation for non-linear random vibrations. *Probabilistic Engineering Mechanics*, *20*(2), 136–147. https://doi.org/10.1016/j.probengmech.2005.04.001

[18] Boltyanski, V. G., Gamkrelidze, R. V., Mishchenko, E. F., & Pontryagin, L. S. (1960). The maximum principle in the theory of optimal processes of control. *IFAC*

Proceedings Volumes, *1*(1), 464–469. https://doi.org/10.1016/s1474-6670(17)70089-4

[19] Romiti, A. (1966). Some extensions of the L. S. Pontryagin maximum principle for optimum control problems. *Meccanica*, *1*(1-2), 21–28. https://doi.org/10.1007/-bf02128404

[20] Priestley, M. B. (1965). Evolutionary Spectra and Non-Stationary Processes. *Journal of the Royal Statistical Society: Series B (Methodological)*, *27*(2), 204–229. https://doi.org/10.1111/j.2517-6161.1965.tb01488.x

[21] Housner, G. W., & Jennings, P. C. (1964). Generation of artificial earthquakes. *Journal of the Engineering Mechanics Division*, *90*(1), 113–150. https://doi.org-/10.1061/jmcea3.0000448

[22] Stafford, P. J., Sgobba, S., & Marano, G. C. (2009). An energy-based envelope function for the stochastic simulation of earthquake accelerograms. *Soil Dynamics and Earthquake Engineering*, *29*(7), 1123–1133. https://doi.org/10.1016/j.soildyn.2009.-01.003

[23] Shinozuka, M., & Deodatis, G. (1991). Simulation of Stochastic Processes by Spectral Representation. *Applied Mechanics Reviews*, *44*(4), 191–204. https://doi.org-/10.1115/1.3119501

[24] Kanai, K. (1957). 210) Semi-empirical Formula for the Seismic Characteristics of Ground (Structure). *Transactions of the Architectural Institute of Japan*, *57.1*(0), 281–284. https://doi.org/10.3130/aijsaxx.57.1.0_281

[25] Tajimi, H. (1958). 2005) Estimation of the Maximum Response of Building to Earthquake Motions by the Statistical method (Structure). *Transactions of the Architectural Institute of Japan*, *60.1*(0), 249–252. https://doi.org/10.3130/aijsaxx.-60.1.0_249

[26] Liu, S.-C., & Jhaveri, D. P. (1969). Spectral Simulation and Earthquake Site Properties. *Journal of the Engineering Mechanics Division*, *95*(5), 1145–1168. https://doi.org/10.1061/jmcea3.0001168

[27] Faravelli, L. (1988). Stochastic modeling of the seismic excitation for structural dynamics purposes. *Probabilistic Engineering Mechanics*, *3*(4), 189–195. https://doi.org/10.1016/0266-8920(88)90011-2

[28] Bolotin, V. V. (1970). Statistical methods in structural mechanics. *Journal of the American Statistical Association*, *65*(332), 1693. https://doi.org/10.2307/2284360

[29] Shinozuka, M., & Brant, P. (1969). Application of the Evolutionary Power Spectrum in Structural Dynamics. *Proceedings of the ASCE-EMD Specialty Conference on Probabilistic Concepts and Methods*, 12–14.

[30] Liu, S. C. (1970). Evolutionary power spectral density of strong-motion earthquakes. *Bulletin of the Seismological Society of America*, *60*(3), 891–900. https://doi.org/10.1785/bssa0600030891

[31] Bogdanoff, J. L., Goldberg, J. E., & Bernard, M. C. (1961). Response of a simple structure to a random earthquake-type disturbance. *Bulletin of the Seismological Society of America*, *51*(2), 293–310. https://doi.org/10.1785/bssa0510020293

[32] Shinozuka, M., & Sato, Y. (1967). Simulation of nonstationary random process. *Journal of the Engineering Mechanics Division*, *93*(1), 11–40. https://doi.org/10.-1061/jmcea3.0000822

[33] Amin, M., & Ang, A. H.-S. (1968). Nonstationary stochastic models of earthquake motions. *Journal of the Engineering Mechanics Division*, *94*(2), 559–584. https://doi.org/10.1061/jmcea3.0000969

[34] Iyengar, R. N., & Sundara, T. (1969). A nonstationary random process model for earthquake accelerograms. *Bulletin of the Seismological Society of America*, *59*(3), 1163–1188. https://doi.org/10.1785/bssa0590031163

[35] Levy, R., Kozin, F., & Moorman, R. B. B. (1971). Random processes for earthquake simulation. *Journal of the Engineering Mechanics Division*, *97*(2), 495–517. https://doi.org/10.1061/jmcea3.0001377

[36] Lin, Y. K. (1963). Application of Nonstationary Shot Noise in the Study of System Response to a Class of Nonstationary Excitations. *Journal of Applied Mechanics*, *30*(4), 555–558. https://doi.org/10.1115/1.3636617

[37] Cornell, C. A. (1964). *Stochastic process models in structural engineering*. Technical Report No. 34, Department of Civil Engineering, Stanford University.

[38] Lin, Y.-K. (1986). *Probabilistic theory of structural dynamics*. Robert E. Krieger.

[39] Liu, S.-C. (1970). Dynamics of Correlated Random Pulse Trains. *Journal of the Engineering Mechanics Division*, *96*(4), 455–470. https://doi.org/10.1061/jmcea3.-0001258

[40] Lin, Y. K. (1986). On random pulse train and its evolutionary spectral representation. *Probabilistic Engineering Mechanics*, *1*(4), 219–223. https://doi.org-/10.1016/0266-8920(86)90015-9

[41] Shields, M. D., & G. Deodatis. (2013). Estimation of evolutionary spectra for simulation of non-stationary and non-Gaussian stochastic processes. *Computers & Structures*, *126*, 149–163. https://doi.org/10.1016/j.compstruc.2013.02.007

[42] Metropolis, N., & Ulam, S. (1949). The Monte Carlo Method. *Journal of the American Statistical Association*, *44*(247), 335–341. https://doi.org/10.1080/0162-1459.1949.10483310

[43] Hastings, W. K. (1970). Monte Carlo sampling methods using Markov chains and their applications. *Biometrika*, *57*(1), 97–109. https://doi.org/10.1093/biomet/57.1.97

[44] Metropolis, N., Rosenbluth, A. W., Rosenbluth, M. N., Teller, A. H., & Teller, E. (1953). Equation of State Calculations by Fast Computing Machines. *The Journal of Chemical Physics*, *21*(6), 1087–1092. https://doi.org/10.1063/1.1699114

[45] Martin, J., Wilcox, L. C., Burstedde, C., & Ghattas, O. (2012). A stochastic Newton MCMC method for large-scale statistical inverse problems with application to seismic inversion. *SIAM Journal on Scientific Computing*, *34*(3). https://doi.org/10.1137/110845598

[46] Au, S. K., & Beck, J. L. (2003). Subset simulation and its application to seismic risk based on dynamic analysis. *Journal of Engineering Mechanics*, *129*(8), 901–917. https://doi.org/10.1061/(asce)0733-9399(2003)129:8(901)

[47] Melchers, R. E. (1990). Improved Importance Sampling Methods for Structural System Reliability Calculation. *Structural Safety and Reliability*, 1185–1192.

[48] Ibrahim, Y. (1991). Observations on applications of importance sampling in structural reliability analysis. *Structural Safety*, *9*(4), 269–281. https://doi.org-/10.1016/0167-4730(91)90049-f

[49] Julier, S. J., & Uhlmann, J. K. (2004). Unscented Filtering and Nonlinear Estimation. *Proceedings of the IEEE*, *92*(3), 401–422. https://doi.org/10.1109-/jproc.2003.823141

[50] de Angelis, M., Patelli, E., & Beer, M. (2015). Advanced Line Sampling for efficient robust reliability analysis. *Structural Safety*, *52*, 170–182. https://doi.org/-10.1016/j.strusafe.2014.10.002

[51] Schuëller, G. I., Pradlwarter, H. J., & Koutsourelakis, P. S. (2004). A critical appraisal of reliability estimation procedures for high dimensions. *Probabilistic Engineering Mechanics*, *19*(4), 463–474. https://doi.org/10.1016/j.probengmech.-2004.05.004

[52] Zio, E., & Pedroni, N. (2009). Subset simulation and line sampling for Advanced Monte Carlo Reliability Analysis. *Reliability, Risk, and Safety*. https://doi.org/-10.1201/9780203859759.ch94

[53] Tenne, D., & Singh, T. (2003). The higher order unscented filter. *Proceedings of the 2003 American Control Conference*, *3*, 2441–2446. https://doi.org/10.1109/-acc.2003.1243441

[54] Ponomareva, K., Date, P., & Wang, Z. (2010). A new unscented Kalman filter with higher order moment-matching. *Proceedings of the 19th International Symposium on Mathematical Theory of Networks and Systems – MTNS 2010*, 1609–1613. https://doi.org/10.13140/2.1.1472.6089

[55] Wu, Y., Wu, M., Hu, D., & Hu, X. (2004). An Improvement to Unscented Transformation. *AI 2004: Advances in Artificial Intelligence - 17th Australian Joint*

Conference on Artificial Intelligence, 3339, 1024-1029. Springer, Berlin, Heidelberg. https://doi.org/10.1007/978-3-540-30549-1_96

[56] Liu, J., Wang, Y., & Zhang, J. (2014). A linear extension of unscented Kalman filter to higher-order moment-matching. *53rd IEEE Conference on Decision and Control*, 5021–5026. https://doi.org/10.1109/cdc.2014.7040173

[57] Du, X. (2005). Chapter 7: First Order and Second Reliability Methods. In *Probabilistic Engineering Design*.

[58] Li, J., & Chen, J. B. (2004). Probability density evolution method for dynamic response analysis of structures with uncertain parameters. *Computational Mechanics*, *34*(5), 400–409. https://doi.org/10.1007/s00466-004-0583-8

[59] Der Kiureghian, A., Lin, H., & Hwang, S. (1987). Second-order reliability approximations. *Journal of Engineering Mechanics*, *113*(8), 1208–1225. https://doi.-org/10.1061/(asce)0733-9399(1987)113:8(1208)

[60] LeVeque, R. J. (2007). *Finite difference methods for ordinary and partial differential equations: Steady-state and time-dependent problems*. Society for Industrial and Applied Mathematics, 1st edition.

[61] Richtmyer, R. D., & Morton, K. W. (1967). *Difference Methods for Initial Value Problems*. J. Wiley & Sons, 2nd edition.

[62] Sengupta, B., Friston, K. J., & Penny, W. D. (2014). Efficient gradient computation for dynamical models. *NeuroImage*, *98*, 521–527. https://doi.org/-10.1016/j.neuroimage.2014.04.040

[63] Giles, M. B., & Pierce, N. A. (2000). An introduction to the adjoint approach to design. *Flow, Turbulence and Combustion*, *65*(3/4), 393–415. https://doi.org/-10.1023/a:1011430410075

[64] Wang, Q. (2013). Forward and adjoint sensitivity computation of chaotic dynamical systems. *Journal of Computational Physics*, *235*, 1–13. https://doi.org/-10.1016/j.jcp.2012.09.007

[65] Deneux, T., & Faugeras, O. (2006). Using nonlinear models in fMRI data analysis: Model selection and activation detection. *NeuroImage*, *32*(4), 1669–1689. https://doi.org/10.1016/j.neuroimage.2006.03.006

[66] Jensen, H. A., Valdebenito, M. A., Schuëller, G. I., & Kusanovic, D. S. (2009). Reliability-based optimization of stochastic systems using line search. *Computer Methods in Applied Mechanics and Engineering*, *198*(49-52), 3915–3924. https://-doi.org/10.1016/j.cma.2009.08.016

[67] Hager, W. W., & Zhang, H. (2005). A New Conjugate Gradient Method with Guaranteed Descent and an Efficient Line Search. *SIAM Journal on Optimization*, *16*(1), 170–192. https://doi.org/10.1137/030601880

[68] Keshtegar, B., & Miri, M. (2014). Introducing conjugate gradient optimization for modified HL-RF method. *Engineering Computations*, *31*(4), 775–790. https://doi.-org/10.1108/ec-09-2012-0225

[69] Pontryagin, L. S., & Gamkrelidze, R. V. (1986). *The mathematical theory of optimal processes.* Gordon and Breach, 1st Edition.

[70] Peng, S. (1990). A general stochastic maximum principle for optimal control problems. *SIAM Journal on Control and Optimization*, *28*(4), 966–979. https://doi.-org/10.1137/0328054

[71] Wang, G., & Chen, S. (1999). Maximum principle for optimal control of some parabolic systems with two-point boundary conditions. *Numerical Functional Analysis and Optimization*, *20*(1–2), 163–174. https://doi.org/10.1080/01630569908816886

[72] Van Damme, L., Zeier, R., Glaser, S. J., & Sugny, D. (2014). Application of the Pontryagin maximum principle to the time-optimal control in a chain of three spins with unequal couplings. *Physical Review A*, *90*(1). https://doi.org/10.1103/-physreva.90.013409

[73] Özparpucu, M. C., Haddadin, S., & Albu-Schäffer, A. (2014). Optimal Control of Variable Stiffness Actuators with Nonlinear Springs. *IFAC Proceedings Volumes*, *47*(3), 8487–8495. https://doi.org/10.3182/20140824-6-za-1003.01193

[74] Li, L., Fang, M., Chen, G., & Yang, D. (2022). Reliability-based stochastic optimal control of frame building under near-fault ground motions. *Mechanical*

Systems and Signal Processing, *163*, 108098–108098. https://doi.org/10.1016/-j.ymssp.2021.108098

[75] Peng, Y., & Zhang, Z. (2020). Optimal MR Damper–Based Semiactive Control Scheme for Strengthening Seismic Capacity and Structural Reliability. *Journal of Engineering Mechanics-Asce*, *146*(6). https://doi.org/10.1061/(asce)em.1943-7889.0001768

[76] Li, J., Peng, Y.-B., & Chen, J.-B. (2010). A physical approach to structural stochastic optimal controls. *Probabilistic Engineering Mechanics*, *25*(1), 127–141. https://doi.org/10.1016/j.probengmech.2009.08.006

[77] Rao, A.V. (2009). A survey of numerical methods for trajectory optimization. *AAS/AIAA Astrodynamics Specialists Conference*, *135*(1), 497-528.

[78] Betts, J. T. (1998). Survey of Numerical Methods for Trajectory Optimization. *Journal of Guidance, Control, and Dynamics*, *21*(2), 193–207. https://doi.org/-10.2514/2.4231

[79] Morrison, D. D., Riley, J. D., & Zancanaro, J. F. (1962). Multiple shooting method for two-point boundary value problems. *Communications of the ACM*, *5*(12), 613–614. https://doi.org/10.1145/355580.369128

[80] Bock, H. G., & Plitt, K. J. (1984). A Multiple Shooting Algorithm for Direct Solution of Optimal Control Problems. *IFAC Proceedings Volumes*, *17*(2), 1603–1608. https://doi.org/10.1016/s1474-6670(17)61205-9

[81] Campbell, K. W., & Bozorgnia, Y. (2008). NGA Ground Motion Model for the Geometric Mean Horizontal Component of PGA, PGV, PGD and 5% Damped Linear Elastic Response Spectra for Periods Ranging from 0.01 to 10 s. *Earthquake Spectra*, *24*(1), 139–171. https://doi.org/10.1193/1.2857546

[82] Abrahamson, N., Atkinson, G., Boore, D., Bozorgnia, Y., Campbell, K., Chiou, B., Idriss, I. M., Silva, W., & Youngs, R. (2008). Comparisons of the NGA Ground-Motion Relations. *Earthquake Spectra*, *24*(1), 45–66. https://doi.org/10.1193/1.2924363

[83] Wan, E. A., & Van Der Merwe, R. (2000). The unscented Kalman filter for nonlinear estimation. *Proceedings of the IEEE 2000 Adaptive Systems for Signal Processing, Communications, and Control Symposium (Cat. No.00EX373)*, 153–158. https://doi.org/10.1109/asspcc.2000.882463

[84] Fujimura, K., & Der Kiureghian, A. (2007). Tail-equivalent linearization method for nonlinear random vibration. *Probabilistic Engineering Mechanics*, *22*(1), 63–76. https://doi.org/10.1016/j.probengmech.2006.08.001

[85] Butcher, J. C. (2000). Numerical methods for ordinary differential equations in the 20th century. *Journal of Computational and Applied Mathematics*, *125*(1-2), 1–29. https://doi.org/10.1016/s0377-0427(00)00455-6

[86] Dormand, J. R., & Prince, P. J. (1980). A family of embedded Runge-Kutta formulae. *Journal of Computational and Applied Mathematics*, *6*(1), 19–26. https://doi.org/10.1016/0771-050x(80)90013-3

[87] Shampine, L. F., & Reichelt, M. W. (1997). The MATLAB ODE Suite. *SIAM Journal on Scientific Computing*, *18*(1), 1–22. https://doi.org/10.1137/s1064827-594276424

[88] Rabinowitz, P., & Davis, P. J. (2007). *Methods of numerical integration*. Dover Publications, 2nd edition.

[89] Baydin, Atilim, G., Barak, A. P., Alexey A. R., & Jeffrey M. S. (2018). Automatic Differentiation in Machine Learning: A Survey. *The Journal of Machine Learning Research*, *18*(153), 1–43. https://doi.org/10.48550/arXiv.1502.05767

[90] *Automatic Differentiation Background - MATLAB & Simulink - MathWorks United Kingdom*. Uk.mathworks.com. https://uk.mathworks.com/help/optim/ug/auto-diffbackground.html

[91] Schuëller, G. I., & Pradlwarter, H. J. (2007). Benchmark study on reliability estimation in higher dimensions of structural systems – An overview. *Structural Safety*, *29*(3), 167–182. https://doi.org/10.1016/j.strusafe.2006.07.010

[92] Gutenberg, B., & Richter, C. F. (1944). Frequency of earthquakes in California*. *Bulletin of the Seismological Society of America*, *34*(4), 185–188. https://doi.org/-10.1785/bssa0340040185

[93] Gutenberg, B. (2013). *Seismicity of the Earth and Associated Phenomena*. Read Books Ltd.

[94] Press, W. H., Teukolsky, S.A., Vetterling, W.T., & Flannery, B.P. (2007). Section 18.1. The Shooting Method. In *Numerical Recipes: The Art of Scientific Computing*. New York: Cambridge University Press, 3rd edition.

[95] Griffiths, D. F., & Higham, D. J. (2011). Numerical methods for ordinary differential equations: Initial value problems. Springer.

[96] Press, W. H., Teukolsky, S.A., Vetterling, W.T., & Flannery, B.P. (2007). Chapter 9. Root Finding and Nonlinear Sets of Equations. In *Numerical Recipes: The Art of Scientific Computing*. New York: Cambridge University Press, 3rd edition.

[97] Powell, M. J. D. (1988). A Fortran Subroutine for Solving Systems of Nonlinear Algebraic Equations. In *Numerical Methods for Nonlinear Algebraic Equations* (P. Rabinowitz, Ed.). Gordon and Breach Science Publishers.

[98] Yamamoto, Y., & Baker, J. W. (2013). Stochastic Model for Earthquake Ground Motion Using Wavelet Packets. *Bulletin of the Seismological Society of America*, *103*(6), 3044–3056. https://doi.org/10.1785/0120120312

[99] Vlachos, C., Papakonstantinou, K. G., & Deodatis, G. (2016). A multi-modal analytical non-stationary spectral model for characterization and stochastic simulation of earthquake ground motions. *Soil Dynamics and Earthquake Engineering*, *80*, 177–191. https://doi.org/10.1016/j.soildyn.2015.10.006

[100] Vlachos, C., Papakonstantinou, K. G., & Deodatis, G. (2017). Predictive model for site specific simulation of ground motions based on earthquake scenarios. *Earthquake Engineering & Structural Dynamics*, *47*(1), 195–218. https://doi.org/-10.1002/eqe.2948

[101] Dabaghi, M., & Der Kiureghian, A. (2016). Stochastic model for simulation of near-fault ground motions. *Earthquake Engineering & Structural Dynamics*, *46*(6), 963–984. https://doi.org/10.1002/eqe.2839

[102] Lynne, S. B., & Baker, J. W. (2016). A predictive model for fling-step in near-fault ground motions based on recordings and simulations. *Soil Dynamics and Earthquake Engineering*, *80*, 119–126. https://doi.org/10.1016/j.soildy-n.2015.10.010

[103] Rosenblueth, E. (1975). Point estimates for probability moments. *Proceedings of the National Academy of Sciences*, *72*(10), 3812–3814. https://doi.o-rg/10.1073/pnas.72.10.3812

[104] Julier, S. J. (2003). The spherical simplex unscented transformation. *Proceedings of the 2003 American Control Conference*, *3*. https://doi.org/10.1109-/acc.2003.1243439

[105] Amir, M., Papakonstantinou, K. G., & Warn, G. P. (2022). Scaled Spherical Simplex Filter and State-Space Damage-Plasticity Finite-Element Model for

Computationally Efficient System Identification. *Journal of Engineering Mechanics-Asce, 148*(2). https://doi.org/10.1061/(asce)em.1943-7889.0001945

[106] Papakonstantinou, K. G., Amir, M., & Warn, G. P. (2022). A Scaled Spherical Simplex Filter (S3F) with a decreased n + 2 sigma points set size and equivalent 2n + 1 Unscented Kalman Filter (UKF) accuracy. *Mechanical Systems and Signal Processing*, *163*, 107433. https://doi.org/10.1016/j.ymssp.2020.107433

[107] Ko, M., & Papakonstantinou, K. G. (2024). Quadratic point estimate method for probabilistic moments computation. *Probabilistic Engineering Mechanics*, *79*(0266-8920), 103705. https://doi.org/10.1016/j.probengmech.2024.103705

[108] Andrieu-Renaud, C., Sudret, B., & Lemaire, M. (2004). The PHI2 method: a way to compute time-variant reliability. *Reliability Engineering & System Safety*, *84*(1), 75–86. https://doi.org/10.1016/j.ress.2003.10.005